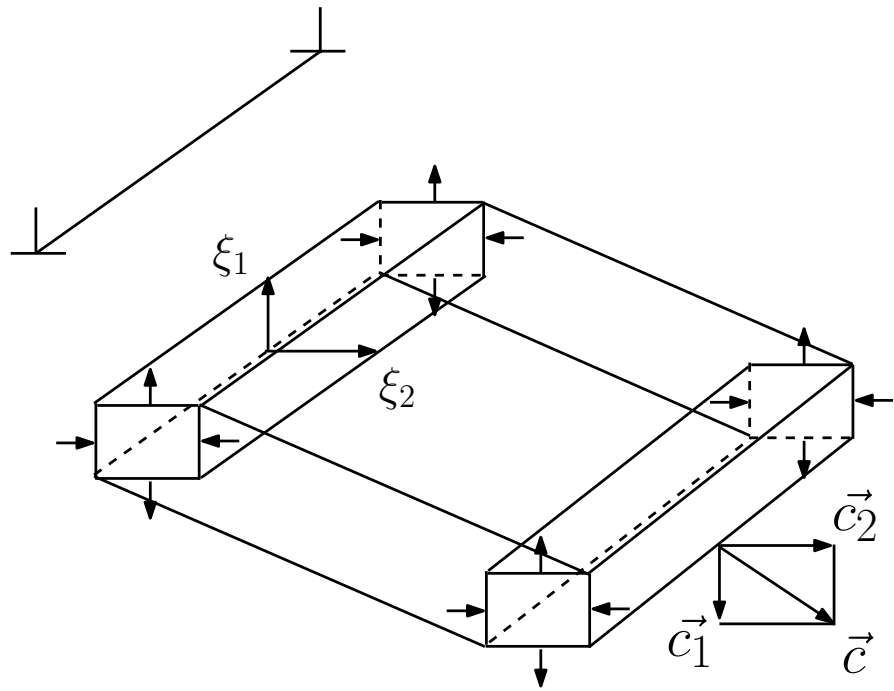


M. P. KASHCHENKO

THE WAVE MODEL OF MARTENSITE GROWTH
FOR THE $\gamma - \alpha$ TRANSFORMATION
OF IRON-BASED ALLOYS



EKATERINBURG 2005

M.P.KASHCHENKO

THE WAVE MODEL OF MARTENSITE GROWTH
FOR THE $\gamma - \alpha$ TRANSFORMATION
OF IRON-BASED ALLOYS

Prof. Michael P. Kashchenko
Ural State Forest Engineering University
Physics Chair
Sybirskiy Tract 37
620100 Ekaterinburg
RUSSIA
mpk@usfeu.ru or mpkathome@usfeu.ru

Ekaterinburg
UIF Publishing-House "Nauka"
Original Russian Edition 1993

English Edition 2005.
Translation from Russian by J. Gerlts and U. Kayser-Herold

Contents

Preface	8
Introduction	11
1 Basic notions on the γ-α martensitic transformation in iron based alloys	15
1.1 Position of the γ - α martensitic transformation in relation to other solid state structural transformations	15
1.2 Characteristic features of the spontaneous γ - α martensitic transformation	18
1.3 Lattice-stability near the M_S -temperature and the problem of nucleation during the γ - α martensitic transformation	22
1.4 Solved and unresolved problems on the theoretical description of the γ - α - martensitic transformation	28
1.5 General physical tasks and objectives	39
2 Particularities of an electronic energy spectrum as required for realization of a Phonon-Maser	49
2.1 The Hamiltonian Problem	49
2.2 Form of a non-equilibrium addend to the electronic distribution function and definition of points separating inversely occupied states in a one-dimensional electronic spectrum	50
2.3 Definition of boundary surfaces separating inversely occupied states for a 3-dimensional electronic spectrum	52
2.4 Limitations imposed by the equidistance relations in (1.9)	58
2.5 Potentially active pairs of electronic states in the electronic-spectrum of fcc iron	64
2.6 Summary of Chapter 2	73
3 Constitutive equations of the electron-phonon system and the threshold wave generation conditions	77
3.1 Threshold conditions for single-mode generation	77
3.2 Threshold conditions for two- and three-mode wave generation and characteristics of a phase transition of a radiation system	84

3.3	The lattice strain induced by the generated waves	91
3.4	Conclusions from Chapter 3	95
4	Coordination between of the γ-α martensitic transformation temperature and the optimum wave generation temperature in iron-based alloys	99
4.1	Definition of the task	99
4.2	Modified electronic distributions and their derivatives in the case of a rectangular spectral density function	102
4.3	Region of T' , Γ' values with optimum conditions for phonon-generation in the case of a Lorentz-shaped SD-function	108
4.4	Mapping of the functions $M_S(C)$ into the T' , Γ' region of optimum phonon-generation, with analysis of the electronic configurations of atoms in binary substitutional alloys	111
4.5	Discussion of the results on substitutional alloys	118
4.5.1	Determination of the parameter a_0 and of electronic atom-configurations on the basis of electrical and optical characteristics of alloying components	118
4.5.2	Effect of variations of lattice-parameter and the s-band width on the difference of the charge numbers ΔZ of alloying components	122
4.5.3	Estimation of the chemical potential differences of some γ - and α - phases, for the sub-system of d-electrons	128
4.6	The $M_S(C)$ function for steel and degree of ionization of carbon-atoms	129
4.7	Summary of Chapter 4	131
5	Interpretation of a variety of characteristic morphological features of martensite within the notion of a phonon-maser	135
5.1	Habit-planes in Fe-Ni, Fe-C-alloys	136
5.1.1	Matching of a plane with a pair of waves	136
5.1.2	Habit (225)	136
5.1.3	Habit (557). Criterion for transition from habitus (557) to (225)	139
5.1.4	Habits $\{15\ 3\ 10\} \div \{9\ 2\ 5\}$	140
5.2	Grouping laws for packet-martensite crystals	142
5.3	Effect of the magnetic state of austenite and of an externally applied magnetic field on the martensitic $\gamma - \alpha$ - transformation	145
5.3.1	Possible causes for the transition of habit-planes	145
5.3.2	Single peak density of states (DOS) model, exchange-splitting and electronic redistribution	147
5.3.3	Oriented lattice-growth of athermal martensite in an externally applied magnetic field	153
5.4	Summary of chapter 5	157

6	Wave-model of motion for a martensitic lattice boundary	162
6.1	Coordinated propagation of a displacement-wave with a switching-wave of chemical potential or temperature	164
6.2	Coordinated propagation of a pair of displacement-waves with the switching-wave of $T(\mu)$	167
6.3	Stationary wave of relative spatial deformation $\tilde{\epsilon}$ during the $\gamma - \alpha$ - transformation	170
6.3.1	$\tilde{\epsilon}$ - trigger-switching - wave in absence of displacement-waves	170
6.3.2	Effect of the displacement-waves on the velocity of the $\tilde{\epsilon}$ - switching-wave	174
6.3.3	The $\tilde{\epsilon}$ - Modified-Switching-Wave	175
6.4	Summary of Chapter 6	179
	Synopsis and outlook	183
	Bibliography	193
	Epilogue	213
	Summary	218

Preface

Since the early seventies, the Author and his Team have been engaged in their still ongoing task and vision of developing a comprehensive physical notion of the $\gamma - \alpha$ Martensitic Transformation ($\gamma - \alpha$ MT). The main results of their research work are published in this monograph. Shortly after an initial review and analysis of existing literature on the subject, the following initial conclusions could be drawn:

- The $\gamma - \alpha$ MT is a cooperative lattice transformation proceeding under highly pronounced deviations from local equilibrium conditions;
- The velocity of rapid controlled growth of α -Martensite crystals is so large that only a wave-model has the physical potential for a conclusive detailed and comprehensive explanation of the transformation and growth ;
- A microscopic theory of the transformation is missing.

From the very beginning, the development of a new and comprehensive growth model of a single martensite crystal was mainly guided by the following two factors: On the one hand, the realization that a substantial fraction of energy released during the martensitic transformation process is immediately being converted into the energy of cooperative lattice displacement waves, by the mechanism of stimulated emission of coherent phonons, becoming most effective in a subsystem of non-equilibrium 3-d electrons, which "jump" down to a lower energetic level at the very instant and location of the martensitic lattice transformation, and on the other hand, the formulation of a simple two-wave scheme of the crystal growth control mechanism. Even though these two factors were known to the author since 1976, considerable efforts were necessary to figure out in detail the kind and sequence of events during lattice wave generation, and to consistently interpret in their entirety the observed morphological and kinetic particularities of the $\gamma - \alpha$ MT, including those of some binary alloys in a wide range of concentrations of their second component, as well as to prove experimentally a variety of postulates and predictions related to the problem. The matter described in this monograph nearly reproduces the contents of the habilitation paper of the Author at the Department of Radiating Materials Science of the Ural Polytechnical Institute (nowadays the Ural State Technical University) and at the Cathedra of Physics of the Ural Forest

Engineering Institute (nowadays Ural Forest Engineering State University) completed in 1986.

The decision to publish this monograph was motivated, on the one hand, by several wishes expressed during the many and extensive discussions with specialists in the disciplines of Solid State Physics and Phase-Transitions, as well as with Metal- and Materials scientists, and on the other hand, by the presently achieved success in the realization of theoretical and experimental research programs on α -Martensite nucleation focusing on the specific aspects of the Wave-Growth-Model. The results obtained from 1989 to 1991 are supposed to be worth a presentation in a single special monograph. The short survey in the final part of this monograph is to complete the notion of the $\gamma - \alpha$ MT. Here, let us only mention the most important:

- It has been found that 60° straight line dislocations with $\langle 110 \rangle$ lines could act as dislocation nucleation centers (DNC) for α -Martensite crystals with habit planes close to $\{557\} - \{225\}$, whereas 30° dislocations with $\langle 112 \rangle$ lines were acceptable candidates for the role of DNC for crystals with habits close to $\{259\} - \{3\ 10\ 15\}$.
- Physical models have been developed for the excited pre-martensitic lattice condition, being typical of the state of nucleation. It was also possible to reproduce the physical conditions prevailing in the transformation wave-front, by means of picosecond-laser irradiation directed onto the surface of a Fe - 31,5 Ni single crystal. The results of these investigations can be interpreted as supportive and further detailing the qualitative notion of nucleation, which had been presupposed during the development of the growth model.

This is the first time that the mechanism of phonon generation during a solid state transformation has been analyzed and identified as a fundamental aspect of the $\gamma - \alpha$ transformation. Obviously, the newly developed model of spontaneous martensitic nucleation and growth is also suitable for a physical description of the reverse martensitic $\alpha - \gamma$ -transformation, as well as for other transformations of the type (i.e. cubic-bcc \leftrightarrow cubic-fcc lattice of Cu-Zn alloys). Moreover, the example of the $\gamma - \alpha$ MT shows that the key for comprehensive understanding of the mechanism controlling the growth of a new phase during reconstructive cooperative transformations is to reveal the dynamic characteristics of an excited lattice in the non-equilibrium system conditions developing in the frontal zone of a non-linear transformation wave. This latter conclusion is fundamental as it includes the essence of the paradigm complementing the traditional conceptual notion of equilibrium thermodynamics.

The Author hopes that this monograph will close (to some degree) the gap which previously had existed in the theory of reconstructive martensitic transformations, and will attract the attention of other scientists to the problem, and be useful to a wider audience of readers.

The Author wants to express his thanks and acknowledgments to all his Colleagues and Specialists who discussed this matter with him, thereby promoting the progress in research, as well as to the cooperative "Alvo-Materialovedenie", who sponsored the publication of this monograph.

Introduction

Since many epochs, the production and use of steel and ferrous alloys have been of high and ever increasing importance, for almost any branch of industry and economy. Thus the development of new types of steel with prescribed combinations of the desired mechanical and physical properties, as well as economical benefits, have been the final aim of numerous and still ongoing metallurgical research projects. On the one hand, such research traditionally comprises the empirical development of highly sophisticated metallurgical production methods, like new thermo-mechanical methods of treatment, by making use of the most suitable phase- and structural transformations and, on the other hand, has the final aim of comprehensive and fundamental theoretical understanding of the underlying phase transitions and related physical processes.

In the metallurgy of steel, the spontaneous martensitic $\gamma - \alpha$ -transformation plays a key role among structural transformations, as it constitutes the most important hardening process ending up in the formation of martensite. Traditionally, the spontaneous martensitic transformation (MT) is produced by quenching of the high-temperature (austenitic) phase. The spontaneous MT of ferrous alloys is intriguing and challenging from a scientific point of view. One of the most characteristic features of MT is their diffusionless transformation mechanism, by means of rapid cooperative rearrangement of the face-centered cubic (fcc) high-temperature γ -phase (austenite) into the body-centered cubic (bcc) or body-centered tetragonal (bct) low temperature α -phase (martensite). The results of specific research focusing on martensitic transformations substantially contributed to the increase of understanding of the many relevant details of diffusionless structural transformations. However until recently, some key features of martensitic transformations, like the growth process and lattice-dynamics of the spontaneous transformation, remained as one of metal physics greatest intractable problems. The disclosure of the dynamical mechanisms and principles underlying the process of martensitic transformations would enlighten their intrinsic characteristics and physical nature, and can thus be regarded as one of the fundamental problems of metal physics. Till now, dynamic approach has only been (partially) developed for transformations of the distortional type, in which the lattice symmetry groups of the final and of the initial phases are mutually subordinated. In principle, the transformations of the distortional type are close to a second-order phase transition (as a rule they exhibit weakly pronounced characteristics of first-order transitions). Such

transformations are almost satisfactorily explained within the "Soft-Mode" theory, which, for the most part, focuses around the Shape-Memory-Effect (SME). In contrast, the reconstructive phase transitions, to which the spontaneous $\gamma - \alpha$ MT is related, demonstrate pronounced features of the first-order transitions, namely, considerable temperature hysteresis (between the direct and reverse transformations) and thermal and volume effects. Therefore, the "Soft-Mode" theory cannot be directly applied to them. Theoretical research on the $\gamma - \alpha$ MT is mainly characterized by the parallel development of the lattice-geometrical, thermodynamic and wave approaches. The few attempts to describe the martensite growth within the wave theory remained uninformative, mainly due to the poorly understood mechanisms of wave excitation and stabilization, as well as of the types of waves and their directions of propagation. On the other hand, the results of such investigations remained in the shadow of an impressive success in the interpretation of the morphology of the martensite crystals, which had mainly been achieved by means of lattice-geometrical and thermodynamic investigations. At the same time it turned out more and more obvious that only the wave approach would have the full potential for a comprehensive description of the dynamical aspects of the transformation process. This circumstance determines the immediateness of development of the wave models of martensite crystal growth.

The main problems of the wave theory of the α -phase growth are the type of the wave process and the mechanism of energy supply that ensures their steady-state propagation. Experimental results indicate that the frontal velocity of martensitic lattice growth only weakly depends on temperature. Its speed of propagation of about $\sim 10^3$ m/s is of the same order of magnitude as the sound velocity, presumably exceeding the velocity of longitudinal elastic waves. Supersonic growth speed, on the one hand, is a clear indication of a complicated, non-linear character of a wave-process and on the other hand, of its adiabatic nature, which, in combination with supercooling by about $\Delta T \approx 200\text{K}$ below phase equilibrium temperature T_0 , together with considerable heat- and volume-transformation effects, must inevitably lead to a strongly pronounced non-equilibrium condition with large temperature- and chemical potential gradients, in the area between the two phases and, finally, to intensive electronic flows. In accordance with the general laws of non-equilibrium thermodynamics, specific self-organizing processes and structures can in principle emerge within any kind of pronounced non-equilibrium system. In the particular case of interactions between radiation fields comprising photons or phonons with inversely occupied radiative (electronic) sub-systems, such conditions may strongly support the generation of coherent waves. To achieve our final aim of determination of the mechanism controlling the cooperative atom displacements (in a microscopic frame of description) associated with the $\gamma - \alpha$ MT, it is necessary to analyze the dynamical properties of a non-equilibrium system comprising essential electron-phonon interactions. The direction of research initiated by this work, being mainly related to the $\gamma - \alpha$ martensitic transformation of ferrous alloys, can essentially be formulated as follows:

A theoretical description of rapid growth of a martensite crystal as a self-organizing process being inherently associated with the propagation of displacement waves generated and amplified by non-equilibrium 3-d electrons.

Thus the aim of this work will focus on the substantiation of a wave-model of martensite growth, which in principle should enable us to determine the basic relationships between the microscopic particularities of the electronic structure and the macroscopic (morphologic) features of the transforming systems.

To achieve this goal, the following basic prerequisites will have to be met:

1. The development of a methodology for specific search and the identification of pairs of electronic states, that are potentially active for the generation of displacement waves in a local non-equilibrium medium, and an assessment of the amount of such pairs in the electronic spectrum of fcc-iron during the $\gamma - \alpha$ MT.
2. Definition of the threshold conditions for the generation of elastic displacement -waves by nonequilibrium electrons, including an estimation of maximum wave amplitudes.
3. Substantiation of the possibility to realize the conditions required for wave generation within a wide range of temperatures and concentrations of the second component in ferrous alloys.
4. Creation of a model associating a variety of morphologic features of martensite crystals with the coordinated propagation of lattice displacement waves.
5. Investigation of the motion of the martensitic crystal interface within the concept of a coordinated propagation of a "switching-wave" for relative volume deformation and displacement waves ensuring the onset of threshold deformation.

A qualitative notion of the physical state of rapid frontal growth of martensitic lattice, as obtained from theoretical analysis, thus must at least comprise the following key features:

1. Frontal growth of martensite is controlled by quasi-longitudinal lattice distortion waves fastly propagating through a γ - phase;
2. The characteristics of such waves define the basic spatial and temporal scales of martensitic growth, and as a consequence the gradients of the chemical potential of electrons (and thereby also the magnitudes of the electrical field strength and current density) and of temperature in the transformation zone;
3. During martensitic lattice growth, the physical parameters of the interphase region comprise key characteristics of a highly pronounced non-equilibrium condition;

4. The amplitudes of lattice distortion waves are maintained owing to the process of stimulated emission of phonons by non-equilibrium 3-d electrons located in the transformation zone, thereby revealing the physical nature of the real process controlling a spontaneous martensitic reaction.

Detailed physical information on the various field characteristics (i.e. displacements, temperature, electrical and magnetic fields) within the non-equilibrium area in the vicinity of a growing lattice will be of fundamental importance for the design of experiments aiming at a simulation of the process of lattice nucleation of the α -phase, as well as for the design of experimental devices for dynamical excitation of a pre-martensitic lattice condition by hypersonic frequencies in a range of $\sim 10^{10}s^{-1}$, which would have to coincide with the range of frequencies of the distortion waves controlling martensite lattice growth. There exists a variety of possibilities for controlled oriented lattice growth during the $\gamma - \alpha$ - transformation of austenitic single crystals, for example by means of the combined influence of hypersonic, mechanical stress and strong external magnetic fields. In particular, the effect of controlled orientation of martensitic crystal growth by means of a strong magnetic field, as predicted by the author, has experimentally been confirmed at the "Institute of Physics of Metals" of the Academy of Sciences of the USSR.

The first chapter of this monograph includes a short review of the most important results of theoretical and experimental research on the subject of $\gamma - \alpha$ martensitic transformations. The theoretical difficulties arising at the description of a martensite nucleation and rapid growth of a martensite crystal will be discussed (in particular, the deficiencies of existing theories dealing with the wave model), also the discussion of the physical problem will be presented in detail.

Contents of Chapters 2 to 6 is the absolutely original and corresponds to the objectives of the aforementioned points 1 to 5. Briefly it is presented in a synopsis. In this synopsis, the conclusions playing a major role in understanding of the dynamical sequence of processes during the $\gamma - \alpha$ martensitic transformation with a survey of results relating to a description of the martensitic nucleation process are presented. In addition, some objectives of proposed further research are outlined.

In order to understand this monograph, it is essential to read Chapter 1. However, some alternatives exist for the further sequence of reading. For instance, those readers only being interested in an explanation of the morphology of the products of the $\gamma - \alpha$ MT, can immediately skip over to Chapter 5. Chapter 2 is of interest for the experts in kinetic properties of metals and alloys. In Chapter 4, specialists in phase-diagrams and electronic structures of alloys can find new information related to the dependence between concentration and optimum temperature for the onset of the $\gamma - \alpha$ MT, from the point of view of the growth theory. None the less, the author recommends to read this monograph in sequence to those readers who want to thoroughly understand such a complicated process as the $\gamma - \alpha$ MT.

Chapter 1

Basic notions on the $\gamma - \alpha$ martensitic transformation in iron based alloys

1.1 Position of the $\gamma - \alpha$ martensitic transformation in relation to other solid state structural transformations

The proposition that the causal dependence between a structural state and physical properties of a material is fundamental for solid state physics and defines thus raising permanent interest and intensive research efforts on structural transformations (ST). From the point of view of symmetry-theory, the following two types of ST may be emphasized [1]. The transformations are related to the first type (ST1) if the spatial group of one of the phases (as a rule, the low-temperature phase) is a subgroup of the initial phase symmetry group. They are called distortional transitions. The success of lattice-dynamical theories can mainly be attributed to the notion of "Soft-Phonons". Accordingly, the frequencies of certain phonons exhibit a strong temperature-dependence and can even vanish at temperature T_0 (Ms) owing to interactions in the system. At the critical point T_0 , a macroscopic amount of zero-frequency phonons emerges, and the associated static rearrangements of atoms can be interpreted and visualized by the concept of Soft-Modes "frozen" in initial crystal. At present, this approach for ST-I is well elaborated and described in detail in the literature (i.e. [1-4]). For this reason, we shall neither dwell on examples of ST-1 nor on details of the mechanism of the phonons softening, only remarking here that such structural transformations may proceed as second-order phase transitions (as a rule, the features of the first-order phase transitions are only weakly expressed).

In contrast, for the structural transformations of the second type (ST-2) there is no subordination between the symmetries of the initial phase and the final

phase. Phase transitions from the fcc to a bcc or to a close packed hexagonal phase are the examples of the ST-2 transitions. ST-2 exhibits the pronounced characteristics of the first-order phase transitions, namely, the significant thermal and volume effects and a temperature hysteresis (between the direct and reverse transformations). This type of transition is called "reconstructive".

A separate class (ST-3) of structural transitions belongs to the type "order-disorder", during which the atoms occupy mainly one of the quasi-equilibrium positions on temperatures below a transition temperature T_0 whereas at temperatures above T_0 different (not less than two) positions are occupied with the same probability. In addition to [1-4], an extensive survey of ST-3 transformations is given in [5].

As to the fourth type (ST-4) of structural transitions, it is possible to assign them as "symmetric-noncommensurate-commensurate" phase transition, in which an intermediate phase features a "super-structure" with a lattice period that is non-commensurate with the period of the parent structure (see more in detail [1, 4, 6]).

The term "Martensitic Transformation" is used as a common attribute for diffusionless structural transitions proceeding by a cooperative rearrangement of the lattice structure. With such an extensive definition, the term MT would equally apply to the above defined ST-1, ST-2 and ST-4 transitions, with specific exclusion of such ST-3 transformation, for which atomic displacements over distances comparable to the inter-atomic distances would be an indispensable prerequisite, typical of this transformation process. It should however be noted that the term "Martensite" originally was used for designation of the lamellar component in the microstructure of hardened steel [7]. If the extensive definition of MT encompasses the below mentioned totality of transformation characteristics, then we would rather prefer to use term MT in a more restricted sense, i.e. only for the subset of MT relating to diffusionless transformations of the ST-2 type. As mentioned in articles [8,9] it is necessary to refine the terminology. Among the reasons for the insufficient present classification of MT are, on the one hand, its incompleteness, and on the other hand, the dissimilarities between the microscopic mechanisms of structural transformations of various types, whose clarification would require an utmost differentiation of MT from the outset. And vice-versa, in a lattice-geometrical or thermodynamic model of MT, it would suggest itself to strive for a standardized interpretation of all the numerous classes of MT.

If kinetic characteristics [10,11] were used for the classification of diffusionless spontaneous phase transitions, and if their speed of transformation was mainly determined by the velocity of their mobile phase boundaries, then the distinguishing features of MT would be their cooperative way of lattice transformation and their large velocity of growth (with a magnitude of about the sound velocity), being practically independent on temperature. In contrast, "normal" or polymorphic transformations are characterized by an alternative group of distinguishing features (like non-correlated migration of atoms over the phase boundaries, as well

as relatively slow, thermally activated motion of phase boundaries).

Due to a missing of the standardized classification it is obvious to regard the existing approaches as complementary, each of them is focused on a different set of features and aspects of a MT.

Within the frame of this theoretical research work on the $\gamma - \alpha$ MT (related to fcc, bcc or bct lattice, respectively), particular attention will be paid to steel and iron-based (ferrous) alloys. Thus in this paper, the term "Martensitic Transformation" (MT) will only be used in its more restricted meaning, if not otherwise explicitly noted. In addition to its great practical importance, the choice of the $\gamma - \alpha$ MT as a subject of research has also been guided by the large amount of already available experimental data. As contemporary well matured lattice-geometrical and thermodynamical approaches are not able to provide a comprehensive notion of MT, there is an increasing need to extend them by a microscopic description, with the final aim to develop a dynamical model of the $\gamma - \alpha$ MT. Of course, the objectives of this work are more modest than the development of a complete microscopic theory of the $\gamma - \alpha$ MT. We shall formulate our objectives after a brief review of the main and well established notions on the $\gamma - \alpha$ MT in steel and ferrous alloys.

1.2 Characteristic features of the spontaneous $\gamma - \alpha$ martensitic transformation

There exist many monographs [10–16] and survey papers (i.e. [7, 17–19]) dealing with the history of research, as well as with basic aspects of the $\gamma - \alpha$ MT. For this reason there is no need here to dwell with history. We only would like to remark that the basis for quantitative research on the subject of $\gamma - \alpha$ MT has been founded in the twenties. In those days it had already been determined by means of X-ray investigations [20] that the low-temperature phase in steel (martensite) features a body-centered tetragonal (bct) lattice, whereas the high-temperature phase (austenite) features a fcc-lattice. A bct lattice is typical of interstitial alloys (Fe-C, Fe-N), in which tetragonality increases with increasing concentration of the interstitial component, whereas a bcc-lattice is more typical of substitutional alloys (Fe-Ni, Fe-Mn). Martensitic transformations of both kinds of alloys feature similar characteristics. As for their classification, we shall preferentially follow [13] and choose the systems Fe-C and Fe-Ni for a quantitative presentation.

The definition of the martensitic transformation (MT) mechanism by G.W. Kurdjumov essentially postulates that a MT is a spontaneous process of lattice transformation following certain rules, one of them being that the relative migration distance of neighbor atoms does not exceed the interatomic distance of the parent lattice. An immediate conclusion from this definition is that a MT is as a phase transition without change of composition, analog to phase transitions in a one-component system. For 1st order transitions, the equilibrium-temperature T_0 of phases [21] is determined by the Helmholtz-Equation of free energy F: $F_\gamma(T_0) = F_\alpha(T_0)$. Thus the energy to be invested for creation of a new phase-boundary always requires a given amount of supercooling below T_0 (or, conversely, of superheating above T_0 , during the reverse transition). Typical measured values of the temperature-hysteresis between these two transformations are quite substantial and amount to $(M_S - A_S) \simeq 400$ K, with similar magnitudes of supercooling and super-heating, respectively: $T_0 - M_S \approx A_S - T_0 \approx 200$ K. Here M_S is the starting temperature of the $\gamma - \alpha$ MT and A_S the starting temperature of the reverse $\alpha - \gamma$ MT. The change of specific volume also is considerable and has been assessed by different authors up to values within a range of 2 to 5%, where the larger figures of the specific volume effect (per unit weight) are more characteristic of the α -phase. The specific heating effect [22] during a MT amounts to some hundreds of calories per mol, resulting in an increase of the temperature of a sample by some dozens of centigrades [22, 23].

Let us now enumerate some of the indisputable structural (morphologic) characteristics of the $\gamma - \alpha$ MT.

1. Martensite emerges in the shape of lamellae featuring a low ratio of thickness to the other of their characteristic linear dimensions, or in the shape of lenticular crystals, in the middle of which a lamella (midrib) sets off in the

first stage of a MT. The thickness of such lamellae varies between 10^{-7} and 10^{-6} m (i.e. from 0.1 to a few μm).

2. The habit-plane of a lamellae (i.e. the phase-boundary or flat midrib-boundaries) has some stable orientations (depending on constitution), in relation to the crystallographic axis of the γ - and α -phases. In the systems Fe-C, Fe-Ni, there have been observed habit-planes coming close to the $\{557\} \div \{111\}$ (up to 0,6 weight% C, up to 29 % Ni), $\{2\ 2\ 5\} - (0,6 \div 1,4 \text{ weight.}\% \text{ C})$, $\{2\ 5\ 9\} \div \{3\ 10\ 15\} - (1,4 \div 1,8 \text{ weight.}\% \text{ C, } 29 + 34 \text{ \% Ni})$.¹
3. The shape of the transformed areas changes with the emergence of a surface-relief, the shape of which being characterized by distinct macroscopic shear-parameters. This latter feature suggested the commonly used designation "Shear-Transformation" as a synonym for MT.
4. There exists an orientational relationship among the γ - and the α -phase, indicating parallelism (or approximate parallelism) among the densely packed phase-planes: $\{111\}_{\gamma} \parallel \{110\}_{\alpha}$ and among angles of rotation in relation to the orientation of the densely packed parallel planes.
5. Martensite crystals exhibit an ordered internal structure, and in many cases a more or less ordered relative arrangement. This way, crystals with habit-planes $\{557\} \div \{111\}$ are characterized by a rather complicated lattice displacement structure. They form colonies (packets) of crystals with almost equal orientation, whereas for crystals with habit-planes $\{225\}$, $\{259\} \div \{3\ 10\ 15\}$, the formation of internal transformation twins and other crystal arrangements are more typical (more detailed in [24]).

An important conclusion raised in [16] states that "...In a single crystal of martensite, its habit-plane incorporates a substantial aspect of an orientational relation, being closely linked to the macroscopic shear parameters or, in other words, only a single way of martensitic transformation corresponds to a given habit-plane."

Any classification of the kinetic characteristics of MT should therefore clearly distinguish between micro-kinetics, which characterize the growth of a single lamella, and macro-kinetics, which characterize the increase of the bulk amount of martensite in a sample.

In terms of micro-kinetics, a MT can be classified as athermal, because firstly, the speed of transformation and growth of a single lamella is very large (in the order of magnitude of the speed of sound) and independent on temperature, even though the MT may occur within a wide range of temperature $T - (0 \div 10^3)$ K, and secondly, because the transformed volume is determined by the emergence of

¹In the following, the crystallographic terms without notation will relate to the axis of the γ -parent-phase (i.e. three right-hand vectors along the axis of symmetry of the 4th order $\langle 001 \rangle$).

discrete new crystals and not by the steady growth of previously existing ones. Thus the growth proceeds with almost non-existent thermal activation, giving reason for the attribute "athermal".

In terms of macro-kinetics, it can be distinguished between isothermal and athermal MT. Isothermal MT can proceed at constant temperature, attainable by an isothermal high-capacity heat receptacle (in relation to the transforming volume), while there exists a characteristic temperature (depending on the composition of an alloy) at which the rate of increase of the macroscopic amount of martensite is utmost. If significant deviations from the optimum temperature are forced in (i.e. by rapid quenching), then isothermal MT can be suppressed. This category of macro-kinetics is typical for the formation of packet-martensite.

If athermal macro-kinetics predominate, then the amount of martensite is determined by the degree of supercooling below M_S , while isothermal stops of the quenching process would not cause any increase in the transformed volume. These characteristics are typical of the growth of crystals with habit planes $\{259\} \div \{3\ 10\ 15\}$. The extreme case of athermal growth is the "explosive" MT, during which an appreciable fraction (some dozens of percents) of the total transformed volume is produced almost instantaneously within a short "explosive" period.

Remarkably, there have also been discovered alloys featuring both types of reaction kinetics [25]. Though, as a rule, the athermal martensite formation normally proceeds after isothermal (during the cooling process), the observation of the reverse sequence has also been reported in [26].

In spite of the crucial importance of data required for a precise determination of the speed of growth of martensite crystals, as well as of the transformation mechanism, only few experimental data with quantitative details like those shown in Table 1.1 have been published.

Table 1.1. Experimental data on the speed of growth of martensite

Material	Speed of growth 10^3 m/s	Source
Fe - 29,5 % Ni	1	[27]
Fe - 30 % Ni	(1,8 \div 2)	[28]
Fe - 32 % Ni	0.1	[23]
	1.1	[29]
	0.2	[29]
Fe - 0,35 % C - 8 % Mn	6,6	[30, 31]
Steel Type 18-8	(0,1 \div 0,2)	[32]

Let us now comment the data shown in Table 1.1. Obviously, the emergence of a single martensite crystal immediately changes the electrical resistance of a sample and, in turn, triggers an electrical signal which can be registered by means of a simple oscilloscope, as reported in [27]. The speed $v = l \cdot \tau^{-1}$ has been determined

from previously known values of the signal period τ and the grain size l . Basically in the same way, the speed v has been estimated in [28]. The different order of magnitude of the data presented in [23] can mainly be deduced from the different experimental method of determination of the signal period τ , which in this case was obtained by observation of the change in reflectivity of the sample, being caused by a dull surface relief showing up simultaneously with the MT and remaining engraved in the aftermath. Instead of a characteristic timescale $\tau \approx 10^{-7}$ s, as used in [27, 28], a timescale of $\tau \approx 5 \cdot 10^{-6}$ s was used in [23], which however is not directly related to the growth of a single crystal, but to the "explosive" bulk growth of the crystals as a whole. It has been clarified in [29] that the speed of $2 \cdot 10^2$ m/s only relates to the lateral speed of crystal growth, while a radial (frontal) speed of growth of an order of magnitude of 10^3 m/s could be confirmed. In [27], the potential coexistence of two different, superimposed stages of growth of martensite crystals has been postulated for the first time, based on signal-form analysis. In another analysis of [27] by Arskij, published in [33], it was further asserted that the initially upshooting edge of the signal is caused by the rapid formation of a two-dimensional crystal nucleus, in conjunction with radial growth. We note that the surface of such a nucleus represents an inhomogeneity, immediately prompting an increase in electrical resistance. Based on this assumption, it can be inferred that the observed declining signal edge, having a period 5 to 6 times as large as that of the increasing edge, can be used as a natural time gauge for lateral growth of the nucleus (bearing in mind that the specific resistance of martensite is less than that of austenite). Based on such differentiation of growth stages and on data published in [27], Lokschin [30, 31] obtained a value of $7 \cdot 10^3$ m/s for radial growth velocity, clearly exceeding the velocity of longitudinal sound waves in austenite. This evaluation was substantiated in [30, 31] by measurements of the propagation of detonation waves in steel. In the case where the MT was initiated by an external detonation, the speed of wave propagation was $(6, 5 \div 6, 6) \cdot 10^3$ m/s. By contrast, in cases where a MT in steel was induced by a precooling, the speed of the detonation wave was remarkably lower: $(4, 8 \div 4, 9) \cdot 10^3$ m/s. Assuming a measurement error of 4 % in [31], this difference can be interpreted as an indication of a large proper speed of the transformation. Even though in [28] no reason is given for a differentiation of the growth mechanism into two different stages, the observations reported in [34–36], relating to the nucleation of thin martensite lamellae being triggered by a strong magnetic field, where an initially rapid nucleation process was followed up by a significantly slower growth stage, convincingly support the assumption that a differentiation or classification of the growth mechanism is realistic. Without doubt from a methodological point of view, such nucleation and growth phenomena would be most promising for further experimental research aiming at the measurement of frontal velocity of growth, by systematic measurement and analysis of signals. And finally, it should be noted that the data reported in [32], which were obtained by evaluation of acoustic signals, only pertain to the average speed of growth of martensite crystals

and not to that of a single lamellae, as would be required. Thus, on the basis of experimental data, an order of magnitude of 10^3 m/s for radial (frontal) growth of a martensite crystal during the $\gamma - \alpha$ MT presumably would be realistic. The results of direct experiments reported in [30,31] further support the assumption that the frontal velocity of growth is greater than the velocity of longitudinal elastic waves.

1.3 Lattice-stability near the M_S -temperature and the problem of nucleation during the $\gamma - \alpha$ martensitic transformation

The pronounced characteristics of a first-order transition of the $\gamma - \alpha$ MT suggest to assume the separate existence of a nucleation and of a growth stage of the new phase. Thus an important question is related to the stability of the austenitic lattice at M_S - temperature, being closely related to the question of the possible existence of a temperature T_C at which the stability of the austenitic lattice would completely vanish. In fact, the existence of an absolute temperature $T_C > 0$, at which a supposedly perfect lattice becomes unstable with respect to infinitesimally small fluctuations, will lead us to the conclusion that a MT is almost inevitable during the cooling process. Due to an obvious disparity indicated by the inequality $M_S > T_C$, it can be inferred for alloys with isothermal reaction kinetics, which can normally be suppressed by sufficiently rapid quenching below M_S , that a distinguished T_C - temperature is missing. This in turn is a clear indication of metastability (relative stability) of the parent lattice at temperatures comprising not only the $T_0 > T \geq M_S$ region, but also the $T < M_S$ region. An important characteristic of alloys with athermal transformation kinetics, being mentioned in most relevant publications, is the independence of M_S from the quenching rate, which can be interpreted as a clear indication of the impossibility of supercooling below M_S . However, according to experimental results reported in [37], it has also been possible to supercool an Fe -33,7% Ni alloy down to 4.2 K and to trigger an "explosive" MT only in a subsequent reheating process, which also included some isothermal holding stages. Further indication of the non-existence of an unequivocal T_C for athermally transforming alloys may also be inferred from the character of incompleteness, being typical of them: The transformation process ceases at a temperature M_f , with $0 < M_f < M_S$, whilst subsequent cooling will not lead to any further growth of martensite, in spite of the existence of a substantial volumetric fraction (up to some dozens of percent) of residual, non-transformed parent phase.

Investigations on the temperature-dependence of elastic moduli published in [38,39], as well as of dispersion curves of phonon-spectra [38–41] show that, in most cases, not even a faint tendency towards loss of lattice stability is evident. The observed abnormal course of the temperature-dependency of elastic moduli [38]

of alloys of the Fe-Ni-systems ($> 30\%$ Ni), which already attain a ferromagnetic state of order for $T > M_S$, can easily be attributed to the effect of ferromagnetic ordering [42, 43], instead of lattice instability. This means that in general, a normal temperature characteristic of the elastic moduli of ferromagnetic systems is the case. In other words, an austenitic lattice essentially maintains its inherent stability against certain phonon-modes of small amplitude.

The results of experiments with small particles (diameter $> 10^{-6}$ m), reported in [44], convincingly demonstrated that when particles of similar size are cooled down, a MT only occurs in a certain fraction of the involved particles, this being further evidence of the heterogeneous nature of martensite nucleation in certain preferred centers. The same conclusion can also be drawn from observations of thermo-cycling, during which repeated (cyclic) growth of parent crystals and of martensite crystals takes place at the same location. A variety of electron-microscopical observations documented in [45] give evidence of an intimate relationship between dislocations and the process of martensitic nucleation.

Even though there is no doubt in general on the heterogeneous character of nucleation, there exists a variety of experiments related to the microscopic mechanism of nucleation [46], like diffuse electron- and X-ray scattering [47] (see also [45, 48]), and measurements of reactive forces against microscopic deformations at temperatures near M_S [47], all of them providing evidence of a special state of the austenitic lattice prior to its transformation, manifesting itself by an anisotropic increase of the squared mean of the oscillatory amplitudes of lattice modes with wave-vectors of selected orientation (and of selected polarization), as well as in a reduction of the mechanical resistance to small deformation [49]. In the case of a perfect lattice being free of phonon-mode softening, this particularity can be interpreted as the result of non-linear (anharmonic) mode-interaction, associated with the emergence of isolated, near-order regions of displacements (NORD), as proposed in [50].

The investigations performed in [50] mainly deal with constitutive thermodynamic aspects of MT (Investigation of lattice stability against quasi-static lattice deformations, as modeled by a package of "frozen-in" waves). Obviously, the more normal situation would be characterized by a transformed spectrum of elementary lattice oscillations, leading to the emergence of movable near-order domains of the soliton type [51], their stability being endorsed by the accumulation (localization) of electrons in the vicinity of isolated NORD (in a similar way as in the case of the fluctuational model in [52]). From our point of view, a reasonable qualitative notion of martensite formation, comprising both heterogeneous and homogeneous nucleation, would have to be a nucleation model encompassing the basic process of NORD -localization in the vicinity of inhomogeneities produced by single or grouped dislocations. Obviously this point of view is both in accordance with pure thermodynamical concepts [10, 53], because any weakening of the binding energy in the proximity of a lattice defect would compensate for the increase in energy related to the creation of a boundary area, as well as with the Pinning-effect [54] in non-linear lattice dynamics. This model thus is closely related to the

”reactive path” model by Cohen, Machlin and Paranyan [7] in that:

1. A coordinated motion of atoms proceeds by means of ”rapid sequential change of intermediate structures in a given range...” growing ”...in a similar way as the propagation of an elastic wave”.
2. ”The activation occurs by means of fluctuating rearrangements of the atomic configuration within the nucleus, and not through changes of its size”
3. Nucleation occurs in the centers of lattice distortion, including dislocation rows.

An important feature reported in [50] is the possible loss of stability of NORD, which could be related to their increase in size in conjunction with partial lattice-softening. However, as local softening is always existent in the vicinity of a dislocation, the lateral dimension $2 \cdot r_0$ of a settling NORD must be larger than the dimension of mobile NORD without defect.

In pure dislocation nucleation models (e.g. in [55]), the M_S -temperature is put into relation with the emergence of the first dislocation loop, whereas the creation of follow-up dislocation loops is supposed to occur spontaneously. Subsequently, a rapid nucleation process up to macroscopic dimensions would be possible by means of expansion of such dislocation loops, at a speed close to the speed of sound. With the assumption that a nucleus would have the following main linear dimensions: Length as determined by the straight section of the dislocation line, lateral diameter $2 \cdot r$, for $r \approx (10^{-6} \div 10^{-7})\text{m}$ as a realistic gauge for the thickness of a typical lamella, it is possible to assess the period of macro-nucleation t_N by $t_N \approx r \cdot c^{-1} \approx (10^{-9} \div 10^{-10})\text{ s}$, where c is a speed close to the speed of sound. A model based on the notion of localized NORD thus would have to presuppose an initial quantity r_0 of a NORD, being significantly smaller than r ([50] assumes $r_0 \approx 10^{-9}\text{ m}$), whilst the event of NORD-localization would simultaneously stimulate the creation of the first dislocation loop. The follow up expansion of these loops would then be characterized by synchronized growth from r_0 to a macroscopic size r . It should however be considered that the NORD-model as defined in [50], is inherently confined to short wave length displacements. For this reason, the existence of soliton solutions with dimensions r_0 of about the order of magnitude of r cannot generally be excluded. The transformation of NORD from their initial size $r_0 \approx 10^{-7}\text{m}$ into a macro-nucleus takes place within a period of $t_N \approx 10^{-11}\text{ s}$, as the participating atoms would only have to overcome a distance of about $\varepsilon \cdot r$, within a period t_N , where the quantity $\varepsilon \approx 0, 1$ suggests itself to be taken as a natural gauge of relative deformation during the $\gamma - \alpha$ MT [56]. We have to remark that the usually assumed shape of the nucleus as a thin, flattened spheroid was mainly determined, on the one hand, by thermodynamical reasons, and on the other hand, by a presupposed inherent similarity between the initial shape of the nucleus and the lenticularly shaped final crystal. The last circumstance led to a nucleation growth model in the pattern of expanding dislocation loops, where

the edges of the growing crystal would feature mono-atomic thickness in radial orientation. The model of a slowly thickening spheroid for lenticularly shaped crystals requires some further explanation related to its central lamellar zone - the midribs - whose constant thickness can, for good reasons, be regarded as a characterizing gauge of the bulk structure. In terms of thermodynamics, this would be analog to a gauge for critical crystal thickness [57], being related to phenomena of transition between different mechanisms of additional deformation (i.e. low thickness by twinning vs. larger thickness by slipping). Thus, in principle, the creation of midribs and their expansion from mono-atomic size to their final dimensions of $r \approx 10^{-6} \div 10^{-7}$ m would be feasible.

Another alternative might be the above mentioned possibility for rapid emergence of a macro-nucleus, whose dimension r determined the length of lattice-displacement waves excited under non-equilibrium conditions. Thus, if a mechanism for effective maintenance of the wave amplitude would exist in such a way that the amplitude ε of deformation associated with these waves exceeded the threshold-value required for initiation of the martensitic transformation, then the growth had to proceed in a wave-mode, with characteristic structural gauges of the macro-nuclei corresponding to certain wave-lengths. Obviously, the notion of non-equilibrium conditions, being typical of the nucleation process, will constitute the focus of such a model. It is fairly obvious that the highly pronounced non-equilibrium conditions prevailing in the vicinity of a rapidly growing phase can only be maintained if the process of heat liberation is adiabatic [58,59]. Then, the temperature difference between the γ - and the α - phase $\Delta T \approx Q \cdot C_{sp}^{-1}$ (where Q - heat energy density, C_{sp} - specific heat), would be comparable with the magnitude of supercooling $T_0 - M_S$. This in turn allows to refine the formulation of our basic task:

Investigation of a non-equilibrium electron-phonon system with the final aim of clarification and substantiation of the principles and conditions for efficient generation of lattice-displacement waves.

In the above outlined qualitative pattern, the transition from nucleation to the growth stage features some characteristics of a continuous transition, thus being an indication of a potential instability with respect to rapid growth of nuclei emerging under non-equilibrium conditions. Such a conclusion would however have to presuppose the existence of effective rapid growth mechanisms. This latter circumstance may thus play the crucial role in the transition process of the initial system into a new state. In fact, the following basic rule of non-stationary thermodynamics applies: If a given system can potentially exist in different states, each of them having a relative minimum of free energy, then " . . . those states emerging at the greater speed will be realized first". Just this way, the kinetic factor comes to the fore, which is quite natural in a growth stage. Even though the kinetic aspect of the transformation does not belong to the classic realm of thermodynamics, there exists a link between the thermodynamical and the kinetic conditions of such phase generation. In our case however, we shall confine the role of thermodynamics to

the determination of the thermodynamic stimulus of the transformation, and of the activation energies required for nucleation and growth.

The missing quantity T_0 , and therefore the asserted relative stability of the fcc-lattice at M_S -temperature, implies a question related to the magnitude of the energy barrier, which has to be overcome by the system during the processes of nucleation and growth. Obviously, this question is closely related to the problem dealing with the large observed magnitude of supercooling $T_0 - M_S \approx 200$ K, which has been clearly formulated in [58, 59]. This specific problem arises from a consideration of the remarkably small temperature difference $\Delta T = T_0 - M_S \approx 45$ K, being required to satisfy the energy requirement of $E_e \approx 50$ kcal/mol to carry out the exterior mechanical work during a MT, and of the great observed magnitude of the supercooling. One of the acceptable explanations stated in [7] is that "... the kinetics of the process is determined by the speed at which the transient system overcomes the energy barrier associated with the formation of the nucleation center of the new phase, as further growth of martensite crystals proceeds almost instantly." Thus, any explanation of the magnitude of supercooling $T_0 - M_S$ must inevitably consider the key thermodynamic and kinetic process parameters.

In the above discussed model of adiabatic generation of a macro-nucleus, the heating effect Q associated with the transformation, treated in [56], can be interpreted as a result of the distribution of atomic oscillation energy E in the vicinity of new equilibrium states, among all available $3 \cdot N_N$ oscillatory modes of the nucleus (N_N - number of atoms in the nucleus), with only a small number of polarization orientations excluded (for anisotropic deformation). We evaluate E by the assumption that during the process of nucleation, the excitation of longitudinal oscillations being polarized in two orientations (called x and y), will be predominant. Let an oscillatory mode be enumerated by a wave-vector of components \mathbf{q}_i ($i = x, y$). Then, their contribution to E will be

$$E_{\mathbf{q}_i} = \frac{1}{2} M \omega_{\mathbf{q}_i}^2 |\mathbf{u}_{\mathbf{q}_i}|^2 N_N, \quad (1.1)$$

where M - atomic mass, $\omega_{\mathbf{q}_i}$ - cyclic frequency, $\mathbf{u}_{\mathbf{q}_i}$ - oscillatory amplitude.

Further, the relative deformation ε associated with such oscillations can be determined by the extreme condition

$$\varepsilon_m = \frac{2u}{\lambda/2} = \frac{2uq}{\pi}, \quad (1.2)$$

where $\lambda/2$ is the distance between two adjacent planes, supposed to oscillate in mutually opposed phases (λ - wave-length). We further assume the same ε for all q_i , replacing $\omega_{\mathbf{q}_i}$ by $\omega_{\mathbf{q}_i} = cq_i$, where c - speed of sound, and consider that $q_x q_y$ attain the value $N_{N_x} \approx N_{N_y} \approx 2r_N/a$ (r_N - radius of the macro-nucleus, a - lattice parameter). Then from (1.1) and (1.2):

$$E = \sum_{i, \mathbf{q}_i} E_{\mathbf{q}_i} \approx \frac{\pi^2}{2a} r_N N_N M c^2 \varepsilon_m^2. \quad (1.3)$$

At the instant of nucleation $t = t_N$ we get

$$\frac{E}{N_N M} \approx \frac{\pi^2}{2} r_N c^2 \varepsilon_m^2 \approx Q, \quad (1.4)$$

where Q is the specific transformation heating effect [J/kg]. Using $Q \approx 4 \cdot 10^4$ J/kg (for a Fe-30 Ni - alloy according to [22]) we get $r_N \approx 10^{-7} m$, $a \approx 3 \cdot 10^{-10}$ m, $c = 5 \cdot 10^3$ m/s and from (1.4): $\varepsilon_m \approx 10^{-3}$.

This way we can reasonably infer a threshold-value for the deformation ε_{th} of about a magnitude $\varepsilon_m \approx 10^{-3}$, at least for long-living modes with quasi-momenta $q \approx q_{min} \approx \pi \cdot r_N^{-1}$ at the instant $t = t_N$, coinciding with the final instant of the nucleation stage and with the moment of growth initiation. With respect to the effect of external stress on MT, it would be useful to compare our estimate of ε_m with data published in [13, 49].

The reasons for such comparison - for instance with data of the strain effect - are obvious, if we consider that the term $\lambda/2$ in (1.2) plays the role of the initial length l of the sample, while the amplitude u corresponds to the incremental length Δl , and that the quantity $\lambda_{max} = 2 \cdot \pi / q_{min} \approx (10^{-7} \div 10^{-6})$ m is a multiple of the lattice parameter a . In conclusion, the order of magnitude of these quantities appears to be fairly adequate for a description by continuum mechanics. Useful information can further be inferred from the mere existence of a temperature M_{elast} (in the notion of [49] M_{elast} is close to M_S , i.e. $M_{elast} - M_S \approx 35 \div 40$ K), the quantity M_{elast} being such that if a MT proceeded within the temperature range $M_S < T < M_{elast}$ it could be induced by elastic stress σ_m , thus satisfying the inequality $\sigma_m < \sigma_y$ (σ_y - yield stress). Remarkably, an evaluation of the stress-strain curve shows that the values of $\sigma \leq \sigma_y$ correspond to strains $\varepsilon_{th} \leq 10^{-3}$. This observation may further support our estimate of $\varepsilon_{th} \approx 10^{-3}$ for threshold deformation. Thus in the notion of a developing macro-nucleus, supposed to be inherently unstable in the growth process, a strongly pronounced supercooling $T_0 - M_S$ is regarded as an imperative condition for the excitation of oscillations with final (peak) amplitudes (and frequencies) satisfying the condition $\varepsilon > \varepsilon_{th} \approx 10^{-3}$. Moreover, the same condition could be used as a qualitative criterion for lattice stability (or instability) of the γ - phase at the M_S - point.

1.4 Solved and unresolved problems on the theoretical description of the $\gamma - \alpha$ - martensitic transformation

Any comprehensive reasoning on the theory of phase transitions will inevitably lead to the following two fundamental questions, as noted in [10]:

1. Why does a given phase transition occur?
2. Which is its transformation mechanism?

The first question will normally be approached by investigations on the relative stability of different possible phases. In this case, the phase with lowest value of free Gibbs-Energy $G(P,T)$ will usually be in the focus of interest. A generalized expression for G is given by the constitutive expression in [60]:

$$G(P, T) = H - TS = U + PV - TS \quad (1.5)$$

where H , U , S , V are the commonly used specific values of enthalpy H , internal energy U , entropy S , volume V and pressure P (relating to 1 mol).

A calculus of the (macroscopic) thermodynamic quantities in (1.5) within the frame of a strict (quantum-statistical) approach would be an extraordinarily complicated task, as the G -values of different phases differ almost inappreciably, and to the worse, any such calculus cannot be effectively simplified. Nonetheless, today there exist sufficiently clear and substantiated notions on the causes and mechanisms of polymorphic transitions in pure iron.

Presumably, the high-temperature transition fcc-bcc ($\gamma - \delta$) at $T_{\gamma-\delta} = 1665$ K is determined by the entropy term in (1.5), as the contribution to S from atomic oscillations in the more weakly bound bcc lattice, as well as from disordered (large) magnetic moments, is relatively larger for the δ -phase than for the γ -phase [61]. The low-temperature transition fcc-bcc ($\gamma - \alpha$) at $T_{\gamma-\alpha} = 1183$ K, which would appear paradox from the aspect of the oscillatory contributions of the atoms to S , can be put into relation with the reduction of internal energy of the α -phase in the ferromagnetic state of order [62–64]. Taking for granted that the answers are already given, we shall refrain from dealing here any more in detail with questions related to phase stability.

Of course, a constitutive solution to our initial question "Why" related to the $\gamma - \alpha$ MT has not yet been found, as the second part of our question, being related to a "given phase transition", belongs to the particularities of the $\gamma - \alpha$ MT and is intimately linked up with the question for the mechanism of this particular transition.

The morphological (phenomenological) features of low-temperature martensite with habit planes $\{2\ 5\ 9\} \div \{3\ 10\ 15\}$ (see 1.2) have successfully been interpreted by the crystallographic theory. A detailed description of its most important results

is published in [13, 18]. From a crystallographic point of view, MT are regarded as a lattice deformation process, characterized by a macroscopically invariant plane, the habit plane. This deformation includes pure lattice-distortion (PLD), as well as lattice invariant deformation (LID). PLD can either be described within a pattern including two (or more) shear motions, onto which a dilatation mechanism is superimposed, or within the pattern of Bain-Distortion (BD) with consecutive rotations satisfying the constitutive orientational relationships. The BD-pattern is shown in Fig. 1.1, which has been extracted from [13]. Imagine an elementary bct-lattice cell (with a tetragonality of $\sqrt{2}$) being partially configured by two adjacent fcc-cells. Then, in order to transform that bct-cell into a cubic bcc-cell, the bct-cell has to be subjected to a compression by 20 % along its [001] axis and to a dilatation by about 13 % along its [100] and $[0\bar{1}0]$ axis (or along its [110] and $[\bar{1}\bar{1}0]$ axis). In Fig.1.1, the principal orientations of compression and dilatation are marked by bold arrows. The densely packed $(111)_\gamma \parallel (011)_\alpha$ plane is hatched. Fig.1.2 shows an inhomogeneous lattice resulting from LID in the case of shearing Fig.1.2a and twinning Fig.1.2b. It is mandatory to consider LID, because pure BD does not comprise a deformation with an invariant plane (DIP) (during DIP, one of the main components vanishes, whereas the two remaining deformation components feature opposite sign). Thus, if LID is used as a method to introduce auxiliary deformation, it is possible in some cases to attribute the bulk macro-deformation of the transformed region to a deformation with an invariant plane. Among other aspects, the twinning mechanism of low-temperature martensite was used to prove LID, in that different volumetric fractions of twins were predicted, as confirmed later on by experimental evidence. Among the drawbacks of this approach are those mentioned in [65], as there are: The lack of physical justification for the selection of a specific mechanism of deformation, as well as " . . . of some of the most essential principles like: attainment of minimum surface energy, minimum active shear parameter, or minimum of atomic motion." In addition, the aforementioned phenomenological theories are not suitable to reasonably explain "any change of a crystallographic feature of martensitic transformations in relation to changes of their composition or of transformation temperature."

The thermodynamical approach in [17, 19, 66], which takes into consideration the energy and enthalpy associated with internal stress, within a given system of coexisting γ - and α -phases, is mainly based on the assumption that the formation of a final structure reflects the tendency of the system to minimize its free energy (i.e. a minimum of elastic energy caused by internal stress), thus giving reasonable justification for regarding the crystallographic pattern of martensite as an isolated case of phases being in immediate contact in an invariant plane, without consideration of the appearance of mechanical stress. In addition, it explains the lamellar equilibrium shape of the crystals, particularities of their internal structure (like autocatalytic twinning) and other general features related to the emergence of crystal groups, under the conditions of a sample with free external boundaries as well as under the conditions imposed by an externally applied field of mechanical

tension [67–69]. An interpretation of the kinetic particularities must be based on an evaluation of: a) the level of the energy-barriers which have to be surmounted during this type of growth. b) The thermodynamic driving force of the transformation. c) The role of relaxation processes in this environment. To take an example, the observed differences between lath-shaped and lamellar martensite might be deducible to differences between the dominating relaxation mechanisms (i.e. slipping processes in austenite and twinning in martensite).

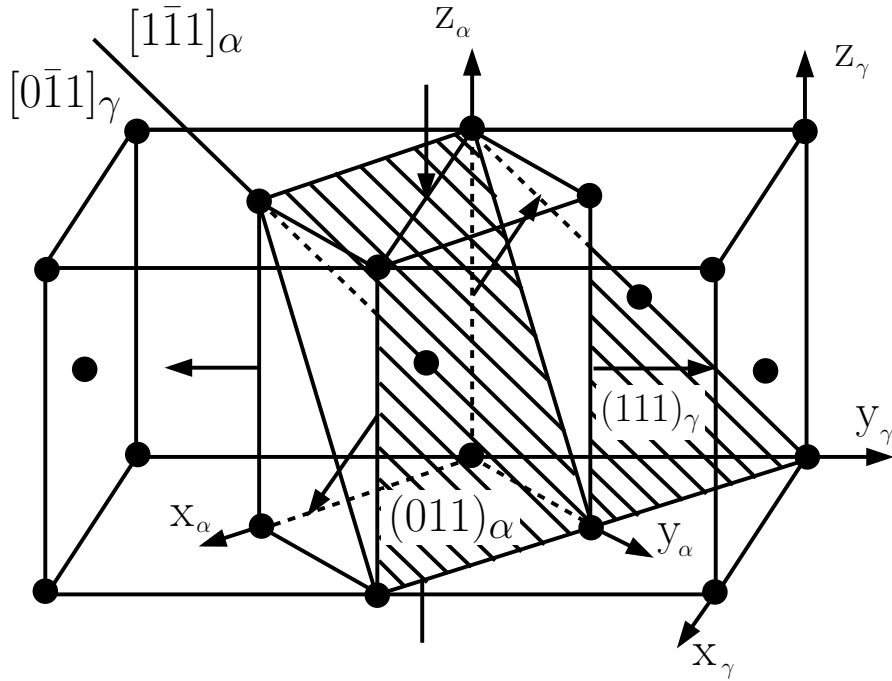


Figure 1.1. Conformance of austenitic and martensitic planes during a fcc \rightarrow bcc Bain- transformation [13]. Planes $(111)_\gamma \parallel (011)_\alpha$ are hatched. Bold arrows point to orientations of compression $[001]_\gamma$ and tension $[100]_\gamma$, $[010]_\gamma$, respectively.

The question about the growth mechanism will lead us into a consideration of the model of a phase-boundary and into an evaluation of its mobility. For example, in [17, 19, 70] there has been investigated a model of a phase boundary arising during a MT, with a transformation pattern characterized by an invariant plane. In Fig. 1.3, which has been taken from [19], the phase boundary is represented by a transition layer together with a transition vector \mathbf{S} of variable size and orientation, indicating the locations of atoms (l_0 - thickness of the boundary layer, being about the size of several lined up lattice parameters). The term f_n relates to free energy density, x - coordinate axis oriented parallel to the normal \mathbf{n} of the invariant plane of the boundary layer, f_n^a and Δf indicate the magnitude of the activation energy threshold, or of the thermodynamic driving force, respectively. This representation of a phase boundary thus is akin to that of a ferromagnetic domain [71], which also includes a term related to the free energy gradient.

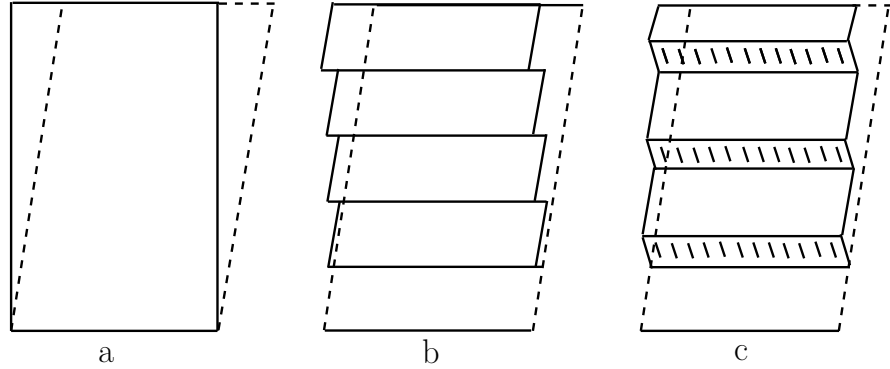


Figure 1.2. Reconstruction of the shape of a transformed region by additional deformation [13]: (a) = Mode of transformation; (b) = Reconstruction of the shape by means of slipping; (c) = Reconstruction of the shape by twinning.

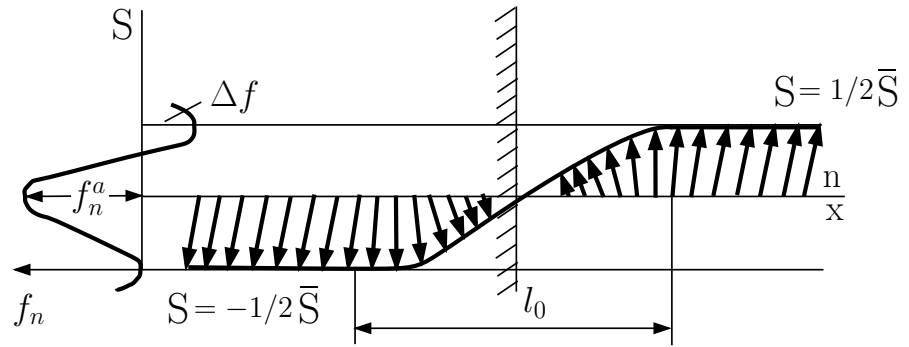


Figure 1.3. Structural pattern of a phase boundary [19]

As for the MT of alloys of the Fe - Ni, Fe - C systems, a realistic representation of a phase boundary would, at the first sight, have to satisfy the following two, obviously contradicting requirements: the pronounced persistence of metastable austenite at the M_S temperature (see also the explanation in 1.3) implies the existence of a finite energy threshold f_n^a . The almost temperature-independent speed of growth of an individual martensitic crystal (at least within a wide range of temperature) is a typical feature of a thresholdless type of growth or motion. In [17, 19, 70] it is proposed to consider the mobility of a phase boundary analogous to the mobility of a dislocation through a periodic potential as determined by the lattice with its structural periodicity in \mathbf{n} - orientation, in a similar way as that described by the Frenkel-Kontorova-Model. As a result, the f_1^a threshold is considered instead of the f_n^a threshold, (see Fig.1.4 as taken from [19]), which separates the relatively unstable states in the boundary area (i.e. where the location of individual atoms deviates significantly from the stable location with minimum potential energy in relation to the peaks of the potential "comb") from relatively stable ones (i.e. the atoms are located near the bottom of the periodic lattice potential), if put into relation with the driving force Δf . Thus for $\Delta f > f_1^a < f_n^a$

a boundary would move (jump) nearly unhindered over a threshold, at a speed comparable to the velocity of (transversal) sound waves, nearly independent of temperature. However it has to be considered that a calculus of the above postulated speed of propagation has not yet been performed (as this would not be a typical problem of thermodynamic analysis). Thus the postulate of a large velocity of boundary propagation still needs to be proven. Moreover, according to data published in [30,31], the velocity of growth of martensite crystals not only exceeds the velocity c_t of transversal, but also the velocity c_l of longitudinal elastic waves. Thus any concept based on an upper velocity limit $c_t < c_l$ would be fundamentally inadequate for the description of radial (frontal) growth of a lamellar martensitic crystal, even though an interpretation of lateral growth might be conceivable within such a concept.

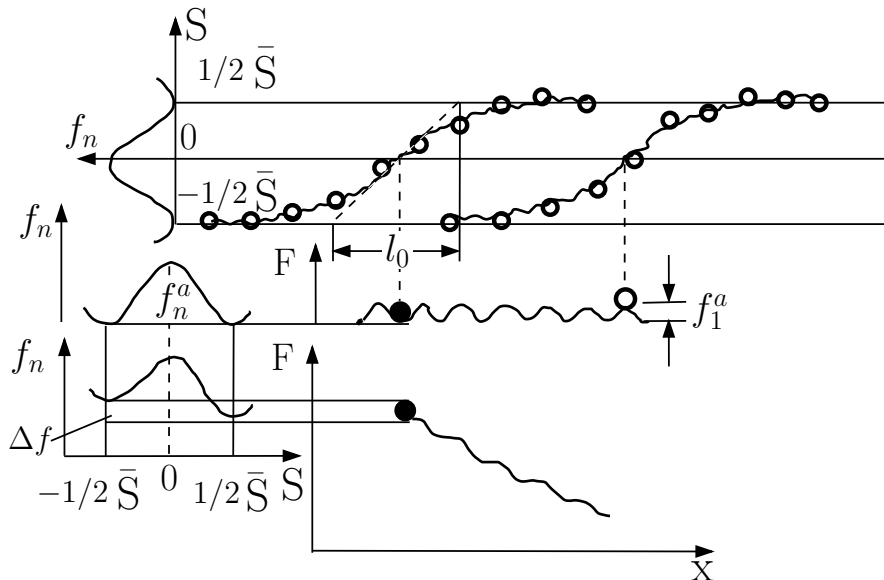


Figure 1.4. Determination of the f_1^a -threshold at the phase boundary, analogous to the Peierls-threshold of a dislocation [19]

What's more, the assumption of supersonic velocity of martensitic crystal growth will inevitably lead into another problem: The usually observed $\gamma - \alpha$ -phase boundaries belong to the semi-coherent type [12]. High mobility of semi-coherent boundaries usually is put into relation with the existence of parallel rows of slipping dislocations making up a boundary [72]. Under the assumption that the motion of a boundary, including that of a martensite crystal, is produced by slipping dislocations, then we must inevitably conclude that the motion speed v of such dislocations will also take place at the of sound velocity c_t . We remember that the supposed motion of dislocations at a velocity exceeding c_t is prohibited within the frame of a continuous model [73]. In principle however, this could yet be possible in crystals of a discrete atomic structure [74]. Moreover, we must consider that a dislocation in supersonic motion $v > c_t$ would inevitably and per-

manently emit acoustic radiation energy, due to an effect analogous to the emission of Tscherenkov-radiation. In accordance with [74], it is possible to calculate the stress σ needed to maintain a dislocation speed $v > c_t$, by the relation

$$\sigma \approx \left[\frac{v^2}{c_t^2} - 1 \right] \cdot \frac{\mu b}{2 \pi a} \quad (1.6)$$

where μ - shear-modulus; b - Burgers-Vector, a - distance between the planes of shear.

For example, if $v \approx 2 c_t$, and $b \approx a$ were inserted in (1.6), then σ would exceed the theoretical yield stress $\approx 0,1 \cdot \mu$, a result which makes no physical sense. The same kind of problem would basically also appear in any investigation of shock-wave propagation in solid state matter. Some alternative opinions about the role of dislocations in shock-wave propagation are outlined in the papers by Wirthman, Meyers and Moor in [75]. According to Wirthman, supersonic propagation of dislocations (Smith-dislocations) should theoretically be possible in conjunction with the propagation of a shock-wave at a maximum stress level being equivalent to the yield strength. Meyers and Moor, whose position is based on experimental evidence however reject this point of view, arguing that dislocations generated in conjunction with a shock wave would lag behind the shock wave and soon come to a stop. Rejecting the thesis that the level of stress during the $\gamma - \alpha$ MT is close to theoretical yield strength, the motion of the phase boundary should rather be regarded as some kind of non-linear wave process producing dislocations which at the same time set up a boundary between the phases arising immediately behind the propagating wave front.

Machlin and Cohen in [76] were first to clearly formulate a wave model as a conceptual approach for resolving the martensitic growth problem. Without getting into details on the meaning of velocities, the authors of [76] propose a pattern of two sequential deformation waves. The first of the waves spreads out into radial orientations starting from a minute platelet-shaped martensitic nucleus, thereby causing a homogenous deformation of a lamellarly shaped area, the surface of which (i.e. the habit plane) matches with the invariant plane. As soon as the deformation induced stress delivered by the first wave attains certain amount (presumably the yield limit), the second wave starts to spread into a direction perpendicular to the habit plane, thereby causing shear deformation (being homogenous only at a macroscopic scale). The residual inhomogeneous shear deformation completes the growth process of a martensite lamella. In principle, such wave pattern would make possible a direct interpretation of the crystallographic (geometrical) theory: The first wave produces pure lattice deformation, and the second one the required lattice invariant deformation. But in contrast to the geometrical pattern, in which the invariant (habit) plane can only arise during a combined lattice-variant and lattice-invariant deformation, [76] requires that the development of a habit plane must already occur in the first step of pure deformation. Obviously, there do not exist any reasons for assuming that inhomogeneous deformation (i.e. by twinning)

takes place only after formation of the lamellar region. At present, there is no doubt about inhomogeneous deformation occurring during a martensitic transformation (transformation twinning according to [13]). Nonetheless, the notion of a clear distinction between two stages of crystal growth still appears to be current.

Essentially, the aforementioned basic ideas are also proposed in [77]. In addition, it is postulated therein that the radially propagating wave is of the longitudinal type, leading to a MT in the central area (midrib) of a martensitic crystal. The transformed midrib-regions thus are about to play the role of second-order nuclei for excitation of a transversal transformation wave, which would propagate into an orientation perpendicular to the habit plane. In conclusion, it can only be the transversal wave which initiates the growth process in the region adjacent to a midrib. The most important single factor ensuring growth initiation is the high pressure (about $7,4 \cdot 10^9$ Pa) being produced in the immediate vicinity of the midrib, due to its increase in width by about 5 %. This way, right in front of the transformation wave, short compressive and plastic shear wave pulses are surmised to move about, slowly widening until the growth process has ceased, after which the wave-pulses fade down to the level of ordinary elastic waves. The whole scenario is shown in Fig.1.5, extracted from [77]. Fig.1.5 shows a cross-section of a growing lenticular crystal (the drawing plane is assumed to run perpendicular to the habit-plane).

The midrib is represented by a straight line, splitting the lenticular region into two symmetrical halves, while the arrows are pointing into the orientation of wave propagation. The hatched region represents the region of compressive and shear wave pulses, and the broken line intersecting the crystal indicates how an originally straight line of reference (dotted line in Fig.1.5d) is distorted during and after a MT. Using this pattern of transformation, together with the assumption that the longitudinal and the transversal transformation waves propagate at $v_l = c_l$, and $v_t = c_t$, respectively, there has been reported in [77] an equation for the shape of the surface of a lenticular crystal, which has been the final aim of that work. We would further like to remark that the notion of dislocation generation under the condition of a high level of mechanical stress being built up in the waves, as postulated in [77], is justified, whilst the motion of the boundary is not put into clear relation with the motion of the dislocations. Even though the values of v_l in [77] appear to be estimated too low, and too high for v_t (see also the interpretation of the data related to the speed of growth in 1.2), the qualitative model looks quite promising. However, what is obviously missing in [76, 77] is a description of the development of a midrib with an internal twinning structure, which is supposed to take up a leading role during the formation of lenticular crystals.

In [31, 78, 79], the growth of martensite has been treated from the point of view of the shock wave theory. Lokschin also investigated the case of strong shock waves, opening up a possible explanation for supersonic speed of growth. According to estimates in [31, 78], the compressive stress or tension being developed within a

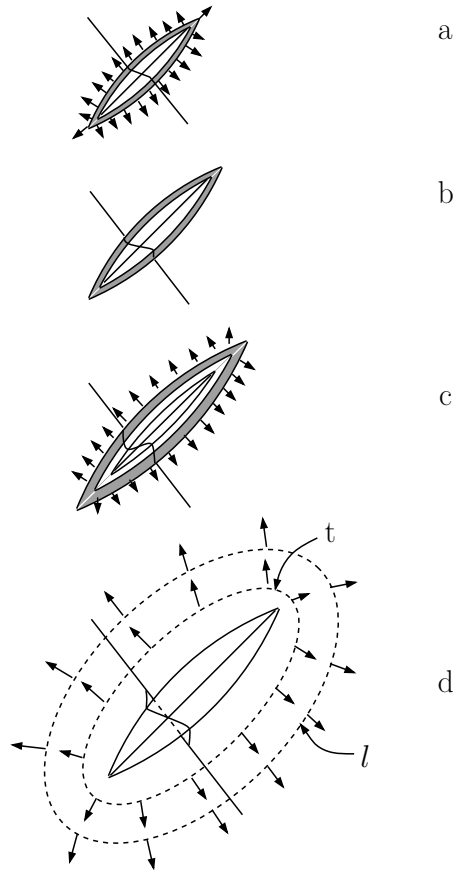


Figure 1.5. Growth pattern of a lenticularly shaped martensite crystal [77]: (a): Plastic shear and compression waves are propagating ahead of the transformation front; (b) and (c): Crystal growth process has ceased, but abating waves of plastic deformation are still propagating in the aftermath; (d): Waves of plastic deformation faded away, after having excited elastic transverse-(t) and longitudinal (l) waves.

shock wave amounts to about $(1, 4 \div 1, 6) \cdot 10^{10}$ Pa, being about twice as large as the value used in [77], thus attaining the same order of magnitude as theoretical yield stress. Based on data published in [27], Crussard analyzed the case of weak shock waves with a speed of propagation lower than sonic speed. The common weakness of these treatises is their lack of interpretations of the extensive amount of morphological transformation characteristics.

If the role of dislocations during formation and propagation of the phase boundary was not properly considered in the aforementioned models, then the motion of a phase boundary could simply be regarded as the propagation of a lonely front (called "switching" wave in [80]), akin to a step like excitation (as shown in Fig. 1.3. To the left and to the right of such a "switching" wave, different values of deformation $\varepsilon_{\alpha,\gamma}$ would be produced, being typical of the γ - and α - phases. Such a process can usually be described on the basis of a quasi-linear parabolic equation

(non-linear diffusion equation), to be dealt with in Chapter 6.

Let us now briefly discuss the theories focusing on the role of hyperbolic waves during a MT. Generally, these waves correspond to solutions of non-linear equations arising from a basic linear hyperbolic equation (i.e. a classical wave equation featuring spatial and temporal derivatives of the second order) for which (harmonic) sinusoidal waves are fundamental solutions. In our opinion, the general interest on waves of this category is due to their potential for simple representations by (quantized) totalities of phonons. Our next logical step will thus be to pass over to phonon theory, which will finally enable us to take advantage of the well developed and efficient microscopic models of solid state physics, and to establish later on an important link between microscopic and macroscopic descriptions of MT.

The assertions in [81] advocate for a description of MT in the wave model. Remarkably in [81], a decidedly passive role is assigned to dislocations, including the proposal to reject a differentiation between the nucleation and growth stages, apparently justified by the lack of observable static nuclei. Thus the kinetics of any kind of MT should in general be allocated within the explosive type. (Even the case of slow macroscopic growth of a martensite crystal can easily be explained within the general notion of explosive transformation, by assuming small micro-explosions occurring in sequence, with fairly long interruptions in between). In addition to the above thesis we want to point to another assertion stated in [81]: It is being proposed to interpret the particularities of the martensitic structure as a result of the interaction of a combination of one (or more) lattice oscillation modes, propagating at the velocities of elastic waves).

Kayser [82] was first in trying to associate the athermal activation of explosive MT in ferrous alloys with the principle of stimulated emission of phonons, which led to the conceptual notion of a phonon-maser² effect coming into being at a given amount of supercooling below the equilibrium temperature T_0 of both phases. The optimum frequency assumed in [82] is the Debye-frequency $\nu_{AM} \approx 10^{13}$ Hz, while the associated phonon energy $h\nu_{AM}$ would equate with the free energy difference $G_A - G_M$ (related to one atom) between metastable (pre-martensitic) austenite G_A and stable martensite G_M . The radiation system is supposed to be given by the lattice atoms, which, during the MT, perform a coordinated (cooperative) jump from an energy level G_A down to a level G_M , simultaneously with a structural transformation. As the initial occupation of the G_M - level is assumed to be nil (i.e. when the atoms make up the austenitic lattice) and if the condition $G_A > G_M$ was given, then the starting scenario would correspond to the utmost possible inversion between the occupations G_A and G_M . The propagation of the emitted phonons through the transforming lattice is supposed to proceed in such

²Editorial note: Phonon-maser and laser research and development proceeded almost in parallel in their initial theoretical and experimental stages in the sixties, but phonon-maser development was abandoned later on due to lack of practical need for phonon-masers. See e.g. Phys. Rev. Lett. vol. 12, pp. 592-595, May 1964.

a way that the amount of phonons would steadily increase, resulting in a steadily increasing amplitude of the acoustic wave, up to a magnitude enabling the creation of lattice defects. Kayser also proposed to interpret the zigzag structures, comprising a macroscopic group of relatively small martensite crystals, grown and confined within the space enclosed by two larger, pre-existing lamellae, as a sequence of multiple reflections of stimulated phonon radiation between the lamellae. Fig. 1.6a shows a schematic illustration of the observed zigzag structure (being more commonly known in metallurgy under the term ("lightning" or "lace" structure), whereas Fig. 1.6b shows the Kayser-pattern (arrow lines). Typical of this structure are two groups of lamellae: Any two lamellae selected from the same group are parallel, whilst lamellae belonging to different groups adjoin at an acute angle. We would however like to remark that any two of such totalities of lamellae cannot be built up only on the basis of reflections between non-parallel larger lamellae. Thus the interpretation by Kayser cannot be regarded as consistent. Obviously the structure shown in Fig. 1.6b represents nothing more than an observed phenomenological rule, which however does not reconcile with the classical laws of reflection. The general definition of the radiating system as well as of the radiation frequency also appear to be contestable. In fact, in a well developed two-level maser (i.e. see [83]), pairs of inversely occupied energy levels would simultaneously exist at certain points of space, and the active radiating sub-system normally is subjected to the Fermi-Dirac-Statistik. However in the Kayser-pattern, the physical state corresponding to G_M -energy would only potentially be possible, as the atoms are in a state with G_A -energy. Furthermore, short-wave phonons generally have a highly pronounced rate of decay, corresponding to short average lifetimes and ranges, thus the argument for the possibility of being generated by the proposed mechanism appears fairly improbable.

A more promising description of the emission of radiation in conjunction with atomic jumps is obviously set up by the concept of vacant atomic states, being closely linked with the physical state of quenched austenite (i.e. see [84]).

An explanation of the mechanism of phonon generation has also been tried by Zhang in [85]. Refraining here from further and detailed enumeration or discussion of the various theoretical possibilities, we can conclude that, in the aforementioned papers, a more or less reasonable concept of the microscopic mechanism of phonon generation during MT is missing. This can be easily realized by comparing points 2 and 3 of Table 1.2 (next page) which has been borrowed from [85].

In Table 1.2, it has been tried to draw some general analogies (theoretical and phenomenological) between the laser or maser effect and the MT. Moreover, we assume that the requirement of a critical rate of cooling down to M_S (pt. 3 in Table 1.2) is not mandatory.

In order to suppress diffusion, it would suffice to rapidly pass through the high-temperature region, where diffusion processes predominate, whilst further cooling can succeed at a rather slow rate. For a description of the lateral displacement

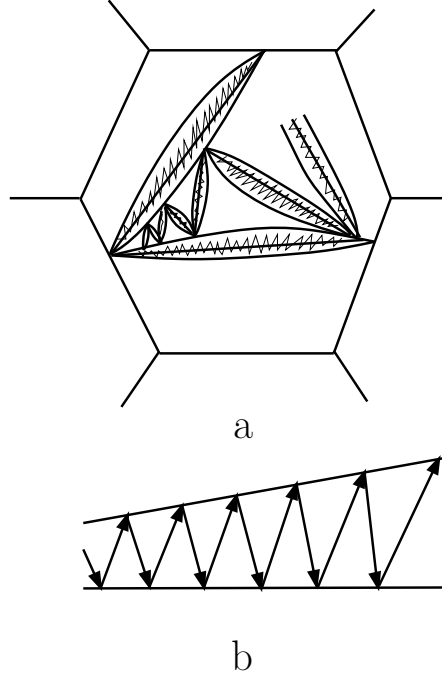


Figure 1.6. Schematic structural arrangement of typical martensite crystals: (a): Totality of the lenticularly shaped twinned crystals in a realistic pattern [24]; (b): Idealized pattern of multiple reflections of excited phonons [82].

wave, Zhang proposes a wave equation borrowed from Laser-Theory:

$$\nabla^2 \vec{\xi} + \frac{1}{c^2} \frac{\partial^2 \vec{\xi}}{\partial t^2} = -\frac{\partial^2 \mathbf{p}}{\partial t^2}, \quad (1.7)$$

where: c - speed of sound; $\vec{\xi} = [\nabla, \mathbf{u}]$ - axial vector of rotation is correlated with the antisymmetric rotation tensor [86]; \mathbf{u} - vector of translational displacement; ∇ - gradient operator in a spatial frame of reference; \mathbf{p} - analog to the polarization-vector of a lasing medium as used in laser-theory, given by $\mathbf{p} = c^{-2} \hat{\varepsilon} \vec{\xi}$, where $\hat{\varepsilon}$ - matrix of lattice distortion during a lattice-transformation. As reported in [85], there have been performed investigations on the characteristics of stationary wave amplitudes, using a phenomenological approach by the commonly known Van-der-Pol and Duffing equations, under the assumption that, in a harmonic approximation, the square of oscillatory frequencies exhibit a critical dependence on temperature, thus resembling a typical characteristic of "Soft-Modes", i.e.: $\omega_0^2 \sim (T - T_0)$.

A discussion of reports related to investigations on the effects of externally applied magnetic fields and of magnetic ordering in austenite on MT will be subject of Chapter 5.

³A laser-resonator, being a characteristic part of most lasers, is not an absolute requirement for realization of laser/maser radiation, as in some radiating systems comprising a sufficiently high

Table 1.2. Analogies between the Laser-effect and martensitic transformations

Laser	Martensitic Transformation
1. Coherent photons	1. Coherent phonons
2. Occupational inversion	2. Mechanism ensuring a (potential) possibility for stimulated emission of phonons
3. Under the conditions of an occupational inversion, coherent photons are emitted during the transition of electrons to the lower energy level.	3. Under given conditions (critical rate of cooling, supercooling down to a certain temperature), the transition of atoms occurs from their initial lattice position of the high-temperature-phase into lattice positions of the low temperature equilibrium phase. Simultaneously with this phase transition, coherent phonons are emitted.
4. Resonator ³	4. Lattice boundary, plane lattice defects, grouped point defects, dislocations etc.
5. Van-der-Pol-Equation	5. Van-der-Pol- and Duffing-Equation

1.5 General physical tasks and objectives

A brief review of existing publications dealing with the spontaneous MT of paramagnetic austenite lead us to the conclusion that the wave-approach, though being regarded as most promising for further development of a microscopic dynamical MT-theory and description of the $\gamma - \alpha$ - MT, presently is only weakly developed.

At first, the mechanism of wave-generation (and -amplification, respectively) in the stage of martensite growth has to be determined, and secondly, the substantial variability of crystallographic characteristics of Martensite must be interpreted in the wave-model, as without such an interpretation, the wave-approach would be largely invalidated with respect to materials science.

1. Let us assume that the process of fast development of a macro-nucleus of a lateral dimension of about $2r \approx (10^{-6} \div 10^{-7})$ m (see 1.3) occurs within a period of $t_N \approx (10^{-9} \div 10^{-10})$ s. Then it is fairly easy to realize that this postulate represents some kind of specification going beyond the normally used model of fluctuation nucleation. Let us further assume that

population inversion density (threshold-inversion), a "single-shot" or "superradiance" (Dicke) laser/maser-effect can emerge. (Superradiance however mostly is an undesired, potentially destructive and hardly controllable side-effect in many high-intensity lasers.) Moreover, there have also been discovered innumerable cosmic sources of (continuous) laser/maser radiation, clearly demonstrating that laser/maser activity is a natural effect, not requiring sophisticated laboratory equipment like a resonator at all.

certain spatial scale l can be defined along an orientation perpendicular to the axis of nucleation, in such a way that l would be complementary to r , as shown in Fig. 1.7. Then l indicates the width of a specific region (we call

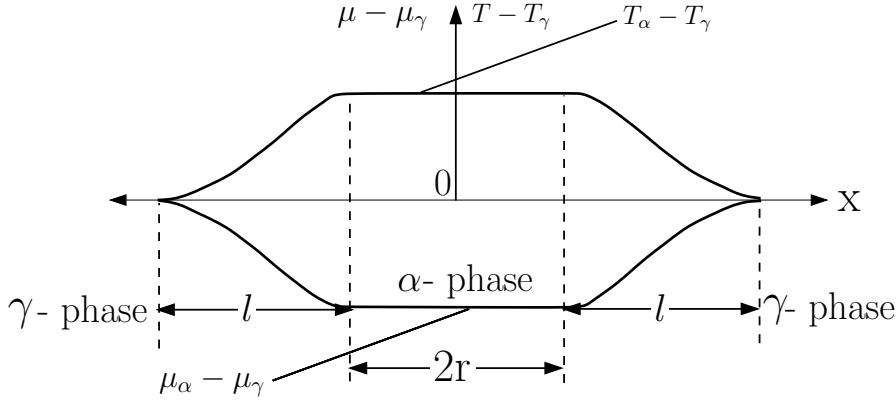


Figure 1.7. Assumed distribution of temperature T and chemical potential μ at the instant of macro-nucleation of the α -phase. The x -axis is oriented perpendicular to the axis of nucleation.

it $B_{\gamma-\alpha}$) characterized by significant inhomogeneities of such fundamental macro-parameters like temperature T and chemical potential μ ⁴. In other words, the magnitudes of the spatial gradients ∇T and $\nabla \mu$ in the a.m. $B_{\gamma-\alpha}$ -region are relatively large. In order to evaluate the size of l , we start from the assumption that heat liberation as well as a remarkable volume change simultaneously occur in the region penetrated by an elasto-plastic wave-front (being closely linked up with the $\gamma - \alpha$ -transformation). Let us further assume that the wave-front propagates at a speed of $c \sim 10^3$ m/s, through a region transforming within a period t_N , rendering: $l \sim c \cdot t_N \sim (10^{-6} \div 10^{-8})$ m (see also an evaluation of l under 6.3.3). The order of magnitude of the quantities ∇T , $\nabla \mu$ can easily be assessed from the relations:

$$\nabla T \sim \frac{\Delta T}{l} \approx \frac{T_\alpha - T_\gamma}{l}, \quad \nabla \mu \sim \frac{\Delta \mu}{l} \approx \frac{\mu_\alpha - \mu_\gamma}{l}. \quad (1.8)$$

The quantity ΔT is comparable with the degree of supercooling $T_0 - M_S$, i.e., $\Delta T \sim 100$ K (see also the beginning of 1.2) and, as a result, the temperature gradient would become $\nabla T \sim (10^8 \div 10^{10})$ K/m. In assessing $\nabla \mu$, we take into consideration that the specific volume of the α -phase increases due to the volume-effect, and that simultaneously the concentration of electrons n , and thus also μ , decrease. Let $\mu \sim n^{2/3}$ be the generally used relation between μ and n in the free-electron model (see for example [87]).

⁴The designation μ , having been used in 1.4 as the designation of the shear-modulus, will from now on exclusively be used as the designation of chemical potential.

Then we get

$$\frac{\Delta\mu}{\mu} = -\frac{2}{3} \frac{\Delta V}{V}. \quad (1.9)$$

For an assumed ratio of volume change $\Delta V/V \approx 2,4 \cdot 10^{-2}$, being typical of the Bain-deformation, and with $\mu \sim 10$ eV, we get from (1.9): $\Delta\mu = 0,16$ eV, being equivalent to 1860 K at a temperature scale. This way, the quantity $\nabla\mu/k_B$ (k_B - Boltzmann-Factor) can easily exceed the value of ∇T by one order of magnitude, for the same value of l . It should be noted that our estimate of $\Delta\mu$ with adequate consideration of the volume-effect should be essentially correct, due to the use of the relation $\mu \sim n^{\frac{2}{3}}$ for a sub-system of s-electrons. Of course the same results can be obtained analytically for a d-electron subsystem (see 4.5).

The remarkable gradients ∇T and $\nabla\mu$ however require further analysis under non-equilibrium conditions of the electron- and phonon-subsystems of the $B_{\gamma-\alpha}$ -region. A substantiation of such non-equilibrium conditions will then enable us to confine our further task to the determination of the mechanism of generation (or selective amplification) of phonons by non-equilibrium electrons.

2. We recall that the physical basis of the maser-effect is that the processes of stimulated absorption are outnumbered by simultaneously occurring processes of stimulated emission in a given region of a system, provided an inverted occupation is given in the radiating system (i.e. in a lasing system the occupation of higher energy levels must substantially exceed that of the lower energy levels). If we choose a group of electrons as a radiating system and further assume that the band model is correct, then it will be straight forward to conclude that inversely occupied energy levels are present wherever electronic flows exist, provided their assumed energy levels are correct. Let $f_{j\mathbf{k}}$ denote the non-equilibrium distribution function of electrons in the state (j, \mathbf{k}) , where j is a band number, \mathbf{k} is the wave vector and $\hbar\mathbf{k}$ the quasi-momentum (\hbar - Planck's constant) associated to a given electron of energy $\varepsilon_{j\mathbf{k}}$. Let us now regard the graphs pertaining to a non-equilibrium distribution of electrons (ref. i.e. [87]) being already known from the theories of heat (for $\nabla T \neq 0$) and of electrical conductivity (for $\nabla\mu \neq 0$). In Fig.1.8, an equilibrium function $f_{\mathbf{k}}^0$ (normal line), and a non-equilibrium function $f_{\mathbf{k}}$ (dotted line) are plotted, the degree of non-equilibrium being determined by the quantities ∇T Fig.1.8a and $\nabla\mu$ Fig.1.8b. In case (a), it is clearly obvious that two oppositely oriented electronic flows arise (namely, electrons with energy $\varepsilon > \mu$ predominantly move from the warmer to the cooler regions, i.e., against the temperature-gradient ∇T , whereas electrons with $\varepsilon < \mu$ predominantly move parallel to the direction being set by ∇T).

Thus, if the quasi-momentum $\hbar \mathbf{k}$ of electrons is oriented anti-parallel to the temperature-gradient ∇T , a non-equilibrium term $\Delta f_{\mathbf{k}} > 0$ for $\varepsilon_{\mathbf{k}} > \mu$, with $\Delta f_{\mathbf{k}} < 0$ for $\varepsilon_{\mathbf{k}} < \mu$, has to be considered. And vice-versa, if $\hbar \mathbf{k}$ is oriented parallel to ∇T , then $\Delta f_{\mathbf{k}} > 0$ for $\varepsilon_{\mathbf{k}} < \mu$ and $\Delta f_{\mathbf{k}} < 0$ for $\varepsilon_{\mathbf{k}} > \mu$. Thus the states with quasi-momentum $\hbar \mathbf{k}$ oriented anti-parallel or parallel to ∇T would be inversely occupied above or below the Fermi-level μ . In Fig.1.8a, two such inversely occupied energy levels are plotted by thin horizontal lines, in relation to the Fermi level μ . In Fig.1.8b, the particular case of parallel electron motion towards decreasing chemical potential, i.e. against $\nabla \mu$, is illustrated, where the sign of the non-equilibrium addend to the equilibrium distribution function $f_{\mathbf{k}}^0$ is independent of the relation between $\varepsilon_{\mathbf{k}}$ and μ , i.e.: $\Delta f_{\mathbf{k}} > 0$ for $\mathbf{k} \uparrow \downarrow \nabla \mu$, and $\Delta f_{\mathbf{k}} < 0$ for $\mathbf{k} \uparrow \uparrow \nabla \mu$. The above concept of formation of inversely occupied states related to the non-equilibrium conditions during the stage of growth of the α -phase has been proposed in [88–90].

3. Our investigation of the generation of elastic waves by non-equilibrium electrons should most reasonably start with a definition of the conditions required for the excitation (or amplification) of a plane wave of atomic displacement, in the ideal case of a crystal of infinite dimensions, with homogenous and stationary temperature- and chemical potential gradients.

From the point of view of quantum-mechanics, a plane wave of relative atomic

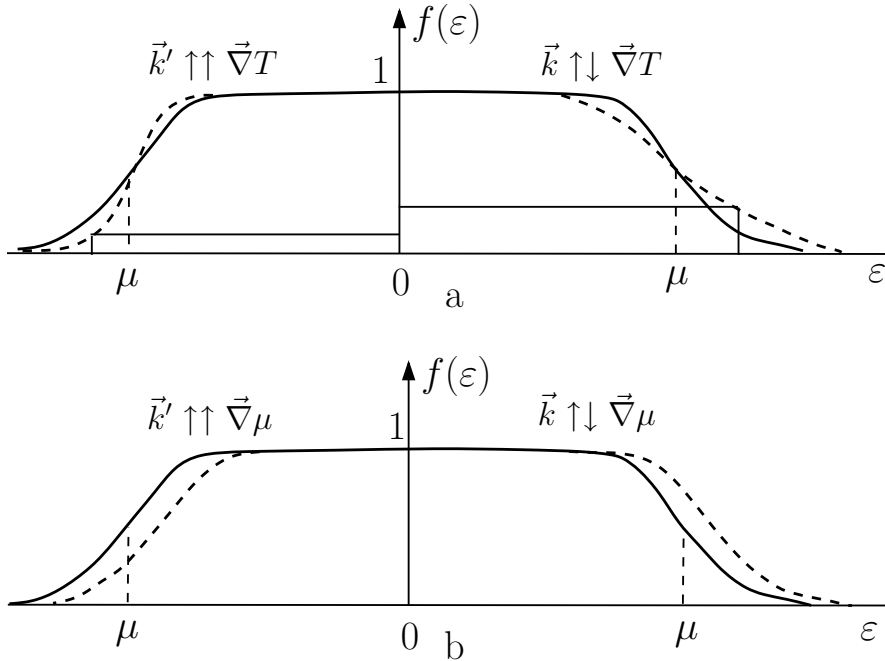


Figure 1.8. Equilibrium (normal line) and non-equilibrium (dashed line) electron energy distributions: (a): $\nabla T \neq 0$; (b) $\nabla \mu \neq 0$

displacement: $\mathbf{u}(\mathbf{r}, t) = \mathbf{u}_0 \cos(\omega_{\mathbf{q}} t - \mathbf{q} \cdot \mathbf{r})$ represents the macroscopic effect of a totality of coherent phonons of energy $\hbar\omega_{\mathbf{q}}$, with wave-vectors \mathbf{q} . This means that the generation of waves by a maser-mechanism would become feasible whenever a macroscopic number of inversely occupied electronic states (\mathbf{k}, \mathbf{k}') was existent, and transitions between them would predominantly result in the emission of phonons, in accordance with the laws of energy- and quasi-momentum conservation:

$$\varepsilon_{i\mathbf{k}} - \varepsilon_{i'\mathbf{k}'} = \omega_{j\mathbf{q}}, \quad (1.10)$$

$$\mathbf{k} - \mathbf{k}' - \mathbf{q} = 0, \mathbf{Q}. \quad (1.11)$$

In (1.10), j is the index of the phonon-branch, whereas the equality of (1.11) depends on whether the electronic transitions belong to a normal "N-process" or to a "U-process" [87] (see Fig.1.9). For an N-process, the right side of

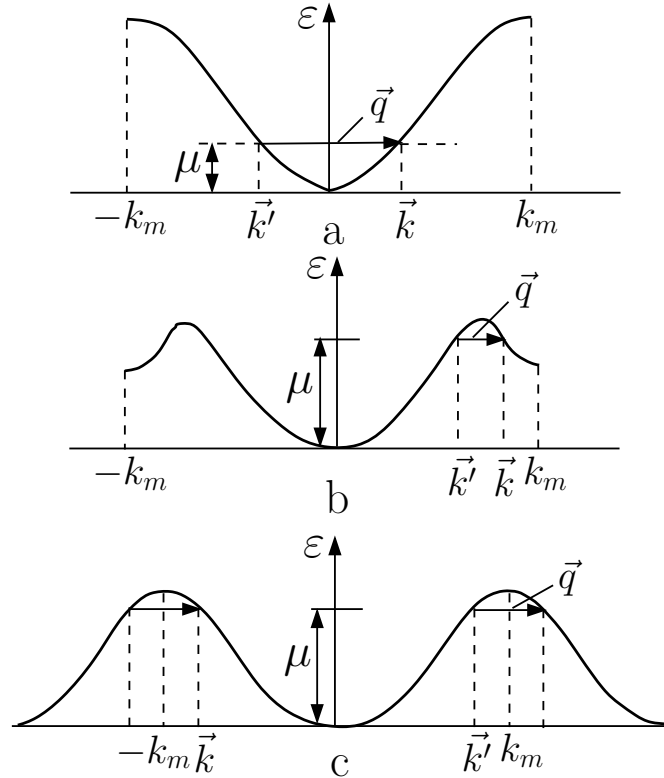


Figure 1.9. One-dimensional pattern of N-processes (cases a and b) and U-process (case c) k_m – upper momentum limit in the 1st BZ, \mathbf{q} – phonon-momentum. The energy difference $\varepsilon_{\mathbf{k}} - \varepsilon_{\mathbf{k}'}$ is not considered, μ – Fermi-level.

(1.11) vanishes, while for a U-process, the right side of (1.11) is the vector \mathbf{Q}

of the reciprocal lattice. This way, our task is equivalent to finding macroscopic sets of pairs of inversely occupied electronic states in \mathbf{k} -space, which would have to be equidistant to satisfy the conditions of (1.10,1.11). The main objective in processing with this task will thus be the identification and classification of such pairs of electronic states, starting with the definition of points located in a surface separating inversely occupied states in \mathbf{k} -space. Thus it will be important from the outset of our analysis, to identify and pre-select such lattice oscillations being characterized by an implicit tendency to become unstable under non-equilibrium conditions. This analysis will be based on the assumption that the structure of the electronic spectrum in the transforming $B_{\gamma-\alpha}$ -region maintains all relevant properties of the electronic spectrum of the fcc-phase of iron, this being a significant prerequisite from the viewpoint of the phonon-generation mechanism.

If we think of a MT as the manifestation of a particular kind of lattice-instability, it would be reasonable to identify some key features of solid-state instabilities in general. Firstly, it can be stated that, except for some specific aspects of non-equilibrium states, basically the same - finally stated - particularity of an electronic spectrum is used to explain lattice-instabilities like the Peierls-instability of a three-dimensional lattice, as well as during a variety of electronic and magnetic phase transitions, within the frame of a wave concept for charge- and spin-densities [4, 91–94]: The key point thus is: The macroscopicity and collectivity of a number of electronic states, corresponding to (1.10, 1.11). In fact: For the presented examples, there is a requirement for the existence of more or less large regions on the Fermi-surface which must nest during a translation by a given vector \mathbf{q} . This very vector \mathbf{q} thus characterizes the resulting structure. The existence of such particularities must manifest itself through the appearance of density-peaks of the electronic states in the proximity of the Fermi-energy μ [95–97]. Of course, the pairs of electrons that will attract our particular interest later on, must also have energies near μ .

4. By analogy with a photon-maser [98], it can be expected that, in order to realize a phonon-maser, mere satisfaction of the threshold-condition

$$\sigma_0 > \sigma_{th} = \frac{\Gamma \varkappa}{|W|^2 R}, \quad (1.12)$$

would be sufficient, which already considers that the inverted initial difference of the σ_0 -populations has to exceed a given threshold σ_{th} . This threshold value thus is proportional to the inherent attenuation Γ of radiating electrons, as well as to the rate of damping \varkappa of generated phonons, and inversely proportional to the square of the matrix-element W of electron-phonon interaction, as well as to the number of pairs of equidistant electronic states R . It should be noted that Debye-Phonons turn out to be incompetent, due to

their high attenuation in relation to the attenuation of phonons with longer waves, as indicated by (1.12).

5. It has to be clearly distinguished between a dynamical instability, as manifested by the excitation of elastic waves (in accordance with (1.12)) and the lattice-instability arising as soon as the waves attain a threshold amplitude of $\varepsilon_{th} \sim 10^{-3}$, as required to initiate plastic deformation (see 1.3). Thus, in order to materialize the lattice instability to be dealt with here, a more demanding condition than that of (1.12) has to be satisfied.
6. As the $\gamma - \alpha$ MT of ferrous alloys occurs in a wide range of concentrations of its other component (-s), causing significant variations of the M_S -temperatures (from $M_S < 10^3$ K, for low Ni-concentrations, down to $M_S < 4,2$ K, for 34% Ni in a Fe - Ni - System), we have to identify a specific criterion for an effective working principle of phonon-maser-excitation, which must be valid for the observed wide range of temperatures and concentrations. The specific difficulties arising from this task can most easily be overcome by a two-band model of the electronic spectrum of a metal, comprising s and d electrons (a more comprehensive definition of this task will be given under 4.1).
7. After having established a conceptual notion of a phonon-maser for single wave generation, let us now get into an interpretation of some morphological characteristics of martensite. It would be most convenient to select the habit plane as a basic characteristic of a MT, as the habit plane is unequivocally linked up with a MT, as already mentioned under 1.2. For further interpretation of MT, it will be convenient to start with an outline of the following geometrical representation, which will play a key role in our further analysis: Imagine a straight line of fixed (non-rotating) orientation, moving with a constant velocity relative to an inertial reference frame (associated, for example, with crystal axes $\langle 100 \rangle$). As a flat surface can geometrically be defined as the location of all points in space through which such a line has passed, then this line in motion will generate a plane. (Analogously, a line can be generated by the trail of a moving point imprinted in a given plane). In our next step, we assume that the moving line itself is defined and generated by the geometric locus of a moving intersection of two flat (non-parallel) wave fronts (i.e. with non-collinear wave-vectors). (The idea of using a combination of waves has first been expressed in [81]). Further substantiation of the wave characteristics should aim at defining the class of waves (i.e. longitudinal or transversal), their direction(s) of propagation, and their phase-relationships. It can however be anticipated that the combined action of such waves might suffice to build up favorable conditions for a structural transition. With respect to the $\gamma - \alpha$ -transformation, longitudinal (or quasi-longitudinal) waves, supposed to propagate near to the

orientations $\langle 001 \rangle$, $\langle 110 \rangle$ will be selected. In addition and in accordance with the pattern of Bain-deformation (see Fig.1.1), let us further suppose that the growth of a martensite lamella proceeds by progressive unification with its adjacent areas, which are subjected to the synchronized dilatational and compressive action of the waves intersecting them. In Fig.1.10, two selected perpendicular directions of wave propagation are marked by indices 1 and 2, while the velocities and lengths of the two waves are marked by c_1 , c_2 , λ_1 , λ_2 , respectively. The hatched cross-sections represent the areas of favorable transformation conditions with respect to the orientations of compressive- (acting in direction 1) and tensile stress (acting in direction 2). Each of the waves is shown at a given starting time t_0 and at a somewhat later instant t . Obviously in Fig.1.10, the area enclosed by the bold lines represents an idealized cross-section of a lamella with an approximate width of $(1/2)\lambda_{1,2}$, thus resembling a prototype image of a growing martensite lamella.

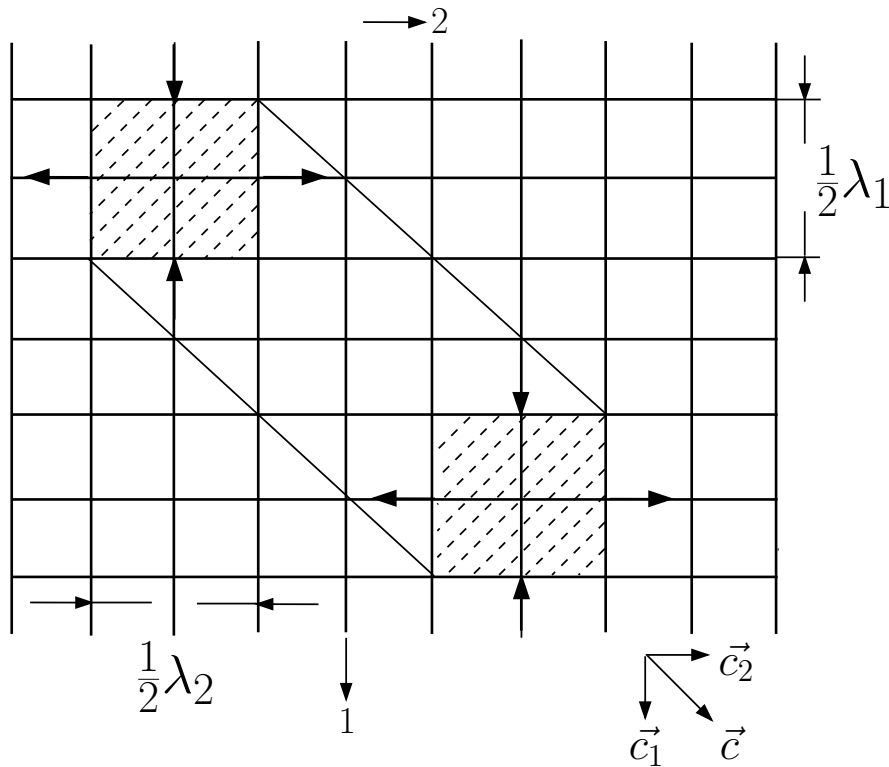


Figure 1.10. Fundamental growth pattern of a martensite lamella in the notion of two flat longitudinal waves propagating perpendicular to each other: c_1 , c_2 – wave - velocity, λ_1 , λ_2 – wavelength.

It is easy to conceive from Fig.1.10 that the hatched area of wave-superposition, as well as the intersecting area of the wave-fronts, are simultaneously propagating at the velocity equivalent to the vector-sum (i.e.

geometrical sum) of their individual velocities $\mathbf{c}_1, \mathbf{c}_2$ ⁵, i.e.

$$\mathbf{c} = \mathbf{c}_1 + \mathbf{c}_2, \quad c = |\mathbf{c}| = \sqrt{c_1^2 + c_2^2}. \quad (1.13)$$

As the value of $|\mathbf{c}|$, on the one hand, characterizes the frontal speed of growth of a martensite lamella, and on the other hand can exceed the longitudinal velocity of sound in direction of \mathbf{c} in Fig.1.10, it is possible in principle to explain this way the aligned supersonic growth of martensite crystals (being controlled by a pair of ordinary longitudinal waves), thus inherently representing an important kinetic particularity of the growth stage. This interpretation was proposed for the first time in [99]. We should also keep in mind that the dominating role of longitudinal waves in the formation stage of midribs was postulated in [77] too. If, on the one hand, the types of generated waves were put in relation with the particularities of the electronic spectrum and on the other hand, with the morphology of the end product, then we could expect new explanations of structural and kinetic particularities of the MT (including the effects of changes in concentration of the second component), which might be complementary to some important conclusions drawn from thermodynamic analysis of MT.

8. After having convinced ourselves of the "functionality" of a two-wave pattern, we shall deal in our next step with the various implications related to the coordinated propagation of displacement waves in the model of "switching waves", as we will call the isolated, step-shaped fronts of temperature, chemical potential and distortion. This might finally consolidate our understanding of the key phenomena associated with the motion of the interface of a martensite crystal in the growing stage.

The following chapters will mainly be devoted to the solution of the tasks defined in above sub-points 3 to 8. In brief, the ultimate objective of this work is to analyze and understand the growth stage of a martensitic crystal during the $\gamma - \alpha$ -transformation of ferrous alloys, within the conceptual frame of a self-organizing process, during which the mechanism of generation (and amplification) of lattice-displacement-waves by means of non-equilibrium electrons will play a dominant role.

To avoid any misunderstandings when reading this monograph, the author recommends to bear in mind that different physical quantities may sometimes be denoted by one and the same symbol. For this reason, the indices appended to symbols, as well as the "local" definition of abbreviations, will normally be introduced in the "local" text and should be duly considered. Thus in one instance, ε_k may represent the energy of an electron of wave-vector \mathbf{k} , whereas ε may represent linear deformation, and $\tilde{\varepsilon}$ represents rel-

⁵In case of non-orthogonality between c_1, c_2 , the velocity c would deviate from (1.13)

ative volume deformation. Vectors will be represented either by bold letters or by an arrow placed above a letter.

Chapter 2

Particularities of an electronic energy spectrum as required for realization of a Phonon-Maser

2.1 The Hamiltonian Problem

In accordance with No. 1 and 2 of point 1.5 of this monograph we associate to each state of an electron a band-index j and a wave-vector \mathbf{k} . Let us further assume that the basic characteristics of the band-structure of γ - iron will essentially also apply to other ferrous alloys with fcc-lattice, at least in a coherent potential approximation [100, 101] (also see [102]). Thus our consistent first step will be to analyze the dynamical characteristics of the electron-phonon system under non-equilibrium conditions, within the frame of energy of the band spectra of the involved electrons and phonons.

We choose the standard formulation of the Hamiltonians for non-interacting electrons H_e and Phonons H_p , respectively

$$H_e = \sum_{j\mathbf{k}} \varepsilon_{j\mathbf{k}} a_{j\mathbf{k}}^+ a_{j\mathbf{k}}, \quad (2.1)$$

$$H_p = \sum_{i\mathbf{q}} \hbar\omega_{i\mathbf{q}} (b_{i\mathbf{q}}^+ b_{i\mathbf{q}} + \frac{1}{2}), \quad (2.2)$$

where $a_{j\mathbf{k}}^+$, $a_{j\mathbf{k}}$, $b_{i\mathbf{q}}^+$, $b_{i\mathbf{q}}$ - are the creation and annihilation operators for electrons and phonons, respectively. Accordingly, the acoustic branches of the phonon spectrum with frequencies ω and wave-vectors \mathbf{q} will be enumerated by $i = 1, 2, 3$. In consideration of the predominance of single-phonon processes during electron-phonon interactions, it is justified to use the Fröhlich-Hamiltonian H_{ep} as interaction operator, being linear in the operators b^+ and b :

$$H_{ep} = \sum_{\mathbf{q}\mathbf{k}i\mathbf{j}\mathbf{j}'} W_{i\mathbf{q}\mathbf{j}\mathbf{j}'}^* b_{i\mathbf{q}} a_{\mathbf{j}\mathbf{k}}^+ a_{\mathbf{j}'\mathbf{k}'} + W_{i\mathbf{q}\mathbf{j}\mathbf{j}'} b_{i\mathbf{q}}^+ a_{\mathbf{j}'\mathbf{k}'}^+ a_{\mathbf{j}\mathbf{k}}. \quad (2.3)$$

In this case the quasi-momenta obey to the conservation-law (1.9b), and $W_{\mathbf{q}}$ is the matrix-element pertaining to electron-phonon interaction ($W_{\mathbf{q}}^*$ is complexly coupled to $W_{\mathbf{q}}$). In the tight binding approximation it is possible to get an estimated value for $W_{\mathbf{q}}$ by limiting the calculus to a linear reduction of the resonance integral G , with respect to atomic displacements, where the magnitude of G determines the width of the electron band [92]. For $q < q_{max}$ with $q_{max} \sim \pi/a$, near the boundary of the 1st Brillouin-Zone (BZ), we get for Normal (N-processes) as well as for Umklapp (U-processes):

$$W_{\mathbf{q}} \approx i \left[\frac{\hbar}{2MN\omega_{\mathbf{q}}} \right]^{\frac{1}{2}} G(\mathbf{e}_{\mathbf{q}}, \mathbf{q}), \quad (2.4)$$

where M - atomic mass, N - number of atoms, $\mathbf{e}_{\mathbf{q}}$ - phonon polarization vector, i - imaginary unit in (2.4) (we omitted the band and branch indices).

Apart from the Hamiltonians (2.1)-(2.3), the complete Hamiltonian of system H would also have to take into account electron-electron interactions H_{ee} as well as anharmonic phonon-phonon interactions H_{pp} , the explicit form of which will however not be used further.

2.2 Form of a non-equilibrium addend to the electronic distribution function and definition of points separating inversely occupied states in a one-dimensional electronic spectrum

The task related to the identification of pairs of potentially active electronic states (ES) being involved in the generation of phonons (see sub-point 3 under point 1.5) requires that some additional conditions have to be satisfied, besides those already defined in (1.9). Above all we have to remark that in the context of this monograph, the notion "potentially active" addresses the population inversion of pairs of ES under non-equilibrium conditions in a transforming lattice. As a population inversion of the kind to be discussed here always coexists with electronic flows, it can be anticipated that the uppermost inversion between pairs of ES will only be realized for such orientations of the group-velocities $\mathbf{v}_{\mathbf{k}} \uparrow \downarrow \mathbf{v}_{\mathbf{k}'}$ of electrons (with wave-vectors \mathbf{k} , \mathbf{k}' , respectively) being mutually opposed to the relevant gradient of a locally existing spatial inhomogeneity.

It is easy to convince ourselves of the correctness of this latter statement by writing out a stationary non-equilibrium addend $f_{\mathbf{k}} - f_{\mathbf{k}}^0$ (for stationary and ho-

mogenous temperature and chemical potential gradients), as determined by the standard kinetic equations of electronic populations $f_{\mathbf{k}}$ and using the relaxation time approximations presented in [87]. Our determination of relaxation time τ will be based on the consideration that the impact-integral can be replaced by expression $(f - f^0)\tau^{-1}$, where τ is the average relaxation time to equilibrium distribution f^0 .

$$f_{\mathbf{k}} - f_{\mathbf{k}}^0 \approx \frac{\partial f_{\mathbf{k}}^0}{\partial y_{\mathbf{k}}} \frac{y_{\mathbf{k}} \tau}{T} (\mathbf{v}_{\mathbf{k}}, \vec{\nabla} T), \quad (2.5)$$

$$f_{\mathbf{k}} - f_{\mathbf{k}}^0 \approx \frac{\partial f_{\mathbf{k}}^0}{\partial y_{\mathbf{k}}} \frac{\tau}{k_B T} (\mathbf{v}_{\mathbf{k}}, \vec{\nabla} \mu). \quad (2.6)$$

In (2.5) and (2.6) $f_{\mathbf{k}}^0$ - Fermi-Distribution

$$f_{\mathbf{k}}^0 = \frac{1}{e^{y_{\mathbf{k}}} + 1}, \quad y_{\mathbf{k}} = \frac{\varepsilon_{\mathbf{k}} - \mu}{k_B T}, \quad (2.7)$$

k_B - Boltzmann-Factor.

It immediately follows from (2.5) and (2.6) that the non-equilibrium addends in brackets simultaneously change their own signs with a change of the orientation of $\mathbf{v}_{\mathbf{k}}$, as indicated by the change of sign of the respective scalar products $(\mathbf{v}_{\mathbf{k}}, \vec{\nabla} T)$ or $(\mathbf{v}_{\mathbf{k}}, \vec{\nabla} \mu)$. Bearing in mind that $\partial f_{\mathbf{k}}^0 / \partial y_{\mathbf{k}} < 0$, we can easily note the correspondence of equations (2.5) and (2.6) with Fig. 1.8.

The requirement of anti-parallelism $\mathbf{v}_{\mathbf{k}} \downarrow \mathbf{v}'_{\mathbf{k}}$ bears a more generalized character than the singular requirement of anti-parallelism for quasi-momenta $\hbar \mathbf{k} \uparrow \downarrow \hbar \mathbf{k}'$ of a pair of ES, as indicated under sub-point 2 of point 1.5. The requirement $\mathbf{k} \uparrow \downarrow \mathbf{k}'$ is actually satisfied for N and U-processes, near the lower and the upper edge of an energy band (cases a and c in Fig.1.9). However it would not be satisfied if an N-process occurred at an intermediate location (case b in Fig. 1.9), whereas the requirement $\mathbf{v}_{\mathbf{k}} \downarrow \mathbf{v}_{\mathbf{k}'}$ would be satisfied in any case. Obviously, a consideration of the one-dimensional spectrum Fig. 1.9 shows that mutually opposed velocity orientations correspond to pairs of ES separated by a point corresponding to a quasi-momentum \mathbf{p} (see below) for which the energy distribution $\varepsilon(\mathbf{k})$ features an extreme value. This means that for $\mathbf{k} = \mathbf{p}$ the group velocity

$$\mathbf{v}_{\mathbf{k}} = \frac{1}{\hbar} \frac{\partial \varepsilon(\mathbf{k})}{\partial \mathbf{k}} \Big|_{\mathbf{p}}$$

vanishes (with $\mathbf{p} = 0$: in case a; $\mathbf{p} = \mathbf{k}_m$: in case c; and $0 < \mathbf{p} < \mathbf{k}_m$: in case b). This way it will be convenient to select pairs of ES in one-dimensional \mathbf{k} -space by looking for points \mathbf{p} corresponding to equilibrium population, which in this case separate the states \mathbf{k} and \mathbf{k}' of an ES-pair.

2.3 Definition of boundary surfaces separating inversely occupied states for a 3-dimensional electronic spectrum

We shall now apply the results of point 2.2 for the case of a 3-dimensional electronic spectrum. Let $R(\mathbf{q}) = \{|i\mathbf{k}\rangle, |i'\mathbf{k}'\rangle\}$ be sets of equidistant ES-pairs satisfying the conditions of (1.9), which at the same time are potentially active during the creation of phonons with quasi-momenta $\hbar\mathbf{q}$. As already discussed under sub-point 3 of point 1.5, the contribution of stimulated radiative transitions between ES within a set $R = \{|\mathbf{k}\rangle, |\mathbf{k}'\rangle\}$ can in some instances become a macroscopic quantity, provided that the number of ES-pairs in R also is a macroscopic quantity and a population inversion of the majority of such pairs does exist. For simplicity the radiative transitions are supposed to be confined to one electron energy band, and for this reason the band indices will be omitted further on. In the case of an inhomogeneous spatial electron distribution, a population inversion would be possible if ES-pairs with anti-parallel components of velocities $\mathbf{v} = \hbar^{-1}\vec{\nabla}\varepsilon$ existed along certain directions. This requirement could essentially be satisfied if the ES belonging to one pair were separated in \mathbf{k} -space by certain geometrically defined boundary surfaces, including planes, which we shall generally denote as P-surfaces. In such case the general condition

$$(\mathbf{v}(\mathbf{k}), \mathbf{n}(\mathbf{k})) = 0 \quad (2.8)$$

will apply. Here $\mathbf{n}(\mathbf{k})$ - unit normal vector in point \mathbf{k} of surface P. This enables us to allocate to each of the P-surfaces a totality of ES-pairs with antiparallel velocity components being collinear to the axis of \mathbf{n} , being localized in the proximity of a layer with thickness $\sim q$ (we assume that $q \sim (10^{-3} \div 10^{-1})\pi/a$, a - lattice-parameter). However, not all of the P-surfaces actually determine a set of ES-pairs, as the general requirement of macroscopicity of the number of inversely occupied ES-pairs, as well as the need of compatibility with (1.9) have to be equally met. Let a given orientation of the spatial inhomogeneity be denoted by \mathbf{e} . Then, in the proximity of those points of the P-surface where \mathbf{n} is collinear to \mathbf{e} , an inverted population (IP) of ES-pairs should actually exist, as in the \mathbf{q} -proximity of these points the existence of states with antiparallel velocity components along the orientation determined by \mathbf{e} would be inevitable. Obviously, the number and density of these specific points mostly depend on the shape of the P-surface, and attain a maximum in the case that the P-surface is a plane. For this reason, among the totality of P-surfaces, the sub-set of P-planes (defined by $\mathbf{n} = \mathbf{const}$) will be highlighted.

By definition, the P-plane is a plane in which the velocity component $\mathbf{v}_{\mathbf{n}}$ (along to the normal \mathbf{n} of the plane) vanishes for all points of the plane. Obviously, planes satisfying this specific definition match with the symmetry-planes of the reciprocal lattice. (We recall the classical rule of reflection which simply states that all normal

velocity components conserve their magnitudes and only change their signs, before and after reflection at a plane.) Consequently, on the points of a symmetry plane, the velocity \mathbf{v} (as an invariant during a reflective transformation) does not feature non-vanishing components collinear to the normal \mathbf{n} of that plane.

Of course such symmetry considerations do not exclude in general the possible existence of P-planes not coinciding with symmetry planes. For this reason we need to find certain specific equations which may enable us to determine such P- planes not being defined by symmetry considerations alone, but still being in accordance with the dispersion law. It should be noted that in case that a surface is a P-plane, Eqs. (2.8) must be satisfied for all points of this plane and the next relationship (2.9) occurs

$$(\mathbf{n}, d\mathbf{v})|_{\mathbf{P}} = (\mathbf{n}, (d\mathbf{k}, \vec{\nabla})\mathbf{v})|_{\mathbf{P}} = 0, \quad (2.9)$$

where $d\mathbf{k}$ corresponds to the requirement $(d\mathbf{k}, \mathbf{n}) = 0$. It is further possible to define two independent vectors $d\mathbf{k} = d\mathbf{k}_1, d\mathbf{k} = d\mathbf{k}_2$. Supposing that $d\mathbf{k}_1 = [\mathbf{n}, \mathbf{v}]|_{\mathbf{P}} dl$ and $d\mathbf{k}_2 = \mathbf{v}|_{\mathbf{P}} dl$, then we get from (2.9):

$$(\mathbf{n}, ([\mathbf{n}, \mathbf{v}] \vec{\nabla})\mathbf{v})|_{\mathbf{P}} = 0, (\mathbf{n}, (\mathbf{v}, \vec{\nabla})\mathbf{v})|_{\mathbf{P}} = 0. \quad (2.10)$$

If we write the equation for the P-plane in the form $(\mathbf{n}, \mathbf{k}) = C$, then it will be possible to find the normal-vector \mathbf{n} and the constant C by resolving (2.8) and (2.10) for the components of \mathbf{n} and C with a given value $\mathbf{k} = \mathbf{k}_0$ corresponding to the requirement $\mathbf{v}(\mathbf{k}_0) \neq 0$. The vector \mathbf{k}_0 , which determines a point in the P-plane, possesses two independent components, which can be chosen arbitrarily. For practical reasons however it is more convenient to choose \mathbf{k}_0 in such a way that Eqs. (2.8) and (2.10) attain their most simple form for $\mathbf{k} = \mathbf{k}_0$.

In the particular case of a curved surface P, both its normal vectors \mathbf{n} and the velocity vectors \mathbf{v} change their orientation from point to point, with respect to the orientation of \mathbf{e} . Thus the number of ES-pairs with anti-parallel velocity components \mathbf{v}_e (collinear to \mathbf{e}) located in the \mathbf{q} -layer can be small. And vice versa, from the point of view of a population inversion, only such specific ES-pairs are highlighted whose mutually anti-parallel velocity components are oriented collinear to the local spatial inhomogeneity \mathbf{e} . In \mathbf{k} -space, such ES-pairs are separated by boundary surfaces of a different category (we denote them by S or S-surface) for which

$$(\mathbf{v}, \mathbf{e}) = 0. \quad (2.11)$$

This means that at any point in S, the projection of \mathbf{v} onto \mathbf{e} vanishes, i.e. $\mathbf{v} \perp \mathbf{e}$. According to (2.11) the surface S comprises the geometric loci of all singularity points (i.e. the extremes and flex points) of a function $\varepsilon(\mathbf{k})$, if \mathbf{k} varies parallel with \mathbf{e} . Obviously, the scalar products $(\mathbf{v}(\mathbf{k}), \mathbf{e}), (\mathbf{v}(\mathbf{k}'), \mathbf{e})$ will attain different signs for each pair of points \mathbf{k}, \mathbf{k}' located at opposed sides of S, but still remain in the proximity of S (i.e. where $|\mathbf{k} - \mathbf{k}'| \leq 0, 1\pi/a$), provided the intersection of the

vectors $\mathbf{k} - \mathbf{k}'$ with S corresponds to a relative extreme of the function $\varepsilon(\mathbf{k})$ in such intersections, i.e. for $(\mathbf{k} - \mathbf{k}', \vec{\nabla})\mathbf{v}|_s \neq 0$. Let $(\mathbf{k} - \mathbf{k}', \vec{\nabla})\mathbf{v}|_s = 0$ define a flex point of the function $\varepsilon(\mathbf{k})$ on the surface S. Then, in the proximity of such a flex point, there will not occur a change of sign of the scalar product $(\mathbf{v}(\mathbf{k}), \mathbf{e})$. Consequently, ES-pairs \mathbf{k}, \mathbf{k}' corresponding to such flex points will not be considered further.

The equations of surfaces S can also be written in a form not explicitly depending on \mathbf{e} . It will be reasonable to use such a notion when searching for certain S-surfaces with specific characteristics. Doing this way, the \mathbf{e} vectors will not be given from the outset, but can be derived from the already known equations of an S-surface. We note that in any point of the S-surface, the velocity vectors $\mathbf{v}(\mathbf{k})$ - according to (2.11) - are oriented parallel to a fixed plane. Consequently, if three arbitrary points in the S-surface are defined by vectors $\mathbf{k}, \mathbf{k}_1, \mathbf{k}_2$ we get

$$(\mathbf{v}(\mathbf{k}), [\mathbf{v}(\mathbf{k}_1), \mathbf{v}(\mathbf{k}_2)]) = 0. \quad (2.12)$$

Assuming that $\mathbf{k}_1 = \mathbf{k} + \Delta\mathbf{k}$, $\mathbf{k}_2 = \mathbf{k} + \Delta\mathbf{k}'$, we can develop (2.12) by powers of $\Delta\mathbf{k}, \Delta\mathbf{k}'$, however confining our decomposition of $\mathbf{v}(\mathbf{k}_1), \mathbf{v}(\mathbf{k}_2)$ to the linear terms.

$$(\mathbf{W}(\mathbf{k}), [\Delta\mathbf{k}, \Delta\mathbf{k}']) \approx 0, \quad (2.13)$$

where

$$\mathbf{W} = \frac{1}{2} \sum_{ijn} \mathbf{e}_i \varepsilon_{ijn} \left(\mathbf{v}, \left[\frac{\partial \mathbf{v}}{\partial k_j}, \frac{\partial \mathbf{v}}{\partial k_n} \right] \right) \quad (2.14)$$

and $\mathbf{e}_1, \mathbf{e}_2, \mathbf{e}_3$ are the orthogonal unit vectors of a right-hand Cartesian frame of reference, with $\varepsilon_{ijn} = (\mathbf{e}_i, [\mathbf{e}_j, \mathbf{e}_n])$. If $\Delta\mathbf{k}, \Delta\mathbf{k}' \rightarrow 0$, then the vector $[\Delta\mathbf{k}, \Delta\mathbf{k}']$ adopts the orientation of the normal \mathbf{n} of the surface S in point \mathbf{k} . For this reason, the vector $[\Delta\mathbf{k}, \Delta\mathbf{k}']$ can be replaced by \mathbf{n} when reaching the limit $\Delta\mathbf{k}, \Delta\mathbf{k}' \rightarrow 0$ in (2.13). In result, we obtain the general equation for the S-surfaces we were searching for:

$$(\mathbf{W}(\mathbf{k}), \mathbf{n}(\mathbf{k})) = 0. \quad (2.15)$$

In our specific task of search for and identification of the subset of flat S-surfaces, we shall essentially use (2.15). Formally, our task of finding such planes, determined by a vector-field $\mathbf{W}(\mathbf{k})$, is equivalent to the task of finding P-planes associated with a velocity-field $\mathbf{v}(\mathbf{k})$, as (2.8) and (2.15), which define both the P and S surfaces, are formally equivalent. Thus their resolution will also lead to a resolution of Eqs. (2.8), (2.10), only by replacing \mathbf{v} by \mathbf{W} . By way of illustration let us analyze a cubic (fcc) lattice, using the definition of the basis vectors of the real and of the reciprocal lattice given in [103]. This will then enable us to use the simplest dispersion law in the tight binding approximation for fcc lattice [104]:

$$\varepsilon = \varepsilon_0 - 2\varepsilon_1 \sum_{ij} (1 - \delta_{ij}) \cos \eta_i \cos \eta_j, \quad (2.16)$$

where $\varepsilon_0, \varepsilon_1$ - constants, $\eta_i = (ak_i/2)$, a - lattice-constant. In this case, the set of P-planes will be confined to planes of symmetry with $k_i = 2m_i(\pi/a)$, $k_i \pm k_j = 4m_{ij}(\pi/a)$, $i \neq j$, $i, j = 1, 2, 3$; $m_i, m_{ij} = 0, \pm 1, \dots$. In our further search for S-planes, it will be convenient to distinguish between the following 2 variants of planes: 1) planes oriented parallel to the coordinate planes (or axes) of the lattice and 2) planes intersecting the coordinate planes or axes. The subset of planes oriented parallel to the coordinate planes can be defined by the condition $k_i = c_i$, ($i = 1, 2, 3$). The constants c_i can be determined from the relation

$$(\mathbf{n}, \mathbf{W})_{k_i=c_i, k_j=k_l=0} = 2B \sin\left(\frac{1}{2}c_i a\right) \left(1 + \cos\frac{1}{2}c_i a\right)^2, \quad (2.17)$$

where $B = 2a^5 \hbar^{-3} \varepsilon_1^3$, being satisfied for $c_i = 2m_i \pi/a$, $m_i = 0, \pm 1, \pm 2, \dots$. The specific planes oriented parallel to a coordinate axis, for example the k_3 -axis, can be defined by the condition $n_1 k_1 + n_2 k_2 = c_{12}$. The unknown quantities n_1, n_2 and c_{12} are determined by

$$(\mathbf{n}, \mathbf{W})|_{k_3=0} = 32BD^2 K(n_1 \sin \eta_1 + n_2 \sin \eta_2) = 0, \quad (2.18)$$

$$(\mathbf{n}, (\mathbf{W}, \vec{\nabla})\mathbf{W})|_{k_3=0} = 32aB^2 D^4 K \{n_1 \sin \eta_1 [K(\cos \eta_1 + K - 2) - \sin^2 \eta_1 - \sin^2 \eta_2] + (1 \leftrightarrow 2)\} = 0 \quad (2.19)$$

where

$$D = \cos \frac{1}{2}\eta_1 \cos \frac{1}{2}\eta_2, K = \frac{1}{2} \cos \frac{1}{2}(\eta_1 + \eta_2) \cos \frac{1}{2}(\eta_1 - \eta_2).$$

The factor is $K = 0$, if $k_1 \pm k_2 = 2(2m + 1)\pi/a$, $m = 0, \pm 1, \dots$. We can easily convince ourselves that the term in brackets in (2.18) can only vanish if the condition $|n_1| = |n_2|$ is satisfied, i.e. for planes with $k_1 \pm k_2 = 4\pi m/a$. The Eqs. $k_1 \pm k_2 \pm k_3 = 4\pi m/a$ defining the planes intersecting all coordinate axes can immediately be identified taking into account that all sections being cut out from the coordinate axes by such planes must be equally sized, as demanded by (2.17), (2.18), (2.19). However, the requirement of (2.15) will not be met on these planes, which means that they would not be S-planes.

It should be kept in mind that the requirement for attainment of maximum population inversion, which actually selects the flat S-surfaces (planes), is not the only one. For this reason, also curved S-surfaces have to be included in our considerations. The Eqs. defining such surfaces can be derived from (2.11) if certain \mathbf{e} are given, as each \mathbf{e} is associated with a multi-sheeted S-surface, whose shape would change with varying \mathbf{e} . Using the spectrum given by (2.16), it is possible to obtain the view about a modification of the shape of S-surfaces setting \mathbf{e} along symmetry axes. For $\mathbf{e}||[001]$ (fourfold axis), $\mathbf{e}||[111]$ (threefold axis) and $\mathbf{e}||[110]$ (twofold axis) the Eqs. describing the S-surfaces are:

$$S_{[001]} : \sin(\eta_3) \cos \frac{\eta_1 + \eta_2}{2} \cos \frac{(\eta_1 - \eta_2)}{2} = 0, \quad (2.20)$$

$$S_{[111]} : \sin(\eta_1 + \eta_2) + \sin(\eta_1 + \eta_3) + \sin(\eta_2 + \eta_3) = 0, \quad (2.21)$$

$$S_{[110]} : \sin \frac{(\eta_1 + \eta_2)}{2} \left[\cos \frac{(\eta_1 + \eta_2)}{2} + \cos \frac{(\eta_1 - \eta_2)}{2} \cos(\eta_3) \right] = 0. \quad (2.22)$$

Typical shapes of some sheets of the surfaces (2.20 -2.22), being confined within the 1st BZ, are shown in Figs. 2.1 -2.3. (In the following, we shall denote those specific sheets of S-surfaces being located within the 1st BZ as "reduced sheets").

For $\mathbf{e} \parallel [001]$, (2.20) describes a totality of planes:

$$\eta_3 = m\pi \rightarrow k_3 = 2m\pi/a, m = 0, \pm 1, \pm 2, \dots, \quad (2.23)$$

$$\eta_1 \pm \eta_2 = (2m + 1)\pi \rightarrow k_1 + k_2 = 2(2m + 1)\pi/a \quad (2.24)$$

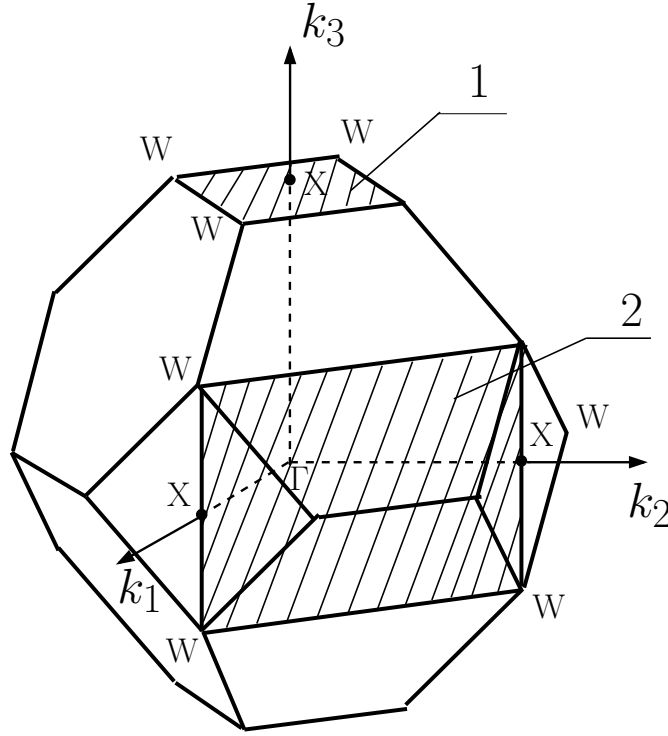


Figure 2.1. Image of the reduced Surface $S_{[001]}$ for the dispersion-law given by (2.16); Sheets 1 and 2 are determined by: $k_3 = 2\pi/a$, $k_1 + k_2 = 2\pi/a$, where a - parameter of the fcc-lattice.

In Fig. 2.1, the hatched quadratic sheet of the 1st BZ corresponds to the plane defined by (2.23) for $m = 1$ (the opposed quadratic face corresponds to $m = -1$, and the flat region including the point Γ corresponds to $m = 0$). The vertically hatched rectangle in Fig. 2.1 corresponds to one of the four planes given by (2.24) for $m = 0$: $k_1 \pm k_2 = 2\pi/a$.

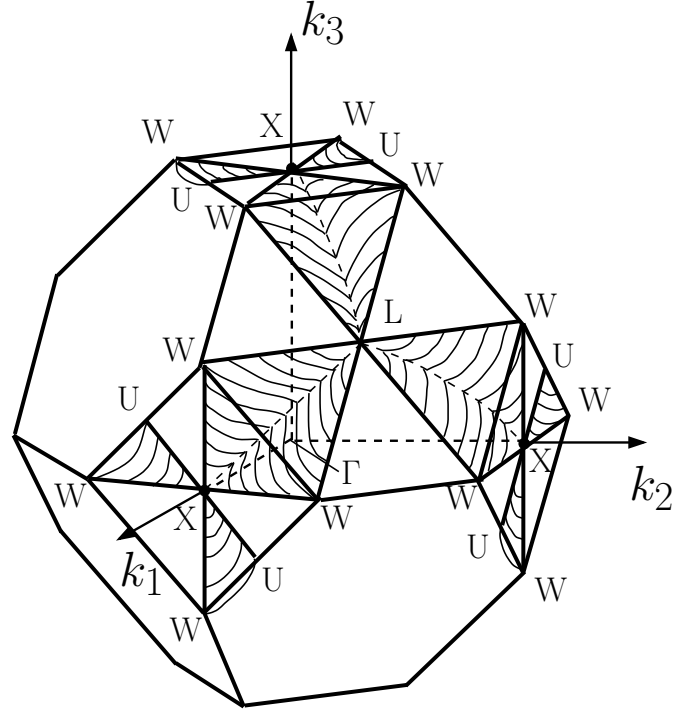


Figure 2.2. Image of one reduced curved sheet of the $S_{[111]}$ surface for dispersion-law (2.16)

For $\mathbf{e} \parallel [111]$, all sheets of the surface given by (2.21) are curved. Figure 2.2 shows one of the three reduced sheets. It is possible to obtain the sheet of similar shape by means of the geometric operation of the inversion in relation to point Γ . (The sheet including the point Γ is not shown in Fig. 2.2).

For $\mathbf{e} \parallel [110]$, (2.22) is satisfied for S-planes with $k_1 + k_2 = 4\pi m/a$ (the reduced flat sheet corresponds to $m = 0$) as well as for curved S-surfaces (whenever the expression included in brackets in (2.22) vanishes). Figure 2.3 shows one of the reduced curved sheets (the second one is produced by the inversion in relation to point Γ).

In Fig. 2.3, showing the intersections of the S-surfaces (including those not shown in Fig. 2.1 - 2.3 with planes $k_1 = k_2$ for $\mathbf{e} \parallel [11\psi]$, it is possible to track their continuous transformation with varying \mathbf{e} . For $\psi \gg 1$, the traces of the S-surfaces attain a step-like shape with pronounced linear (nearly vertical and horizontal) regions, which, for $\psi \rightarrow \infty$, will steadily transform into groups of perpendicular straight lines, which also represent the traces of planes (2.20). The

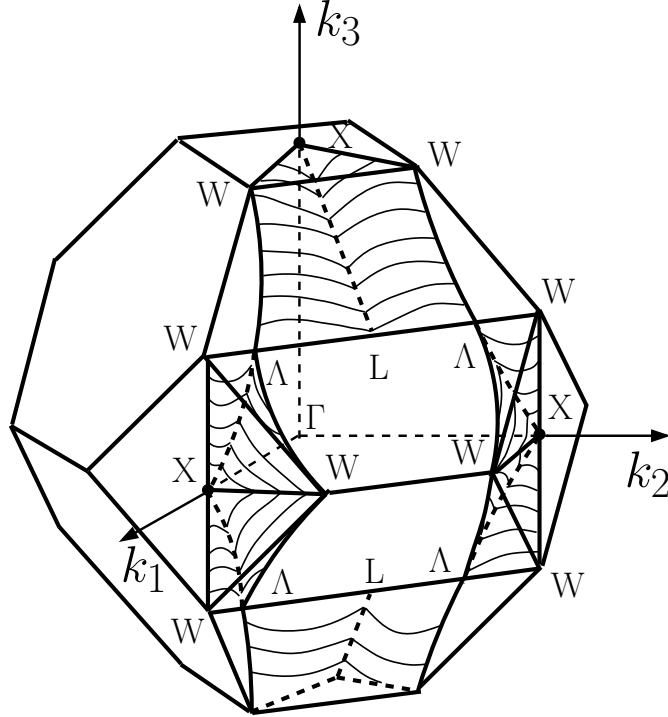


Figure 2.3. Image of the reduced curved sheet of the $S_{[110]}$ surface for dispersion-law (2.16)

trace of that sheet of the S-surface, which includes the point Γ , will be subjected to the most pronounced changes. This trace changes over from a nearly horizontal section for $\psi \gg 1$, to the almost vertical, for $0 < \psi \ll 1$ (for $\psi = 0$, the vertical line can be regarded as trace of the plane $k_1 = -k_2$, corresponding to (2.22)). The particular signs in figure 2.4 are used to mark and distinguish the different traces (quadrangles, triangles and ellipses) and also indicate the proximity of \mathbf{e} to the fourfold ($\psi \gg 1$), threefold ($\psi = 1$) and twofold ($\psi \ll 1$) axes of symmetry.

2.4 Limitations imposed by the equidistance relations in (1.9)

The first of the implicit conditions in equation (1.9), as well as the requirement of macroscopicity of the number of ES-pairs with inverted population will now enable us to develop an initial conceptual view of the S-surfaces (We should however bear in mind that P-planes are a sub-set of the totality of S-planes, defined by $\mathbf{n} = \mathbf{e}$, and for this reason the general symbol S will also include P-planes), justifying the exclusion from further consideration of all ES except those for which $R = \{R^s\} = \{ \{ |\mathbf{k}\rangle, |\mathbf{k}'\rangle \}^s \}$ with wave-vectors $\mathbf{k} = \mathbf{s} + 1/2\mathbf{q} + \delta(\mathbf{q}/q)$ and $\mathbf{k}' = \mathbf{s} - 1/2\mathbf{q} + \delta(\mathbf{q}/q)$, being localized in the proximity of S-surfaces within a layer of thickness $\sim q \sim$

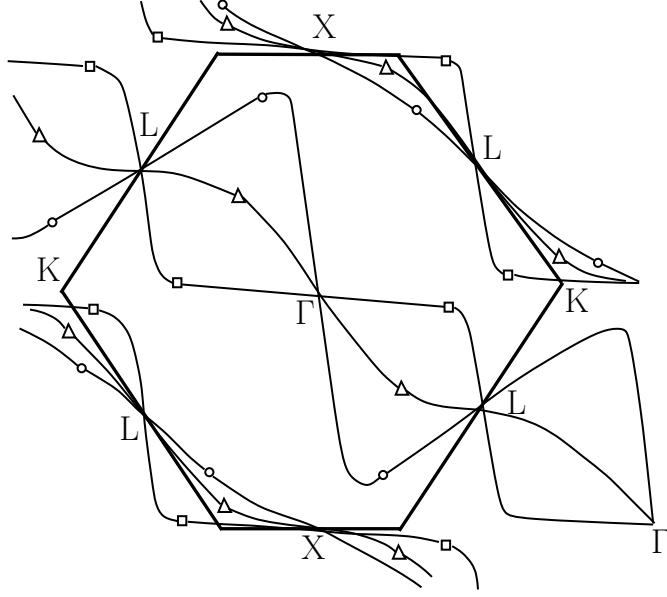


Figure 2.4. Image of the intersection of the $S_{[11\psi]}$ surfaces with planes $k_1 = k_2$ for dispersion-law (2.16):

—□— $\psi \gg 1$, —△— $\psi = 1$, —○— $\psi < 1$.

$(10^{-3} \div 10^{-1})\pi/a$, with $\delta = \delta(s) = q^{-1}(\mathbf{q}, (\mathbf{k} + \mathbf{k}')/2 - \mathbf{s})$, $|\delta| \leq 1/2q$ (using $|\mathbf{q}| = q$). But even within R , not all states are equivalent. Among them, we shall highlight those energy states located within an interval 2Δ near the Fermi-energy μ , just because they can attain significant population differences, as will be shown later on. Let $R_{\mu\Delta}$ denote the set of ES-pairs satisfying the conditions

$$\mu - \Delta \leq \varepsilon(k), \quad \varepsilon(\mathbf{k}') \sim \varepsilon(\mathbf{s}) \leq \mu + \Delta. \quad (2.25)$$

where $R_{\mu\Delta}$ represents a unification of the subsets $R_{\mu\Delta}^s$, in which each set is connected with its particular S-surface. For a given Δ , each of these sets is determined by the dispersion law $\varepsilon = \varepsilon(\mathbf{s})$ on its S-surface.

Obviously, $R_{\mu\Delta}^s = R^s$, if the following two inequalities are satisfied for the S-surface

$$\varepsilon_{min} \geq \mu - \Delta, \quad \varepsilon_{max} \leq \mu + \Delta \quad (2.26)$$

and $R_{\mu\Delta} = R$, if the inequalities (2.26) are satisfied for any of the S-surfaces. Let us take for example the spectrum described by (2.16): For $\varepsilon_1 \approx 0, 3$ eV, corresponding to a band width of 5 eV, together with $\Delta \approx 0, 1$ eV and for μ values close to the upper band boundary, (i.e. $\mu \sim \varepsilon_{max} = \varepsilon_0 + 4\varepsilon_1$), the whole reduced sheet 1 of the surface $S_{[001]}$ (see Fig. 2.1) is confined between the isoenergetic surfaces $\varepsilon = \mu \pm \Delta$, thus the inequalities (2.26) are satisfied. For ferrous alloys, $\Delta \approx 0, 24$ eV may be typical (as shown in Chapter 4) and thus large enough for the limitation imposed

by (2.25) not becoming too restrictive.

The set $R_{\mu\Delta}$ includes all ES-pairs whose contribution to stimulated radiative transitions may prove to be a potentially macroscopic quantity. Thus our next task, being immediately related to the determination of the spectrum of generated phonons, will essentially comprise the isolation of those sub-sets $R_{\mu\Delta}(\mathbf{q})$ from $R_{\mu\Delta}$ which contain equidistant ES-pairs being directly involved in the emission of phonons with the fixed magnitude and orientation of \mathbf{q} . In resolving this task we shall consistently take into account the requirements of : Macroscopicity of the quantity $|R_{\mu\Delta}(\mathbf{q})|$ - i.e. of the number of ES-pairs in $R_{\mu\Delta}(\mathbf{q})$, Maximum of population inversion and the requirements implied by (1.9), as dominant, while the electronic energy states will be considered as stationary quantities. Each of the sub-sets $R_{\mu\Delta}^s$ included in $R_{\mu\Delta}$ will have to be considered separately. Let us now decompose the energies associated with the states $|\mathbf{k}\rangle, |\mathbf{k}'\rangle$, being localized close to the S-surface, into powers of the deviations $\mathbf{k} - \mathbf{s}, \mathbf{k}' - \mathbf{s}$, and confine our further analysis to the square terms. Using this approximation and considering (2.25), we get from (1.9):

$$(\vec{\xi}, \mathbf{v}(\mathbf{s})) + \hbar\delta m^{-1}(\mathbf{s}, \vec{\xi}) = q^{-1}\omega_j(\mathbf{q}) = c_{j\vec{\xi}}, \quad (2.27)$$

where $m^{-1} = \hbar^{-2}(\vec{\xi}, \vec{\nabla})^2\varepsilon$; $\vec{\xi} = \mathbf{q}/q$, $c_{j\vec{\xi}}$ - velocity of sound. If we now ignore the second addend in (2.27), then (2.27) will be satisfied anywhere on the S-surface, provided the condition

$$(\vec{\xi}, (\vec{\tau}, \vec{\nabla})\mathbf{v})|_s = 0, \quad (2.28)$$

is satisfied. In (2.28): $\vec{\tau}$ - arbitrary unit-vector, located in a tangential plane of S. According to (2.28) and by definition of the S-surface, the vector $(\vec{\tau}, \vec{\nabla})\mathbf{v}$ is oriented perpendicular to $\vec{\xi}$ and \mathbf{e} . Thus (2.28) can be satisfied for any $\vec{\xi}$ being non-collinear to \mathbf{e} , provided the vector $(\vec{\tau}, \vec{\nabla})\mathbf{v}$, being associated with the S-surface, is collinear to fixed vector \vec{v}_0 i.e., if the velocity field on the S-surface is prescribed by

$$\mathbf{v}(\mathbf{s}) = v_0(\mathbf{s})\vec{v}_0 + \tilde{\mathbf{v}}, \quad \vec{v}_0, \tilde{\mathbf{v}} \perp \mathbf{e} \quad (2.29)$$

where $\tilde{\mathbf{v}}$ is a constant vector. Eq. (2.27) only applies to the velocity field (2.29) if the second term in (2.27) is omitted, and if $\vec{\xi}$ is perpendicular to \vec{v}_0 , and if $(\vec{\xi}, \tilde{\mathbf{v}}) \approx c_{j\vec{\xi}}$. The second term in (2.27) must be considered if $(\vec{\xi}, \mathbf{v})|_s = const \approx c_{j\vec{\xi}}$. In this case (2.27) is satisfied on the S-surface if, for any displacement in the S-surface, the incremental change of the first term can be compensated by the incremental change of the second term. The dependence of the second term in (2.27) on an additional parameter δ enables us to achieve such compensation at any point of the S-surface, only by choosing a matching value for δ out of an interval $[-1/2q, 1/2q]$, taking advantage of the less rigid restrictions of the dispersion law $\varepsilon = \varepsilon(\mathbf{s})$ in relation to (2.28). This way the parameter δ can be considered as a function of \mathbf{s} ,

not explicitly given by relation (2.27). After conversion of (2.27) with respect to δ , we get

$$\delta = \hbar^{-1}m(\mathbf{s}, \vec{\xi})[c_{j\vec{\xi}} - (\vec{\xi}, \mathbf{v}(\mathbf{s}))]. \quad (2.30)$$

Obviously the contribution of each term in (2.27) depends on the relative orientation of $\vec{\xi}$ versus \mathbf{e} . For $\vec{\xi} \rightarrow \pm\mathbf{e}$ the first term in (2.27) will decrease, whereas for $\vec{\xi} = \pm\mathbf{e}$, only the second term remains unchanged on the S-surface, provided $\delta = \hbar^{-1}m(\mathbf{s}, \mathbf{e})c_{je}$. We must further note the possible existence of certain points on the S-surface, in the proximity of which there is a tendency for $m^{-1} \rightarrow 0$, corresponding to flex points of the function $\varepsilon(\mathbf{k})$. Then, the second term in (2.27) will become small, as the terminating values of δ cannot compensate for the decrease of m^{-1} . For the same reason, (2.27) cannot be satisfied in the proximity of such points, if (2.27) was obtained by a 2^{nd} order approximation of (1.9) for $\mathbf{k} - \mathbf{s}$, $\mathbf{k}' - \mathbf{s}$, so that these points have to be excluded.

As $|\delta| \leq 1/2\mathbf{q}$, the relation (2.30) defines certain limitations on the range of variation of the functions $m(\mathbf{s}, \vec{\xi})$, $\mathbf{v}(\mathbf{s})$, if certain \mathbf{q} is given. And vice-versa, if \mathbf{m} and \mathbf{v} are given, then relation (2.30) determines the lower limit of possible \mathbf{q} -values, in any point of the S-surface:

$$q \geq q_{min}(\mathbf{s}, \vec{\xi}) = 2|\delta(\mathbf{s}, \vec{\xi})|. \quad (2.31)$$

In the case of P-planes with $\vec{\xi} \parallel \mathbf{n}$ we get $(\vec{\xi}, \mathbf{v}(\mathbf{s})) = 0$. Thus from (2.30) and (2.31):

$$q_{min} = 2\hbar^{-1}m(\mathbf{s}, \vec{\xi})c_{j\vec{\xi}}, \quad (2.32)$$

where m corresponds to the $\vec{\xi}$ -component of the effective mass-tensor $m = m_{\xi\xi}^*$. For $m = (1 \div 5)m_0$ (m_0 - free electron mass) and assuming $c_{j\vec{\xi}} \sim 10^3$ m/s we get $q_{min} \sim (10^{-3} \div 10^{-2})\pi/a$. If $\vec{\xi}$ deviates from \mathbf{n} , then q_{min} decreases, depending on the magnitude of $(\vec{\xi}, \mathbf{v}(\mathbf{s})) \neq 0$. For $|\mathbf{v}(\mathbf{s})| < c_{j\vec{\xi}}$, always is $q_{min} > 0$, but for $|\mathbf{v}(\mathbf{s})| > c_{j\vec{\xi}}$, there exists one orientation \mathbf{q} for which $q_{min} = 0$. (If $|\mathbf{v}(\mathbf{s})|c_{j\vec{\xi}}^{-1} \gg 1$, then this orientation is close to \mathbf{n} but if $|\mathbf{v}(\mathbf{s})|c_{j\vec{\xi}}^{-1} \sim 1$, then it will deviate significantly). It has to be taken into account that the orientation of $\mathbf{v}(\mathbf{s})$ on the P-plane does not necessarily remain constant. In this case the reduction of q_{min} , being caused by the deviation between the $\vec{\xi}$ and \mathbf{n} , will be achieved due to the decrease in the number of inversely occupied ES-states, already being attached to a smaller region of the P-surface (related to the case $\vec{\xi} \parallel \mathbf{n}$). Thus wherever $\vec{\xi}$ is non-collinear to \mathbf{n} , the P-plane can be partitioned into sections P_i . In such cases each P_i will be associated with an individual orientation of $\vec{\xi}$. Curved P-surfaces, on the other hand, can only be considered if they can be divided into a totality of sufficiently small sections. Finally, each of them would approximate flat sections. For example, in the proximity of the hexagonal face of the 1st BZ, the shape of the P-surface is close to that of the S-surface, as shown in Fig. 2.2. On the hexagonal

face, the lines LW, which intersect the surface in regions with opposite sign of those electron group velocity components being oriented normal to the surface, belong to the P-surface. This means that those P-regions protruding from the upper side of the hexagonal surface alternate with those P-regions protruding from below.¹ It is reasonable to infer that, in the proximity of the hexagonal faces, the P-surface is divided into roughly six flat regions (with median lines LW), being projected towards those faces of the hexagonal face of the 1st BZ being limited by the lines LK, LU. The normals \mathbf{n}_j ($j = 1, \dots, 6$) to these regions are grouped in the proximity of one of the threefold axes $\langle 111 \rangle$, and the degree of deviation from \mathbf{n}_j depends on the magnitude of the velocity component \mathbf{v}_p of the electrons along the lines LW.

Now let us inspect the S-surfaces. The particularity of this case is that the first addend in (2.27) also exists when S is a plane and $\vec{\xi} = \pm \mathbf{n}$ (in the case of P-planes $(\vec{\xi}, \mathbf{v})|_p = 0$ for $\vec{\xi} = \pm \mathbf{n}$). Induced radiative transitions from states of higher energy into states with relatively lower energy correspond to such $\vec{\xi}$ pointing towards regions with increasing electronic energy. For this reason $\vec{\xi}$ must have such characteristics that the product $(\vec{\xi}, \mathbf{v}(\mathbf{s}))$ in (2.27) results into a positive quantity. According to (2.31) q_{min} depends on $\vec{\xi}$ and varies from point to point of the S-surface. Let us denote by $q_m(\vec{\xi})$ the maximal value of $q_{min}(\mathbf{s}, \vec{\xi})$, corresponding to a given $\vec{\xi}$. Among the totality of possible $\vec{\xi}$ we shall highlight those specific $\vec{\xi}$ satisfying the following conditions:

1. $(\vec{\xi}, \mathbf{v}(\mathbf{s})) \geq 0$ for the majority of points of the S-surface;
2. Maximum population difference with uniform sign at opposed sides of the S-surface;
3. Small ($\leq 10^{-1}\pi/a$) magnitudes of q_m .

It should however be noted that for a given S-surface it is possible in principle that not even a single $\vec{\xi}$ may exist for which compliance with all of these conditions would simultaneously be given at all of its points. In such cases the possibility of partitioning the S-surface into individual sectors $S^{(i)}$ with an individually assigned orientation $\vec{\xi} = \vec{\xi}_i$ should be considered. The requirement of macroscopicity $|R_{\mu\Delta}^{s(i)}(\mathbf{q}^{(i)})|$ for each of the desired $\mathbf{q} = \mathbf{q}^{(i)}$ must however presuppose the correctness of (2.27) for the majority of points of the section $S^{(i)}$ of an S-surface and can be satisfied at any point of the section for

$$q^{(i)} \geq q_m(\vec{\xi}^{(i)}). \quad (2.33)$$

For a given $\vec{\xi}^{(i)}$ the inequality (2.33) determines the minimum magnitude of the wave vector of those phonons being emitted during stimulated transitions of electrons between ES from the set $R_{\mu\Delta}^{s(i)}(\mathbf{q}^{(i)})$.

¹ We note that such characteristics of a surface are not related to a specific kind of dispersion law $\varepsilon(\mathbf{k})$, as they rather result from pure symmetry considerations [105].

It should be noted that the requirement of compliance with the conditions of equidistance (1.9) enables us to compare the S-surfaces being linked up with different \mathbf{e} and to sort out those ones which, for a given \mathbf{q} , dispose over the largest total area $\Sigma_{s(\mathbf{q})}$ of the S(\mathbf{q})-regions within the reduced sheets of the S-surface. Obviously the number of ES-pairs being active immediately after their generation in the proximity of S(\mathbf{q}) must be proportional to $\Sigma_{s(\mathbf{q})}$. Taking the spectrum (2.16) as an example, there exist for $\mathbf{e} \parallel [001]$ and $\mathbf{e} \parallel [110]$ each a planar (see sheet 2 in Fig. 2.1) and a curved (Fig. 2.3) reduced sheet of the S-surfaces, for which the vector $\mathbf{q} \parallel [110]$ is highlighted from the point of view of maximum population inversion. Now, let us compare these particular sheets of the S-surfaces. It is easy to realize that both of the requirements of maximum population inversion, for positive amount of $(\vec{\xi}, \mathbf{v})$ as well as for conservation of the sign of the population difference, are satisfied for $\vec{\xi} = \pm 1/\sqrt{2}(\mathbf{e}_1 + \mathbf{e}_2)$ in half of the section $S_{[001]}$. However, for small values of ε_1 and $q < 0, 1\pi/a$, the majority of points of this section does not satisfy Eq. (2.27). This is due to the fact that in $S_{[001]}$, the quantity $(\vec{\xi}, \mathbf{v})$ varies within the wide range between 0 and $2\sqrt{2}a\varepsilon_1$, whereas the term $m^{-1} = -\hbar^2 a^2 \varepsilon_1$ remains constant. Due to the small variations of δ (not exceeding $0, 1\pi/a$), (2.27) is valid only for a small number of points in sheet 2 of the surface $S_{[001]}$. As a result, the associated amount of pairs of equidistant states is small and would not even significantly increase with variations of $\vec{\xi}$. And vice-versa, in case of a curved surface (2.22) (see also Fig. 2.3) then (2.27) could be satisfied for the same $\vec{\xi}$ in a region being comparable with that of the sheet $S_{[110]}$ of the surface S, located within the 1st BZ. The dimensions of this region depend on ε_1 and q . The first addend in (2.27), being related to the surface (2.22), indeed vanishes for $\vec{\xi} = (1/\sqrt{2})(\mathbf{e}_1 + \mathbf{e}_2)$, while the factor $m^{-1} = -\hbar^2 a^2 \varepsilon_1 \sin^2 1/2(\eta_1 + \eta_2)$ varies. Considering that $m^{-1} \rightarrow 0$ for $(\eta_1 + \eta_2) \rightarrow 0$, we must exclude from the possible range of variables η_1, η_2 the specific range

$$|\eta_1 + \eta_2| \leq 2 \arcsin [2\hbar c_{j\vec{\xi}}(q\varepsilon_1 a^2)^{-1}]^{1/2}, \quad -|\eta_1 + \eta_2| \leq \eta_1 - \eta_2 \leq |\eta_1 + \eta_2|,$$

in which $|\delta| \geq |\delta|_{max} = q/2$. For example, taking $c_{j\vec{\xi}} = 5 \cdot 10^3$ m/s, $a = 3, 5 \cdot 10^{-10}$ m, $\varepsilon_1 = 10^{-19}$ J, we obtain $|\eta_1 + \eta_2| \leq \pi/4$ for $q = 0, 2\pi/a$, and $|\eta_1 + \eta_2| \leq \pi/2$ for $q = 0, 02\pi/a$. The results of this estimate indicate that for $S_{[110]}$, the part of the area to be excluded amounts to about 10 % in the first case and to about 30% in the second case. As the area Σ of the sheet $S_{[110]}$ is large ($\Sigma \sim 10\pi^2/a^2$), the number of equidistant pairs of states in the proximity of the sheet $S_{[110]}$ also becomes large. Thus in the case of the dispersion law defined by (2.16), and with due consideration of the conditions of equidistance, a comparison between flat and curved S-surfaces turns out in favor of the curved surfaces.

2.5 Potentially active pairs of electronic states in the electronic-spectrum of fcc iron

Within the framework of our final aim to describe the $\gamma - \alpha$ - MT, our interest will now focus on an analysis of the S-surfaces of the fcc iron lattice. A detailed analysis however appears to be difficult, as this would imply substantial knowledge on the spectrum $\varepsilon(\mathbf{k})$ as well as on the velocity-fields $\mathbf{v}(\mathbf{k})$, within a region limited by isoenergetic surfaces $\varepsilon(\mathbf{k}) = \mu \pm \Delta$. The data published in the relevant literature however only refer to symmetry lines (predominantly relating the bcc-phase of iron), whereas data on the velocity field are totally missing. Thus it would be reasonable to investigate to which extent the results obtained for the model spectrum (2.16) can be used further. Above all we have to remark that all symmetry planes of the reciprocal lattice: $k_i \pm k_j = 4\pi m/a$ are S-planes, independent of the underlying spectrum $\varepsilon(\mathbf{k})$. Yet any of the S-planes corresponds to a vector \mathbf{e} , oriented in the normal of the plane. This immediately follows from symmetry considerations. The velocity \mathbf{v} , being an invariant with respect to reflective transformations in the symmetry-plane, can't feature a non-vanishing component oriented normal to the symmetry-plane and thus must completely lie within the symmetry-plane. Based on this consideration it can be concluded that the reduced sheet 1 of the surface $S_{[001]}$ (see Fig. 2.1) at $\mathbf{e} \parallel [001]$ also remains conserved for the $\varepsilon(\mathbf{k})$ -spectrum of iron. However, there exist no reasons to surmise that the reduced sheet 2 of this surface maintains its shape. Even the slightest modification of the dispersion-law (2.16):

$$\varepsilon = \varepsilon_0 - 2\varepsilon_1 \sum_{ij} (1 - \delta_{ij}) \cos \eta_i \cos \eta_j + 2\varepsilon_2 \sum_i \cos 2\eta_i \quad (2.34)$$

taking into account the interaction with the second neighbor from [104], results into a curved sheet 2, associated with an expansion of its area. Depending on the sign of ε_2 , the curvature of sheet 2 will take shape within the 1st Brillouin-Zone (1st BZ) for ($\varepsilon_2 > 0$), or be oriented towards the faces of the 1st BZ for ($\varepsilon_2 < 0$), as shown in Fig. 2.5. Thus the flattening of sheet 2 follows from particularities of the dispersion law. It can further be stated for the iron spectrum that sheet 2 will intersect the hexagonal surfaces of the 1st BZ in the same horizontal WLW-lines as sheet 2 in figs. 2.1 and 2.5. Symmetry considerations in fact lead to the conclusion that the velocity \mathbf{v} is oriented along the lines WL (as well as WX), i.e., $\mathbf{v}|_{WLW} \perp \mathbf{e} \parallel [001]$, whereas the horizontal lines WLW belong to sheet 2 of surface $S_{[001]}$. In the case of an iron spectrum, the intersecting region of sheet 2, comprising the square surfaces of the 1st BZ $k_1 = 2\pi/a$, $k_2 = 2\pi/a$ can only go along the line WXW if the dispersion ε vanishes in the lines WX, in the same way as for the spectrum (2.16), or in other words, if the velocity vector \mathbf{v} vanishes along these lines. Otherwise the intersection would be located either along the curved line Λ , being defined by the requirement $(\mathbf{v}, \mathbf{e})|_{\Lambda} = 0$, as shown in Fig. 2.5a, or in

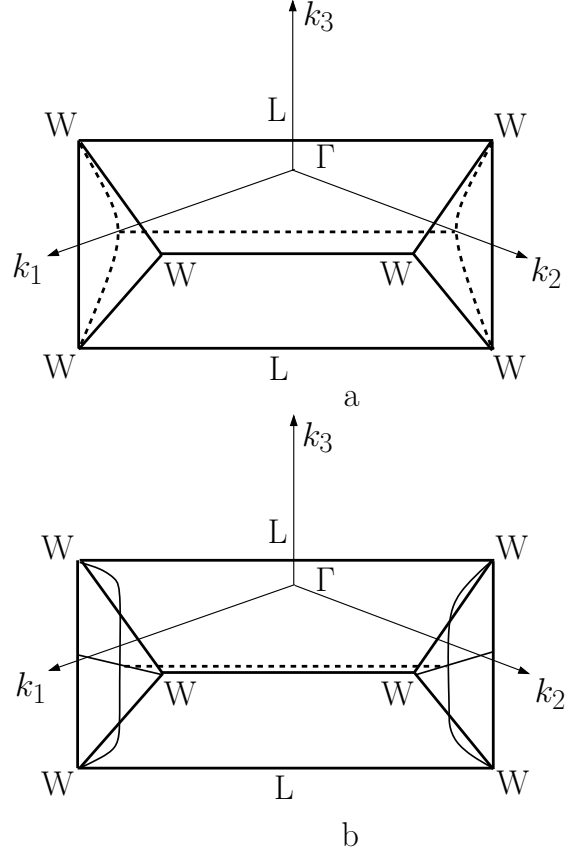


Figure 2.5. View of reduced curved sheets 2 of the surface $S_{[001]}$ for the spectrum (2.34): a - Parameter $\epsilon_2 > 0$; b - Parameter $\epsilon_2 < 0$. The intersection of surface $S_{[001]}$ with the plane $k_3 = 0$ is shown by the horizontal dashed line.

singl points W, as shown in Fig. 2.5b. We emphasize that from the point of view of materialization of a maser-effect the curved sheets 2 imply a promising advantage over the flat sheets. The ES-pairs located in the proximity of the flat sheets 2 cannot contribute to the generation of phonons with $\mathbf{q} \parallel [001]$, as they don't feature inverted populations in this direction, and for $\mathbf{q} \parallel [110]$, their contribution would only be small, as already mentioned. This means that for $\mathbf{q} \parallel \mathbf{e} \parallel [001]$ and flat sheets 2 only ES-pairs located in the proximity of the flat sheets 1 would have the potential to actively contribute to phonon generation. However, in the case of curved faces 2, phonon generation with $\mathbf{q} \parallel [001]$ would not be generally forbidden. Therefore, an appreciable increase of the number of ES-pairs being active during phonon generation with $\mathbf{q} \parallel [001]$ can be expected, if compared with the spectrum (2.16).

For $\mathbf{e} \parallel [111]$, the shape of the reduced sheet of surface $S_{[111]}$, as shown in Fig. 2.5, must not differ appreciably from the reduced sheet of surface $S_{[111]}$ of the iron spectrum $\varepsilon(\mathbf{k})$. This way the lines WLW at the hexagonal face of the 1st BZ, and the lines UXU at the square faces of the 1st BZ will also belong to the surface

$S_{[111]}$ of iron, as the velocity there is oriented perpendicular to $[111]$, due to the symmetry requirements. It should also be noted that the aforementioned remarks on the intersecting lines of face 2 of surface $S_{[001]}$ with the square surface of the 1st BZ also apply to the allocation of lines WXW to surface $S_{[111]}$.

For spectrum (2.16) and for that of iron at $\mathbf{e} \parallel [110]$, the common features of the reduced sheets of the surface $S_{[110]}$ are the vertical lines WXW, being located on the square faces of the 1st BZ, $\mathbf{k}_1 = 2\pi/a, \mathbf{k}_2 = 2\pi/a$, and the horizontal lines WLW located on the hexagonal surfaces of the 1st BZ, being an immediate result of the orthogonality relation for the velocity $\mathbf{v} \perp [110]$ in these lines. It will however be necessary to specify the intersection lines of the surface $S_{[110]}$ with the horizontal square surfaces of the 1st BZ (in the same way as in the previous cases), as well as the location of the lines WAW (see Fig. 2.3).

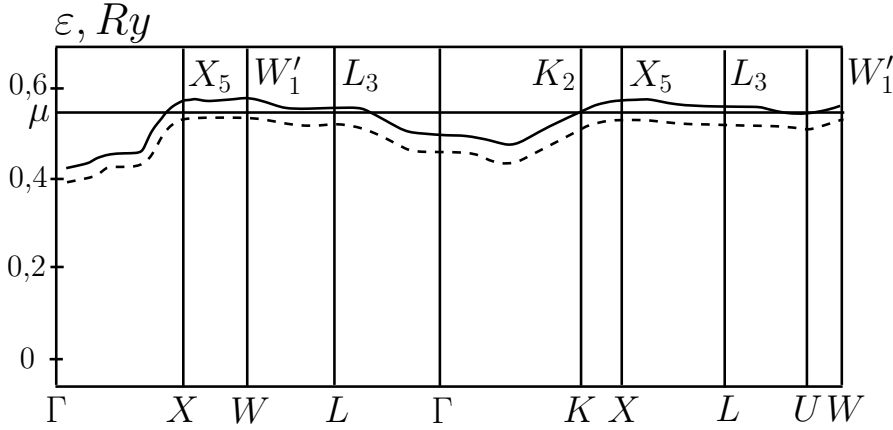


Figure 2.6. Extract of the calculus in $[110]$ of the dispersion curves of ferromagnetic nickel with fcc lattice. The solid lines indicate spin-down states, dashed lines spin-up states, $\mu =$ Fermi-energy.

Let us now deal with questions related to the possible existence of electronic bands in the energy-spectrum of fcc iron, featuring weak dispersion at the reduced sheets of the S-surfaces, which at the same time dispose of an acceptable energetic interval $\Delta \sim 0,2\text{eV}$ in the proximity of the Fermi-energy μ , in accordance with inequality (2.25). As the bcc lattice modification of iron predominates in the temperature range between 0 and 1183 K, most calculus related to structure deal with this modification. Nonetheless, the results published in [106–109], dealing with the energy spectrum of the fcc lattice modification of iron [106, 107], as well as with nickel in [108–110], will enable us to answer the first part of the question. The similarity between the energy spectra of iron and nickel, becoming evident from a comparison of the results in [107] for spin-up sub-bands with the results in [108–110], enables us to use the more comprehensive calculus of [110] for Ni, with the aim to reveal those bands featuring a weakly pronounced dispersion. Figure 2.6 shows data published in [110], related to those branches of the ε_{L_3} energy spectrum featuring the weakest dispersion of the lines corresponding to the

above discussed S-surfaces. As can be seen in Fig. 2.6, the energy along the lines LW, LU and LX is close to ε_{L_3} , and along the line XW is close to ε_{X_5} . According to [106], the difference between the energies $\varepsilon_{X_5} - \varepsilon_{L_3} \approx 0,02Ry \approx 0,27 \text{ eV}$. (It should be noted that in [106] only the curves $\varepsilon(\mathbf{k})$ for the γ -phase of iron along $\Gamma X, \Gamma L, \Gamma K$, as well as the term - energies in the points Γ, X, K, L are presented).

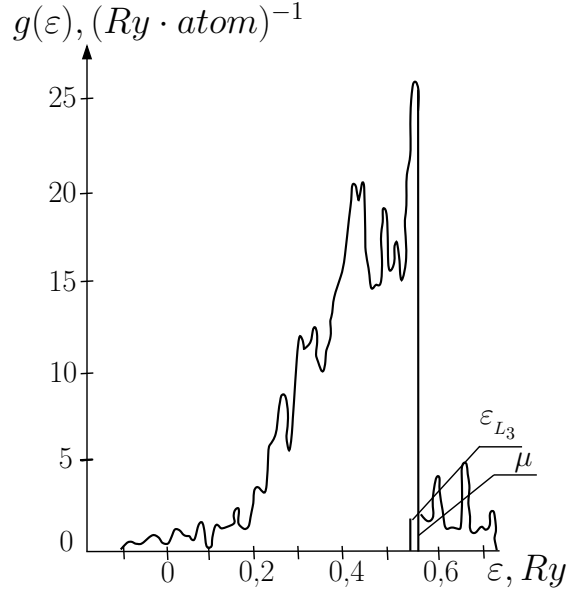


Figure 2.7. Density of states (DOS) for the non-magnetic state of nickel with fcc-lattice [110]. The loci of the Fermi-energy μ and of the energy ε_{L_3} are labeled.

Thus it can be inferred from the available details of energy spectra that there is an appreciable probability for the existence of S-surfaces with weak energy dispersion.

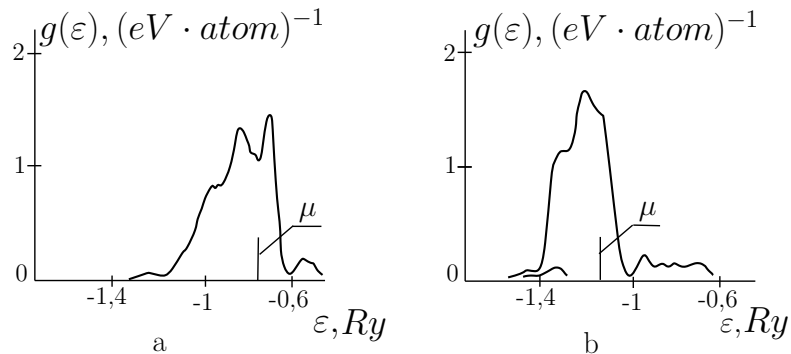


Figure 2.8. DOS-functions of iron with fcc-lattice from [111], for two different electronic configurations of the iron atoms: $a - 3d^74s^1$; $b - 3d^64s^2$

The second part of our question will be more difficult to answer: Which are the mutual arrangements of the energy level μ and of the energies $\varepsilon(\mathbf{s})$ on the S-

surfaces or, put in another way: How can the size of the interval $\Delta = |\mu - \varepsilon|$ be unambiguously determined on the basis of existing calculations of electronic spectra, with a required precision of at least $\leq 0,1\text{eV}$. If we denote by ε_{L_3} the spatial average energy on the S-surface, then we will note from the calculus in [108–110] that ε_{L_3} is localized in the peak area of the DOS $g(\varepsilon)$, whose energy is close to the top of the 3d-band, as shown in Fig. 2.7. Provided the electronic configuration is known, and after having determined the location of μ , it would be reasonable to assume $\Delta = \varepsilon_{L_3} - \mu$. However, the precise electronic configuration of iron atoms in the solid (metallic) state is not precisely known and the quantity $\varepsilon_{L_3} - \mu$ varies significantly with changes in the electronic distribution between the 3d and 4s states. In figure 2.8, which has been extracted from [111], the characteristics of the curves $g(\varepsilon)$ are compared for the $3d^7 4s^1$, $3d^6 4s^2$ configurations. The change of configurations is associated with a reduction of the difference between the peak-energies $\varepsilon \approx \varepsilon_{L_3}$ (in the proximity of the top of the d-band) and μ from $\approx 0,6\text{ eV}$ down to $\approx 0,2\text{ eV}$. In the last case, the peak degenerates to a step like shape. The intermediate configuration $3d^{6,5} 4(sp)^{1,5}$ of the γ - and α -phases of iron has been used in [112]. (However an explicit form of the $g(\varepsilon)$ is not presented in [112]).

It should be noted here that the results of the calculated configurations ($3d^{9,4} 4s^{0,6}$ in [108,109] and $3d^{8,6} 4(sp)^{1,4}$ in [110]) differ appreciably for the fcc modification of Ni. If preference was given to the self-consistent calculus in [110,112], then the configurations $3d^{6,5} 4(sp)^{1,5}$ for Fe and $3d^{8,6} 4(sp)^{1,4}$ for Ni would be in harmony with the lemma of increased probability of population of states with a fraction of s-electrons, during passage from the elements of the mean of the 3d-group towards its end [113]. A value of $\Delta = \varepsilon_{L_3} - \mu \approx 0,4\text{ eV}$ can be expected, which would be intermediate in relation to the $\Delta = \varepsilon_{L_3} - \mu$, for the configurations $3d^7 4(sp)^1$, $3d^6 4(sp)^2$.

One point however, being related to the vague interpretation of paramagnetism of the γ - phase of iron, is important enough to deserve a remark: Experimental results published in [114,115] clearly show that the magnetic susceptibility of the γ - phase is less by a factor of about $1.5 \div 2$ in comparison with that of the α - or δ -phase and, moreover, does not obey to the Curie-Weiss law [62]. In [62], these facts are reasonably explained by the Pauli-characteristics (including exchange amplification) of the paramagnetism of the γ - phase. In contrast, the experimental results of diffuse magnetic neutron scattering published in [116,117] provide clear evidence of a remarkable amount of magnetic moment density in the γ - phase (being of an order of magnitude of Bohr's magneton μ_B per atom). As stated in [62], it is possible to interpret these observations without contradiction by the theory of spin-fluctuations, stating that the average spin-moment of a given "knot" vanishes, due to permanent statistical fluctuations, and thus cannot be observed or derived from magnetic susceptibility measurements under static conditions. However, if the measurements are performed at a timescale being comparable with the average lifetime of these fluctuations (like neutron diffraction), then the spin moment fluctuations can clearly be observed.

In a paramagnetic state, the existence of disordered local magnetic moments of finite magnitude implies that the local DOS varies from point to point, with the same probability for a spin-up or a spin-down condition of a spin-polarized state. Thus, in such cases there must also exist spin-up \uparrow and spin-down \downarrow states located on S-surfaces, with identical difference $\Delta = |\varepsilon(\mathbf{s}) - \mu|$. As described in [118], the average DOS is broadened and characterized by displaced and diffuse peaks of the DOS function, if compared with a ferromagnetic (or non-magnetic) state.

We should also recall that in [119, 120], the existence of two atomic states (γ_1 and γ_2) of iron in the γ -phase has already been hypothesized, essentially stating that a γ_1 state coexists with a smaller atomic volume V_1 and a smaller magnetic moment, together with a γ_2 state characterized by a relatively larger atomic volume $V_2 > V_1$ and larger magnetic moment. In [107, 112, 121, 122] (see also [123]), this hypothesis received some verification within the frame of the simple Stoner-model. As has been shown therein, for an existing exchange-splitting of the bands into

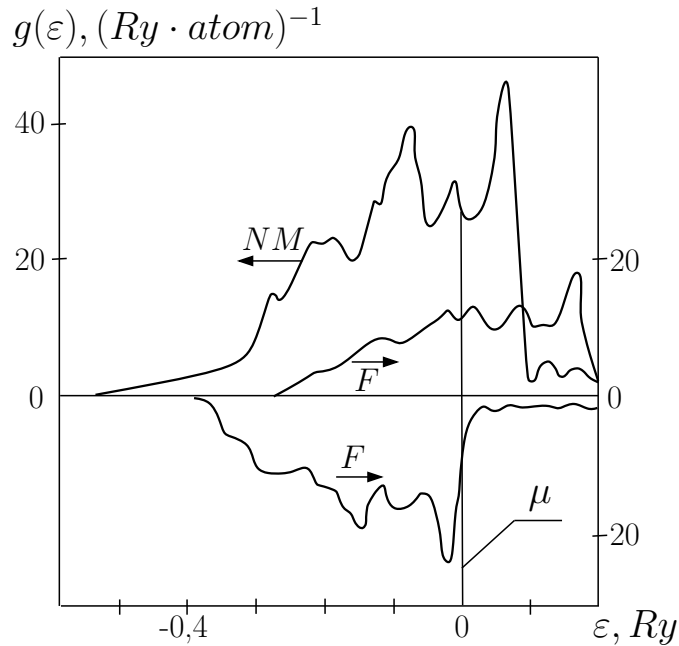


Figure 2.9. DOS-functions of iron with fcc-lattice. NM - non-magnetic state, F - ferromagnetic state (lower curve - spin-up, upper curve - spin-down) [122]

spin-up \uparrow and spin-down \downarrow sub-bands, together with the assumption of steady increases of the lattice parameters at certain $a = a_0$ ($a_0 \approx 3,58 \text{ \AA}$ in [122] and $3,63 < a_0 < 3,71 \text{ \AA}$ in [107]), a stable ferromagnetic state with a magnetic moment of $(2,3 \div 3)\mu_B$ per atom will arise, being separated from states with vanishing magnetic moment by an energy gap of 0.1 eV [112] (in [120] an energy-gap of 0,037 eV is given). In Fig. 2.9, borrowed from [122], both the DOS functions $g(\varepsilon)$ of the non-magnetic and of the spin-polarized state are shown for $a \approx a_0$. Obviously, the peak of the nearly filled spin-up \uparrow sub-band is located below the Fermi-level,

in the proximity of μ , $\mu - \varepsilon_{L3\uparrow} \approx 0,2$ eV. If we took the location of μ between two large peaks of the DOS function $g(\varepsilon)$ of the non-magnetic state as a criterion for selection of the electronic configuration, then the electronic configuration of iron would be near the $3d^7 4s^1$ configuration (as can be confirmed by comparison with Fig. 2.8a). However, due to the existence of exchange-splitting, the values of the parameters $\Delta \sim 0,2$ eV are also possible for this configuration. It should be noted that the value $\varepsilon_L - \mu \approx 0,78$ eV for the non-magnetic state of the γ -phase (published in [122]) is larger than the corresponding value of 0,6 eV published in [111].

As the martensitic transformation temperature M_S of pure iron (or of iron with small content of nickel or carbon) is $M_S \sim 10^3$ K, it would be possible for the iron atoms to simultaneously coexist in both states γ_1 and γ_2 , with the same probability at $T \sim M_S$. If we assigned to the state γ_1 the configuration $(3d \uparrow)^3(3d \downarrow)^3(4sp)^2$, which does not feature a local magnetic moment, and to the state γ_2 the configuration $(3d \uparrow)^5(3d \downarrow)^2(4sp)^1$, featuring an atomic moment of $3\mu_B$, as surmised in the modified Weiss-pattern [124], then the states located above and below the Fermi-level μ , being linked up with the γ_1, γ_2 - states of iron, would be interchangeable on the S-surfaces (with values $\Delta \sim 0,2$ eV).

On the basis of energy spectrum calculus however, substantial difficulties arise in unambiguously determining both the magnitude and the sign of the chemical potential difference $\mu_\alpha - \mu_\gamma$ of the electrons in the α - and γ - phase (Let's remind that the specified difference is the significant characteristic of a non-equilibrium condition of an electronic system). According to [111], the chemical potentials of non-magnetic phases are practically indistinguishable in the configuration $3d^7 4s^1$. For the configuration $3d^6 4s^2$, a value of $\mu_\alpha - \mu_\gamma \approx -0,2$ eV is proclaimed. However, the calculus in [125], which was performed by the cluster method (for the configuration $3d^6 4s^2$), delivered $\mu_\alpha - \mu_\gamma \approx +0,2$ eV, the sign thus being opposed to the aforementioned sign. However, it should be remarked that the limitation to three regions of nearest neighbors, used in [125], presumably is inadequate for a sufficiently precise evaluation of the small difference $\mu_\alpha - \mu_\gamma$. Thus the calculus by the augmented plane wave method in [111] should be given preference.

There still remains one unconsidered aspect: During the $\gamma - \alpha$ - MT (with exception of Fe-Ni alloys with a Ni-content of > 30 %), the MT is associated with a transition from the paramagnetic γ - into the ferromagnetic α - phase (we recall that the Curie-temperature $T_c = 1041$ K of the α - phase of iron is higher than the M_S temperature at the onset of a martensitic transformation). This means that μ_γ of paramagnetic and μ_α of ferromagnetic iron must be compared among themselves. Estimates in [118], based on a DOS model, indicate that during the process of ferromagnetic ordering, the magnitude of μ_α decreases, that would be an argument in favor of a negative sign of the difference $\mu_\alpha - \mu_\gamma < 0$. Of course this question could most easily be resolved by a proper experimental method, taking advantage of the fact that the large temperature hysteresis between martensitic transformations of Fe-Ni alloys and their reverse transformation (see Pt. 1.2)

enables us to measure the difference of the contact potential at one and the same temperature between a sample which has undergone practically the total $\gamma - \alpha$ - MT (as with Fe-Ni alloys containing up to 28 % Ni), and an austenitic sample of same composition. In our further evaluations, a value of $\mu_\alpha - \mu_\gamma = -0,16$ eV will generally be assumed. This latter value was determined under adequate consideration of the volume-effect of the MT, as described in Pt. 1.5. A more detailed treatment of this question will be resumed under Pt. 4.5.3.

Some additional remarks

1. In addition to the ES with least dispersion (see Fig. 2.6), there may also exist active ES belonging to other energy bands. For example, in the proximity of point X, potentially active ES are those associated with point X_2 and energies $\varepsilon_{X_2} \approx \varepsilon_{L_3}$.
2. From the point of view of compliance with the energetic criterion (2.25), a curvature of sheet 2 of surface $S_{[001]}$ oriented towards the faces of the 1st BZ, would be more favorable (see Fig. 2.5b), as on the one hand, the dispersion along line ΓK is remarkably pronounced, and on the other hand, a curvature towards the center of the 1st BZ (see Fig. 2.5a) would come into conflict with the conditions implied by (2.25), for the largest part of sheet 2, and would thus finally lead to a contraction of the region adjacent to lines LWL.
3. A weak dispersion $\varepsilon(\mathbf{k})$ (comparable with the dispersion of the phonon-branches) in the essential sections of lines LW and LV of the P-surfaces in the proximity of the hexagonal Brillouin-faces (as well as for similarly shaped $S_{[111]}$ surfaces) opens up the possibility for participation of ES-pairs - being mutually separated by these surfaces - on the generation of long-wave phonons with quasi-momentum $\hbar\mathbf{q}$, whose orientation would significantly deviate from the threefold axes of symmetry $[111]$ towards the twofold axes of symmetry $[\bar{1}10]$, $[10\bar{1}]$, $[0\bar{1}1]$ (also see the remarks following (2.31) of Pt. 2.4). We also remind that the component of electron group velocity being oriented normal to the P-surface would vanish by definition of (2.8). This in turn implies that the non-equilibrium addends relating to the occupation of states on both sides of a P-plane would essentially be proportional to the projection of \mathbf{e} (\mathbf{e} - orientation of spatial inhomogeneity) onto the normal \mathbf{n} of the P-plane. In contrast to the S-surfaces, which vary with variations of the orientation of \mathbf{e} , the P-planes are independent of \mathbf{e} . Thus only the magnitude of occupational inversion would depend on \mathbf{e} . Therefore it will be necessary to correct our conclusions initially inferred from the analysis of ES located in the proximity of S-surfaces, if they should also apply to ES-pairs located in the proximity of flat (or nearly flat) sections of P-surfaces. To take an example: Instead of the generation of phonons with quasi-momenta $\mathbf{q} \parallel \langle 110 \rangle$ strictly aligned with twofold axes of symmetry, which would be most

obvious due to the extensiveness of the $S_{\langle 110 \rangle}$ surfaces (see Fig. 2.3), there must be expected a deviation of \mathbf{q} with respect to the axis $\langle 110 \rangle$. As the area Σ of the reduced S-surfaces steadily changes with varying \mathbf{e} , a deviation of \mathbf{e} from the axis $[110]$ by a small angle of let us say 10° , ($\mathbf{e} \parallel [11\eta]$, $\eta \approx 0,3$) could not significantly diminish the area of the reduced surface $S_{[11\eta]}$, if compared with $S_{[110]}$. The additional contribution to the generation of phonons with $\mathbf{q} \parallel [11\eta]$ comprises about one sixth of the ES-pairs located in the proximity of the P-planes, in the surroundings of the hexagonal faces of the 1st BZ with normal vectors \mathbf{n} oriented parallel to $[\bar{1}11]$, $[1\bar{1}1]$, corresponding to areas of P-planes $\sim 2\sqrt{3}(\pi/a)^2$, thereby not only compensating for the losses but leading to a surplus of area. This means that a consideration of ES located in the proximity of P-planes ensures a low generation threshold for waves whose wave-vectors \mathbf{q} lie within orientations confined by a cone centered around $[110]$, with respect to the threshold for $\mathbf{q} \parallel [110]$. The deviation of \mathbf{q} from $[110]$ will however be essential for an interpretation of the particularities of the morphology of the product of the $\gamma - \alpha$ -MT (see Chap.5), as well as for any reasoning about the actually occurring choice of the pathway of a martensitic reaction.

4. The conclusion on the existence of S-surfaces with weak energy dispersion in the proximity of values $\varepsilon = \varepsilon_L$ means that the shape of the isoenergetic surface $\varepsilon = const \approx \varepsilon_{L_3}$ must be more or less akin to the shape of the S-surfaces. As in the case of ferromagnetic Ni discussed in [108]- [110], the location of the Fermi-level with partially filled minority sub-band (electron spin-down \downarrow oriented against the orientation of the magnetic field) is close to the energies $\varepsilon_{L_{3\downarrow}}$ ($\varepsilon_{L_3} - \mu \approx 0,3$ eV), the method of Fermi - surface calculus can be used. In Fig. 2.10, the intersections extracted from [109] are depicted (see also [126]) and the overview of the sheet corresponding to the d-like sheet of the Fermi-surface in [127] (5β in accordance with the designations used in [109]). Obviously, the curved surface pronouncedly protrudes towards the orientation of the WKW-rib of the 1st BZ. Thus condition (2.25) is satisfied for the similarly curved sheet 2 of surface $S_{[001]}$. In \mathbf{k} -space, the sheet of the Fermi-surface is more remotely located from sheet 1 of the $S_{[001]}$ surface than from sheet 2, featuring the shape of a double-saddle in the region opposite the square surface of the 1st BZ. Obviously with increasing energy, the isoenergetic surface will come closer to the faces of the 1st BZ, which in turn will enhance the effectivity of those ES-pairs being located in the proximity of the vastly extended curved surfaces $S_{[110]}$, $S_{[111]}$ (see also Figs. 2.2, 2.3).

2.6 Summary of Chapter 2

A consideration of the crucial conditions for phonon generation to be satisfied by a radiative electronic sub-system led us to the following conclusion: Potentially active ES in \mathbf{k} -space are localized near regions of S-surfaces being limited by isoenergetic surfaces $\varepsilon(\mathbf{k}) = \mu \pm \Delta$. In \mathbf{k} -space such S- surfaces separate ES with the opposite signs of group velocity projections $\mathbf{v}(\mathbf{k}) = \hbar^{-1} \vec{\nabla}_{\mathbf{k}} \varepsilon(\mathbf{k})$ on the direction of the local spatial inhomogeneity \mathbf{e} .

Even if the dispersion law $\varepsilon = \varepsilon(\mathbf{s})$ on the S- surface was arbitrarily chosen, the conditions for inversely occupied and equidistant ES-pairs would still demand a slow rate of change of the electron energy on the S- surfaces, hence satisfying the inequalities (2.25) for the macroscopic majority of points on the S- surface. It can thus reasonably be expected for systems with high density of electron states in the proximity of the Fermi-level to satisfy this requirement. Those S- surfaces (as well as the associated orientations of \mathbf{e}) for which the greatest part of their area is located within the 1st Brillouin-Zone (BZ) (for reduced sheets) are highlighted, as they correspond to (2.27) and, at the same time, satisfy the requirement of sign invariance of the population difference of ES associated with a given pair \mathbf{k}, \mathbf{k}' , where a phonon-wave-vector \mathbf{q} connects the pair of points defined by \mathbf{k}, \mathbf{k}' , at opposed sides from S. The quantity \mathbf{q} is limited from below, where the minima of \mathbf{q} are mainly determined by the characteristics of the group-velocities $\mathbf{v}|_s$, as well as by the inverse effective masses $m^{-1}|_s$ on the S- surfaces (note that the inverse effective masses are essentially independent of the orientation of \mathbf{q} , see eq.(2.27)). For $\mathbf{q} \parallel \mathbf{e}$, the smallest value of $q = q_{min}$ attains an order of magnitude of $(10^{-3} \div 10^{-2} \pi/a)$.

As the vast majority of points of the reduced sheets of the S-surfaces are located within the 1st BZ, and not at its boundaries, the elementary processes of phonon-emission with wave-vectors $q \geq q_{min}$ can be regarded as N-processes, as they are determined by electronic transitions of the type $\mathbf{k} \rightarrow \mathbf{k}'$ being localized in the proximity of the S- surfaces. Thus, under the pronounced non-equilibrium conditions locally prevailing in a $\gamma - \alpha$ - MT region, there will predominantly be emitted or amplified longitudinal (or quasi-longitudinal) phonons, as both the scalar products $(\mathbf{e}_q, \mathbf{q})$, and the matrix-elements (2.4) of electron-phonon-interaction would vanish for pure transversal waves related to N-processes.

The emission of phonons with \mathbf{q} vectors collinear with \mathbf{e} becomes most probable under condition of maximum population inversion. Using the conservation law of quasi-momentum (1.9) and the non-equilibrium addenda, to the electronic distribution function expressed in (2.5), (2.6), it is easy to find the relative orientation of \mathbf{q} and \mathbf{e} according to the sign of the expression $m^{-1}|_s, (\varepsilon - \mu)|_s$ on the S-surface, for two different sources of non-equilibrium. Table 2.1 shows the relative orientation between \mathbf{q} and the unit vectors defined by $\mathbf{e} \parallel \mathbf{e}_T \parallel \vec{\nabla} T, \mathbf{e} \parallel \mathbf{e}_\mu \parallel \vec{\nabla} \mu$. Positive $m^{-1}|_s \rightarrow (+)$ correlate with the points of minimum, while negative $m^{-1}|_s \rightarrow (-)$ correlate with the points of maximum of the function $\varepsilon(\mathbf{k})$ on the S-surface. For

example, for $m^{-1}|_s < 0 \rightarrow (-)$, $(\varepsilon - \mu)|_\varepsilon > 0 \rightarrow (+)$, $\mathbf{e} \parallel \mathbf{e}_\mu$ in Table 2.1 we get $\mathbf{q} \uparrow\uparrow \mathbf{e}_\mu$. The latter statement means that for $\mu_\alpha < \mu_\gamma$, there will be generated (or amplified) the longitudinal waves propagating from the growing martensite crystal (into the austenite area being free from martensite). Thus it can also be concluded from Table 2.1 that for $\mathbf{e} = \mathbf{e}_\mu$ the relative orientation of \mathbf{q} and \mathbf{e} is independent of the sign of the term $(\varepsilon - \mu)|_s$, whereas such a dependence does exist for $\mathbf{e} = \mathbf{e}_T$. This latter conclusion immediately results from the consideration that for $\nabla\mu \neq 0$, there must exist an electron flow oriented from regions with relatively larger chemical potential μ towards regions with lower μ (thus being linked up with charge transfer), while for $\nabla T \neq 0$, there must exist two mutually opposed electron flows of equal density, however not contributing to effective charge transfer in that region (see also the legend to Fig. 1.8).

Table 2.1. Orientation of the wave-vectors of generated phonons relative to the orientation of spatial inhomogeneity

$(\varepsilon - \mu) _s$	$m^{-1} _s$	
	+	-
+	$\mathbf{q} \downarrow\uparrow \mathbf{e}_T$	$\mathbf{q} \uparrow\uparrow \mathbf{e}_T$
	$\mathbf{q} \downarrow\uparrow \mathbf{e}_\mu$	$\mathbf{q} \uparrow\uparrow \mathbf{e}_\mu$
-	$\mathbf{q} \uparrow\uparrow \mathbf{e}_T$	$\mathbf{q} \downarrow\uparrow \mathbf{e}_T$
	$\mathbf{q} \downarrow\uparrow \mathbf{e}_\mu$	$\mathbf{q} \uparrow\uparrow \mathbf{e}_\mu$

Considering that $T_\alpha > T_\gamma$ and bearing in mind that $\mu_\alpha < \mu_\gamma$, (see also final statement of Point (2.5)) the anti-parallelism of \mathbf{e}_μ and \mathbf{e}_T becomes evident. Then the effect of the sources of non-equilibrium for the states with $(\varepsilon - \mu)|_s > 0$ will partially be counterbalanced (in that the non-equilibrium addenda of (2.5) and (2.6) are mutually subtracted), whereas they will mutually be amplified for $(\varepsilon - \mu)|_s < 0$ (i.e. the non-equilibrium addenda of (2.5) and (2.6) add up). Of course, during the process of generation and amplification of longitudinal waves propagating ahead of the growing martensitic phase, the dominating quantity is the inhomogeneity (gradient) of the chemical potential μ and not the temperature gradient $\vec{\nabla}T$. This conclusion is evident as the order of magnitude of the difference $\mu_\alpha - \mu_\gamma = -0,16\text{eV}$ is about one order of magnitude greater than that of the temperature difference $T_\alpha - T_\gamma$ (after the temperature is adequately converted into its energy equivalent). Following an evaluation of our electronic band-analysis under Point 2.5 it appears to be most likely that the value of the parameter Δ is approximately some tenths of eV for fcc-iron lattice, and that ES-pairs in the proximity of the surfaces $S_{[001]}$, $S_{[110]}$, $S_{[111]}$ can be active during the generation of longitudinal phonons with orientations \mathbf{q} in the proximity of symmetry axis.

The most important results of our analysis of electronic spectra under the particular aspect of the general requirements for realization of a phonon maser are

published in [55, 88, 89, 128–130].

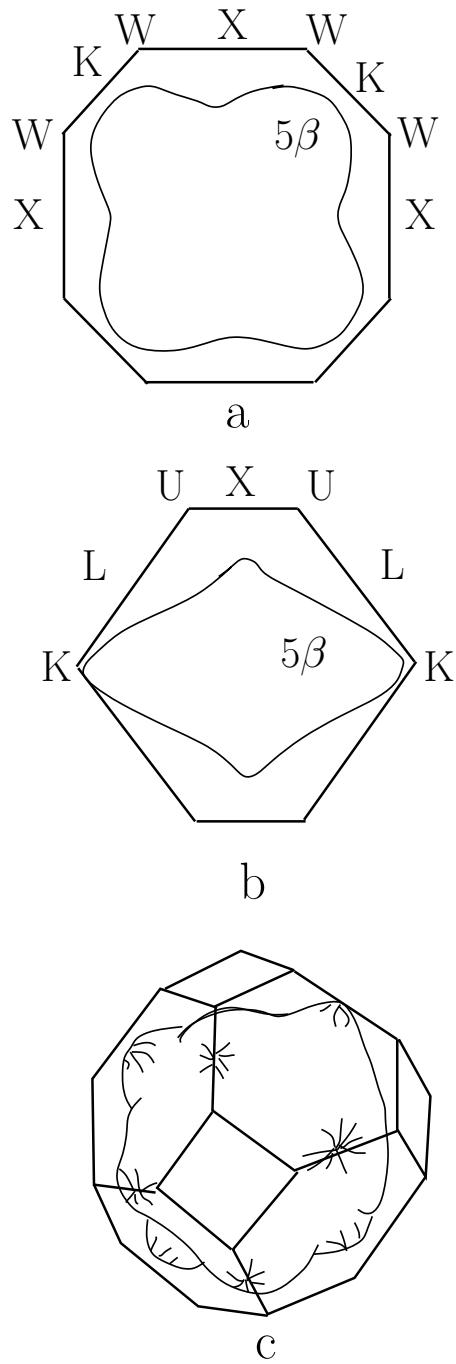


Figure 2.10. Sheet of the d-like band (5β with spin-down) for Ni with fcc lattice: a - sectional view by the plane (001); b - sectional view by the plane (011) [126]; c - general view [127].

Chapter 3

Constitutive equations of the electron-phonon system and the threshold wave generation conditions

The theoretical finding of pairs of electronic states with the inverted population (see the previous chapter) is the most essential stage in our aim to disclose the phonon-generation mechanism. Next it is necessary to get a determination of the physical conditions required for the functioning of a phonon maser (see Sub-Pt 4 in Pt.1.5) or, put in another way, to determine the threshold value of an inverted population difference. Thanks to the already existing comprehensive theory of the maser-effect (for example in [98, 131–133]) this task does not comprise any fundamental difficulties and can thus be resolved on the basis of well-proven approaches and methods. The simplest approach is semi-phenomenological. Then the crucial interaction of a radiating sub-system (in our case the non-equilibrium 3-d electrons) with a radiating field (in our case a specific class of longitudinal phonons) has to be defined as precisely as possible, while the creation of the inverted population (i.e. the pumping), as well as dissipation processes, are treated by a phenomenological method.

3.1 Threshold conditions for single-mode generation

Following [132, 133] we shall start with a brief consideration of the simplest derivation of the expression for a threshold-difference of population (1.12), related to the case of single-mode generation. As the generation of phonons normally begins with that specific mode for which the required population difference is minimal, it would be reasonable to start with a consideration of single-mode generation. Thus

in this case we start with our analysis by sorting out one specific Hamiltonian H_1 from the general set of Hamiltonians 2.1-2.3 of an electron-phonon system:

$$H_1 = \hbar \omega_{\mathbf{q}} b_{\mathbf{q}}^+ b_{\mathbf{q}} + \sum_{\mathbf{p}} \varepsilon_{\mathbf{p}} a_{\mathbf{p}}^+ a_{\mathbf{p}} + \sum_{\mathbf{k}} W_{\mathbf{q}}^* b_{\mathbf{q}} a_{\mathbf{k}}^+ a_{\mathbf{k}'} + W_{\mathbf{q}} b_{\mathbf{q}}^+ a_{\mathbf{k}'}^+ a_{\mathbf{k}}. \quad (3.1)$$

Here $b_{\mathbf{q}}^+$, $b_{\mathbf{q}}$ and $a_{\mathbf{p}}^+$, $a_{\mathbf{p}}$ are the phonon and electron creation and annihilation operators, respectively, and $W_{\mathbf{q}}$ is the matrix-element of electron-phonon interaction. Then, our next step is the decomposition of the complete Hamiltonian H of our task into the sum

$$H = H_1 + H_2,$$

The Hamiltonian H_2 describes the action of other sub-systems like heat reservoirs, on the segregated system (3.1). In (3.1), we omitted the indices of bands related to electron-energies and -operators (in the case of a 3d - electron band), as well as the polarization index of phonon-energies and -operators (the polarization is supposed to be longitudinal); \hbar - Planck's constant.

In the Heisenberg-representation, the following constitutive equations of motion can be assigned to any operator x :

$$\frac{\partial x}{\partial t} \equiv \dot{x} = \frac{i}{\hbar} [H, x] = \frac{i}{\hbar} [H_1, x] + \frac{i}{\hbar} [H_2, x] \equiv \dot{x}_1 + \dot{x}_2. \quad (3.2)$$

Using the commutation rule

$$[b_{\mathbf{p}}^+, b_{\mathbf{q}}] = \delta_{\mathbf{q}, \mathbf{p}}, \quad [b_{\mathbf{q}}^+, b_{\mathbf{p}}^+] = [b_{\mathbf{q}}, b_{\mathbf{p}}] = 0$$

and the anticommutation

$$[a_{\mathbf{p}}^+, a_{\mathbf{q}}]_+ = \delta_{\mathbf{q}, \mathbf{p}}, \quad [a_{\mathbf{p}}^+, a_{\mathbf{q}}^+]_+ = [a_{\mathbf{p}}, a_{\mathbf{q}}]_+ = 0,$$

we find from (3.1) and (3.2) that the following expressions describe the phonon field operators $b_{\mathbf{q}}^+$, electron-polarization operators $d_{\mathbf{k}, \mathbf{k}'}^+ = a_{\mathbf{k}}^+ a_{\mathbf{k}'}$ and the operator of the population-difference $\sigma_{\mathbf{k}\mathbf{k}'} \equiv \sigma = a_{\mathbf{k}}^+ a_{\mathbf{k}} - a_{\mathbf{k}'}^+ a_{\mathbf{k}'}$ (where \mathbf{k} , \mathbf{k}' correspond to those used in (1.9)):

$$\begin{aligned} \dot{b}_{\mathbf{q}}^+ &= (i\omega_{\mathbf{q}} - \varkappa_{\mathbf{q}}) b_{\mathbf{q}}^+ + \frac{i}{\hbar} \sum_{\mathbf{k}} W_{\mathbf{q}}^* d_{\mathbf{k}, \mathbf{k}'}^+, \\ \dot{d}_{\mathbf{k}, \mathbf{k}'}^+ &= (i\omega_{\mathbf{k}, \mathbf{k}'} - \Gamma) d_{\mathbf{k}, \mathbf{k}'}^+ - \frac{i}{\hbar} W_{\mathbf{q}} b_{\mathbf{q}}^+ \sigma, \\ \dot{\sigma} &= \frac{\sigma_0 - \sigma}{t_{\sigma}} + \frac{2i}{\hbar} W_{\mathbf{q}} d_{\mathbf{k}, \mathbf{k}'} b_{\mathbf{q}}^+ - \frac{2i}{\hbar} W_{\mathbf{q}}^* d_{\mathbf{k}, \mathbf{k}'}^+ b_{\mathbf{q}}, \\ \dot{b}_{\mathbf{q}} &= (\dot{b}_{\mathbf{q}}^+)^+, \quad \hbar \omega_{\mathbf{k}, \mathbf{k}'} = \varepsilon_{\mathbf{k}} - \varepsilon_{\mathbf{k}'}. \end{aligned} \quad (3.3)$$

Here, Γ is the electron-attenuation.

Let us now discuss (3.3): As our interest is focused on the average values of the operators in (3.3), we can ignore the fluctuational action of heat reservoirs in (3.3), without introducing any significant error. Then, the effect of dissipation can be considered phenomenologically by introduction of relaxation times t_σ of electron populations, of phonon attenuation $\varkappa_{\mathbf{q}}$, and of electron attenuation Γ . (It is agreed that an attenuation Γ for the dipole - moment $d_{\mathbf{k},\mathbf{k}'}$ of transition between a pair of electronic states (ES-pair) \mathbf{k} , \mathbf{k}' , emitting phonons with the quasi-momentum \mathbf{q} , is of the same order of magnitude as the electronic states attenuations, i.e., $\Gamma \sim \Gamma_{\mathbf{k}} \sim \Gamma_{\mathbf{k}'}$); σ_0 - inverse initial population difference of states \mathbf{k} , \mathbf{k}' located on opposite sides of the S-surface, being produced by electronic flows (drift-pumping mechanism), as well as by other non-coherent processes in absence of maser radiation.

In principle, the constitutive set of equations (3.3) represents an analog to the Bloch-equations of magnetic resonance theory. This becomes obvious from [134, 135] and by comparing σ , d^+ , d with the projections of the spin-operators S^z , S^+ , S^- , and the parameters t_σ , Γ^{-1} with the longitudinal- and transversal relaxation times T_1 , T_2 , respectively. This immediately leads to the restriction (3.4) already known from [134]:

$$T_1 \geq T_2 : t_\sigma \geq \Gamma^{-1}. \quad (3.4)$$

In the phonon generation (stimulated emission) regime, the number of quanta of the mode to be emitted becomes macroscopic and the operators $b_{\mathbf{q}}^+$, $b_{\mathbf{q}}$ represent satisfactory approximations of c - number functions of time. From the above presentation it becomes obvious that, in the generation regime, the equations of the system (3.3), averaged by a density matrix of the system, are identical with the classical expressions, if all operators were replaced by their average values. In below equations, this replacement has already been considered. Hence, the previously used designations of operators now simply pertain to their averages. The oscillatory dependence on time can then simply be eliminated by adoption of the quantities

$$\begin{aligned} \tilde{b}_{\mathbf{q}}^+ &= \exp[-i\Omega_{\mathbf{q}}t] b_{\mathbf{q}}^+, & \tilde{b}_{\mathbf{q}} &= \exp[i\Omega_{\mathbf{q}}t] b_{\mathbf{q}}, \\ \tilde{d}^+ &= \exp[-i\Omega_{\mathbf{q}}t] d^+, & \tilde{d} &= \exp[i\Omega_{\mathbf{q}}t] d, \end{aligned} \quad (3.5)$$

with consideration of the case of exact resonance:

$$\hbar\Omega_{\mathbf{q}} = \hbar\omega_{\mathbf{q}} = \varepsilon_{\mathbf{k}} - \varepsilon_{\mathbf{k}'} = \hbar\omega_{\mathbf{k},\mathbf{k}'}. \quad (3.6)$$

Under stationary conditions, we get from (3.3) - under consideration of (3.5) and (3.6) - the following system of non-linear algebraic equations:

$$\varkappa_{\mathbf{q}} \tilde{b}_{\mathbf{q}}^+ - \frac{i}{\hbar} W_{\mathbf{q}}^* \sum_{\mathbf{k}'} \tilde{d}_{\mathbf{k},\mathbf{k}'}^+ = 0,$$

$$\begin{aligned}
\Gamma \tilde{d}_{\mathbf{k},\mathbf{k}'}^+ + \frac{i}{\hbar} W_{\mathbf{q}} \tilde{b}_{\mathbf{q}}^+ \sigma &= 0, \\
\Gamma \tilde{d}_{\mathbf{k},\mathbf{k}'} - \frac{i}{\hbar} W_{\mathbf{q}}^* \tilde{b}_{\mathbf{q}} \sigma &= 0, \\
\frac{\sigma_0 - \sigma}{t_\sigma} + \frac{2i}{\hbar} W_{\mathbf{q}} \tilde{d}_{\mathbf{k},\mathbf{k}'} \tilde{b}_{\mathbf{q}}^+ - \frac{2i}{\hbar} W_{\mathbf{q}}^* \tilde{d}_{\mathbf{k},\mathbf{k}'}^+ \tilde{b}_{\mathbf{q}} &= 0.
\end{aligned} \tag{3.7}$$

The stationary value of the population difference σ , being the result of a balance between gains and losses, is the threshold value σ_{th} . Assuming the existence of solutions $\tilde{b}_{\mathbf{q}}^+ \neq 0$, we find from the first of two equations of system (3.7) that

$$\sum_{\mathbf{k}'} \sigma_{th} = \frac{\hbar^2 \Gamma \varkappa_{\mathbf{q}}}{|W_{\mathbf{q}}|^2}. \tag{3.8}$$

We note that the attenuation Γ included in (3.8) represents certain mean attenuation of the dipole-moment \mathbf{d} of the pairs of state \mathbf{k} , \mathbf{k}' , being localized in the vicinity of the S-surface. It is further convenient to introduce an average value σ_{th} for those σ_{th} associated with the S-surface, by substituting in (3.8) in accordance with the mean-value rule:

$$\sum_{\mathbf{k}'} \sigma_{th} = \bar{\sigma}_{th} R_{\mathbf{q}}. \tag{3.9}$$

Here $R_{\mathbf{q}}$ - number of ES-pairs of state \mathbf{k} , \mathbf{k}' which emit phonons with quasi-momentum $\hbar\mathbf{q}$ during $\mathbf{k} - \mathbf{k}'$ transitions. As the energy of the pairs of state \mathbf{k} , \mathbf{k}' must settle within certain interval Δ (see (2.25)), the substitution in (3.9) requires from $\bar{\sigma}_{th}$ to be associated with certain constant amount of energy $\bar{\varepsilon}$ within the interval Δ : $\varepsilon - \mu \in \Delta$. This requirement is equivalent to the replacement of a non-isoenergetic S-surface by an isoenergetic one. Considering the weakly pronounced dispersion of $\varepsilon(\mathbf{k})$ near the S-surfaces, such a substitution suggests itself as natural. Using (3.9) and omitting the mean value sign (horizontal dash on top of σ_{th}) we can write (3.8) in the form

$$\sigma_{th} = \frac{\hbar^2 \Gamma \varkappa_{\mathbf{q}}}{|W_{\mathbf{q}}|^2 R_{\mathbf{q}}}. \tag{3.10}$$

It immediately follows from (3.10) that σ_{th} becomes the less, the greater: the lifetimes of the quasi-particles Γ^{-1} , \varkappa^{-1} ; electron - phonon interaction; the number of pairs of state with inverted population $R_{\mathbf{q}}$, being proportional to the area $\Sigma_{S(\mathbf{q})}$ of the reduced sheet of the S-surface.

If we express (with the aid of the last of the three Eqs. of (3.7)) the value \tilde{d}^+ by $\tilde{b}_{\mathbf{q}}^+$ and $\tilde{b}_{\mathbf{q}}$ and insert the result into the first of Eqs. (3.7), then, by consideration of (3.10), we get

$$\tilde{b}_{\mathbf{q}}^+ \left[\frac{\sigma_0}{\sigma_{th}} \left(1 + \frac{4t_\sigma |W_{\mathbf{q}}|^2}{\hbar^2 \Gamma} \tilde{b}_{\mathbf{q}}^+ \tilde{b}_{\mathbf{q}} \right)^{-1} - 1 \right] = 0, \tag{3.11}$$

with the two solutions:

$$\tilde{b}_{\mathbf{q}}^+ = 0, \quad \sigma_0 < \sigma_{th}, \quad (3.12)$$

$$\tilde{b}_{\mathbf{q}}^+ \tilde{b}_{\mathbf{q}} = \frac{\hbar^2 \Gamma}{|W_{\mathbf{q}}|^2 4t_{\sigma}} \left[\frac{\sigma_0}{\sigma_{th}} - 1 \right], \quad \sigma_0 > \sigma_{th}, \quad (3.13)$$

which clearly verify that the displacement amplitude

$$u_{\mathbf{q}} = \left[\frac{2\hbar^2}{MN\omega_{\mathbf{q}}} \right]^{\frac{1}{2}} \tilde{b}_{\mathbf{q}} \quad (3.14)$$

is vanishing below and non-vanishing above the generation threshold, thus indicating essentially classical characteristics of the displacement. In fact, it is obvious from (3.13) and (2.4) that for $\sigma_0 > \sigma_{th}$ the number of phonons $\tilde{b}_{\mathbf{q}}^+ \tilde{b}_{\mathbf{q}} \sim |W_{\mathbf{q}}|^{-2} \sim N$ becomes a macroscopic quantity. Consequently, the energy of this mode is comparable with the energy of the remaining non-coherent phonons.

In order to evaluate σ_{th} , the relaxation-parameters $\varkappa_{\mathbf{q}}$, Γ and the number of pairs of active states $R_{\mathbf{q}}$ must be known. To perform such evaluation, we can use as an upper limit of the parameters $\varkappa_{\mathbf{q}}$, Γ their respective values in the high temperature domain, where scattering by short - wave phonons predominates (i.e. where T exceeds the Debye-temperature T_D).

For an evaluation of $\varkappa_{\mathbf{q}}$, let $q \ll \pi/a$ and use the results of Woodruff-Ehrenreich (see [136]) for the case $\omega_{\mathbf{q}}\tau \ll 1$, where τ - average lifetime in the free path of thermal phonons for $T > T_D$:

$$\varkappa_{\mathbf{q}} = \frac{\lambda_l T \gamma_0^2 \omega_{\mathbf{q}}^2}{\rho c_{\mathbf{q}}^4} \equiv \frac{\pi \lambda_l T \gamma_0^2}{\rho c_{\mathbf{q}}^3 a} \left[\frac{qa\omega_{\mathbf{q}}}{\pi} \right]. \quad (3.15)$$

In (3.15), we used (4.63) of [136], after multiplication with the speed of sound $c_{\mathbf{q}}$, in order to get $\varkappa_{\mathbf{q}}$ in frequency units. In (3.15): λ_l - heat-conductivity of the lattice, γ_0 - Gruneisen-constant, ρ - density, a - lattice-parameter. In the case of fcc-iron lattice with $\lambda_l \approx 0,03\lambda_t$ (λ_t - is the total heat conductivity), $T \sim 10^3$ K, $\lambda_t \approx 34$ W/(m K) [137], $\gamma_0 = 2$, $\rho = 7900$ kg/m³, $c_{\mathbf{q}} = 5 \cdot 10^3$ m/s, $a = 3,57 \cdot 10^{-10}$ m, we get from (3.15):

$$\varkappa_{\mathbf{q}} \approx 3,5 \cdot 10^{-2} \frac{aq}{\pi} \omega_{\mathbf{q}}, \quad (3.16)$$

i.e., within our region of interest $q \sim (10^{-3} \div 10^{-2})\pi/a$, the extinction would be about $\varkappa_{\mathbf{q}} \leq (10^{-4} \div 10^{-3})\omega_{\mathbf{q}}$.

For comparison, let us now find out the extinction $(\varkappa_{\mathbf{q}})_e$ being caused by the interaction of conduction electrons. In the high temperature region, with $q \ll \pi/a$, the condition $ql_e \ll 1$ must be satisfied, where l_e - mean electron free path. Using the Pippard-Formula (8.2) in [136] we get:

$$(\varkappa_{\mathbf{q}})_e \approx \frac{4n_0m}{15\rho\tau}(ql_e)^2 = \frac{4n_0m}{15\rho c_{\mathbf{q}}}(ql_e)\omega_{\mathbf{q}}, \quad (3.17)$$

where n_0 - free electron density, m - mass, $v = l_e\tau^{-1}$ - electron velocity. Assuming that the quantities $n_0 = 8 \cdot 10^{28} \text{ m}^{-3}$, $m \approx 10^{-30} \text{ kg}$, $v \approx 10^6 \text{ m/s}$, ρ , $c_{\mathbf{q}}$ are identical with those used in (3.15), we get from (3.17):

$$(\varkappa_{\mathbf{q}})_e \approx 5 \cdot 10^{-4}(ql_e)\omega_{\mathbf{q}}.$$

In other words, for $q \sim (10^{-3} \div 10^{-2})\pi/a$ and $ql_e \approx 0, 1$, we get a result comparable with that of (3.16), being equivalent to $l_e = (100 \div 10)a$. In the high temperature region however, the value $l_e \sim 10a$ may be more realistic, therefore our estimate (3.16) would not significantly be affected by adequate consideration of $(\varkappa_{\mathbf{q}})_e$. The magnitude of attenuation of the dipole-moment Γ is reciprocal to the average lifetime τ of the states \mathbf{k}, \mathbf{k}' , or to the mean scattering period $\tau = \tau_0$, as defined in [138]. An evaluation of the quantity τ_0 however could easily be obtained if the following quantities were known: relaxation time $\tilde{\tau}$ of the electron energy in the states \mathbf{k}, \mathbf{k}' , the non-elastic relaxation coefficient δ_0 is the reciprocal number of scattering events required for the relaxation of an appreciable fraction of energy:

$$\tau_0 \equiv \frac{\tilde{\tau}}{\delta_0^{-1}}. \quad (3.18)$$

According to [138] for $T > T_D$

$$\delta_0^{-1} \approx (2N_{\mathbf{p}} + 1) \frac{|\varepsilon - \mu|}{\Delta\varepsilon} \approx \frac{2k_B T |\varepsilon - \mu|}{\hbar^2 \omega_{\mathbf{p}}^2}, \quad (3.19)$$

where $N_{\mathbf{p}} \approx k_B T / \hbar \omega_{\mathbf{p}}$ - occupancy of short-wave phonons with frequencies $\omega_{\mathbf{p}} \approx C \pi / a \approx k_B T_D / \hbar$, and $\Delta\varepsilon \approx \hbar \omega_{\mathbf{p}}$ - fraction of energy lost during non-elastic interaction (for $\varepsilon - \mu > 0$) or absorbed (for $\varepsilon - \mu < 0$). The presence of a factor $(2N_{\mathbf{p}} + 1)$ in (3.19) becomes obvious by consideration that, for large occupancies $N_{\mathbf{p}}$, the processes of induced emission and induced absorption of phonons predominate during scattering events, and "... to each $N_{\mathbf{p}} + 1$ events of emission there correspond $N_{\mathbf{p}}$ events of absorption, or, put in another way, during energy relaxation only one event will be effective out of $2N_{\mathbf{p}} + 1$ events" [138].

The effects of rapid heating of an electron-subsystem by means of short pulse of laser radiation, as reported in [139], enables us to assess $\tilde{\tau} \approx 10^{-10} \text{ s}$ for nickel, where τ is a characteristic time of electron-lattice relaxation. In this case, the role of a large heat reservoir is taken up by the short-wave phonons (which cover the maximum spectral density of states in the phonon-spectrum). Under the assumption of [139] that the most part of energy of a laser pulse is absorbed by the 3d - electrons, it would be reasonable to conclude that the scale of τ in Ni is mainly determined by those electrons with energies near the peak area of the density function, i.e. near the upper edge of the 3d - band, as the contribution of these

electrons makes up for the greatest fraction of the heat capacity of an electronic sub-system. We bear in mind that the same electronic states are considered to be active during the generation of phonons in the case of fcc-iron (see Pt. 2.5). Thus our evaluation of $\Gamma \sim \tau_0^{-1}$ can be performed with the aid of Eqs. (3.18) and (3.19), and under the assumption that in accordance with Pt. 2.5: $|\varepsilon - \mu| \sim (0, 2 \div 0, 3 \text{ eV})$ or $|\varepsilon - \mu| \sim (5 \div 8)\hbar\omega_{\mathbf{p}}$, $k_B T \approx 2, 5\hbar\omega_{\mathbf{p}}$ and $\tilde{\tau} = 10^{-10} \text{ s}$. Then we get:

$$\delta_0^{-1} \approx 30 \div 50,$$

$$\tau_0 \approx (3 \div 2) \cdot 10^{-12} \text{ s}, \quad (3.20)$$

$$\Gamma \approx (3 \div 5) \cdot 10^{11} \text{ s}^{-1}.$$

It should be noted here that the final width of the electronic energy levels at $\Gamma > \omega_{\mathbf{q}}$ enables us to use (without getting into contradiction to the conservation laws of energy and momentum) as the maximum number of electronic states $R_{\mathbf{q}}$ the quantity

$$(R_{\mathbf{q}})_{max} \approx 2q\Sigma_{\mathbf{q}}\delta^{-1},$$

$$N\delta \approx 4 \cdot (2\pi/a)^3 \sim q_{max}^3. \quad (3.21)$$

In (3.21): δ - volume of the reciprocal space covering one wave number, the factor 2 is due to the required consideration of two possible spin-orientations, $\Sigma_{\mathbf{q}}$ - area of one sector of the package of sectors oriented parallel to the reduced sheet of the S-surface, without being more distant from it in \mathbf{q} - space than one unit of quasi-momentum $\hbar\mathbf{q}$ of the generated phonons, this way ensuring the transition of electrons from the volume $\Sigma_{\mathbf{q}}q$ of the states with quasi-momenta $\hbar\mathbf{k}$ into the same volume with quasi momenta $\hbar\mathbf{k}'$, being located at opposite sides of the S-surface. Further assuming that $\Sigma_{\mathbf{q}} \approx 20(\pi/a)^2$, we get

$$\Sigma_{\mathbf{q}}\delta^{-1} = \frac{5a}{8\pi}qN, \quad R_{\mathbf{q}} = \frac{5a}{4\pi}qN. \quad (3.22)$$

This means that for $q \sim (10^{-3} \div 10^{-2})\pi/a$ the number of pairs of state being active during phonon generation is about $(10^{-3} \div 10^{-2})$ times from the total number of states $2N$. After substitution with (3.22), (3.16), (2.4) in (3.10) and using $M \approx 10^{-25} \text{ kg}$, $G \approx 10^{-19} \text{ J}$ ($G \approx 0, 6 \text{ eV}$), $\Gamma \sim (10^{11} \div 10^{12}) \text{ s}^{-1}$, we finally get $\sigma_{th} \approx 10^{-4} \div 10^{-3}$.

Using the expressions (2.5), (2.6), being related to additional non-equilibrium terms in the energy distribution of electrons, in conjunction with the energy conservation law (1.9), we can express the inverted initial occupational difference in the pattern

$$\sigma_0(\nabla T) = f_{\mathbf{k}} - f_{\mathbf{k}'} \approx \frac{y_{\mathbf{k}}}{k_B T} \left| \frac{\partial f_{\mathbf{k}}^0}{\partial y_{\mathbf{k}}} \right| \left[k_B \tau (\mathbf{v}_{\mathbf{k}'} - \mathbf{v}_{\mathbf{k}}) \vec{\nabla} T - \hbar \omega_{\mathbf{q}} \right], \quad (3.23)$$

$$\sigma_0(\nabla \mu) = f_{\mathbf{k}} - f_{\mathbf{k}'} \approx \frac{1}{k_B T} \left| \frac{\partial f_{\mathbf{k}}^0}{\partial y_{\mathbf{k}}} \right| \left[\tau (\mathbf{v}_{\mathbf{k}'} - \mathbf{v}_{\mathbf{k}}) \vec{\nabla} \mu - \hbar \omega_{\mathbf{q}} \right]. \quad (3.24)$$

Table 3.1 shows the values of σ_0 obtained for some representative $y_{\mathbf{k}} = (\varepsilon_{\mathbf{k}} - \mu)/k_B T$ (after omission of the last term in (3.23) and (3.24)), using: $T = 10^3$ K, $\nabla T = \Delta T (10 \text{ v}_{\mathbf{k}} \tau)^{-1}$, $\nabla \mu = \Delta \mu (10 \text{ v}_{\mathbf{k}} \tau)^{-1}$, $\Delta T = 100$ K, $\Delta \mu = 0,15 \text{ eV} = 1,74 k_B T$.

It is obvious from Table 3.1 that the crucial condition for excess generation of phonons $\sigma_0 > \sigma_{th}$ is easily satisfied for $\sigma_0(\nabla T)$, as well as for $\sigma_0(\nabla \mu)$, in the latter case even with an excess of the order of magnitude (since $2 \cdot 10^{-1} > \sigma_0(\nabla \mu) > 10^{-2} > 10 \cdot \sigma_{th}$). We have however to remark that for $|\mathbf{q}| \sim (10^{-3} \div 10^{-2})\pi/a$, the value of the projection $\mathbf{v}_{\mathbf{k}}$ towards the orientation given by the heterogeneity gradient attains an order of magnitude of about 10^3 m/s. At the other hand, if 10 average free path lengths of electrons of about $10 \text{ v}_{\mathbf{k}} \tau \sim 10^{-8}$ m were taken as a natural scale of the average size of an heterogeneity, and further assuming $\tau \sim 10^{-12}$ s, then we would get a length one order of magnitude less than half wavelength, as given by the expression $\lambda/2 \sim 4\pi/q \sim 10^{-7}$ m. From the point of view that a MT can be described as a diffusionless lattice deformation process, then at least $\lambda/2$ would fit into our assumed scale of the heterogeneity (see also the treatment of (1.2) in Pt. 1.3 and Sub-Pt. 7 of Pt. 1.5, as well as Chap. 6). In this case however, for an evaluation of ∇T and $\nabla \mu$, it would be more realistic to use a value of $10^2 \text{ v}_{\mathbf{k}} \cdot \tau$, instead of $10 \text{ v}_{\mathbf{k}} \cdot \tau$ (thus in this case the values of σ_0 in Table 3.1 would have to be reduced by one order of magnitude), and for $\sigma_{th} \sim 10^{-3}$ the condition $\sigma_0 > \sigma_{th}$ would only be satisfied for the $\sigma_0(\nabla \mu)$. However, assuming $\sigma_{th} \sim 10^{-4}$, then the condition $\sigma_0 > \sigma_{th}$ would easily be satisfied for both the thermal and the chemical potential of heterogeneities ($\sigma_0(\nabla T)$ and $\sigma_0(\nabla \mu)$). We shall resume our consideration of a realistic spatial scale of an inhomogeneous (non-equilibrium) distribution of T and μ in Pt. 3.3 (from a different point of view).

3.2 Threshold conditions for two- and three-mode wave generation and characteristics of a phase transition of a radiation system

We shall now deal with multi-phonon processes involved in the generation and amplification of waves, using some reasonable and justified approximations within the basic objectives of our analysis. In our notion of the $\gamma - \alpha$ -MT, the electronic transitions between the states \mathbf{k}, \mathbf{k}' , occurring in the vicinity of the $S_{\langle 111 \rangle}$ surface

Table 3.1. Inverted initial population difference as a function of the parameter y

y	$ \partial f^0/\partial y $	$\sigma_0(\nabla T) \cdot 10^3$	$\sigma_0(\nabla \mu) \cdot 10^2$	$\sigma_{th} \cdot 10^3$
0	0,5	0	17,4	(0, 1 ÷ 1)
1	0,197	3,94	6,86	
1,54	0,156	4,78	5,43	
2	0,105	4,2	3,65	
3	0,045	2,7	1,57	

under participation of two or three longitudinal phonons, are supposed to be of real importance. The quasi-momenta of these phonons are oriented either along the two - and fourfold symmetry axes (during a two-phonon process), or along the fourfold symmetry axes (during a three-phonon process). This statement is put into relation with the assumption that predominantly the longitudinal waves, which propagate in the $\langle 001 \rangle$ and $\langle 110 \rangle$ orientations, initiate the process of Bain-deformation (see (1.1)). It would be further interesting to find the conditions for multi-mode generation and to compare them with the conditions for single-mode generation. Such a comparison would then enable us to find a criterion for identification of such cases where multi-phonon processes carry out independent or supportive functions for single-mode generation, during a $\gamma - \alpha$ - MT.

To disclose and enlighten the outstanding features of two-mode generation, it is convenient from the outset to omit single-phonon processes and define a specific model Hamiltonian as the Hamiltonian of the electron-phonon system:

$$H = \hbar\omega_{\mathbf{q}}b_{\mathbf{q}}^+b_{\mathbf{q}} + \hbar\omega_{\mathbf{p}}b_{\mathbf{p}}^+b_{\mathbf{p}} + \sum_{\mathbf{k}} \varepsilon_{\mathbf{k}}a_{\mathbf{k}}^+a_{\mathbf{k}} + W(\mathbf{q}, \mathbf{p}) \sum_{\mathbf{k}} b_{\mathbf{p}}^+b_{\mathbf{q}}^+a_{\mathbf{k}}^+a_{\mathbf{k}} + b_{\mathbf{p}}b_{\mathbf{q}}a_{\mathbf{k}}^+a_{\mathbf{k}}. \quad (3.25)$$

Here, b^+ , b , a^+ , a are the phonon and electron creation and annihilation operators, respectively. During the summation of quasi-momenta of the electrons $\hbar\mathbf{k}$ we shall however only consider those states located in the vicinity of the surface $S_{[111]}$ (see (2.2)). In (3.25), the quasi-momenta $\hbar\mathbf{q}$ and $\hbar\mathbf{p}$ are oriented parallel to the axis $[001]$ and $[110]$ ($\mathbf{q} \perp \mathbf{p}$), thus the following conservation rules are satisfied:

$$\varepsilon_{\mathbf{k}'} - \varepsilon_{\mathbf{k}} - \hbar(\omega_{\mathbf{q}} + \omega_{\mathbf{p}}) = 0, \quad \mathbf{k}' - \mathbf{k} - \mathbf{q} - \mathbf{p} = 0, \quad \mathbf{Q}. \quad (3.26)$$

Here, \mathbf{Q} - vector of the reciprocal lattice, to be considered in the case of U-Processes. However, as the quasi-momenta $\hbar\mathbf{q}$, $\hbar\mathbf{p}$ can be judged as small quantities in relation to the quantity $\hbar\pi/a$, the importance of U-processes is only appreciable for a small fraction of the totality of transitions with quasi-momenta $\hbar\mathbf{k}$, $\hbar\mathbf{k}'$, in the immediate proximity of the lines LW, XW. Thus we will later

consider N-processes, selecting zero in the right-hand side of the quasi-momentum conservation law (3.26).

With quasi-momenta $\hbar q$, $\hbar p \ll \hbar\pi/a$, we get the following expression for a matrix-element of electron-phonon interaction:

$$W(\mathbf{q}, \mathbf{p}) \equiv -\frac{G q p \hbar}{2 M N \sqrt{\omega_{\mathbf{q}} \omega_{\mathbf{p}}}} \equiv W_2, \quad (3.27)$$

where M , N and G have the same meaning as in 2.4.

Let us now perform the same sequence of operations as those already explained in Pt. 3.1:

1. Neglecting the fluctuation effect of heat reservoirs and considering their dissipation by the phenomenological parameters Γ , \varkappa and t_σ , we can formulate the Heisenberg equations of motion for the operators of the phonon-field b^+ , b , the electron-polarization $d_{\mathbf{k}, \mathbf{k}'}^+ = a_{\mathbf{k}}^+ a_{\mathbf{k}'}$, $d_{\mathbf{k}, \mathbf{k}'} = a_{\mathbf{k}'}^+ a_{\mathbf{k}}$, and the occupation inversion σ ;
2. By averaging out the equations of motion with the aid of the system density-matrix, we can get over to the classical equations for the mean values of the relevant operators;
3. We shall confine our considerations to the exact resonance case and, using equations analog to (3.5), we can use the mean values of the operators \tilde{d}^+ , \tilde{d} , \tilde{b}^+ , \tilde{b} , which have no oscillation dependence of time. In the stationary case, we thus get the following system of non-linear algebraic equations:

$$\begin{aligned} \varkappa_{\mathbf{p}} \tilde{b}_{\mathbf{p}}^+ - \frac{i}{\hbar} W_2 R \tilde{b}_{\mathbf{q}} \tilde{d}^+ &= 0, \\ \varkappa_{\mathbf{q}} \tilde{b}_{\mathbf{q}}^+ - \frac{i}{\hbar} W_2 R \tilde{b}_{\mathbf{p}} \tilde{d}^+ &= 0, \\ \Gamma \tilde{d}^+ + \frac{i}{\hbar} W_2 \sigma \tilde{b}_{\mathbf{p}}^+ \tilde{b}_{\mathbf{q}}^+ &= 0, \\ \frac{\sigma_0 - \sigma}{t_\sigma} + \frac{2i}{\hbar} W_2 (\tilde{b}_{\mathbf{p}}^+ \tilde{b}_{\mathbf{q}}^+ \tilde{d} - \tilde{b}_{\mathbf{p}} \tilde{b}_{\mathbf{q}} \tilde{d}^+) &= 0, \end{aligned} \quad (3.28)$$

which is expressed in a shorthand notation, after omission of the coupled equations obtained by the substitutions $\tilde{b}^+ \leftrightarrow \tilde{b}$, $\tilde{d}^+ \leftrightarrow \tilde{d}$, $i \rightarrow -i$. In (3.28), we denoted by R the number of ES for which an electron transition within its own group is associated with the emission of a pair of phonons.

We can now derive the equation for σ from system (3.28):

$$\sigma^2 + \sigma_0 \sigma + \frac{1}{4} \sigma_{t_2}^2 = 0,$$

from which follows

$$\sigma_{1,2} = \frac{\sigma_0}{2} \pm \frac{\sigma_0}{2} \left[1 - \left(\frac{\sigma_{th2}}{\sigma_0} \right)^2 \right]^{\frac{1}{2}}, \quad \sigma_{th2} = \frac{4 \hbar (\Gamma t_\sigma \varkappa_{\mathbf{q}} \varkappa_{\mathbf{p}})^{\frac{1}{2}}}{R |W_2|}, \quad (3.29)$$

where the aim and object of σ_{th2} is the determination of an occupational threshold difference for two-mode generation. By (3.28), we get the following expression for $\tilde{b}_{\mathbf{p}}$:

$$\varkappa_{\mathbf{p}} \tilde{b}_{\mathbf{p}} \left[1 - \frac{R \sigma_0 W_2^2 \tilde{b}_{\mathbf{p}}^2}{\hbar^2 (\varkappa_{\mathbf{q}} \Gamma + 4 W_2^2 \varkappa_{\mathbf{p}} t_\sigma \tilde{b}_{\mathbf{p}}^4)} \right] = 0, \quad (3.30)$$

which only comprises one singular and valid solution $\tilde{b}_{\mathbf{p}} = 0$, for $\sigma_0 < \sigma_{th2}$. For $\sigma_0 > \sigma_{th2}$, there exist two other valid solutions, in addition to $\tilde{b}_{\mathbf{p}} = 0$:

$$(\tilde{b}_{\mathbf{p}})_{1,2} = \frac{1}{2} \left[\frac{R}{\varkappa_{\mathbf{p}} t_\sigma} (\sigma_0 - \sigma_{1,2}) \right]^{\frac{1}{2}} \neq 0. \quad (3.31)$$

For $\sigma_0 = \sigma_{th2}$, we get from (3.29) and (3.31):

$$\sigma_1 = \sigma_2 = \frac{\sigma_0}{2} = \frac{\sigma_{th2}}{2}; \quad (\tilde{b}_{\mathbf{p}})_1 = (\tilde{b}_{\mathbf{p}})_2 = \tilde{b}_{\mathbf{p}th} = \frac{1}{2} \left[\frac{R \sigma_{th2}}{2 \varkappa_{\mathbf{p}} t_\sigma} \right]^{\frac{1}{2}} \quad (3.32)$$

The correct expressions for $\tilde{b}_{\mathbf{q}}$ can be obtained by replacement of \mathbf{p} by \mathbf{q} ($\mathbf{p} \leftrightarrow \mathbf{q}$).

The investigation on the stability of these solutions and their interpretations will be performed by considering the transition in the generating mode as a particular kind of phase transition of a radiation system, as proposed by Haken in [98, 135, 137]. The role of the ordering and temperature parameters will be represented by \tilde{b} and $-\sigma_0$ respectively. The analog expression for free energy B can easily be found by considering Eq.(3.30) as an extreme condition

$$\frac{dB}{d\tilde{b}} = 0.$$

Then, after omission of the irrelevant constant, we get:

$$B \equiv B_2(\tilde{b}) = \varphi(\tilde{b}_{\mathbf{p}}) + \varphi(\tilde{b}_{\mathbf{q}}),$$

$$\varphi(\tilde{b}_{\mathbf{p}}) = \frac{1}{2} \varkappa_{\mathbf{p}} \tilde{b}_{\mathbf{p}}^2 - \frac{R \sigma_0}{16 t_\sigma} \ln \left[1 + \frac{4 t_\sigma W_2^2 \varkappa_{\mathbf{p}} \tilde{b}_{\mathbf{p}}^4}{\hbar^2 \Gamma \varkappa_{\mathbf{q}}} \right]. \quad (3.33)$$

The expression $\varphi(\tilde{b}_{\mathbf{q}})$ can be obtained from $\varphi(\tilde{b}_{\mathbf{p}})$ by the changing $\mathbf{p} \leftrightarrow \mathbf{q}$.

Now it is easy to verify that the function $B_2(\tilde{b})$ attains a single minimum in the region $\sigma_0 < \sigma_{th2}$, corresponding to $\tilde{b} = 0$. For $\sigma_0 = \sigma_{th2}$, a flex point \tilde{b}_t arises, being a forerunner of additional extremes taking shape in the region $\sigma_0 > \sigma_{th2}$. The additional minimum B_2 is associated with the value \tilde{b}_2 (3.31), while the maximum

corresponds to \tilde{b}_1 , which indicates an instability of the solution \tilde{b}_1 and a stability of the solution \tilde{b}_2 . This is a distinct indication for the emergence of a scenario of a typical 1st order phase-transition (see (3.1)), where the value $\sigma_0 = \sigma_{th2}$ determines the limit of absolute loss of stability of the phase with non-vanishing magnitude of order parameter.

The analog of the critical temperature of a 1st - order phase transition is the critical value of occupation inversion $\sigma_0 = \sigma_c$, at which the minimum values of the function B_2 match, i.e.

$$B_2(\tilde{b} = 0) = B_2(\tilde{b}_2) = 0. \quad (3.34)$$

We can now determine \tilde{b}_2 by substituting the expression for σ_2 from (3.29) in (3.31). After insertion of \tilde{b}_2 in (3.33), we are able to express (3.34) in such a manner that we can determine σ_c :

$$1 + (1 - \psi^{-2})^{1/2} - \ln \left[1 + \psi^2 \left[1 + (1 - \psi^{-2})^{1/2} \right]^2 \right] = 0, \quad (3.35)$$

where $\psi = \sigma_c \sigma_{th2}^{-1}$. The numeric solution of (3.35) renders:

$$\psi \approx 1,25, \quad \sigma_c \approx 1,25 \sigma_{th2}.$$

For $\sigma_0 > \sigma_c$ we get $B_2(\tilde{b}_2) < B_2(0)$, indicating a higher relative stability of the phase corresponding to $b \neq 0$. After further analysis, we can realize a decrease of the maximum of $B_2(\tilde{b}_1)$, which plays the role of a potential-barrier between the states with $\tilde{b} = 0$ and $\tilde{b}_2 \neq 0$, as well as a decrease of the actual value of \tilde{b}_1 with increasing parameter $\sigma_0 \sigma_c^{-1} > 1$ ($B_2(\tilde{b}_1) \rightarrow 0$ only for $\sigma_0 \sigma_c^{-1} \rightarrow \infty$). As the value of σ_0 is limited ($\sigma_0 < 1$), the satisfaction of Eqs. $\tilde{b}_1 = 0$ and $B_2(\tilde{b}_1) = 0$, indicating an absolute loss of stability of the phase with vanishing order-parameter, will only be possible at $\sigma_c = 0$. However, if $\sigma_c \sim \sigma_{th} \neq 0$, it is not possible to introduce a value σ_c corresponding to the temperature of absolute loss of stability of the high-temperature phase.

A consideration of three-mode generation with frequencies $\omega_{\mathbf{k}}, \omega_{\mathbf{p}}$ and $\omega_{\mathbf{q}}$ would lead us to qualitatively similar conclusions. For this reason, we will only denote the expressions for the threshold- and for the critical occupational differences.

$$\sigma_{th3} = \frac{3}{R} \left[4 \Gamma t_\sigma^2 \hbar^2 \varkappa_{\mathbf{k}} \varkappa_{\mathbf{q}} \varkappa_{\mathbf{p}} \right]^{\frac{1}{3}}, \quad \sigma_c \approx 1,41 \sigma_{th3} \quad (3.36)$$

where

$$W_3 \equiv W(\mathbf{k}, \mathbf{p}, \mathbf{q}) = \frac{i G k p q \hbar^{3/2}}{(2MN)^{3/2} (\omega_{\mathbf{k}} \omega_{\mathbf{p}} \omega_{\mathbf{q}})^{1/2}}.$$

We can realize the difference between two- and three phase generation on the one hand and single-phase generation on the other hand, which can thus be defined

as a second-order phase transition of a radiation field at threshold occupational differences σ_{th1} (3.10), which we shall write once more, for comparison,

$$\sigma_{th1} = \frac{\Gamma \varkappa_{\mathbf{q}} \hbar^2}{R |W_1|^2}, W_1 \equiv W(\mathbf{q}) = \frac{i\hbar^{1/2} G q}{(2 M N \omega_{\mathbf{q}})^{1/2}} \quad (3.37)$$

and which can be interpreted as an analog to the expression of the Curie-temperature. In fact, if we regard (3.11) in 3.1 as a prerequisite for a minimum of the free energy equivalent $B_1(\tilde{b})$, then we get:

$$B_1(\tilde{b}) = \frac{\varkappa \tilde{b}^2}{2} - \frac{\sigma_0 R}{8 t_\sigma} \ln \left[1 + \frac{4 t_\sigma |W_1|^2 \tilde{b}^2}{\hbar^2 \Gamma} \right]. \quad (3.38)$$

It can easily be verified that - in the region $\sigma_0 < \sigma_{t1}$ - the function $B_1(\tilde{b})$ attains a minimum at $\tilde{b} = 0$, and in the region $\sigma_0 > \sigma_{th1}$ another minimum at $\tilde{b} \neq 0$. This is a clear indication of a non - stability of the ordered state below the generation threshold, and of the disordered state above the generation threshold. Moreover, a typical feature of 2nd order transitions can be inferred from the smoothly changing of the order parameter while approaching to $\sigma_0 = \sigma_{th1}$.

The expressions $\sigma_c \sim \sigma_{th2,3}$ also differ significantly from σ_{th1} . By definition, σ_c implicitly includes a time-variable t_σ , in addition to the parameters specifying σ_{th1} . We thus determine the relations $\sigma_{th2} \sigma_{th1}^{-1}$ and $\sigma_{th3} \sigma_{th1}^{-1}$, using the assumption that frequencies of a given order of magnitude will be generated in a single mode, as well as in two or three modes, respectively. Then we get from Eqs. (3.29), (3.36) and (3.37), within an accuracy given by factors of order

$$\frac{\sigma_{th2}}{\sigma_{th1}} \sim \frac{G}{\hbar} \left(\frac{t_\sigma}{\Gamma} \right)^{1/2}; \quad \frac{\sigma_{th3}}{\sigma_{th1}} \sim \left[\frac{G}{\hbar} \left(\frac{t_\sigma}{\Gamma} \right)^{1/2} \right]^{4/3}. \quad (3.39)$$

Thus for $\hbar^{-1} G t_\sigma^{1/2} \Gamma^{-1/2} < 1$, multi-mode generation could formally start sooner than single-mode generation. It has however to be considered that this inequality can only be satisfied by a reduction of G or by raising of Γ within the region of the threshold condition $\sigma_{thj} > 1$, $j = 1, 2, 3$, being unattainable in reality due to the limitation $\sigma_0 < 1$. But also the parameter t_σ has a natural lower limit. According to (3.4), $(t_\sigma)_{\min} = \Gamma^{-1}$, but $(\sigma_{th2} \sigma_{th1}^{-1})_{\min} \sim G(\hbar \Gamma)^{-1}$, and for the previously used values $G \sim 10^{-19}$ J, $\Gamma \sim 10^{12}$ 1/s we get $\sigma_{th2} \sigma_{th1}^{-1} \sim 10^3$. Thus the role of processes with two and three participating phonons can mainly be attributed to the amplification (and possible synchronization) of modes generated by single-phonon processes.

Our common consideration of single- and two-phonon processes has been performed for the most favorable case of generation, being characterized by electronic transitions with one or two participating phonons, occurring in the proximity of different S-surfaces. To take an example, during the generation of a pair of waves along the orientations Δ -[001] and Σ -[110], it is possible to analyze single-phonon

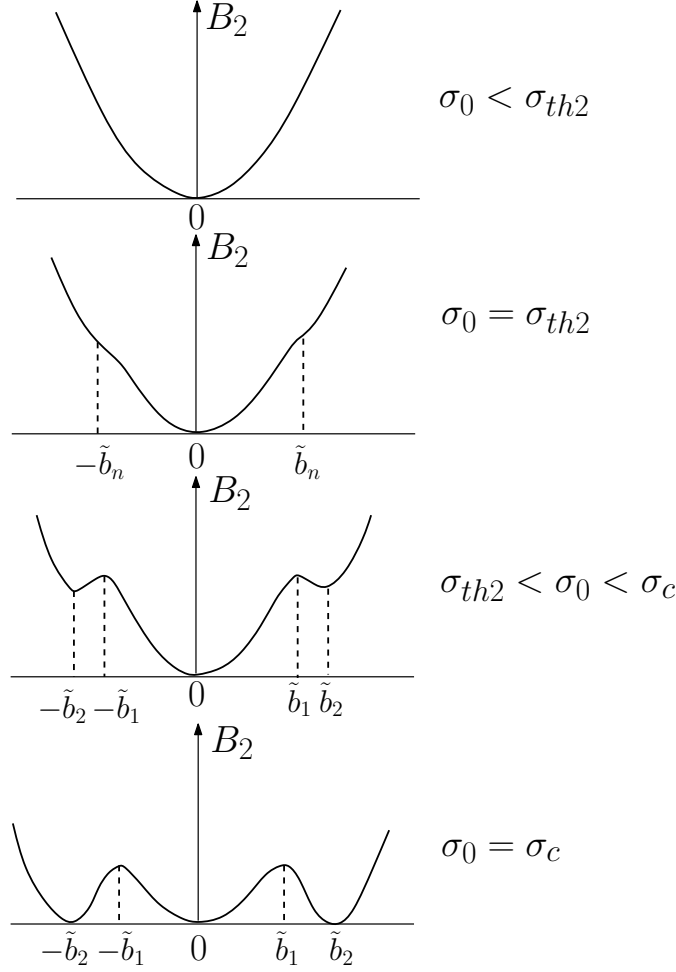


Figure 3.1. Image of the function $B_2(\tilde{b})$ at different values of occupational difference σ_0 .

processes in the proximity of the surfaces $S_{[001],[110]}$, and two-phonon processes between states in the proximity of $S_{[111]}$. Omitting some usual considerations, being negligible for our purposes, and considering $\sigma_0 \sigma_{th2}^{-1} \geq \sigma_{th1} \sigma_{th2}^{-1}$ as a small quantity, we can present a stationary solution for the simplest case of equalities: $\tilde{b}_\Delta^2 = \tilde{b}_\Sigma^2 = \tilde{b}^2$ for the numbers of generated phonons; $R_\Delta = R_\Sigma = R$ for the numbers of pairs of electronic states; $\sigma_{0\Delta} = \sigma_{0\Sigma} = \sigma_{0\Lambda} = \sigma_0$ and $t_{\sigma\Delta} = t_{\sigma\Sigma} = t_{\sigma\Lambda} = t_\sigma$ (for the longitudinal relaxation times), confined to the states located in the proximity of different S-surfaces. Then our solution is:

$$\tilde{b}^2 = 0, \quad \sigma_0 < \sigma_{th1}, \quad (3.40)$$

$$\tilde{b}^2 \approx \frac{\hbar^2 \Gamma}{4 |W_1|^2 t_\sigma} \left(\frac{\sigma_0}{\sigma_{th1}} - 1 \right) \left(1 + \left(\frac{2 \sigma_0}{\sigma_{th2}} \right)^2 \right), \quad \sigma_0 > \sigma_{th1},$$

being distinguished from the solution for single-mode generation (3.13) by a fac-

tor $1 + (2 \sigma_0 \sigma_{th2}^{-1})^2$, thus clearly indicating the amplification effect by two-phonon processes.

3.3 The lattice strain induced by the generated waves

For realization of martensitic transformation, in accordance with the wave-model, it is necessary that the amplitudes of the generated waves have exceeded the threshold ($u_t(\lambda, T)$), which essentially depends on the wave-length λ and on the temperature T . The maximum of $u_t(\lambda)$ can be evaluated by geometrical considerations alone, taking into account that - for pure Bain-deformation [13] - the transition to new equilibrium conditions is associated with a relative displacement of $0,1a$ (a - lattice-parameter) of the atoms neighboring in the orientation $\langle 001 \rangle$. This means that an instability must be expected for relative lattice displacements greater than $\approx 0,05a$. If such displacements were associated with a wave, then the amplitude of such waves would obviously be $\sim 0,05 \lambda/2 = u_t(\lambda)$. The value $u_t(\lambda)$ being independent of temperature can be put into natural correspondence with the threshold $u_t(\lambda, T_0)$, where T_0 - equilibrium temperature between austenite and martensite.

The supercooling below the equilibrium temperature (for definiteness, the straight MT under cooling is considered) must occur with the decreasing of austenite stability and hence:

$$u_t(T, \lambda) < u_t(T_0, \lambda).$$

Let's remind (see Pt. 1.3) that wave-amplitudes creating the threshold-deformation ε_{th} of about 10^{-3} are anticipated in the proximity of M_S .

In evaluating the stationary amplitudes u of the generated waves, we can disregard the influence of electron-phonon interaction associated with multi-phonon processes. Then, using the link between u and \tilde{b} by (3.14), as well as the expressions (3.40) and (3.37), we get the following relation:

$$u_{\mathbf{q}} = \left[\frac{2\hbar}{MN\omega_{\mathbf{q}}} \right]^{\frac{1}{2}} \tilde{b}_{\mathbf{q}} \approx \frac{\hbar}{Gq} \left[\frac{\Gamma}{t_{\sigma}} \left(\frac{\sigma_0}{\sigma_{th1}} - 1 \right) \right]^{\frac{1}{2}}. \quad (3.41)$$

The deformation ε in turn is linked up with the amplitude by the relation (1.2) in Pt. 1.3:

$$\varepsilon = \frac{2}{\pi} u_{\mathbf{q}} q \approx \frac{2\hbar}{\pi G} \left[\frac{\Gamma}{t_{\sigma}} \left(\frac{\sigma_0}{\sigma_{th1}} - 1 \right) \right]^{\frac{1}{2}}. \quad (3.42)$$

Assuming $t_{\sigma} = \Gamma^{-1}$, $\sigma_{th1} \sim 10^{-3}$, $(\sigma_0 \sigma_{th1}^{-1} - 1) \approx 1,6$ - corresponding to the value $\sigma_0(\nabla\mu)$, $y = 2$ in Table 3.1 - and using the quantity $10^2 v_k \cdot \tau$ as a natural gage of heterogeneity (see end of Pt. 3.1), with $G \sim 10^{-19}$ J and $\hbar \Gamma \sim 10^{-22}$ J, we get

from (3.42): $\varepsilon \approx 3, 2/\pi \cdot 10^{-3}$. As a result, the existence of waves with amplitudes ensuring a lattice deformation near the elastic (yield-) limit, should be reasonably possible. We further note that for $\lambda/2 \sim 10^{-6}$ m and $\varepsilon \sim 10^{-3}$ the wave-amplitude ($u = \varepsilon \lambda/4 \approx 5 \cdot 10^{-10}$ m $\approx 1, 4a$) becomes even greater than the lattice-parameter.

Let us now discuss the applicability of our estimates, taking into account that they are based on stationary solutions. Above all, the lifetimes of spatially inhomogeneous distributions of temperature and chemical potential have to be evaluated. Let these times be $t_{\nabla T}$, $t_{\nabla \mu}$ and, taking into account that such heterogeneities rapidly fade away, mainly as a result of conduction and diffusion processes, we can obtain an estimate of these times t_{∇} , becoming clearly obvious from dimensional considerations:

$$t_{\nabla T} \approx \frac{l_T^2}{d_T}, \quad t_{\nabla \mu} \approx \frac{l_\mu^2}{d_\mu}, \quad (3.43)$$

where $l_{T, \mu}$ - characteristic gages of inhomogeneity, determining $\nabla T \approx \Delta T \cdot l_T^{-1}$, $\nabla \mu \approx \Delta \mu \cdot l_\mu^{-1}$; d_T and d_μ - heat-conduction and diffusion coefficients, respectively.

The typical value of $d_T \approx 10^{-5}$ m²/s for $T > T_D$ can easily be obtained from below equation (3.44), by linking up d_T with heat-conductivity λ_t , specific heat capacity C_{sp} and density ρ :

$$d_T = \frac{\lambda_t}{\rho C_{sp}}, \quad (3.44)$$

where $\lambda_t = 34$ W/mK, $\rho = 7900$ kg/m³, $C_{sp} \approx 4, 6 \cdot 10^2$ J/kg K (the specific heat capacity has been derived from the Dulong-Petit-Law, being substantiated for $T > T_D$).

Taking into account that the term d_μ is a coefficient of proportionality which combines an electric current density j with the gradient ∇n_γ of conduction electron concentration in the γ - phase, we are able to express the term d_μ by the specific conductivity σ_γ of the γ - phase. For this purpose, we start with an appropriate conversion of the expression for current-density j , presupposing that $\mu \sim n_\gamma^{2/3}$:

$$j = -\frac{\sigma_\gamma}{e} \nabla \mu = -\frac{2}{3} \frac{\sigma_\gamma \mu_\gamma}{e n_\gamma} \nabla n_\gamma. \quad (3.45)$$

After division of both sides of (3.45) by the electron charge e , we get:

$$\frac{j}{e} = -\frac{2 \sigma_\gamma \mu_\gamma}{3 e^2 n_\gamma} \nabla n_\gamma \equiv -d_\mu \nabla n_\gamma, \quad d_\mu = \frac{2 \sigma_\gamma \mu_\gamma}{3 e^2 n_\gamma}. \quad (3.46)$$

After insertion of $\sigma_\gamma \approx 10^6$ m⁻¹ Ohm⁻¹, $n_\gamma = 10^{29}$ m⁻³, $\mu_\gamma \approx 10$ eV = $1, 6 \cdot 10^{-18}$ J into (3.46), we get $d_\mu \approx 4 \cdot 10^{-4}$ m²/s.¹

¹The order of magnitude of the current density j being generated by the chemical potential gradient 10⁶eV/m in the transformation front is 10¹² A/m² for σ_γ about 10⁶ m⁻¹ Ohm⁻¹ and substantially greater than any drift current observed in semiconductors.

Obviously in our assessment of the quantities ∇T , $\nabla\mu$ the usage of the quantities $\Delta T \sim 10^2 \text{ K} \sim (T_0 - M_S)$ and $\Delta\mu = |\mu_\alpha - \mu_\gamma| \approx 0,15 \text{ eV}$ can be justified if the nucleation time t_N is less or of the same order of magnitude than that the time of existence of the gradient t_∇ . Otherwise, conduction- and diffusion processes would smooth down the jumps of temperature and concentration at the phase boundary. In the nucleation model of the macro-nucleus, we can determine the minimum values $(l_T)_{min}$ and $(l_\mu)_{min}$ from the requirement $t_N = t_\nabla$, using (3.43), further assuming $t_N \sim 10^{-11} \text{ s}$ (see treatise under Pt. 1.3), which would correspond to a nuclear radius $r_N \sim 10^{-5} \text{ cm}$ and to a speed of propagation of the nuclear boundary of $V \sim 10^3 \text{ m/s}$:

$$(l_T)_{min} = (t_N d_T)^{1/2} \sim 10^{-8} m,$$

$$(l_\mu)_{min} = (t_N d_\mu)^{1/2} \sim 6 \cdot 10^{-8} m.$$

If $\nabla\mu$ was considered as a stationary quantity, then the quantity $l_\mu \sim 10^{-7} \text{ m}$ would be a natural gage. We remind that, at the end of Pt. 3.1, we came to a similar conclusion (which however resulted from different considerations).

The issue related to the applicability of stationary estimates of the amplitudes $u = u_{st}$ and deformations $\varepsilon = \varepsilon_{st}$ is more complex. In fact, the transition to virtually stationary values of u , ε , within certain characteristic period $t_u = t_\varepsilon$, will not depend on the values of u_0 , ε_0 at the starting moment t_0 , provided $t_u \ll t_\nabla$. Thus in this particular case, a soft mode of wave excitation with $u_0 \ll u_{st}$, $\varepsilon_0 \ll \varepsilon_{st}$ would be possible. But if $t_u \gg t_\nabla$, the values $u \approx u_{st}$ and $\varepsilon_0 \approx \varepsilon_{st}$ cannot be materialized by a soft mode of excitation. Consequently, a stationary estimate would only be realistic for a hard mode of excitation with $u_0 \leq u_{st}$, $\varepsilon_0 \leq \varepsilon_{st}$. Of course, for $u_0 > u_{st}$, $\varepsilon_0 > \varepsilon_{st}$, the stationary estimate then would deliver the lower limit of u , ε (for $\sigma_0 > \sigma_{th1}$).

For an evaluation of t_u , the non-stationary solution of $\tilde{b}(t)$ must be known. However, it cannot be found for the general case, but in the vicinity of the threshold for single-mode generation, the equation for \tilde{b} leads to the Van-der-Pol equation (see for example § (3,a) in the lectures of Haken-Weidlich [132]):

$$\left(\frac{d}{dt} - D \right) \tilde{b}^+ + \beta \tilde{b}^+ \tilde{b} \tilde{b}^+ = 0,$$

$$D = \varkappa \left(\frac{\sigma_0}{\sigma_{th1}} - 1 \right), \quad \beta = \frac{4 t_\sigma \varkappa |W_1|^2 \sigma_0}{\Gamma \sigma_{th1} \hbar^2}. \quad (3.47)$$

Formally, the Van-der-Pol equation can be obtained if the temporal derivatives of system (3.7) are only re-established for the quantities \tilde{b}_q^+ , \tilde{b}_q , by writing $-\dot{\tilde{b}}_q^+$ for the right side of the first Eq. (3.7), instead of zero, leaving the other equations unchanged (Of course, this is an adiabatic approximation, which means that the

radiating sub-system will immediately be subordinated to the ordering-parameter $\tilde{b}_{\mathbf{q}}$). Then, \tilde{d} and σ must be excluded, and a decomposition of the resulting factor

$$\left[1 + \frac{4 t_{\sigma} |W_1|^2}{\hbar^2 \Gamma} \tilde{b}_{\mathbf{q}}^+ \tilde{b}_{\mathbf{q}} \right]^{-1} \approx 1 - \frac{4 t_{\sigma} |W_1|^2}{\hbar^2 \Gamma} \tilde{b}_{\mathbf{q}}^+ \tilde{b}_{\mathbf{q}} \quad (3.48)$$

must be performed with an accuracy up and including to the linear term in $\tilde{b}_{\mathbf{q}}^+ \tilde{b}_{\mathbf{q}}$. As we already excluded the dipole-moment \tilde{d} and the occupation difference σ in our search for a stationary equation for $\tilde{b}_{\mathbf{q}}^+$, we can immediately use Eq. (3.11). It delivers the non-stationary equation for $\tilde{b}_{\mathbf{q}}^+$ in an adiabatic approximation, by multiplication with $-\varkappa_{\mathbf{q}}$ and addition of $\dot{\tilde{b}}_{\mathbf{q}}^+$ to the left side:

$$\dot{\tilde{b}}_{\mathbf{q}}^+ = \varkappa_{\mathbf{q}} \tilde{b}_{\mathbf{q}}^+ \left[\frac{\sigma_0}{\sigma_{th1}} \left(1 + \frac{4 t_{\sigma} |W_1|^2}{\hbar^2 \Gamma} \tilde{b}_{\mathbf{q}}^+ \tilde{b}_{\mathbf{q}} \right)^{-1} - 1 \right] \equiv -\chi \tilde{b}_{\mathbf{q}}^+. \quad (3.49)$$

With consideration of (3.49), we immediately get (3.47) from (3.49). Eq. (3.49) will be further used in Chapter 6, so that we can now deal with to the more simple Eq. (3.47).

Assuming that the quantity \tilde{b} attains the value \tilde{b}_0 , due to fluctuations at the starting time $t = 0$, we get from (3.47):

$$\tilde{b} = \left[\left(\frac{1}{\tilde{b}_0^2} - \frac{\beta}{D} \right) e^{-2Dt} + \frac{\beta}{D} \right]^{-1/2}. \quad (3.50)$$

It follows from (3.50), that for $D > 0$, $t \rightarrow \infty$, $\tilde{b} \rightarrow (D/\beta)^{1/2} \neq 0$, but $\tilde{b} \rightarrow 0$, for $D < 0$, $t \rightarrow \infty$. It also is obvious from (3.50) that the only relevant characteristic time is:

$$t_u = (2D)^{-1}. \quad (3.51)$$

Here, the following observation is striking enough to attract our attention: As a general rule, during approach to the starting temperature of a second-order phase transition, the tendency of t_u to infinity for $\sigma_0 \rightarrow \sigma_{th1}$ would be analog to the critical degradation of fluctuations of the ordering parameter.

Even though the Van-der-Pol equation is not applicable for states located significantly beyond the threshold, an evaluation of the order of magnitude of t_u can nonetheless be performed on the basis of Eq. (3.51). Assuming an attenuation $\varkappa \approx (10^{-4} \div 10^{-3})\omega$, in accordance with (3.16), we can realize that for $(\sigma_0 \sigma_{th1}^{-1} - 1)$ of order 1 the resulting time t_u evaluated on the basis of Eq. (3.51) must be not less than $(10\varkappa)^{-1}$. Hence only the inequality $t_u \gg t_{\nabla}$ is satisfied in the region of parameters interesting for us: $\omega \sim 10^{10} \div 10^{11} \text{ s}^{-1}$, $t_u \geq (10^{-8} \div 10^{-9}) \text{ s}$. In accordance with our above treatise, it must be concluded from this latter inequality that our stationary evaluations of u and ε , having been obtained on the basis of

(3.41), (3.42), would only be justified for hard modes of excitation, i.e. $u_0 \leq u_{st}$, $\varepsilon \leq \varepsilon_{st}$.²

3.4 Conclusions from Chapter 3

From the above analysis of the equations for a non-equilibrium electron-phonon-system, it is possible to draw the following conclusions:

1. Electron-phonon processes with participation of a single phonon play a dominating role during the generation of longitudinal lattice-displacement waves, while the role of multi-phonon processes is limited to the amplification of waves.
2. Wave generation takes place through relatively long-lived ES with an average lifetime of about $\tau_0 \geq 10^{-12}$ s.
3. Among two non-equilibrium sources in electronic subsystems, being defined by the existence of ∇T and $\nabla \mu$, the latter one, being caused by the inhomogeneity of the chemical potential μ , is the more effective one in generating long-wave phonons ($q \sim (10^{-3} \div 10^{-2})\pi/a$).
4. In the case of large-sized reduced sheets of the S-surfaces ($\Sigma \geq (\pi/a)^2$) with weak energy-dispersion near the μ -value, as well as for chemical potential gradients $\nabla \mu \sim 10^6$ eV/m (10^{10} K/m in a temperature-scale) the generation of longitudinal elastoplastic waves, being linked up with lattice-deformations close to the limits of elasticity of about $\varepsilon \sim 10^{-3}$, becomes possible.
5. For some characteristic temporal gauges, the following chain of inequality conditions may be suggested:

$$t_u \gg t_\nabla > t_N > \tau_0 \sim t_\sigma. \quad (3.52)$$

The central term $t_\nabla > t_N$ of (3.52) determines a relation between t_∇ - the lifetimes of ∇T and $\nabla \mu$, respectively - and the time of macro-nucleation $t_N \geq 10^{-11}$ s, which, in turn, also implies minimal spatial gauges $l_T \sim 10^{-8}$ m, $l_\mu \sim 10^{-7}$ m for stationary evaluations of $\nabla T = \Delta T \cdot l_T^{-1}$, $\nabla \mu = \Delta \mu \cdot l_\mu^{-1}$. The first term $t_u \gg t_\nabla$ shows that a realization of the deformation level obtained from an evaluation of (3.42) (for stationary conditions) only becomes feasible for hard-mode wave-excitation. Within the frame of the developed model of the $\gamma - \alpha$ -MT as a deformation- process, being controlled

²Editorial note: If a transformation energy of (0,01 \div 0,1) eV per atom is assumed, then the maximum possible power-density (power per unit surface) of the transformation-wave-front would be of an order of magnitude of $\approx (0,1 \div 1)\text{GW cm}^{-2}$, determining the level of external energy flow being necessary for the martensitic transformation start.

by the threshold-deformation $\varepsilon_{th} \sim 10^{-3}$ of the carrier-waves, this means that the threshold-level ε_{th} must arise simultaneously with beginning growth i.e. for $t_0 = t_N$. This latter conclusion matches very well with the interpretation of the observed pronounced supercooling of the γ -phase below the phase-equilibrium temperature T_0 (including a significant free-energy excess for compensation of the energy required for built-up of the phase boundary, and of the elastostatic distortion field), thus being an essential prerequisite for the excitation of oscillations with an amplitude sufficiently large to produce permanent lattice-deformations of about $\varepsilon_0 \sim 10^{-3}$ in the nucleation stage (see Pt. 1.3 and Pt. 1 of the task defined by Pt. 1.5). Such deformation levels thus will be sufficient to overcome the threshold separating the metastable state of fcc-lattice from the more stable state of bcc-lattice (at $T = M_S$).

The treatise of Chapter 3 is mostly based on the papers [140,141] and, to a lesser extent, on [56], the results of which have been improved in this chapter, mainly by the replacement of the P-planes of the simplified model by S-surfaces and by the specification of the rather illustrative quantitative estimates presented in [140,141].

Some additional remarks

1. The tasks of development of kinetic equations for a non-equilibrium electron-phonon system, as well as the analysis of threshold conditions during single-mode generation within the conceptual notion of isoenergetic P-surfaces with inhomogeneous distribution of temperature has been treated in [142–146] and summarized in [147], within the frame of the method of the non-equilibrium statistical operator of Zubarev and Kalashnikov [148–150]. The results presented in these works, as far as they relate to the $\gamma - \alpha$ -MT, are alike to the results of Pt. 3.1, at least in a qualitative aspect. They can be taken as a justification of the semi-phenomenological approach, being characterized by the introduction of relaxation constants to consider dissipative processes. Furthermore it has been shown in [146,147] that a system of equations with mixed coordinate- and momentum-representation, resulting from a reduction of the macro-variables f, σ, d, b by powers of the respective gradients, attains a local spatial form matching with (3.3), with sufficient precision until the first non-vanishing terms. However, in this case the macro-variables σ, d, b must be considered as functions of the x -coordinate being oriented parallel to the orientation of highest heterogeneity \mathbf{e} . This representation highlights that the probability for the presence of an electron within in the immediate vicinity of a point \mathbf{x} , with simultaneous presence of electronic flows, will largely depend on the orientation of the group-velocity \mathbf{v} of that electron in relation to \mathbf{e} , and that in one and the same point in space states with inverted occupation can exist. The spatially-local nature of such describing justifies the application of the findings obtained in the quasi-momentum rep-

resentation to an analysis of the non-equilibrium state in the proximity of the propagating phase boundary.

2. Generally speaking, the drift mechanism for the creation of a population inversion is well known, being used for example at generation and amplification of elastic waves in semiconductors (see [151, 152]). Usually, the conditions for wave generation by a drift mechanism focus on the requirement that the electron drift velocity \mathbf{v}_d must locally exceed the speed of sound c , i.e. $v_d > c$. Thus this condition is equivalent to that formulated by Tscherenkov for phonon radiation generation by drifting electrons. Within the frame of our designations, the condition $v_d > c$ is equivalent to the condition $\sigma_0 > 0$, being an essentially weaker requirement than $\sigma_0 > \sigma_{th1}$. Obviously from (3.24), the condition $\sigma_0 > 0$ is equivalent to the equation

$$(\mathbf{v}_{\mathbf{k}'} - \mathbf{v}_{\mathbf{k}}) \tau \vec{\nabla} \mu > \hbar \omega_{\mathbf{q}} = \hbar c q. \quad (3.53)$$

Taking into account that the states \mathbf{k} , \mathbf{k}' are located in the vicinity of the S-surface, and that the dispersion-law for these states along the direction \mathbf{e} - is a quadratic function (see Chapter 2), we get:

$$\begin{aligned} \mathbf{v}_{\mathbf{k}'} - \mathbf{v}_{\mathbf{k}} &= \hbar [\mathbf{s} - \mathbf{k}' - (\mathbf{s} - \mathbf{k})] |m|_s^{-1} = \\ &= \hbar (\mathbf{k} - \mathbf{k}') |m|_s^{-1} = \hbar \mathbf{q} |m|_s^{-1}, \end{aligned} \quad (3.54)$$

where \mathbf{s} - vector designating the intersection point \mathbf{s} of the vector $\mathbf{k} - \mathbf{k}' = \mathbf{q}$ with the S-surface, $|m|_s^{-1}$ - reciprocal effective electron-mass in point \mathbf{s} . After substitution by (3.54) in (3.53), we get the condition for Tscherenkov-radiation:

$$v_d = \tau \nabla \mu |m|_s^{-1} > c. \quad (3.55)$$

For $\nabla \mu \sim 10^6$ eV/m = $1,6 \cdot 10^{-13}$ J/m, $\tau \sim 10^{-12}$ s, $|m|_s \approx 3 m_0 \sim 3 \cdot 10^{-30}$ kg, we obtain $v_d \approx 5 \cdot 10^4$ m/s, the magnitude of which exceeds the speed of longitudinal waves by about one order of magnitude and thus is sufficient for satisfaction of the threshold condition $\sigma_0 > \sigma_{th1}$, within a temperature region of $T \sim 10^3$ K. However, the realization of waves carrying a deformation amplitude of $\varepsilon_0 \geq 10^{-3}$ requires the larger values of $\nabla \mu$, corresponding to $v_d \sim 10^5$ m/s. The region of $v_d \sim (10^4 \div 10^5)$ m/s also is typical of semiconductors [151]. To have ended this comparison, we remind that the generation of elastic waves in a semiconductor requires the considerable drift-velocities as well as the large values of the electron-phonon- interaction matrix-elements (semiconductors-piezoelectrics). In the case of the $\gamma - \alpha$ - MT, this interaction is not large. Instead, the number of pairs $(\mathbf{k}, \mathbf{k}')$ of

active electronic states is large, whereas in turn this factor is of minor importance for semiconductors. Of course, neither the drift mechanism of pumping nor the existence of electrical conductivity are exclusive prerequisites for the emergence of a phonon-maser-effect. Alternative principles of a maser-effect are also known (see for example [136, 153, 154]).

3. Finally, we remark that, besides stimulated emission of radiation, in an inversely occupied radiation system the spontaneous collective super-radiation (Dicke)⁸, with the intensity being proportional to the square of the number of pairs of active states, is also possible (see for example [134, 154, 155]). As the time for the development of super-radiation must be less than the relaxation time $\Gamma^{-1} \sim \tau_0$ of the dipole-moment, the generation of a super-radiation pulse is not possible for the frequencies ν of phonons below τ_0^{-1} . Then, assuming $\tau_0 \sim 10^{-12}$ s, it is meaningless to discuss this effect for phonon-radiation with quasi-momenta $q \sim (10^{-3} \div 10^{-2})\pi/a$ or with frequencies $\nu_{\mathbf{q}} < \tau_0^{-1}$. Thus the maser-effect is the predominant generation mechanism of phonons with the relevant region of wave-vectors.

Chapter 4

Coordination between of the $\gamma - \alpha$ martensitic transformation temperature and the optimum wave generation temperature in iron-based alloys

4.1 Definition of the task

Our previous analysis suggests that, in the growth stage of martensite, the existence of lattice-displacement waves with deformation amplitudes of $\varepsilon \sim 10^{-3}$ is a real possibility. Let us remind that the evaluation of the fulfilment of the general threshold-conditions has been performed for the high-temperature region, where the frequency of collisions with short-wave phonons is large. Then there is reason to think that this evaluation in order of magnitude is satisfactory not only for pure iron but also for the iron based alloys. However, to generalize our conclusions and to obtain the optimum conditions of wave generation over the full range of concentrations of the alloying elements (for example up to 10% Mn or up to 34% Ni) and of carbon (up to 1,8 weight%), a special investigation is required.

On the one hand, the existence of a high level of population difference σ_0 in accordance with (3.23), (3.24) would require that the magnitude of the parameter $y = (\varepsilon - \mu)(k_B T)^{-1}$ must not exceed a few units, as the multiplier $|\partial f^0 / \partial y|$ rapidly diminishes with increasing y (see Tab.3.1), and hence also the value σ_0 . On the other hand, with increasing concentration of Ni the temperature (M_S) is decreasing (practically, down to 0 K for 34 % Ni), thus the value of y would have to increase. This difficulty cannot be resolved (vide infra) by the formal assumption about the necessary reduction of the magnitude $(\varepsilon - \mu)$ to ensure practical stability or reduction of the parameter y .

Moreover, the assumption that the increasing of Ni concentration causes a

requisite reduction of the difference $\varepsilon - \mu$, due to the filling of the energy band (the model of hard zone) by excess-electrons (two electrons per Ni-atom), cannot generally be supported, as this model leads to the wrong conclusion about the increasing of M_S for a Fe-Mn-system, because the difference $\varepsilon - \mu$ must increase with increasing Mn concentration. In reality, investigations on binary alloys of the Fe-Ni system (up to 28% Ni), as well as of the Fe-Mn system (up to 10% Mn) clearly show the decreasing of M_S with increasing concentration of the alloying element for the common type (the packet-martensite) of $\gamma - \alpha$ - transformation, therewith the decrease is more pronounced for the Mn-alloys. So, a comparison of data [7] and [156] shows that a reduction of M_S , down to the level of 500 K, requires concentrations of 20% Ni or only 10% Mn.

Assume that the energies of 3d electronic states, belonging to the S-surface, are characterized by a given mean ε_d (see also the context to Eq.(3.9)). Then we can define the following model antithetical to the hard-zone model: In alloys of iron with elements of close neighbors in the 3d row of the transition metals (substitution alloys), the value $\varepsilon_d - \mu$ is considered as non-depending (or weakly depending) on composition and thus conserving the value that is the same as in pure γ - iron. This means is that the alloying element builds up own 3d sub-bands, which overlap with the 3d - bands of iron without a charge exchange flow among the components of alloy. (Hypothesis of minimum polarity [100]). Furthermore, we will assume that the magnitude of the threshold difference σ_t retains a value not exceeding 10^{-3} (as estimated for the region of high temperature), in alloys undergoing a martensitic transformation. Then, fulfilment of the threshold condition $\sigma_0 > \sigma_t$ can be justified within of the two-band model, for a wide region of concentrations C_{ae} of alloying elements, using the assumption that the magnitude of attenuation Γ_s of mobile s electrons is comparable with the value $(\varepsilon_d - \mu)\hbar^{-1}$ and many times larger than the attenuation Γ_d of the 3d - electrons, which are active during the generation of phonons (the typical lifetime of s - electrons $\tau_s \sim 10^{-15}$ s in 3d metals corresponds to the value $\hbar \Gamma_s \sim 0,6$ eV). The population of states with energies $\varepsilon_d > \mu$ can be kept up $f_d^0 \geq 0,1$ by an effective scattering mechanism into d - states of s - electrons with energies ε_s that are corresponding to the condition

$$\varepsilon_d - \mu - \frac{\hbar \Gamma_s}{2} < \varepsilon_s - \mu + \hbar \omega < \varepsilon_d - \mu + \frac{\hbar \Gamma_s}{2}. \quad (4.1)$$

In (4.1) $\hbar \omega$ is the energy of a short-wave phonon, whose participation is required for satisfaction of momentum conservation law, if the uncertainty of the quasimomentums of s - electrons is small (in (4.1), the value $\hbar \Gamma_d$ is disregarded compared to $\hbar \Gamma_s$). Thus, for large Γ_s , the magnitude of thermal excitation $k_B T \sim (\varepsilon_s - \mu)$ can be much smaller than $\varepsilon_d - \mu$, without reduction of the d-state occupation. In a similar way, the mechanism of d - s scattering ensures that the states with the energy ε_d , located below the Fermi-level, despite of an inequality $\mu - \varepsilon_d > k_B T$ have the occupations $f_d^0 < 1$ significantly deviating from unit at the cost of an additional (nonthermal) broadening of the d - electron distribution function.

From the above analysis it is clear that the increase of concentration C of the alloying supplement ($C < 1/2$), which causes a rapid increase of the attenuation-part $\Gamma_s(C) \sim C(1 - C)$ of total attenuation, linked with the scattering on substitution atoms, Γ_s being combined with a temperature-reduction, by the following condition:

$$\hbar \omega + k_B T + \frac{\hbar \Gamma(C, T)}{2} \sim |\varepsilon_d - \mu|. \quad (4.2)$$

It has to be noted that the temperature-dependent contribution $\Gamma_s(T)$ connected with the scattering on thermally activated heterogeneities (vacancies, phonons, magnons etc.) is decreasing with decreasing T and must smooth down the behavior of $\Gamma_s(C, T)$, by stabilizing the broadening of the d-electron distribution function, within a wide range of T and C . Logically, at first we must obtain a modification of the equilibrium distribution function $f^0 \rightarrow \tilde{f}^0$ in such a way that \tilde{f}^0 must simultaneously consider the distribution function broadening determined by the factors T and Γ_s . After that it is necessary to analyze the behavior of the derivatives $\partial \tilde{f}^0 / \partial \mu$, $\partial \tilde{f}^0 / \partial T$ which determine the magnitude of the population difference σ_0 , together with the gradients $\nabla \mu$ and ∇T . Hence we have to find such region of the variables (T and Γ) in which (for a fixed value of $|\varepsilon_d - \mu|$) the value σ_0 attains a maximum that only slightly varies with simultaneous variations of T and Γ . The temperature belonging to this optimum region might then be defined as the optimum temperature \tilde{T} for the martensitic transformation process. If the electronic configurations of the atoms of lattice matrix and of the alloying element are known, it will be possible to determine the dependence $\tilde{T}(C)$, by calculating $\Gamma_s(C)$ and identifying the correlation between \tilde{T} and $\Gamma(C, \tilde{T})$. Then, the concentration-dependencies of $\tilde{T}(C)$ and $M_S(C)$ will be compared. It is also possible to deal with the inverted task:

- i we require a close relation between the dependencies of $\tilde{T}(C)$ and $M_S(C)$;
- ii we choose the electron configuration of one of the alloying components;
- iii we find the electron configuration of the atoms of the other component. It is the latter definition of task, allowing us to gather the additional information which will be used in the fourth chapter, during a comparison of the interdependence between $\tilde{T}(C)$ and $M_S(C)$, in the substitution alloys (Fe-Ni, Fe-Co, Fe-Mn) and in the interstitial alloys (Fe - C).

4.2 Modified electronic distributions and their derivatives in the case of a rectangular spectral density function

A statistically disordered lattice of the binary substitutional type can be considered as the medium comprising an ideal (periodic) arrangement of lattice knots, for which the probability of occupation of a knot (lattice point) with atoms of either one of its two components is equal to C and $1 - C$, respectively, where C - concentration of the dissolved component. The missing of a long-range order in such lattice, being caused by the stochastic nature of its single-knot-potentials, causes the states with predetermined quasi-momenta to become non-stationary. Therefore - within the general notion of some kind of periodic "effective" medium - one of the approaches for the description of substitutional alloys is characterized by the introduction of an effective Non-Hermitian Hamiltonian with complex eigenvalues, the imaginary part of which determines the extinction rate of electronic states [100]. The calculus of mean-values of electronic operators comprises both thermodynamic and configuration averaging, which have to be performed independently from each other for systems without a short-range order. As an example, the modified electronic distribution \tilde{f}^0 of our interest is given by the expression

$$\tilde{f}_{\mathbf{k}}^0 = \int_{-\infty}^{\infty} [1 + \exp(\frac{\varepsilon - \mu}{k_B T})]^{-1} A(\varepsilon, \mathbf{k}) d\varepsilon, \quad (4.3)$$

where the spectral density $A(\varepsilon, \mathbf{k})$ is a configurationally averaged probability in a given alloy for the existence of an electron of energy ε in a state with quasi-momentum $\hbar\mathbf{k}$. Usually, the spectral density obeys the Lorentz (Breit-Wigner) formula:

$$A(\varepsilon, \mathbf{k}) = \frac{1}{2\pi} \hbar \Gamma_{\mathbf{k}} \left[(\varepsilon - \varepsilon_{\mathbf{k}})^2 + \left(\frac{1}{2} \hbar \Gamma_{\mathbf{k}} \right)^2 \right]^{-1}, \quad (4.4)$$

where $\Gamma_{\mathbf{k}}$ - extinction of an electron in a state with energy $\varepsilon_{\mathbf{k}}$, where the extinction corresponds to the width at half of the height of the function $A(\varepsilon, \mathbf{k})$. Furthermore, the normalization condition is satisfied:

$$\int_{-\infty}^{\infty} A(\varepsilon, \mathbf{k}) d\varepsilon = 1. \quad (4.5)$$

Obviously from (4.4), (4.5), the spectral density (SD) function gradually transforms into the δ - function for $\Gamma_{\mathbf{k}} \rightarrow 0$

$$\lim_{\Gamma_{\mathbf{k}} \rightarrow 0} A(\varepsilon, \mathbf{k}) = \delta(\varepsilon - \varepsilon_{\mathbf{k}}), \quad (4.6)$$

and the distribution (4.3) into the Fermi-Dirac distribution:

$$\lim_{\Gamma_{\mathbf{k}} \rightarrow 0} \tilde{f}^0 = \tilde{f}_k^0 = \left[1 + \exp \left(\frac{\varepsilon_{\mathbf{k}} - \mu}{k_B T} \right) \right]^{-1}. \quad (4.7)$$

This is quite reasonable, as the condition $\Gamma_{\mathbf{k}} = 0$ would implicitly require a re-establishment of long-range ordering, as occurring during gradual transition of a binary alloy into a single-component system with $C \rightarrow 0$.

A simple analytical expression for $\tilde{f}_{\mathbf{k}}^0$ can easily be found by choosing a rectangularly shaped spectral density function with a height of $\hbar\Gamma_{\mathbf{k}}^{-1}$ and a width of $\Gamma_{\mathbf{k}}$, being symmetrically arranged with respect to the energy $\varepsilon_{\mathbf{k}}$:

$$A(\varepsilon, \mathbf{k}) = \frac{1}{\hbar\Gamma_{\mathbf{k}}} \left\{ \Theta \left[\varepsilon - \left(\varepsilon_{\mathbf{k}} - \frac{\hbar\Gamma_{\mathbf{k}}}{2} \right) \right] - \Theta \left[\varepsilon - \left(\varepsilon_{\mathbf{k}} + \frac{\hbar\Gamma_{\mathbf{k}}}{2} \right) \right] \right\}, \quad (4.8)$$

where Θ - Heaviside unit-function

$$\Theta(\varepsilon) = \begin{cases} 1 & \varepsilon \geq 0, \\ 0 & \varepsilon < 0. \end{cases} \quad (4.9)$$

After insertion of (4.8) in (4.3), we get:

$$\tilde{f}_{\mathbf{k}}^0 = 1 + \frac{1}{2\eta_{\mathbf{k}}} \ln \left[\frac{1 + \exp(y_{\mathbf{k}} - \eta_{\mathbf{k}})}{1 + \exp(y_{\mathbf{k}} + \eta_{\mathbf{k}})} \right], \quad (4.10)$$

where $y_{\mathbf{k}} = (\varepsilon_{\mathbf{k}} - \mu)(k_B T)^{-1}$, $\eta_{\mathbf{k}} = \hbar\Gamma_{\mathbf{k}}(2k_B T)^{-1}$. It can easily be verified that the limit condition (4.7) is satisfied for (4.10), so that we get for the low-temperature case $T \rightarrow 0$

$$\lim_{T \rightarrow 0} \tilde{f}_{\mathbf{k}}^0 = \begin{cases} 1 & \varepsilon_{\mathbf{k}} < \mu - (\hbar\Gamma_{\mathbf{k}})/2 \\ 1/2 + (\mu - \varepsilon_{\mathbf{k}})(\hbar\Gamma_{\mathbf{k}})^{-1} & \mu - (\hbar\Gamma_{\mathbf{k}})/2 \leq \varepsilon_{\mathbf{k}} \leq \mu + (\hbar\Gamma_{\mathbf{k}})/2 \\ 0 & \mu - (\hbar\Gamma_{\mathbf{k}})/2 < \varepsilon_{\mathbf{k}} \end{cases} \quad (4.11)$$

a distribution with a scattering width $\hbar\Gamma_{\mathbf{k}}$, as shown in 4.1. Moreover, the normalization condition for an electronic distribution $\tilde{f}_{\mathbf{k}}^0 = 1/2$ at $\varepsilon_{\mathbf{k}} = \mu$ is satisfied, independent of T. Disregarding the dependency on \mathbf{k} of the extinction Γ within a coherent potential approximation [100], we note that $\tilde{f}_{\mathbf{k}}^0$ remains constant along isoenergetic areas with $\varepsilon_{\mathbf{k}} = \text{const.}$ in quasi-momentum space, as $\tilde{f}_{\mathbf{k}}^0 = \tilde{f}_{\mathbf{k}}^0(\varepsilon_{\mathbf{k}})$. Accordingly, we shall design our spectral function by $A(\varepsilon, \mathbf{k}) = A(\varepsilon, \varepsilon_{\mathbf{k}})$.

Taking for granted that (4.3) represents the energetic distribution function $\tilde{f}^0(\varepsilon_{\mathbf{k}s}) \equiv \tilde{f}_{\mathbf{k}s}^0$ of the s-electrons in an alloy, we can now show that, for a given d-s-scattering mechanism with involvement of short-wave phonons, the equilibrium distribution: $\tilde{f}_{\mathbf{k}d}^0 = \tilde{f}^0(\varepsilon_{\mathbf{k}d})$ of d-electrons of energy ε_d in an alloy of the

same energy $\varepsilon_s = \varepsilon_d$ is nearly equal to the function $\tilde{f}^0(\varepsilon_s)$. According to [157], the modification of the normalized integral of electron-phonon collisions, being required after consideration of scattering at the substitutional atoms, can be reduced to a replacement of the δ - function, thus reflecting strict compliance with the conservation of energy requirement, by the Lorentz-function:

$$\left(\frac{\partial \tilde{f}_{\mathbf{k}d}}{\partial t}\right)_{col} = \frac{2\pi}{\hbar} \sum_{\mathbf{k}'\mathbf{p}} |W_{\mathbf{p}}|^2 \{A(\varepsilon_{\mathbf{k}'s}, \varepsilon_{\mathbf{k}d} + \hbar\omega_{\mathbf{p}})[N_{\mathbf{p}}(\tilde{f}_{\mathbf{k}'s} - \tilde{f}_{\mathbf{k}d}) + \tilde{f}_{\mathbf{k}'s}(1 - \tilde{f}_{\mathbf{k}d})] + A(\varepsilon_{\mathbf{k}'s}, \varepsilon_{\mathbf{k}d} - \hbar\omega_{\mathbf{p}})[N_{\mathbf{p}}(\tilde{f}_{\mathbf{k}'s} - \tilde{f}_{\mathbf{k}d}) - \tilde{f}_{\mathbf{k}d}(1 - \tilde{f}_{\mathbf{k}'s})]\} \quad (4.12)$$

where $|W_{\mathbf{p}}|$ - modulus of the matrix-element of electron-phonon-interaction, $N_{\mathbf{p}}$ - phonon-distribution function. Proceeding further with the integration of the $\varepsilon_{\mathbf{k}'s}$, under consideration of the definitions (1.1) and (1.3), and in order to find the equilibrium-distribution $\tilde{f}_{\mathbf{k}d}^0$, we require that the collision-integral (4.12) must vanish. Then we get approximately

$$\tilde{f}_{\mathbf{k}d}^0 \approx \frac{\tilde{f}_s^0(\varepsilon_{\mathbf{k}d} + \hbar\omega_{\mathbf{p}}) + [\tilde{f}_s^0(\varepsilon_{\mathbf{k}d} + \hbar\omega_{\mathbf{p}}) + \tilde{f}_s^0(\varepsilon_{\mathbf{k}d} - \hbar\omega_{\mathbf{p}})]N_{\mathbf{p}}}{2N_{\mathbf{p}} + 1 + [\tilde{f}_s^0(\varepsilon_{\mathbf{k}d} + \hbar\omega_{\mathbf{p}}) - \tilde{f}_s^0(\varepsilon_{\mathbf{k}d} - \hbar\omega_{\mathbf{p}})]}. \quad (4.13)$$

If we develop (4.13) by powers of $\omega' = \hbar\omega_{\mathbf{p}}(\varepsilon_{\mathbf{k}d} - \mu)^{-1}$, then we get in a zero-order approximation

$$\tilde{f}_{\mathbf{k}d}^0 \approx \tilde{f}_s^0(\varepsilon_d). \quad (4.14)$$

By consideration of (4.10), the linear supplement in the right hand side of (4.14)

$$\frac{\partial \tilde{f}_s^0(\varepsilon_d)}{\partial(\varepsilon_d - \mu)}(1 - 2\tilde{f}_s^0(\varepsilon_d))\hbar\omega_{\mathbf{p}}$$

can be written in the following form

$$\frac{1}{2\Gamma'} \frac{\sinh \Gamma'(T')^{-1}}{\cosh \Gamma'(T')^{-1} + \cosh(T')^{-1}} (1 - 2\tilde{f}_s^0)\omega', \quad (4.15)$$

where

$$\Gamma' = \frac{\hbar\Gamma}{2(\varepsilon_{\mathbf{k}d} - \mu)}, \quad T' = \frac{k_B T}{\varepsilon_{\mathbf{k}d} - \mu}. \quad (4.16)$$

Let $\varepsilon_{\mathbf{k}d} - \mu \approx 0,2\text{eV}$, and $\omega_{\mathbf{p}}$ be of an order of magnitude of half of the Debye-frequency, then we get $\omega' \leq 10^{-1}$. An order of magnitude of about 0,1 also applies to the product of the other factors in (4.15), so that the corrective factor, being linear in ω' , becomes at least one order of magnitude smaller than in (4.14). Therefore, in an analysis of the non-equilibrium addenda to the function \tilde{f}_d

$$\Delta \tilde{f}_{\mathbf{k}d}(\nabla\mu) \approx \frac{\partial \tilde{f}_{\mathbf{k}d}^0}{\partial \mu'} \frac{\tau \mathbf{v}_{\mathbf{k}} \vec{\nabla} \mu}{\varepsilon_d - \mu}, \quad \mu' = \frac{\mu}{\varepsilon_d - \mu}, \quad (4.17)$$

$$\Delta \tilde{f}_{\mathbf{k}d}(\nabla T) \approx \frac{\partial \tilde{f}_{\mathbf{k}d}^0}{\partial T'} \frac{\tau \mathbf{v}_{\mathbf{k}} \vec{\nabla} T k_B}{\varepsilon_d - \mu},$$

it is possible to replace the function \tilde{f}_d^0 by f_s^0 (4.3) for $\varepsilon_{\mathbf{k}} = \varepsilon_{\mathbf{k}d}$. Under the presumption that this replacement has been performed all over, we can omit in our subsequent analysis the indices d, zero and tilde in our notation of the function $\tilde{f}_d^0 \rightarrow f$. After having fixed in (4.17) the values of $\tau \mathbf{v} \vec{\nabla} \mu$, $\tau \mathbf{v} \vec{\nabla} T$, we only need to analyze the derivatives $\partial f / \partial T'$, $\partial f / \partial \mu'$ for our envisaged determination of the optimum values of Γ and T (see Pt. 4.1), as a function of the dimensionless variables Γ' and T' (4.16). It is convenient to use these variables, as the value of $\varepsilon_d - \mu$ will remain unchanged, according to our assumption in Pt.4.1. In the case of the spectral density (4.8) we can obtain from (4.10) the derivatives $\partial f / \partial T'$, $\partial f / \partial \mu'$ by direct differentiation:

$$\frac{\partial f}{\partial T'} = \frac{1}{2\Gamma'} \left\{ \ln \left[\frac{1 + \exp(y - \eta)}{1 + \exp(y + \eta)} \right] + \frac{y \sinh \eta + \eta (\cosh \eta + \exp y)}{\cosh y + \cosh \eta} \right\}, \quad (4.18)$$

$$\frac{\partial f}{\partial \mu'} = \frac{1}{2\Gamma'} \frac{\sinh \eta}{\cosh y + \cosh \eta}, \quad (4.19)$$

where $\eta = \Gamma' T'^{-1}$, $y = T'^{-1}$.

The results of our calculus of the derivatives $\partial f / \partial \mu'$ and $\partial f / \partial T'$ on the basis of (4.18) and (4.19) are presented in Figs. 4.2 and 4.3. In these figures, the group of thin lines represents the constant values of the functions $\partial f / \partial \mu'$, $\partial f / \partial T'$ (being labeled at each line), while the dashed lines 1 and 2 are defined by the conditions

$$\frac{\partial}{\partial T'} \left(\frac{\partial f}{\partial \mu'} \right) \Big|_{\Gamma'} = 0, \quad \frac{\partial}{\partial \Gamma'} \left(\frac{\partial f}{\partial \mu'} \right) \Big|_{T'} = 0. \quad (4.20)$$

These lines correspond to the maximum values of the derivatives $\partial f / \partial \mu'$, $\partial f / \partial T'$ of the variables T' and Γ' and pass through those points where the parallels to the vertical and horizontal coordinate axes touch the iso-lines. The area enclosed by the lines in Fig. 4.2 represents a region of values of the parameters T and Γ for which the occupational inversion $\sigma_0(\nabla\mu)$ attains maximum values, only slowly varying with T and Γ . Obviously, it is justified to define an optimum temperature for phonon-generation, which decreases with increasing extinction Γ , by highlighting within this region the point corresponding to pure iron. Thus the behavior of the derivative $\partial f / \partial \mu'$ suggests the existence of an optimum temperature \tilde{T}_1 , the derivative of which obeying to the condition $\partial \tilde{T}_1 / \partial C < 0$, where $C = C_{ae}$ is the concentration of the alloying element. The jump of the value of $\partial f / \partial \mu'$ from 0 up to 0,5, during the transition from $\Gamma' < 1$ to $\Gamma' > 1$ (at the point

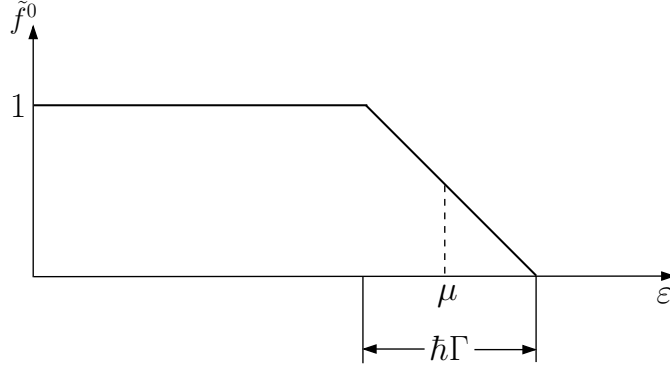


Figure 4.1. Modified SD - function at a temperature of 0 K.

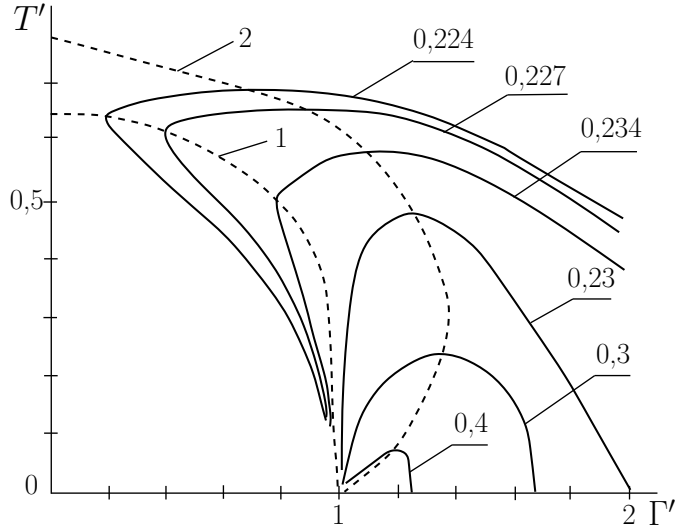


Figure 4.2. Calculated values of the derivative $\partial f/\partial\mu'(\Gamma', T')$, for the case of a rectangular SD- function: — - iso-lines with constant values of the $\partial f/\partial\mu'$ - function (Lines 1 and 2 are defined in the text).

$\Gamma' = 1$ we have $\partial f/\partial\mu' = 0,25$) and for $T' \rightarrow 0$, is obvious from Eq. (4.19), which attains the following form for $T' \rightarrow 0$:

$$\frac{\partial f}{\partial\mu'} \approx \frac{1}{2\Gamma'[1 + \exp(1 - \Gamma')(T')^{-1}]}$$

This jump is due to the extremely rapid decay of the modeled spectral density function (4.8) within a variation of the energy $\varepsilon_{\mathbf{k}}$ by $\pm 1/2\Gamma_{\mathbf{k}}$, and there is no reason for expecting such a jump for a smoother behavior of $A(\varepsilon, \varepsilon_{\mathbf{k}})$.

A comparison of Figs. 4.3 with 4.2 obviously shows that the crucial difference among the behavior of $\partial f/\partial T'$ vs. that of $\partial f/\partial\mu'$ is due to the existence of an ascending section of line 1 for $\Gamma' > 1$, which could serve as the basis for the definition of an optimum phonon generation temperature \tilde{T}_2 , which would increase

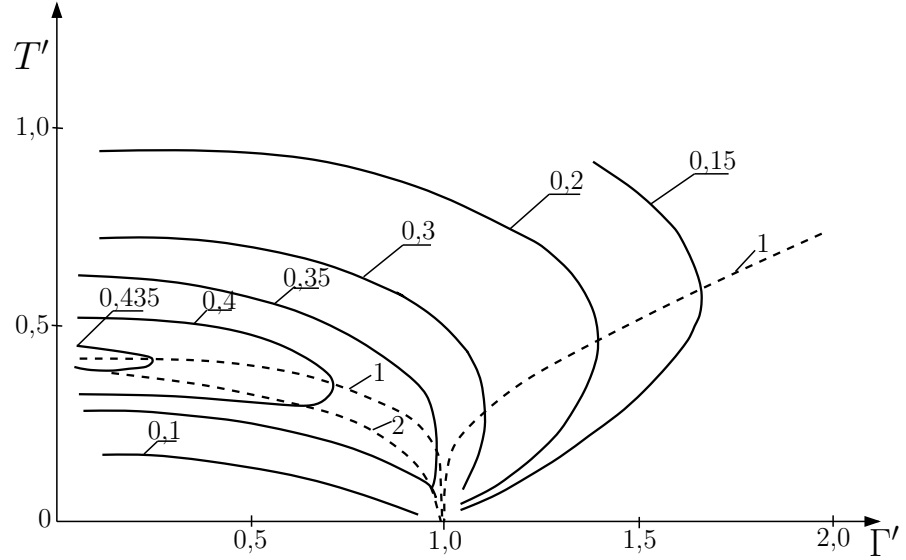


Figure 4.3. Calculated values of the derivative $\partial f(\Gamma', T')/\partial T'$, for the case of a rectangular SD-function: — - iso-lines.

with increasing value of C_{ae} : $\partial \tilde{T}_2 / \partial C_{ae} > 0$. As the abrupt "slump" at $\Gamma' \rightarrow 1$, $T' \rightarrow 0$, along line 1 (at point $\Gamma' = 1$, $T' = 0$, $\partial f / \partial T' = 1/2 \ln 2 \approx 0,347$) is caused by the already mentioned particularity of the spectral density function (4.8). It can be anticipated that this "slump" will vanish when getting over to the more smoothly changing functions $A(\varepsilon, \varepsilon_{\mathbf{k}})$, and that the ascending section of line 1 will broaden out. We also note that the quantity $\partial f / \partial T'$ diminishes more rapidly with increasing Γ' than $\partial f / \partial \mu'$. A convincing explanation for this behavior can immediately be concluded from (4.3), if one considers that derivations on T and μ lead accordingly to factors being odd and even on ε concerning the point μ in the integrand.

If we summarize the results of our calculus with usage of a rectangularly shaped spectral density, it can be concluded that they provide strong evidence for the existence of optimum conditions for phonon generation, within a wide concentration region of the alloying element, a possibility we already tentatively anticipated in Pt. 4.1, on the basis of qualitative thoughts. However, a more detailed treatise of the task of Pt. 4.1 could reasonably be performed by determination of the derivatives $\partial f / \partial T'$ and $\partial f / \partial \mu'$ on the basis of the Lorentz-expression of spectral density, as will be done in the next chapter.

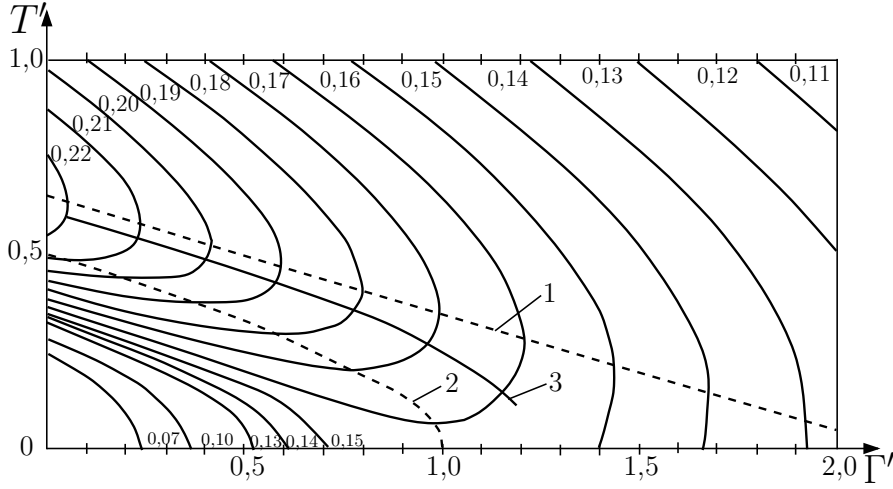


Figure 4.4. Calculated values of the derivative $\partial f(\Gamma', T')/\partial \mu'$, for the case of a Lorentz-shaped SD- function: — - iso-lines.

4.3 Region of T' , Γ' values with optimum conditions for phonon-generation in the case of a Lorentz-shaped SD-function

An explicit determination of $\partial f/\partial \mu'$, $\partial f/\partial T'$ on the basis of (4.3) proves to be difficult in the case of the Lorentz-form (4.4) of the function $A(\varepsilon, \varepsilon_{\mathbf{k}})$. That's why a numeric calculus of T' has been performed, the results of which are presented in Figs. 4.4,4.5. Let us now compare in pairs Fig.4.4 with Fig. 4.2 and 4.5 with 4.3. A comparison of the first pair of results shows that, during a transition to a smoothly changing spectral density (4.4), the optimum region of parameters T' , Γ' is being retained, even though lines 1 and 2 of the maximum value of $\partial f(T', \Gamma')/\partial \mu'$ exchange their relative positions (in Fig. 4.2, line 2 is located above line 1 and in Fig. 4.4 below line 1). In addition, in the region between lines 1 and 2, the values $\partial f/\partial \mu'$ of the Lorentz-form $A(\varepsilon, \varepsilon_{\mathbf{k}})$ slowly decrease with increasing Γ' and with decreasing T' , while the function $\partial f/\partial \mu'$ in Fig. 4.2 behaves non-monotonously, especially in the vicinity of the point $T' \rightarrow 0$, $\Gamma' \rightarrow 1$. The solid line 3 in Fig. 4.4 is the projection of the "crest" of the profile of function $\partial f/\partial \mu'$ on plane (Γ', T') . The function $T'(\Gamma')$ with lines 1, 2, 3 describes the reduction of T' with increasing Γ' , in a similar way as relation (4.2). This means that they can be used as a basis for determination of the temperature \tilde{T}_1 .

The characteristic difference between Figs. 4.5 and 4.3 consists in the missing "slump" of line 1, which - for $0 < \Gamma' \leq 0,8$ - slightly changes in the proximity of $T' \approx 0,4$, attaining its minimum at $T' \approx 0,39$, $\Gamma' \approx 0,42$, being approximated by a straight line for $\Gamma' > 0,8$

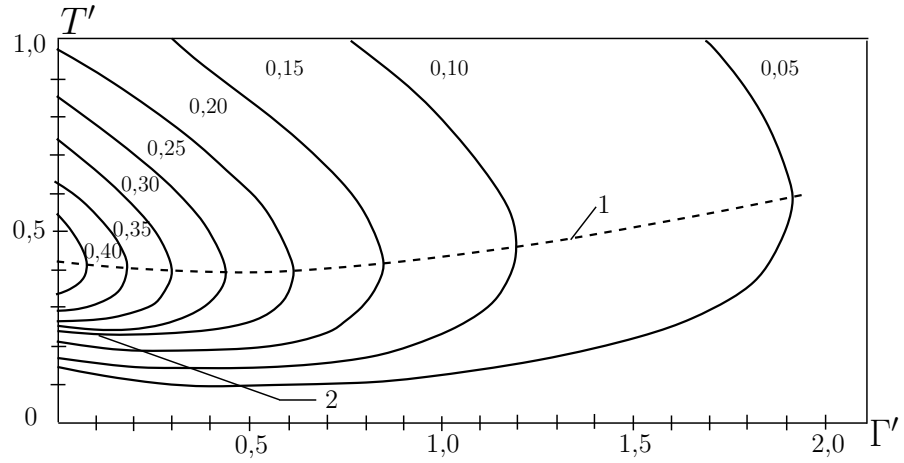


Figure 4.5. Calculated values of the derivative $\partial f(\Gamma', T')/\partial T'$ for the case of a Lorentz-shaped SD-function : ——— - iso-lines.

$$T' \approx 0,25 + 0,175\Gamma'. \quad (4.21)$$

Of course, also a parabolic approximation might be possible. Obviously, by usage of the function $T'(\Gamma')$, corresponding to (4.21), it would be feasible to determine the temperature \tilde{T}_2 , which increases with increasing Γ' . Line 2 in Fig. 4.5 is shifted towards the lower T', Γ' region, both in relation to Fig. 4.3 and to Fig. 4.4 and could thus in principle be used for the introduction of temperature \tilde{T}_1 , provided the starting temperature of the martensitic transformation of the main alloying component is close to it.

Let us surmise that the function $\tilde{T}_{1,2}(\Gamma')$ - being the mapping of the function $\tilde{T}_{1,2}(C)$ onto the plane (Γ', T') - is known. Then, in order to determine the explicit expressions for $\tilde{T}_{1,2}(C)$, we must first discriminate those fractions of total electron extinction Γ being dependent on the concentration of the alloying element:

$$\Gamma(T, C) = \Gamma(T) + \Gamma(C). \quad (4.22)$$

In paramagnetic alloys, at temperatures larger than or close to the Debye-temperature T_D , the extinction $\Gamma(T)$ is mainly caused by s-electron scattering at phonons and magnetic moment fluctuations. The first of these processes leads to a contribution $\Gamma(T)$ exhibiting linear variation with temperature, while the second one only weakly depends on T - for temperatures above the Curie-temperature T_c (or the Neel-temperature T_N respectively) - and rapidly diminishes for $T < T_c$. Measurements of the specific electric resistance ρ [158] (see also §3 of Ch. 25 in [159]) have shown that the contribution to scattering by magnetic inhomogeneities for $T > 500$ K exceeds phonon scattering by about the same order of magnitude. In the region of temperature $T < 1100$ K, being relevant for martensitic transformations, ρ decreases monotonously with decreasing T . Even though

the function $\rho(T)$ is non-linear, we shall use below, for simplification, the linear approximation $\hbar\Gamma(T) = a_0 k_B T$, where a_0 - dimensionless parameter. Obviously, we can already anticipate that a_0 must be a one-digit number greater than 1, as the contribution of pure phonon-scattering already amounts $a_0 \approx 1$ in the case of transition-metals. In principle, it is also possible to include in (4.22) the part being largely independent of T and C, being caused by scattering on static defects (i.e. dislocations, alloying atoms of a third element etc.), but we shall assume that the growth of martensite crystals will proceed within a region being practically devoid of such defects, thus confining ourselves to the contributions of only two terms in (4.22). The usage of the ratio (4.22) takes into account that phonon scattering leads to a more scattered energy distribution function, essentially resulting in the need for replacement of the δ - function by a Lorentz-line of finite width [160]. In this context we should remind that during any consideration of the washout of the Fermi- distribution, the equivalence of different scattering mechanisms will always be confirmed, which inevitably leads to the question about the justification of a well defined Fermi-surface in alloys. Among other arguments, it is being emphasized that a case is possible for which "... an alloy in the proximity of absolute zero temperature represents a better model of an ideal lattice than that of a pure metal lattice at room temperature " [161].

The extinction $\Gamma(C)$ is mostly caused by scattering of s-electrons on alloying elements. In a modeled alloy with diagonal disorder and weak scattering, the following form is true [100]:

$$\hbar\Gamma(C) = 2\pi g_s(\mu) \delta^2 C(1 - C). \quad (4.23)$$

Here $\delta = (\varepsilon_s^{ae} - \varepsilon_s^M)$ - difference of the energy levels of s-states of alloying components;

$g_s(\mu)$ - density of s-electron-states of the matrix at Fermi-level (per spin-orientation). Thus for a numeric assessment of $\Gamma(C)$, the quantities $g_s(\mu)$ and δ must be known. They can be determined if the width W_s of the s-band, the parameter a_0 , and the amount of s-electrons donated by the alloying element Z_{ae} (with matrix Z_M) into the common s-band, i.e. if the electronic configurations of the alloying elements are known. In fact, we have a parabolic s-band:

$$g_s(\varepsilon) \sim \sqrt{\varepsilon}, \quad \int_0^{W_s} g_s(\varepsilon) d\varepsilon = 1, \quad (4.24)$$

$$g_s(\varepsilon) = \frac{3}{2} \left(\frac{\varepsilon}{W_s^3} \right)^{\frac{1}{2}}.$$

Considering that the occupied part of the s-band accepts $Z_M/2$ electrons, i.e.

$$\int_0^{\mu} g_s(\varepsilon) d\varepsilon = \frac{Z_M}{2}, \quad (4.25)$$

we get, after insertion of (4.24) in (4.25):

$$\left(\frac{\mu}{W_s}\right)^{\frac{1}{2}} = \left(\frac{Z_M}{2}\right)^{\frac{1}{3}}. \quad (4.26)$$

Finally we can express (4.26) and (4.24) $g_s(\mu)$ as a function of Z_M :

$$g_s(\mu) = \frac{3}{2W_s} \left(\frac{\mu}{W_s}\right)^{\frac{1}{2}} = \frac{3}{2W_s} \left(\frac{Z_M}{2}\right)^{\frac{1}{3}}. \quad (4.27)$$

According to [100], the parameter δ is linked up with the difference $\Delta Z = Z_{ae} - Z_M$ by means of the relation

$$\Delta Z = -\frac{2}{\pi} \arctan [\pi \delta g_s(\mu) (1 - \delta I(\mu))^{-1}]; \quad (4.28)$$

$$I(\mu) = \int_{-\infty}^{\infty} \frac{g_s(\eta)}{\mu - \eta} d\eta = \frac{3}{2W_s} \left[x \ln \left| \frac{1+x}{1-x} \right| - 2 \right], \quad (4.29)$$

$$x = \left(\frac{Z_M}{2}\right)^{\frac{1}{3}}.$$

In the following, we shall designate by Z_M the number of electrons donated into the s-band by the iron atoms, using $Z_M = Z_{Fe}$.

Obviously, the justification for introduction of the $M_S(C)$ - like function of $\tilde{T}_{1,2}(C)$, can be given on the basis of the analysis performed, by mapping the function $M_S(C)$ onto the plane (Γ', T') , with subsequent determination of those specific values of the parameters $a_0, \delta, \varepsilon_d - \mu$, for which the obtained representations $\tilde{M}_S(\Gamma')$ are located in the vicinities of the dashed lines in Figs. 4.4 and 4.5. Doing this way, it will be possible to bring in accordance various experimental data with the defined above laws.

4.4 Mapping of the functions $M_S(C)$ into the T', Γ' region of optimum phonon-generation, with analysis of the electronic configurations of atoms in binary substitutional alloys

The variation of $M_S(C)$ with concentration mentioned in Pt. 4.1 belongs to the kind of results which have been determined with massive specimen. Besides these

data, there is currently being collected experimental data related to super-rapid quenching (up to $5 \cdot 10^5$ K/s) of foils with a thickness of $\sim 10^{-4}$ m (see for example [162–164] for binary alloys and [165, 166] for steel). It could be shown that in different regimes of cooling-rates of steel and iron-based alloys there can be realized four "stages" of martensitic transformations. An extrapolation of these data towards pure iron delivers the following temperatures M_S^i of these "stages": $M_S^I = 820$, $M_S^{II} = 720$, $M_S^{III} = 540$, $M_S^{IV} = 430$ °C. The existence of various M_S - stages is explained in [164] with the hypothesis of structural particularities of the moving phase-boundaries, as well as by different diffusion mechanisms in their vicinity. During changes of composition, the amount of "stages" will usually decrease, mainly due to the different rates of change of M_S^i during the alloying process, resulting into overlapping of the stages.

Let us now inspect more in detail the Fe - Ni and Fe - Co systems. For this purpose, the corresponding functions M_S^i are shown in Figs. 4.6 and 4.7. For Fe-Ni-alloys, the following inequalities apply for the derivatives (slopes) of the functions $M_S^i(C)$:

$$\left| \frac{d M_S^{II}}{d C} \right| > \left| \frac{d M_S^I}{d C} \right| > \left| \frac{d M_S^{III}}{d C} \right| > \left| \frac{d M_S^{IV}}{d C} \right|, \quad \frac{d M_S^i}{d C} < 0.$$

This means that all M_S^i decline with increasing concentrations of C. By contrast, in Fe-Co-alloys, the temperatures M_S^I , M_S^{III} , M_S^{IV} increase with increasing C, while M_S^{II} decreases:

$$\left| \frac{d M_S^{II}}{d C} \right| > \left| \frac{d M_S^{III}}{d C} \right| > \left| \frac{d M_S^{IV}}{d C} \right| > \left| \frac{d M_S^I}{d C} \right|.$$

If, according to [164], the second MT-stage was combined with the motion of a phase-boundary embodying a Cottrell-atmosphere, then the abnormal M_S^{II} - behavior could be attributed - at least in the case of Fe-Co-alloys - to solute carbon, as the high mobility of carbon atoms can contribute to the rapid formation of a Cottrell-atmosphere. We note here that for Fe- C-alloys, the slope $d M_S^{II}/d C < 0$ is of an order of magnitude of the slope $d M_S^I/d C$, thus exceeding the corresponding derivatives of Fe-Ni, Fe-Co - alloys. This would be evidence for the correctness of our above assumption. As the theory of electron-scattering in substitutional alloys also has to take into account the effects of lattice-deformation, the function $M_S^{II}(C)$ will not be analyzed here.

We also have to point at another particularity of the function $M_S^I(C)$ in Fe-Co-alloys: In the region of small concentrations of C, M_S^I remains almost constant, i.e. $d M_S^I/d C \approx 0$. But if $C \geq 7$ %, then a pronounced slope $d M_S^I/d C > 0$ appears. Assuming an inherent similarity between the functions $\tilde{M}_S^I(\Gamma')$ and $\tilde{T}_2(\Gamma')$, this particularity can easily be explained: It can be taken for granted that the temperature $M_S^I(0)$, when represented on plane (Γ', T') , corresponds to the coordinates $T' \approx 0, 4$, $\Gamma' \approx 0, 42$, in the vicinity of which (as explained in Pt. 4.3) there also is located the minimum of curve \tilde{T}' , where the transition of \tilde{T}' (being

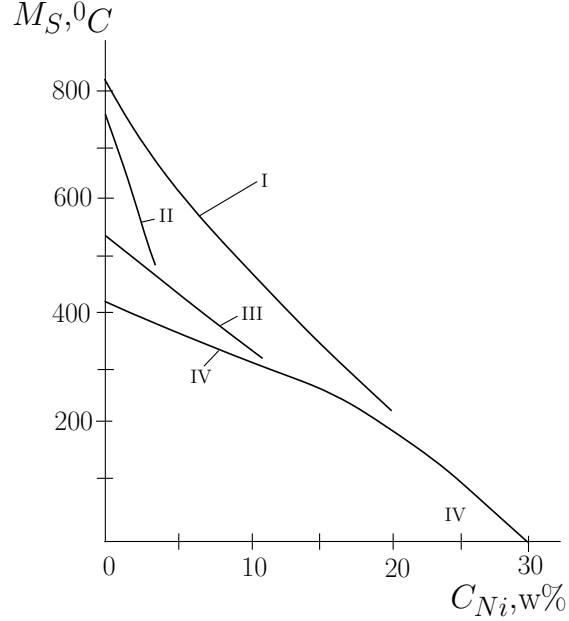


Figure 4.6. Variation with nickel-concentration (weight %) of the temperatures \tilde{M}_S^i , in iron-nickel-alloys [162].

essentially independent of $\tilde{\Gamma}'$) towards the function (4.21) takes place. Then we choose this point as the starting point and get from (4.16):

$$T' = \frac{k_B M_S^I(0)}{\varepsilon_d - \mu} \approx 0,4; \quad \Gamma' = \frac{\alpha_0 k_B M_S^I(0)}{2(\varepsilon_d - \mu)} \approx 0,42, \quad (4.30)$$

from which we can simultaneously determine the values of two parameters: $a_0 \approx 2,1$ and $(\varepsilon_d - \mu)/k_B \approx 2,5$ $M_S^I \approx 2750$ K. If these values were considered as fixed and characteristic of the fcc phases of iron, then it would be possible to perform the mappings of M_S^i onto plane (Γ', T') , simply by varying the parameter ΔZ , being determined by (4.28). This way, it has to be considered that in the case of weak scattering, the parameter δ , being linked with ΔZ , must be a small quantity in relation to the width W_s of the s-band. Let $W_s = 10$ eV, which - for an assumed width $W_d = 5$ eV of the d-band - would correspond to the 10-fold difference of the average densities of the s- and d-electron states.

For the Fe-Ni - system, we shall use the two nickel-atom configurations $3d^{9,4}4s^{0,6}$ and $3d^{8,6}4s^{1,4}$, as configurational references, as proposed in [110, 167]. During our projection of the graphs $M_S^i(C)$ on plane (Γ', T') we choose 5 points being borrowed from [162]: For $C_1 = 0$ (starting points), $C_2 = 5\%$, $C_3 = 12\%$ (in the proximity of C_3 , the curves $M_S^{III}(C)$ and $M_S^{IV}(C)$ intersect), $C_4 = 22\%$ (in the proximity of C_4 , the slope of curve $M_S^{IV}(C)$ changes), $C_5 = 30\%$ (in the proximity of C_5 the curves $M_S^I(C)$ and $M_S^{IV}(C)$ intersect). We further note that for a Ni-concentration $C_{Ni} > C_5$, the slope of the graph $M_S(C)$ abruptly increases, so that variations of Ni-concentrations by about 4% from 30% up to 34% will

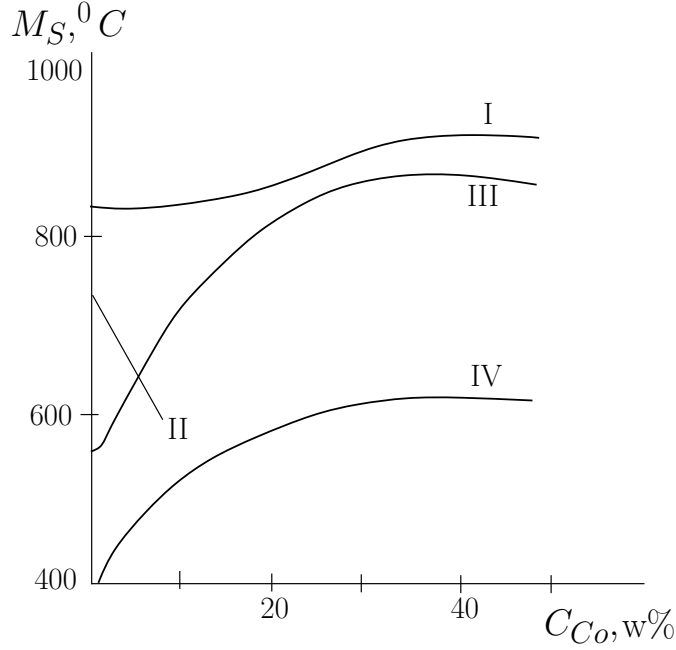


Figure 4.7. Variation with cobalt-concentration (weight %) of the temperature \tilde{M}_S^i , in iron-cobalt alloys [164].

cause a decrease of M_S from 250-270 K close to 0 K. Then we have to introduce the additional requirement that the point $\tilde{M}_S^I = \tilde{M}_S^{IV}$ of the intersection of the first and second stage must fall on the line of extremes 2 (see Fig.4.4), the end of which, close to $\Gamma' \approx 1$, exhibits a section of rapid, non-linear decrease of T' , with only small variation of Γ' . For the a.m. parameters a_0 , W_s , $Z_{Ni} = 0,6$ and $\Delta Z > 0$, it will quite easily be possible to show that, on the basis of (4.16), (4.22), (4.23), (4.27) - (4.29) and by variation of ΔZ , the condition for location of the point $\tilde{M}_S^I = \tilde{M}_S^{IV}$ on line 2 at $Z_{Fe} = 0,91$ can be met. The magnitude of the slope $\partial f / \partial \mu' \geq 0,16$ at point $\tilde{M}_S^I = \tilde{M}_S^{IV}$ remains high. For comparison, we note that at $Z_{Fe} = 1,02$ (point $\tilde{M}_S^I = \tilde{M}_S^{IV}$ on line 1) the slope $\partial f / \partial \mu' \approx 0,13$ is significantly lower. Fig. 4.8 shows the graphs $\tilde{M}_S^i(\Gamma')$ for $Z_{Fe} = 0,91$, corresponding to the configuration $3d^{7,09}4s^{0,91}$ of iron-atoms. During deviations of the point $\tilde{M}_S^I = \tilde{M}_S^{IV}$ from line 2, being associated with a variation of Z in the region $0,88 \leq Z \leq 0,93$, the magnitude of $\partial f / \partial \mu' \approx 0,16$ remains unchanged.

For $\Delta Z < 0$, the iron-atoms will attain configurations with a number of s-electrons less than 0,6. Even though apparently, such a configuration might not be materialized, a consideration of the case $\Delta Z < 0$ may still be useful, from a methodological point of view. An analysis of (4.23), (4.27) - (4.29) in fact leads to the conclusion that, within our notion, the contribution to total extinction $\Gamma(C)$, related to scattering on solute charged atoms, will vanish in the following three specific cases: At $\Delta Z = 0$ (neutral effect), for $Z_M \rightarrow 0$, $x \rightarrow 0$, $g_s(\mu) \rightarrow 0$ (in this case, the Fermi-level corresponds to the bottom of the s-band coinciding with the

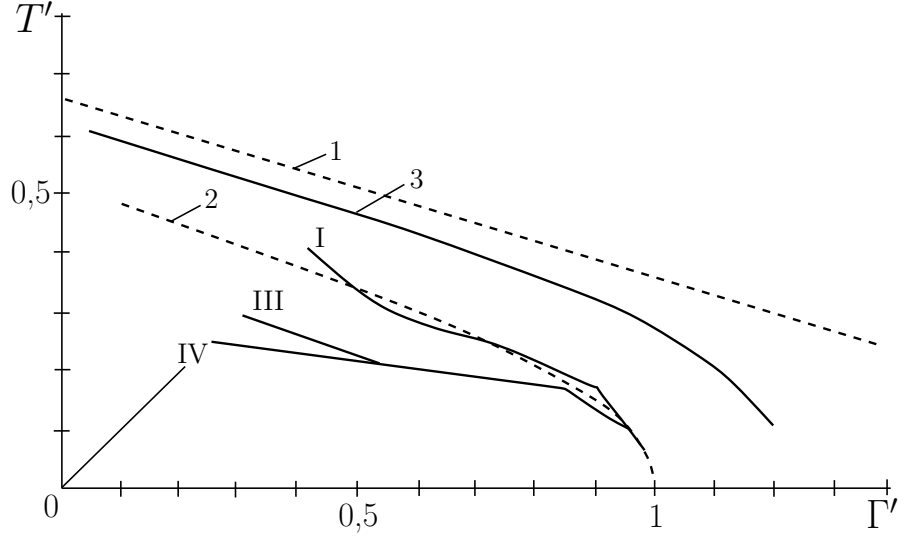


Figure 4.8. Graphs of $\tilde{M}_S^i(\Gamma')$ for Fe-Ni-alloys with $Z_{Ni} = 0,6$, $Z_{Fe} = 0,91$ (or with $Z_{Ni} = 1,4$, $Z_{Fe} = 1,04$): The graphs \tilde{M}_S^i were drawn from the starting points (I, III, IV), which correspond to pure iron; lines 1, 2 and 3 are identical to those in Fig. 4.4.

baseline of the density of states function) and for $Z_M \rightarrow 2$, $x \rightarrow 1$ (in this case, the Fermi-level corresponds to the upper edge of the fully occupied s-band). In these particular cases and in accordance with (4.22), (4.30), total extinction is mainly related to the effects of phonon-scattering and magnetic inhomogeneities, so that the relation $\Gamma' = 1,05 T'$ applies. Point $\tilde{M}_S^I(C_5) = \tilde{M}_S^{IV}(C_5)$ has the coordinates $T' \approx 0,1$, $\Gamma' \approx 0,1$, lying outside of the optimum region, $\partial f/\partial \mu' \approx 0,04$, thus being one fourth as large as the corresponding values in the proximity of line 2 (see Fig. 4.8). For a given value of T' , the approach to the optimum region will also depend on the increase of Γ' , through the scattering effect of the impurities. A path being almost equivalent to that of curves $\tilde{M}_S^i(\Gamma')$ in Fig. 4.8 corresponds to $Z_{Fe} \approx 0,09$, for a configuration $3d^{7,91}4s^{0,09}$ of the iron atoms, being close to the $3d^8 4s^0$ configuration. Full correspondence of the paths of these curves however is not possible, as for $\Delta Z < 0$, the values of Γ' are limited. The existence of the maximum Γ' at fixed T' , for certain Z_{Fe} lying within an interval $0 < Z_{Fe} < 0,6$ is obvious, as the extinction Γ' takes on minimum equivalent values $\Gamma' \approx T'$, at the borders of the interval ($Z_{Fe} = 0,6$ ($\Delta Z = 0$), $Z_{Fe} = 0$). The condition $\Gamma' = \Gamma'_{max} \approx 0,936$ at $T' = 0,1$ also matches with the above mentioned value of $Z_{Fe} \approx 0,09$ with the configuration $3d^{7,91}4s^{0,09}$ of the iron atoms. It is also obvious from Fig. 4.8 that, at the point with coordinates $T' = 0,1$, $\Gamma' \approx 0,936$, the slope is $\partial f/\partial \mu' \geq 0,16$, but line 2 is out of reach for the point $\tilde{M}_S^I = \tilde{M}_S^{IV}$.

For $Z_{Ni} = 1,4$ and $\Delta Z < 0$, the location of point $\tilde{M}_S(C_5)$ on line 2, with coordinates $T' = 0,1$, $\Gamma' \approx 0,96$ (the same as for the case with $Z_{Ni} = 0,6$, $\Delta Z > 0$), corresponds to the value $Z_{Fe} \approx 1,04$ with the iron-atom configuration

$3d^{6,96}4s^{1,04}$. After similar considerations as those done in the case of $Z_{Ni} = 0,6$, $\Delta Z < 0$, we can find out for the difference $\Delta Z > 0$, corresponding to the inequality $1,4 < Z_{Fe} < 2$, an iron-atom configuration $3d^{6,11}4s^{1,89}$, being close to the configuration $3d^6 4s^2$, for which the point $\tilde{M}_S(C_5)$ has the coordinates $T' \approx 0,1$, $\Gamma' = \Gamma'_{max} \approx 0,65$. Even though this point does not merely reach line 2, the corresponding slope $\partial f / \partial \mu' \geq 0,15$ at this point is quite high. Thus the assumption on the existence of two iron-configurations in the γ - phase, being close to the $3d^7 4s^1$ and $3d^6 4s^2$ configurations with $Z_{Ni} = 1,4$ (see Pt.2.5), is compatible with the requirement of conservation of optimum generation conditions for phonon-generation in Fe-Ni-alloys, for both of these configurations.

In [163], the processing of data for the Fe-Mn - system has been performed in a similar way. As reference-configurations, there were used iron-atom configurations like those determined above for the Fe-Ni-system. In addition, satisfaction of the requirement of conformity for points M_S^{IV} , within the systems Fe-Ni and Fe-Mn, with $C_{Ni} = 22\%$ and $C_{Mn} = 11\%$, respectively, was imperative. The results obtained are listed in Table 4.1.

Table 4.1. Charge numbers of manganese- and iron-ions

Z_{Fe}	0,09	0,91		1,04		1,89
Z_{Mn}	0,84	0,53	1,37	1,49	0,63	1,19
ΔZ_{Fe-Mn}	- 0,75	0,38	- 0,46	- 0,45	0,41	0,7

To ease our comparison, Table 4.2 also shows the specifications of the quantities Z and ΔZ , pertaining to the Fe-Ni-system. For "average" iron-configurations near $3d^7 4s^1$ (being equivalent to $Z_{Fe} = 1$), the following conclusion is obvious: To obtain a slope of the relationship $M_S(C)$ in Fe-Mn-alloys, doubly exceeding the corresponding slope in Fe-Ni-alloys, it will suffice that the manganese-atoms must only donate 0,1 more electrons into the s-band than the Ni-atoms. For "marginal"-configurations near $3d^8 4s^0$, $3d^6 4s^2$, this difference would amount to 0,2 electrons per atom.

Table 4.2. Charge numbers of nickel- and iron-ions

Z_{Ni}	0,6		1,4	
Z_{Fe}	0,09	0,91	1,04	1,89
ΔZ_{Fe-Ni}	- 0,51	0,31	- 0,36	0,49

Now let us use the previously determined iron-atom configurations for our foundation of the curves $\tilde{M}_S^i(\Gamma')$ of Fe-Co-alloys. By varying the parameter ΔZ , it is easy to obtain the lines $\tilde{M}_S^i(\Gamma')$ for the function $\tilde{T}'(\Gamma')$, which come close

to line 1 in Fig. 4.5. In Fig. 4.4, the curves $\tilde{M}_S^i(\Gamma')$ are depicted for an "average" iron-atom-configuration $3d^{7,09}4s^{0,91}$ and $\Delta Z = 0, 2$, being in accordance with the correspondence of the path of curve $\tilde{M}_S^I(\Gamma')$ with line 1 (dashed line in Fig. 4.4). The ends of lines \tilde{M}_S^i correspond to a Co-concentration of 40%, and attain maximum values at M_S^I, M_S^{III} (see Fig. 4.7).

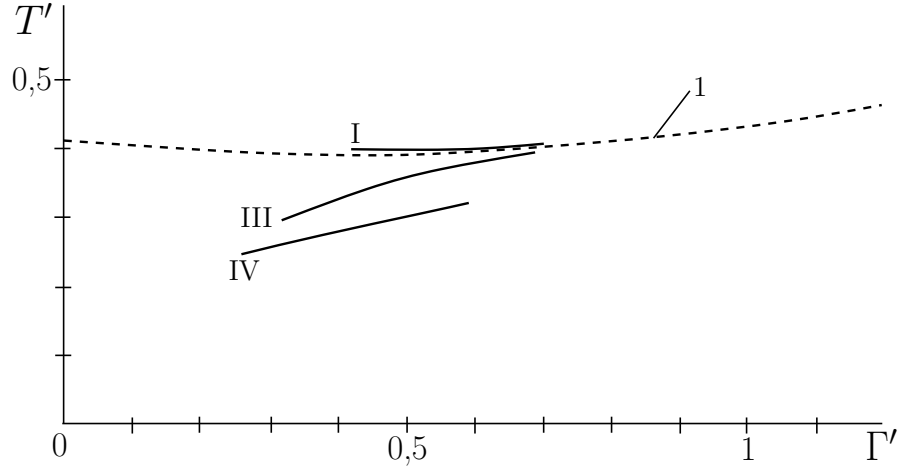


Figure 4.9. Graphs $\tilde{M}_S^i(\Gamma')$ for Fe-Co-alloys with $Z_{Fe} = 0,91, Z_{Co} = 1,12$ (or with $Z_{Fe} = 1,04, Z_{Co} = 1,24$); line 1 is identical to that in Fig. 4.5.

The same general path of curves as those with $\Delta Z = 0, 2$ also results for $\Delta Z = -0,21$, corresponding to a cobalt-atom-configuration $3d^{7,88}4s^{1,12}$. Table 4.3 shows the specifications of some other atom-configurations.

Table 4.3. Charge numbers of cobalt- and iron-ions

Z_{Fe}	0,09	0,91		1,04		1,89
Z_{Co}	0,29	0,71	1,12	0,83	1,24	1,6
ΔZ_{Fe-Co}	- 0,2	0,2	- 0,21	0,21	- 0,2	0,29

A comparison with Fig. 4.4 shows that the coordinates of the ends of lines $\tilde{M}_S^I, \tilde{M}_S^{III}$, being about $T' \approx 0,4, \Gamma' \approx 0,7$, correspond to a point on line 3, and that the coordinates of the end of line M_S^{IV} correspond to a point on line 2, with a slope $\partial f/\partial \mu' \approx 0,18$. In this connection, it is also possible to relate the decrease of M_S^I, M_S^{III} for $C_{Co} > 40\%$ to the onset of shifting of the mapped points $\tilde{M}_S^I, \tilde{M}_S^{III}$ on line 3, thus ensuring a smooth decrease of the slope $\partial f/\partial \mu'$. At the same time, the point \tilde{M}_S^{IV} for $C_{Co} > 40\%$ can shift along the line of constant slope $\partial f/\partial \mu' \approx 0,18$, with smooth increase of M_S^{IV} . Obviously, this interpretation requires an approximated "equality" of two non-equilibrium sources, during a martensitic $\gamma - \alpha$ - transformation in Fe-Co-alloys, while in Fe-Ni- and

Fe-Mn-alloys, the chemical potential gradient $\nabla\mu$ serves as the dominating non-equilibrium source.

4.5 Discussion of the results on substitutional alloys

On the basis of reasonable electronic configurations, our consideration shows that it is possible, in principle, to obtain satisfactory accordance between experimentally $\tilde{M}_S^i(\Gamma')$ and the theoretically obtained relationship $\tilde{T}'_{1,2}(\Gamma')$, provided that the spectral density $A(\varepsilon, \varepsilon_{\mathbf{k}})$ is chosen in the form of a Lorentz-SD-function, as it has to account for the complete extinction of s-electrons.

It would also be interesting to discuss the problems related to the amount of conformity existing between the parameters used for the \tilde{M}_S^i - mappings and other relevant data, and how sensitive the evaluations of the ΔZ - quantities would behave against variations of key parameters, within the frame of an alloying model with diagonal disorder.

4.5.1 Determination of the parameter a_0 and of electronic atom-configurations on the basis of electrical and optical characteristics of alloying components

Let us start with the parameter a_0 . To determine the function $\rho(T)$ of the electric resistance - within a temperature-interval $0 < T < 1100$ K - we use the linear extrapolation for data of [158]. Then we can determine the average slope of the curves $\rho(T)$: $\Delta\rho/\Delta T \approx 10^{-9}$ Ohm \cdot m /K. If we now use the Drude-formula (see for example [87, 168])

$$\frac{1}{\rho} = \frac{e^2 n}{m^* \tau^{-1}} \equiv \frac{\hbar e^2 n}{m^* \Gamma} = \frac{\hbar e^2 n}{m^* a_0 k_B T}. \quad (4.31)$$

we get for a_0 :

$$a_0 = \frac{e^2 n \hbar}{m^* k_B} \frac{\Delta\rho}{\Delta T}, \quad (4.32)$$

where e , m^* - charge and effective electron-mass, n - electron concentration. If we further hypothesize that each iron-atom donates one electron into the s-band ($Z_{Fe} = 1$), we get an s-electron concentration of $n_s \approx 8 \cdot 10^{28} m^{-3}$. Then we determine from (4.32) using $m^* =$ free electron mass $= m_0 = 9,1 \cdot 10^{-31}$ kg a value of $a_0 \approx 17,2$, being 8-times as large as the previously mentioned value $a_0 = 2,1$. For $a_0 \approx 17$, the extinction Γ at point $M_S^I \approx 1100$ K would be about 1,6 eV (Assumed s-electron lifetime $\tau \approx 4 \cdot 10^{-16}$ s). For $\varepsilon_d - \mu \approx 0,24$ eV, point \tilde{M}_S^i in plane (Γ', T') had coordinates $T' \approx 0,4$, $\Gamma' \approx 3,3$, and the level of the value $\partial f/\partial\mu'$ would decrease to 0,08. We remark that the projection of point M_S^I into

the surroundings of the point ($T' \approx 0, 1$, $\Gamma' \approx 1$), including re-establishment of $\partial f / \partial \mu' \approx 0, 15 \div 0, 16$ at $\Gamma' \approx 1, 6$ eV, is possible for $\varepsilon_d - \mu \approx 0, 8$ eV, as shown in [121] for the case of the non-magnetic state of fcc-iron.

Even though in [169] the value $\tau \sim 10^{-16}$ s was used for an interpretation of the thermoelectric effect in Nickel, the quantity τ most probably had been underestimated, and the quantities Γ and a_0 overestimated. This is due to the fact that the Drude-formula (4.31), being correct for the case of a free-electron gas, does not account for the hybridization of s- and d-bands in transition metals. As shown in [111] by calculations, the density of the s-states g_s is only akin to the density of states of free electrons in the proximity of the bottom of the s-band. However, in the overlapping region of s- and d-bands, the s-state density does not exhibit a monotonous increase with increasing energy ε , and thus will only attain values $g_s(\mu)$ of an order of magnitude of 10^{-2} 1/(eV atom), in the proximity of the Fermi-level μ . Thus, for correct interpretation of data substantiating the function $\rho(T)$, it will be more advisable to use the general formula (4.33), which links up both quantities ρ and $g_s(\mu)$:

$$\frac{1}{\rho} = \frac{2}{3} e^2 v^2 \tau g_s(\mu) = \frac{2}{3} \frac{\hbar e^2 v^2 g_s(\mu)}{a_0 k_B T}, \quad (4.33)$$

where v^2 - squared mean value of s-electron velocities at the Fermi-surface [168]. The quantity $g_s(\mu)$ indicates the number of states for a spin-projection within an energy and volume unit interval. For an atom concentration of $8 \cdot 10^{28} \text{ m}^{-3}$, we get the following correspondence for different units of energy density:

$$\frac{1}{\text{eV} \cdot \text{Atom}} = 5 \cdot 10^{47} \frac{1}{\text{J} \cdot \text{m}^3}. \quad (4.34)$$

Let $v \sim 10^6$ m/s, $\Delta\rho/\Delta T \approx 10^{-9}$ Ohm m /K. Then we can determine from (4.33), (4.34) that a value of $g_s(\mu) \approx 2, 3 \cdot 10^{-2}$ 1/(eV atom) is assigned to $a_0 = 2, 1$, thus amounting to only one fifth of the $g_s(\mu)$ as estimated on the basis of (4.27), using $Z_{Fe} = 1$.

Without doubt, the results of optical measurements in the far infrared (at wavelengths of about $10, 6\mu$ m) reported in [170] are interesting, as they enable us to evaluate data related to the plasma - Ω and relaxation-frequencies τ^{-1} for "pure" s- and hybridized s-d-types of the charge-carriers in Fe- and Ni- meltings, and their solutions with Cr, at $T = 1873$ K:

$$\left. \begin{aligned} \Omega_s^2 &= 15 \cdot 10^{30} \text{ s}^{-2}, & \Omega_{s-d}^2 &\approx 33 \cdot 10^{10} \text{ s}^{-2}, \\ \tau_s^{-1} &= 2, 4 \cdot 10^{14} \text{ s}^{-1}, & \tau_{s-d}^{-1} &\approx 4 \cdot 10^{14} \text{ s}^{-1}, \end{aligned} \right\} Fe \quad (4.35)$$

$$\left. \begin{aligned} \Omega_s^2 &\approx 29 \cdot 10^{30} \text{ s}^{-2}, & \Omega_{s-d}^2 &\approx 40 \cdot 10^{10} \text{ s}^{-2}, \\ \tau_s^{-1} &\approx 2 \cdot 10^{14} \text{ s}^{-1}, & \tau_{s-d}^{-1} &\approx 3 \cdot 10^{14} \text{ s}^{-1}. \end{aligned} \right\} Ni$$

Firstly, we note a remarkable conformity among the above data (4.35) and those published in [158], related to the specific resistance ρ . For example we get from

[158] $\rho \approx 1,4 \cdot 10^{-6}$ Ohm m for iron at $T \approx 1900$ K, and an evaluation of the data shown in (4.35) results in

$$\rho_{s-d} = \frac{\tau_{s-d}^{-1}}{\varepsilon_0 \Omega_{s-d}^2} \approx 1,35 \cdot 10^{-6} \text{ Ohm} \cdot m,$$

$$\rho_s = \frac{\tau_s^{-1}}{\varepsilon_0 \Omega_s^2} \approx 1,8 \cdot 10^{-6} \text{ Ohm} \cdot m,$$

where $\varepsilon_0 = 8,85 \cdot 10^{-12}$ F/m - dielectric vacuum field constant. Secondly, the squared ratios of the plasma-frequencies,

$$\frac{\Omega_{sNi}^2}{\Omega_{sFe}^2} \approx 1,93, \quad \frac{\Omega_{s-dNi}^2}{\Omega_{s-dFe}^2} \approx 1,21,$$

being proportional to the ratios of electron-concentrations in Ni and Fe, are greater than 1, a result being in accordance with our initial assumption of the proximity of the effective electron-mass $m_{Ni}^* \sim m_{Fe}^*$, for our chosen configurations $3d^{8,6}4s^{1,4}$, $3d^74s^1$ for Ni and Fe, respectively. Thirdly, a calculus of the n_s - concentration of s-electrons, being included in the formula of the plasma-frequency

$$\Omega_s^2 = \frac{e^2 n_s}{m_s \varepsilon_0}, \quad (4.36)$$

shows that, using $m_s \approx m_0$, the value of n_s , amounting to only one sixteenth of $8 \cdot 10^{28} \text{ m}^{-3}$, corresponds to $Z_{Fe} = 1$. This means that the mean density \bar{g}_s of s-states (being related to the energy-intervals of occupied states in the s-band) is smaller by about one order of magnitude than the \bar{g}_s value of free electrons. This is an immediate indication of the existence of collective s-electrons of the iron-atoms, predominantly in hybridized s-d-states. For our determination of m_{s-d} , we keep in mind the condition $Z_{Fe} = 1$ and apply formula (4.36) for Ω_{s-d}^2 . After insertion of $n_s \rightarrow n_{s-d} \approx 7 \cdot 10^{28} \text{ m}^{-3}$ we obtain an effective mass $m_{s-d} \approx 6,7m_0$. Fourthly, considering that the specific resistance of iron ρ decreases during a change of temperature T from 1900 K to 1100 K by about $20 \div 21\%$ [158], we get the following relaxation-frequencies of iron at T = 1100 K, instead of the values shown in (4.35):

$$\tau_s^{-1} \approx 1,9 \cdot 10^{14} \text{ s}^{-1}, \quad \tau_{s-d}^{-1} \approx 3,2 \cdot 10^{14} \text{ s}^{-1}. \quad (4.37)$$

From this, we can easily evaluate a_0 :

$$a_{0s} = \frac{\hbar \tau_s^{-1}}{k_B T} \approx 1,3, \quad a_{0s-d} = \frac{\hbar \tau_{s-d}^{-1}}{k_B T} \approx 2,2. \quad (4.38)$$

By comparing the results obtained from our interpretation of the concentration-dependency $M_S(C)$ with measured optical data, it is possible to draw the following conclusions:

1. The above used value of $a_0 \approx 2, 1$ corresponds to a washed out distribution of hybridized s-d-carriers.
2. Out of two reference-configurations of nickel, the configuration $3d^{8,6}4s^{1,4}$ should be preferred, and from possible iron-configurations, those being close to $3d^74s^1$.
3. The value of the parameter $\varepsilon_d - \mu \approx 0, 24$ eV indicates a spin-polarized state of iron-atoms, i.e. $\varepsilon_d - \mu = \varepsilon_{d\uparrow} - \mu$ (see Pt.2.5).
4. The location of cobalt in the periodical system of elements, i.e. between nickel and iron, suggests that out of the two "average" configurations of its atoms, with $\Delta Z \approx \pm 0, 2$ (see Table 4.3), the one enabling a rational explanation of the function $M_S(C)$ in Fe-Co-alloys, being close to $3d^{7,8}4s^{1,2}$, i.e. with $\Delta Z \approx -0, 2$, should be chosen. In accordance with the above interpretation of a scenario with plasma-frequencies of s-carriers, it can be anticipated, that the inequalities: $\Omega_{sFe}^2 < \Omega_{sCo}^2 < \Omega_{sNi}^2$, $\Omega_{s-dFe}^2 < \Omega_{s-dCo}^2 < \Omega_{s-dNi}^2$ will be satisfied. However, it has to be taken into account that the partition of the frequencies $\Omega_{1,2}$ and $\tau_{1,2}^{-1}$ for two carrier-groups is no trivial problem, if the frequency of light $\omega < \tau_1^{-1}$, τ_2^{-1} and τ_1^{-1} , τ_2^{-1} are of the same order of magnitude [171]. Thus for example the effective values $\Omega_{ef}^2 = (32 \pm 1, 2)10^{30} \text{ s}^{-2}$, and $\tau_{ef}^{-1} = (0, 8 \pm 0, 04)10^{14} \text{ s}^{-1}$, as determined in [172] at $T = 295$ K for bcc-iron, fit very well with (4.35), taken from [170], for Ω_{s-d}^2 and τ_{s-d}^{-1} , under the assumption that the absorption of light is of Drude-like-character, and if one considers both that the plasma-frequency only weakly varies with temperature, and that the relaxation frequency declines with decreasing T (for $a_0 = 2, 1$ and $T = 295$ K we get $\tau^{-1} = a_0 k_B T \hbar^{-1} = 0, 81 \cdot 10^{14} \text{ s}^{-1}$). The information on frequencies of the s-sub-system however remained hidden. Therefore it cannot be excluded that the values determined for cobalt $\Omega^2 = 31 \cdot 10^{15} \text{ s}^{-2}$, and $\tau^{-1} = 0, 37 \cdot 10^{14} \text{ s}^{-1}$ (see [171, 173]) belong to hybridized s-d-electrons.
5. Assuming that our conclusions drawn from an alloying-model with diagonal disorder in the parabolic band of the s-electrons are correct, this would suggest that the density of states (DOS) $g_s(\mu) \approx 0, 12 \text{ 1/(eV atom)}$ has been determined realistically, with our model for hybridized s-d electrons near the Fermi-level of the γ - phase.

Among the papers dealing with the measurement of the specific electric resistance of Fe-Ni-alloys, we want to emphasize [174–176]. In [174] the "jumps" of the specific electric resistance ρ , in the region of temperatures M_S and A_S , are reported, being most probably directly linked up with the $\gamma - \alpha$ - MT and the $\alpha - \gamma$ -reverse MT ($\rho_\alpha < \rho_\gamma$) occurring during the temperature-cycles. During investigations of alloys with 30% Ni [175], only weak variations of optical data were observed after a $\gamma - \alpha$ - MT. The paper [176]

focuses on measurements of the function $\rho(T)$, in the adjacency of magnetic phase transformations. [156] reports on the behavior of $\rho(T)$ in Fe-Mn-alloys, while [177–179] is related to Fe-C-systems. In our opinion however, a more comprehensive consideration of these results would require additional data on Ω and τ^{-1} , which could in principle be obtained from optical measurements near the M_S - temperatures, for a variety of alloys, in a similar way as with the data for ρ , being presented in [174]. Thus we shall confine ourselves to only two qualitative remarks.

- 1 The values of $\rho(M_S)$ prove to be almost equivalent for various alloys with the same M_S -temperature, an observation satisfying our initial requirement for compliance of the extinction Γ' for Fe-Mn- and Fe-Ni-alloys, with identical M_S - temperature.
- 2 In Fe-Ni-, Fe-Mn-alloys, the function $\rho(M_S)$ slowly declines with decreasing M_S , i.e. with increasing Mn and Ni-concentrations, an observation which, at the first sight, would contradict with our hypothesized increase of s-electron extinction Γ , with decreasing M_S . However, we have to take into account that, for a given d-s, s-d scattering mechanism, the increase of Γ delivers the larger contribution to conductivity by the d-electrons, leading to a decrease of specific impedance. In this case, the increase of Γ leads to the same class of effect as an increase of photon-frequency, the latter one resulting in an increase of the contribution of d-electrons to optically induced conductivity [172].

4.5.2 Effect of variations of lattice-parameter and the s-band width on the difference of the charge numbers ΔZ of alloying components

Due to results of energy band analysis (see for example [106]) we will not only have to expect significant deviations of m^* from m_0 , but also an anisotropy of the values m^* and $g_s(\mu)$, mainly caused by the s-d-hybridization of electronic states. If the value W_s in formula (4.27) was varied for the isotropic function $g_s(\mu)$, it could easily be estimated which electronic configurations will lead to the same optimum functions $\tilde{M}_S^i(\Gamma')$ as previously determined, for new values of W_s . According to the band spectrum of iron [106], the "widths" of the s-band, related to the orientations Δ and Λ of the 1st Brillouin-zone, are close to the above used value $W_s \approx 10$ eV, whilst the "width" of the s-band in Σ - orientation is $W_s \approx 15$ eV. A calculus shows that, for example for $Z_{Ni} = 0,6$, the transition $W_s \approx 10$ eV to $W_s = 15$ eV is associated with a transition of the configurational set $3d^{7,1}4s^{0,9}$, $3d^{8,3}4s^{0,7}$, $3d^{9,4}4s^{0,6}$ (relating to iron, cobalt and nickel, in sequence) into the configurational set $3d^{7,14}4s^{0,86}$, $3d^{8,32}4s^{0,68}$, $3d^{9,4}4s^{0,6}$. This means that the variation of the ΔZ - quantity does not exceed 0,04. Of course, for known

electronic configurations, the deviation of ΔZ could also be larger than 0,04, but we should not overestimate its exactness, under a qualitative aspect. We also note that formula (4.28), establishing the link between ΔZ and the δ parameter (Friedel-summation rule [100]), is only correct in the region of small concentrations of an alloying element. Consequently, the description of the initial path of the curves $M_S(C)$ would be most realistic for small C-concentrations. However, if the function $M_S(C)$ does not significantly deviate from a linear function in a sufficiently large range of concentrations, then a more generous application of the results obtained by means of (4.28) would be justified. For alloys with concentrations $C = 0,2 \div 0,4$, our results undoubtedly only are of qualitative nature. We also note that the parameter $|\delta| W_s^{-1}$, whose magnitude must be less than 1 (being a prerequisite for the applicability of formula (4.23)), has not exceeded the region of $0,23 \div 0,15$, for $W_s = 10 \div 15$ eV, with exception of the case $Z_{Fe} = 0,09$, $Z_{Mn} = 0,84$, and $|\delta| W_s^{-1} = 0,28 \div 0,18$ resembling the least probable "marginal" configuration $3d^{7,91}4s^{0,09}$ of iron atoms in an Fe-Mn-alloy.

Now let us discuss the sensitivity of our calculated results against variations Δa of the lattice-parameter a , essentially depending on temperature and composition of an alloy. It is commonly known that a homogenous distribution of the impurities [180] firstly causes a uniform change of the lattice parameter of an "average" crystal, as well as of the function $a(C)$ of the concentration of a solute, and secondly, the inhomogeneous local static displacements of the lattice, in the adjacency of an impurity atom. The local variation of volume in the adjacency of the impurity atom requires a correction of the quantity ΔZ (4.28), which for an isotropic medium, according to [138], comes to a replacement of the function ΔZ by

$$\Delta Z' = \Delta Z - Z_{Fe} \frac{\Delta V}{a^3} = \Delta Z - Z_{Fe} \frac{1 + \sigma_{Fe}}{1 - \sigma_{Fe}} \frac{1}{a} \frac{da}{dC}, \quad (4.39)$$

where $\sigma_{Fe} \approx 0,3$ - Poisson's number. The corrected expression (4.39) reflects the fact that the shielded charge of the impurity atom must be corrected by consideration of the excessive volume ΔV occupied by the additional atom (in relation of the matrix-atom). To give an example, for Fe-Mn-alloys, the parameter $a(C) = 3,575 - 0,072 C_{Mn}$ (in Angström), according to [156], where C_{Mn} - Mn-concentration. Let $Z_{Fe} = 1$, then we get for the second term in (4.39):

$$Z_{Fe} \frac{1 + \sigma_{Fe}}{1 - \sigma_{Fe}} \frac{1}{a} \frac{da}{dC} \approx 0,037. \quad (4.40)$$

According to data in [181,182], a function $a(C_{Ni})$ for Fe-Ni-alloys is nearly inexistent in the ranges of temperatures above 575 K and concentrations $C_{Ni} < 0,3$, being of interest for a comparison of the functions $M_S(C)$ of Fe-Ni and Fe-Mn-alloys (see Fig. 4.10). Thus, if we ignored the corrective factor for ΔZ in Fe-Ni-alloys, we would note that the difference $Z_{Mn} - Z_{Ni} \approx 0,1$, which originally had been obtained from a comparison of the values shown in Tables 4.1 and 4.2 in

Pt. 4.4, is correlated by nearly 40 % with the corrective factor (4.40) of Fe-Mn-alloys, being related to the case of "average" iron-atom configurations ($Z_{Fe} \approx 1$) and $\Delta Z < 0$. In other words, the actual number of electrons donated by each Mn-atom into the s-band can be less than values shown in Table 4.1 in Pt. 4.4, thus $Z_{Mn} - Z_{Ni} \approx 0,06$.

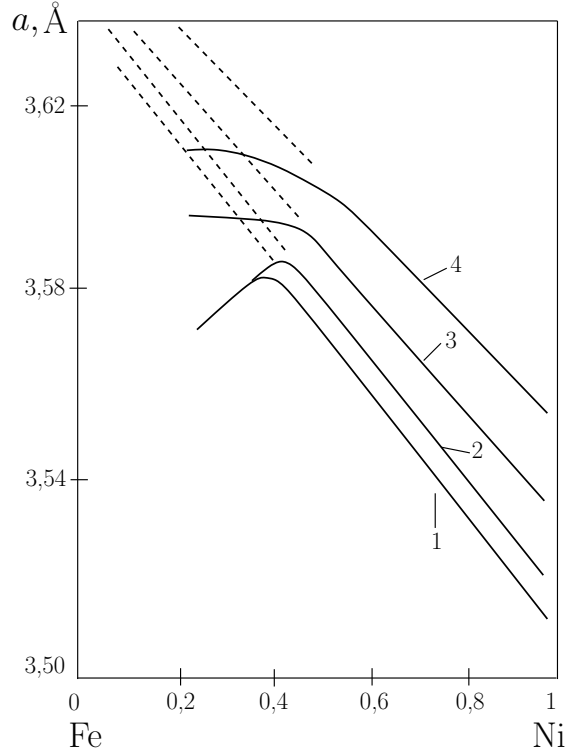


Figure 4.10. Variation of the lattice-constant of Fe-Ni-alloys with Fe-Ni-concentration, at different temperatures [181, 182]: 1 = 0 K, 2 = 288 K, 3 = 575 K, 4 = 875 K.

Now let us get over to an estimate of the increment $\Delta(\varepsilon_d - \mu)$ of the parameter $(\varepsilon_d - \mu)$, being caused by the homogeneous variation of the parameter a , using the tight binding approximation. Above all we have to note that the reduction of a must be associated with increasing probability of transitions of the d-electrons between the knots, with enlargement of the width of W_d - of the d-band. And vice-versa: The width W_d must decrease with increasing a . If we further assume that the relation $|\varepsilon_d - \mu| W_d^{-1}$ will remain unchanged during the variation $a \rightarrow a' = a + \Delta a$, i.e. $|\varepsilon_d - \mu| W_d^{-1} = |\varepsilon'_d - \mu| (W'_d)^{-1}$, then

$$\Delta(\varepsilon_d - \mu) = |\varepsilon_d - \mu| W_d^{-1} \Delta W_d. \quad (4.41)$$

It has to be noted that the correspondence of the incremental signs of ΔW_d , $\Delta(\varepsilon_d - \mu)$ in (4.41) is independent of the sign of the difference $\varepsilon_d - \mu$, as long as the energy ε_d is related to a non-polarized (in terms of magnetism) state of

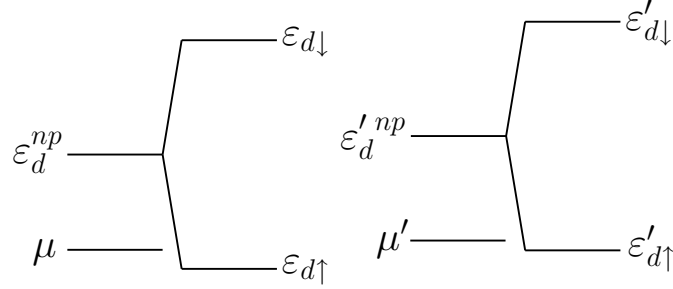


Figure 4.11. Graph of energy levels showing the opposite signs of the increments $\Delta(\varepsilon_d^{np} - \mu) \sim \Delta W_d > 0$ and $\Delta(\varepsilon_{d\uparrow} - \mu) < 0$, during enlargement of the width of the d-band (for $W'_d > W_d$) in the case of $\varepsilon_{d\uparrow} < \mu$.

electrons $\varepsilon_d = \varepsilon_d^{np}$. However, if polarization exists there are two energy levels $\varepsilon_{d\uparrow}$, $\varepsilon_{d\downarrow}$ which emerged after the fission of ε_d^{np} . The energy level $\varepsilon_d = \varepsilon_{d\uparrow}$ is characterizing the lower energy level of the pair. Then the signs $\Delta(\varepsilon_d - \mu)$ and ΔW_d will only correspond for $\varepsilon_{d\uparrow} > \mu$. But if $\varepsilon_{d\uparrow} < \mu$, then the signs will be opposed (see Fig. 4.11). In this case, the ratio (4.41) must be changed:

$$\Delta(\varepsilon_{d\uparrow} - \mu) = -|\varepsilon_d^{np} - \mu| W_d^{-1} \Delta W_d, \quad \varepsilon_{d\uparrow} < \mu. \quad (4.42)$$

As already discussed above under Pt. 2.5, it is both possible for the γ - phase of iron to materialize a non-polarized state with $\varepsilon_d > \mu$ as well as a spin-polarized state with $\varepsilon_{d\uparrow} < \mu$. However, when using (4.41) in the first case, we have to equalize $\varepsilon_d - \mu$ in both the left and right hand side of (4.41), but in the second case, the difference $\varepsilon_{d\uparrow} - \mu$ can significantly deviate from $|\varepsilon_d^{np} - \mu|$. But also $|\varepsilon_d^{np} - \mu|$ can deviate from $|\varepsilon_d - \mu|$ in (4.41). If we further took $\varepsilon_d - \mu = \mu - \varepsilon_{d\uparrow} \approx 2,5 k_B M_S^I(0)$, being equivalent to 2750 K (see (4.30)) at a temperature scale or to 0,237 eV at an energy scale, and the quantity $|\varepsilon_d^{np} - \mu| \approx 0,78$ eV (in accordance with [122]), then we would note that the value $\Delta(\varepsilon_{d\uparrow} - \mu)$ attains a sign opposed to that of $\Delta(\varepsilon_d - \mu)$, being about 3,3 times larger in magnitude. The quantity W_d and its increment ΔW_d can easily be estimated, using the relation from [183]

$$W_d = \frac{6,83 \hbar^2 r_d^3}{m_0 r_0^5}, \quad (4.43)$$

where r_d - atomic parameter, which, in the case of iron, equates to $0,8 \text{ \AA} = 8 \cdot 10^{-11} \text{ m}$, r_0 - radius of the atomic sphere, m_0 - electron-mass. Taking into account that, for an fcc-lattice,

$$\frac{4}{3} \pi r_0^3 = \frac{a^3}{4},$$

then we are able to express the quantities W_d , ΔW_d as a function of a :

$$W_d = \frac{749,3 \hbar^2 r_d^3}{m_0 a^5}, \quad \Delta W = -5 W_d \frac{\Delta a}{a}. \quad (4.44)$$

For $a = 3,6 \text{ \AA} = 3,6 \cdot 10^{-10} \text{ m}$ we get from (4.44) $W_d \approx 4,85 \text{ eV}$. Let us now regard the increment ΔW_d associated with cooling of the γ - phase of iron. According to the data in [184] we can assume a linear heat expansion coefficient $\beta \approx 2,15 \cdot 10^{-5} \text{ K}^{-1}$. Then, as a result of cooling by $\Delta T = -100 \text{ K}$

$$\frac{\Delta a}{a} = \beta \Delta T = -2,15 \cdot 10^{-3}, \quad \Delta W_d = 1,075 \cdot 10^{-2} W_d. \quad (4.45)$$

By insertion of (4.45) in (4.42), (4.41), we get

$$\Delta(\varepsilon_d - \mu) = 0,237 \cdot 1,075 \cdot 10^{-2} \text{ eV} \approx 2,55 \cdot 10^{-3} \text{ eV},$$

$$\Delta(\varepsilon_d - \mu) = -0,78 \cdot 1,075 \cdot 10^{-2} \text{ eV} \approx -8,39 \cdot 10^{-3} \text{ eV},$$

or $k_B^{-1} \Delta(\varepsilon_{d\uparrow} - \mu) \approx 30 \text{ K}$, $k_B^{-1} \Delta(\varepsilon_{d\uparrow} - \mu) \approx -100 \text{ K}$ at a temperature scale. During the cooling process, the starting points $M_S^i(C = 0)$, if mapped onto a plane (T', Γ') in accordance with (4.30), will settle a straight line $1,05 T' = \Gamma'$, so that a variation of the parameter $\varepsilon_d - \mu$ will shift the starting points $\tilde{M}_S^{III, IV}$ along this straight line. In a non-polarized and polarized state, respectively, the coordinates of edge-points \tilde{M}_S^{IV} are $(T' \approx 0,245, \Gamma' \approx 0,257)$ and $(T' \approx 0,298, \Gamma' \approx 0,313)$, whereas in Figs. 4.8, 4.9, the coordinates of the point \tilde{M}_S^{IV} are: $T' \approx 0,256, \Gamma' \approx 0,269$. In case of a spin-polarized state, the point \tilde{M}_S^{IV} will shift from the line of constant slope $\partial f / \partial \mu' \approx 0,14$ towards the line of constant slope $\partial f / \partial \mu' \approx 0,17$. Obviously, this shifting of the points is favorable for realization of optimum conditions for phonon generation. Simultaneously, the shifting of point \tilde{M}_S^{IV} causes a slight reduction of the gradient $\partial f / \partial \mu' \leq 0,14$, in the case of a non-polarized state. For this reason, the polarized state has certain advantage.

The mappings of points M_S , corresponding to alloys with a concentration C_{ae} greater than a few percent, can be performed by consideration of the following: Firstly, we must consider the reduction of the coefficient β , the values of which being about 1,5 to 2-fold smaller (for iron-alloys) during approach to room-temperature (and for Fe-Ni-Invar-alloys 10 times smaller) if compared with γ - iron, and secondly, by adequate consideration of the dependence of the lattice-parameter on the composition of the alloy. Following [181, 182] the value $a \approx 3,58 \text{ \AA}$ corresponds to a Fe - 30% Ni -alloy. It remains almost invariant with varying temperature below 288 K (see Fig. 4.10), whereas at a temperature $M_S^I = 1093 \text{ K}$, corresponding to the value $\varepsilon_d - \mu$ (see (4.30)), $a \approx 3,64 \text{ \AA}$. In Tables 4.4, 4.5, there are presented the Z_{Fe} for the polarized state of iron-atoms, as determined by the requirement of location of point $\tilde{M}_S^I = \tilde{M}_S^{IV}$ on line 2 (at $T' \approx 0,137, \Gamma' \approx 0,92$) and line 3 (at $T' \approx 0,137, \Gamma' \approx 1,17$), taking into account, in each case, the increment $\Delta a = -0,06 \text{ \AA}$.

The data in Tables 4.4, 4.5 only relate to "average" configurations of iron-atoms, in accordance with the assumption in Pt. 2.5 on the polarization of states with a configuration close to $3d^7 4s^1$. A comparison of the data are presented in Tables 4.2, 4.3 also shows that a variation of the lattice-parameter a leads

Table 4.4. Charge-numbers of nickel- and iron-ions with consideration of the lattice parameter variation for the case of location of point $\tilde{M}_S^I = \tilde{M}_S^{IV}$ on line 2 (see explanation in the text)

Z_{Ni}	0,6	1,4
Z_{Fe}	0,87	1,10
ΔZ_{Fe-Ni}	0,27	- 0,30

Table 4.5. Charge-numbers of nickel- and iron-ions with consideration of the lattice parameter variation for the case of location of point $\tilde{M}_S^I = \tilde{M}_S^{IV}$ on line 3 (see explanation in the text)

Z_{Ni}	0,6	1,4
Z_{Fe}	0,90	1,06
ΔZ_{Fe-Ni}	0,30	- 0,34

to a noticeable effect on the quantity $\varepsilon_{d\uparrow} - \mu$, which will diminish by $6,4 \cdot 10^{-2}$ eV (or about 27%) for $\Delta a = -0,06 \text{ \AA}$, as well as on the quantity $|\Delta Z|$, the reduction of which will lead to an additional deviation of Z from 1, by 0,06. For "marginal"-configurations, if put into relation with the non-polarized state of iron, a consideration of $\Delta a = -0,06 \text{ \AA}$ will result into an increase of $|\Delta Z|$ by about 1/3 of the corresponding increment of $|\Delta Z|$ in the polarized condition of iron.

This way, in the spin-polarized state of iron-atoms, the Z_{Fe} - values for $Z_{Ni} = 0,6$ are lying in a range of $0,87 \div 0,91$, and for $Z_{Ni} = 1,4$, in a range of $1,04 \div 1,10$. As to differential-modules of electron-numbers, associated with the s-band of atoms of binary substitutional alloys, we obtain the following inequalities:

$$|\Delta Z_{Fe-Co}| < |\Delta Z_{Fe-Ni}| < |\Delta Z_{Fe-Mn}|. \quad (4.46)$$

It has to be noted here that the value $|\Delta Z_{Fe-Co}| \approx 0,2$, being used in Table 4.3, nearly corresponds to an approximated conformance of the function \tilde{M}_S^I with the sector of line 1 in Fig. 4.5 From the point of view of maintenance of a high level of the slopes $\partial f / \partial \mu'$, $\partial f / \partial T'$ during variations of the Co-concentration, a conformance of the figures Z_{Fe} and Z_{Co} would also be favorable, i.e. $\Delta Z_{Fe-Co} = 0$. For $\Delta Z_{Fe-Co} = 0$, the contribution to extinction being caused by scattering at charged impurities, also vanishes, i.e., $\Gamma(C) = 0$, while the \tilde{M}_S^i - points at the (T', Γ') - plane shift upwards from their initial locations along the straight line $1,05 T' = \Gamma'$. The coordinates of point \tilde{M}_S^I change with variations of Co-concentration from $C = 0$ to $C = 0,4$ from $(T' \approx 0,4, \Gamma' \approx 0,42)$ to $(T' \approx 0,426, \Gamma' \approx 0,447)$, and, for $C = 0,4$, the points \tilde{M}_S^{III} , \tilde{M}_S^{IV} shift into positions close to

that of \tilde{M}_S^I or \tilde{M}_S^{III} for $C = 0$. It can further be seen from Figs. 4.4, 4.5 that the slopes $\partial f/\partial\mu'$ and $\partial f/\partial T'$ increase at the same time. For Fe-Ni- and Fe-Mn-alloys, the vanishing of the quantities ΔZ_{Fe-Ni} , ΔZ_{Fe-Mn} is most unfavorable, as the downshift of points \tilde{M}_S^i along line $\Gamma' = 1,05T'$ will lead to rapid reduction of the magnitudes of slopes $\partial f/\partial\mu'$, $\partial f/\partial T'$.

We further note that in the above performed analysis of the scattering by impurities, we omitted a consideration of non-diagonal disorder existent in binary alloys, being caused by electronic transitions between the knots of the components of binary alloys [100]. Obviously, any additional contribution to extinction $\Gamma(C)$ will cause a decline of the quantity ΔZ . Thus the above determined ΔZ - values should be regarded as estimates lying above the true differences of the number of electrons donated into the s-band by the alloying components.

4.5.3 Estimation of the chemical potential differences of some γ - and α - phases, for the sub-system of d-electrons

Let us use formula (4.43) in order to calculate the chemical potential difference $\Delta\mu = \mu_\gamma - \mu_\alpha$ between austenite and martensite, the magnitude of which will determine the amount of inverted occupational difference σ_0 , in addition to the slope $\partial f/\partial\mu'$. We recall that an elementary assessment of $\Delta\mu$, relating to s-electrons, has already been performed in Pt. 1.5. With regard of the necessary correspondence of the $\Delta\mu$ - assessments for different (s and d) electrons, we now assess $\Delta\mu$ for the sub-system of d-electrons. Let us count μ from the bottom of the d-band upwards, assuming that the ratio μW_d^{-1} applies for both the γ - and the α - phases. Then we get:

$$\Delta\mu = \mu_\gamma - \mu_\alpha = (W_{d\gamma} - W_{d\alpha}) \frac{\mu_\gamma}{W_{d\gamma}} = \left(1 - \frac{W_{d\alpha}}{W_{d\gamma}}\right) \mu_\gamma. \quad (4.47)$$

If we regard the already used quantity $\varepsilon_d^{np} - \mu \approx 0,78$ eV as the energy-difference between the upper edge of the d-band and the Fermi-level of the γ - phase, we get for $W_{d\gamma} \approx 4,85$ eV the value $\mu_\gamma \approx 4,85 - 0,78 = 4,07$ eV. Taking further in consideration that, for a bcc-lattice, the volume associated to one atom is

$$\frac{4}{3} \pi r_0^3 = \frac{1}{2} a_\alpha^3,$$

we then can express by formula (4.43), in a similar way as previously done with (4.44), the value $W_{d\alpha}$ by means of the lattice-constant a_α , and determine the ratio

$$\frac{W_{d\alpha}}{W_{d\gamma}} = \left(\frac{a_\gamma}{2^{1/3} a_\alpha}\right)^5 \approx 0,961, \quad (4.48)$$

using therein the ratio $a_\alpha = 0,8a_\gamma$, being typical of the Bain-deformation (see Fig. 1.1 and its legend). If we now insert $\mu_\gamma = 4,07$ eV in (4.47), under consideration of

(4.48), then we get $\Delta\mu \approx 0,16$ eV, being in good accordance with the previously performed estimate for the sub-system of s-electrons.

4.6 The $M_S(C)$ function for steel and degree of ionization of carbon-atoms

In principle, one could try to extend the approach for an analysis of the concentration-dependence of M_S , from binary substitutional alloys towards interstitial alloys, among which the Fe-C-system would be the most interesting one. We can take for granted that carbon-atoms will only occupy the octahedral interstitial voids in austenite [13]. Let us further surmise that those iron-ions, in the closest adjacency of which a carbon-atom is localized, can be characterized by a charge-number Z_{FeC} , and that these iron-ions will adopt the role of the "alloying-element"-ions, substituting the "normal" iron-ions by a combined charge number Z_{FeC} , being different from Z_{Fe} . Then our search for $\Gamma(C)$, which represents the contribution to s-electron extinction by scattering at the impurity atoms, can be reduced to the task of determination of electron-scattering at octahedral clusters of 6 atoms, whose concentration is identical with the concentration of carbon. This task however is neither trivial nor has it been completely resolved (see for example [102,185]). Thus we shall confine ourselves on a qualitative reflection and start with an estimate of the lower limit by hypothesizing that, during the process of cluster-scattering, the s-electrons will only interact with one of the six "solute" ions (i.e. that one being nearest to the s-electron). In this case, our analysis of $M_S(C)$ can be performed in the same way as in the case of a substitutional lattice in Pt. 4.4, 4.5. According to [165], the rate of reduction of M_S with increasing carbon concentration is about fourfold or twice as large as that for Fe-Ni- or Fe-Mn-alloys. Thus for instance, a temperature $M_S^{IV} \approx 473$ K in Fe-C-, Fe-Mn- and Fe-Ni-systems corresponds to about 4,6 Atom - % C (1 weight-% C), 10,5 atom - % Mn and 22 atom - % Ni. In Table 4.6, there are presented some values of Z_{FeC} , which have been determined for the same parameters as those used in Pt. 4.4, i.e. $W_s = 10$ eV, $\varepsilon_d - \mu \approx 0,237$ eV, without account on the effect of variable lattice parameter.

Table 4.6. Effective charge-numbers of iron-atoms included in octahedral clusters with interstitial carbon atoms (Z_{FeC}), and of iron-ions without association to carbon (Z_{Fe})

Z_{Fe}	0,09	0,91		1,04		1,89
Z_{FeC}	1,08	0,42	1,53	1,62	0,52	0,86
ΔZ	- 0,99	0,49	- 0,62	- 0,58	0,52	1,03

By comparison of the data shown in Tables 4.6 and 4.1, we note that - for "average" iron-configurations - a twofold increase of the rate of reduction of M_S would require an increase of ΔZ - by about $0,1 \div 0,15$. We recall that we came to a similar conclusion in Pt. 4.4, after having compared the rate of change of the M_S temperature in Fe-Ni and Fe-Mn-alloys.

The measured magnetic susceptibility of Fe-C-alloys, as reported in [186], points to an increase of electron-concentration in the d-band with increasing concentration of carbon. In a local interpretation, d-band occupation by carbon-electrons is associated with hybridization of the 2p wave-functions of the carbon with the 3d-functions (e_g - symmetry) of the iron. Such hybridization can associate with a reduction of the charge-number of the iron-atoms in an octahedral cluster. Further hypothesizing that the difference between Z_{FeC} and Z_{Fe} is only caused by the additional charge transfer from the carbon-atom, it is suggested to keep in mind only the following two Z_{FeC} - values of Table 4.6 : $Z_{FeC} = 0,42$ (at $Z_{Fe} = 0,91$) and $Z_{FeC} = 0,52$ (at $Z_{Fe} = 1,04$). $Z_{FeC} = 0,88$ (at $Z_{Fe} = 1,89$) should be omitted, as the adoption of one electron per ion (with $\Delta Z = 1$) would result in complete ionization of the carbon-atom, given an equivalence of six iron-ions per cluster. The degree of ionization of the carbon atom is

$$6 \Delta Z = 6 (Z_{Fe} - Z_{FeC}) \approx \begin{cases} 2,94, & Z_{Fe} = 0,91 \\ 3,12, & Z_{Fe} = 1,04 \end{cases} , \quad (4.49)$$

i.e. one carbon-atom may donate about three electrons into the d-band.

Consideration of the homogenous change of the lattice-parameter (see Pt. 4.5.2) would lead to a reduction of $(\varepsilon_{d\uparrow} - \mu)$ to 0,215 eV, for Fe-C-alloys (1 weight % C) at $T = M_S^{IV} \approx 473^\circ \text{K}$. In Table 4.7, there are presented the corrected Z_{FeC} values, by adequate consideration of the increments of the lattice constant a (the values of Z_{Fe} were extracted from Table 4.4, as determined from the requirement of location of point \tilde{M}_S^{IV} in the adjacency of line 2 in Fig. 4.4 (at $T' \approx 0,19$, $\Gamma' \approx 0,82$), relating to an Fe-C-alloy with 1 weight % carbon.

In calculating the corrective factor for inhomogeneous volume change, we have to consider that the quantity ΔZ in Table 4.7 must equate to the quantity $\Delta Z'$ in (4.39).

Table 4.7. Charge-numbers Z_{Fe} , Z_{FeC} with consideration of a variable lattice-parameter a

Z_{Fe}	0,87	1,1
Z_{FeC}	0,42	0,59
ΔZ	0,45	0,51

Taking advantage of the concentration-dependency of the lattice-parameter of

austenite given in [13]: $a_\gamma = (3,578 + 0,645C)\text{\AA}$, where C - fraction of carbon-atoms, we can determine from (4.39)

$$\Delta Z = \Delta Z' + \frac{1 + \sigma_{Fe}}{1 - \sigma_{Fe}} \frac{Z_{Fe}}{6a} \frac{da}{dC} \approx \begin{cases} 0,47, & Z_{Fe} \approx 0,87 \\ 0,57, & Z_{Fe} \approx 1,1 \end{cases} \quad (4.50)$$

The factor 1/6 in the second term in (4.50) considers that only one sixth of the inhomogeneous volume increase caused by the insertion of the carbon-atom can be assigned to each iron-ion in the octahedral cluster. The ionization degree of the carbon-atoms

$$6 \Delta Z \approx \begin{cases} 2,82, & Z_{Fe} \approx 0,87 \\ 3,42, & Z_{Fe} \approx 1,1 \end{cases} ,$$

which had been determined under consideration of the changes of the austenitic lattice parameter, moderately differs from the results of (4.49). The quantity $6\Delta Z \approx 3,42$ presumably is the upper margin for the degree of ionization of the carbon-atoms, as the hypothesis which transforms the effect of s-electron scattering at the complete cluster to scattering at only one of its six iron-ions, can only be substantiated for a larger number of ions involved in s-electron scattering, which in turn would lead to an increase of Z_{Fe} , with corresponding decrease of ΔZ . However, we note that our conclusion on the maximum value of $6\Delta Z \approx 3,42$ is based on the condition that the point \tilde{M}_S^{IV} for Fe-C-alloys (1 weight % C) arrives at the adjacency of line 2. If we required that the point \tilde{M}_S^{IV} arrives at the adjacency of line 3 in Fig. 4.4 then the degree of ionization would increase to $6\Delta Z \approx 3,78$. This value is an intermediate in relation to the values 3,5 and $3,9 \div 4$, which had been determined in [186] and [187], by analysis of the magnetic susceptibility of Fe-C-systems, within the notion of a quasi-rigid d-band with $Z_{Fe} \approx 1$, and by consideration of data of carbon-diffusion in a constant electric field (electrotransfer-method).

4.7 Summary of Chapter 4

Our assessments of substitutional (Fe-Ni, Fe-Mn, Fe-Co) and interstitial alloys (Fe-C) will now enable us to draw a basic conclusion on the possibility of preservation of the conditions for efficient phonon generation by non-equilibrium 3d-electrons, within a wide range of concentrations of the second alloying component.

The methodological basis of our investigations was the usage of a SD - function, which, besides thermal scattering, also takes into account the effect of scattering (washout) caused by the inhomogeneity of the system. We note that establishment of a modified equilibrium distribution of d-electrons (see Pt. 4.2), whose degree of "washout" is mainly determined by the rate of extinction of s-electrons, is limited by the time τ_{d-s} characterizing d-s-electron scattering. As the non-equilibrium addend to the electronic distribution cannot come into existence prior

to the formation of the real equilibrium distribution, the time τ_{d-s} will determine the minimum time τ_σ for establishment of an inverted occupational difference σ_0 (pumping-time). From this perspective, the value of $\tau_\sigma \sim 10^{-12}$ s, as determined in Chapter 3 in our evaluation of the deformation ε , appears quite acceptable.

Our analysis of the behavior of non-equilibrium addends to the electronic distribution functions revealed the existence of certain region of temperatures T and extinction Γ with optimum conditions for wave generation (Electron extinction depends on the concentration C of the second alloying component). Within this region, during simultaneous change of the key parameters T and C , a high magnitude and slow variation of the non-equilibrium addends are typical.

The next step in our analysis comprised a mapping of the real relationship $M_S(C)$, between temperature and concentration, into the region of optimum values of parameters T and Γ . As for Γ , the contribution of scattering by impurities has already been emphasized, and resulted in our consideration of weak scattering, being intimately related to the diagonal disorder in the system matrix. (Characteristic of this matrix is that it reflects the effect of solute atoms substituting the matrix-atoms in the lattice knots, with conservation of the transition integrals among the lattice-knots).

Our choice of the electronic configurations of the Ni-atoms as a reference configuration, based on published data, enabled us to determine the electronic configurations of iron, cobalt manganese and carbon, in accordance with the mapping of the relationship $M_S(C)$ into the region of optimum values of the parameters T and Γ . Among the analyzed substitutional alloys, the difference ΔZ , indicating the number of electrons donated by an alloying atom into a common s-band, proved to be least for Fe-Co-alloys: $|\Delta Z|_{Fe-Co} = (0 \div 0, 2)$ and largest for Fe-Mn-alloys: $|\Delta Z|_{Fe-Mn} = (0, 4 \div 0, 5)$, for the case of an iron-atom configuration near $3d^7 4s^1$. Interestingly, within our model with diagonal disorder, there can be realized a twice-fold rate of reduction of $M_S(C)$ in Fe-Mn-alloys with increasing manganese-concentration, in relation to the rate of decrease of $M_S(C)$ in Fe-Ni-alloys with $|\Delta Z|_{Fe-Mn} - |\Delta Z|_{Fe-Ni} \leq 0, 1$. This result could also be confirmed by comparison of the rates of reduction among the Fe-Mn and Fe-C-systems.

Good accordance with the values of $0, 2 \div 0, 3$ eV, mentioned in Pt. 2.5, is also given for the parameters $\varepsilon_d - \mu = (0, 17 \div 0, 26)$ eV, which we used for the mapping of the function $M_S(C)$. We recall that the value $\varepsilon_d - \mu \approx 0, 237$ eV has been chosen as an initial value (at a temperature $M_S^I(0) = 1093$ K), and that the range of the $\varepsilon_d - \mu$ values depends on the lattice parameter.

From a quantitative point of view, an evaluation of the derivative $\partial f / \partial \mu'$, which - besides the quantity $\nabla \mu$ - determines the initial occupational inversion σ_0 , appears to be important. It follows from Fig. 4.4 that, in the vicinity of line 2 of the maximum values of the function $\partial f(\Gamma', T') / \partial \mu'$, the inequalities $0, 21 \geq \partial f / \partial \mu' \geq 0, 15$ are satisfied, enabling us to use the value $\partial f / \partial \mu' \approx 0, 15$ as a minimum, in our evaluation of σ_0 . We further note that the value $|\partial f / \partial \mu'| \approx 0, 1$, as used in Pt. 3.3 in our evaluation of the deformation ε (see (3.42)), was 1,5 -times

less than the above value.

We further note that the character of the isolines in Figs. 4.4, 4.5 (mirrored C-shaped curves) does not require that the function $\tilde{M}_S(C)$ strictly follows the path of lines 2 or 3. In the general case, which must not necessarily relate to iron-alloys, a variety of possibilities is permissible. For instance, the mapping of \tilde{M}_S on the plane (T', Γ') (for low M_S -temperatures and $\varepsilon_d - \mu$ - values near $\varepsilon_d - \mu \approx k_B M_S$) can attain the coordinates $(T' \approx 1, \Gamma' \approx 0)$, thus going far beyond of the limits of the region bordered by lines 1 and 2. The value $\partial f / \partial \mu' \approx 0,2$ however is large in this point and remains almost unchanged during a shifting motion along the isolines, being caused by increases of Γ' with simultaneous reduction of T' . Thus, if the starting-coordinates of \tilde{M}_S are located in the adjacency of $T' \approx 0,4, \Gamma' \approx 0$, then the value $\partial f / \partial \mu' \approx 0,18$ can only be conserved with increasing Γ' , if the temperature initially decreases and later on increases. A situation is also possible in which the temperature M_S , along certain section of the branches (steps) of the functions $M_S(C)$, decreases with increasing C , but increases along other sectors of the branches. This situation is illustrated in Fig. 4.12. Obviously, the motion away from point I along the isoline leads to a reduction of \tilde{M}_S^I with increasing Γ' . Cooling (without change of composition) will shift the system away from point I to point II. The shifting away from point II, along isoline $\partial f / \partial \mu' = \text{const}$, is associated with an increase of \tilde{M}_S^{II} , for increasing Γ' , until the intersection of branches \tilde{M}_S^I and \tilde{M}_S^{II} is reached. A similar behavior of the branches $M_S^i(C)$ can also be observed in Fe-Mo-alloys [164,188].

Of course, during an analysis of the functions $M_S^i(C)$ for iron-based alloys, the thermodynamic limitation

$$T_0(C) - M_S(C) \geq |\Delta T|_{\min} \sim 10^2 K, \quad (4.51)$$

may not be ignored.

This limitation shows that, during a $\gamma - \alpha$ - MT, the point M_S is set off by a limited quantity of about 10^2 K, below the temperature T_0 of phase-equilibrium. In the case of a reduction of $T_0(C)$ with increasing C ($\partial T_0 / \partial C < 0$), the condition $\partial M_S / \partial C > 0$ would contradict with the limitation (4.51), thus all functions $M_S^i(C)$ must decrease with increasing C , as can actually be observed in the cases of Fe-Ni-, Fe-Mn- and on Fe-C-alloys. However, if $T_0(C)$ increased with increasing C ($\partial T_0 / \partial C > 0$), then the M_S^i could either increase with increasing C (Fe-Co-, Fe-Al-alloys), or decrease (Fe-Cr-alloys), without contradicting to (4.51). At the same time, the high level of $\partial f / \partial \mu'$ remains conserved, while, in an alloying-model with diagonal disorder, the choice among these two possibilities will be determined by the quantity ΔZ , being the difference among the charge-numbers of the alloying-components. For small $\Delta Z \leq 0,1$, an increase of M_S , and for large $\Delta Z > 0,3$, a decrease of M_S would be favorable.

As to the general case, instead of a ΔZ - comparison, we have to compare, for various alloys, the derivatives $\partial \Gamma(C) / \partial C$. This way the relations (instead of inequalities (4.46))

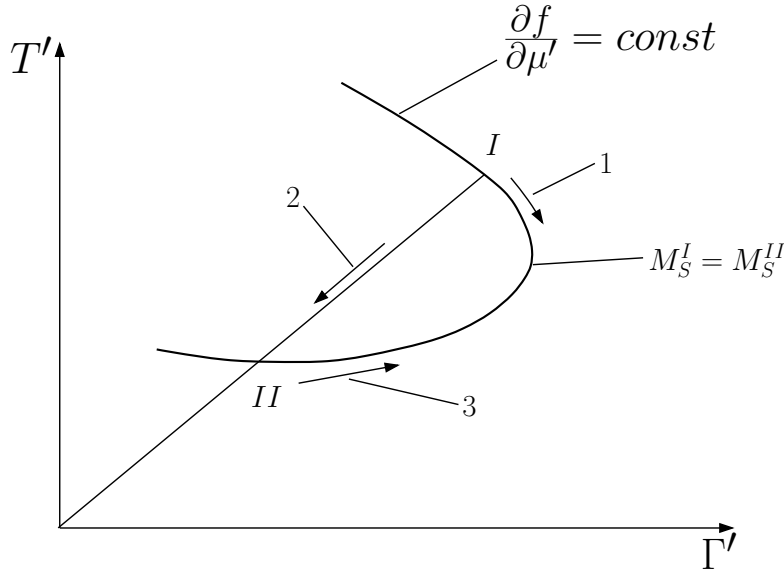


Figure 4.12. One of the variants for description of two stages of the concentration-relationship $M_S^{I,II}(C)$, mapped on the plane of variables Γ' , T' : Shifting motion along the isolines $\partial f / \partial \mu' = const$: Starting at point I and proceeding along route 1 corresponds to a reduction of M_S^I , with increasing concentration of the alloying elements. The motion along route 3 from point II is reflected by an increase of M_S^{II} . Route 2 describes a cooling process without variation of composition.

$$\left. \frac{\partial \Gamma}{\partial C} \right|_{Fe-Co} < \left. \frac{\partial \Gamma}{\partial C} \right|_{Fe-Ni} < \left. \frac{\partial \Gamma}{\partial C} \right|_{Fe-Mn}$$

are materialized in an alloying model with diagonal disorder.

Thus our presentation of the concentration-relationship $M_S(C)$ opens up the possibility of sustaining a high level of occupational inversion, in a wide range of variations of temperature and concentration of alloying-elements, thus delivering a simple explanation for the reasons of the different characteristics of the $M_S(C)$ functions of iron-based alloys, including alloys with elements marking off the limits of the region of existence of the γ - phase (a more comprehensive list of elements than that mentioned in Chapter 4 is given in [7]).

The data on which Chapter 4 is based were published in [90, 189, 190]. The analysis of the electronic configurations of iron-atoms in Fe - Ni - alloys, published in [190], has been used partially [191].

Chapter 5

Interpretation of a variety of characteristic morphological features of martensite within the notion of a phonon-maser

In iron-based alloys, the structural product of the $\gamma - \alpha$ - transformation, mainly bcc or bc-tetragonal martensite, exhibits a large variety of morphological features (see Pt. 1.2). This morphology undoubtedly contains valuable information on the dynamical mechanism of the martensitic transformation (MT). Its disclosure will thus be essential in our search for potential methods of externally influencing a MT. Thus it would be helpful to define certain models which will then enable us to gather such information. The notion of a phonon-maser (see Chapter 2.3) focuses on non-equilibrium conditions emerging in the adjacency of the boundary of the growing phase, as well as on the possibility of generation of lattice-displacement waves with amplitudes being sufficiently large to initiate the necessary plastic lattice deformation. This enabled us to interpret the growth-stage of martensite as a process being controlled by certain waves propagating through the premartensitic lattice phase. It should be emphasized that our task to explain the mechanism of wave generation includes the disclosure of an inherent link between the waves and some specific particularities of the electronic spectrum. Within the notion of the wave-model, our interpretation of morphological features of martensite will define such a link to observable macroscopic features (i.e. habit-planes), which will then allow us to analyze the physical causes of changes being linked up with variations of composition or of external boundary conditions.

5.1 Habit-planes in Fe-Ni, Fe-C-alloys

The qualitative pattern of definition of a habit-plane, which represents a fundamental morphological feature of martensite, has already been outlined in Sub-Pt.7 of the definition of our task under Pt. 1.5. Within our aim to resolve this task, let us start with a qualitative matching of characteristic lattice-planes and waves.

5.1.1 Matching of a plane with a pair of waves

It is generally possible, in principle, to link up planes with waves: Firstly, by directly associating them with the wave-front of a plane wave, and secondly, by associating them with the geometrical pattern of those points defined by a frozen-in trace of a moving line of intersection of two plane wave-fronts, propagating into different orientations. As the first case is rather trivial, let us consider more in detail the second case: Let \mathbf{c}_1 and \mathbf{c}_2 be two non-parallel wave-velocity vectors, taking into consideration that their vector-product $[\mathbf{c}_1, \mathbf{c}_2]$ is collinear with the line of intersection of the wave-fronts, which propagates with velocity \mathbf{c} . Then we will be able to define a vector \mathbf{N} , being collinear with the normal vector of the plane defined by the vectors $[\mathbf{c}_1, \mathbf{c}_2]$ and \mathbf{c} , by the following vector-product

$$\mathbf{N} = [\mathbf{c}, [\mathbf{c}_1, \mathbf{c}_2]] = \mathbf{c}_1 c_2^2 - \mathbf{c}_2 c_1^2. \quad (5.1)$$

Relation (5.1) immediately resolves the task of determination of \mathbf{N} for given \mathbf{c}_1 , \mathbf{c}_2 . The resolution of the inverted task however (i.e. the search for a pair of waves associated with a given \mathbf{N}), is ambiguous from the outset. Nonetheless, with the aid of (5.1), it is possible to determine conditions limiting the degree of ambiguity. As \mathbf{N} is a linear combination of the vectors \mathbf{c}_1 , \mathbf{c}_2 , the vectors \mathbf{c}_1 , \mathbf{c}_2 define a plane. Thus their vector triple product will vanish, for any factorial combination of them:

$$\mathbf{N} [\mathbf{c}_1, \mathbf{c}_2] = \mathbf{c}_1 [\mathbf{N}, \mathbf{c}_2] = \mathbf{c}_2 [\mathbf{N}, \mathbf{c}_1] = 0. \quad (5.2)$$

Inserting the factor $\mathbf{c}_2 c_1^2$ in (5.1), we get a representation of (5.1) in the form:

$$\mathbf{N} \parallel \mathbf{n}_1 \varkappa - \mathbf{n}_2 \quad (5.3)$$

where

$$\mathbf{n}_1 = \mathbf{c}_1 c_1^{-1}, \quad \mathbf{n}_2 = \mathbf{c}_2 c_2^{-1}, \quad \varkappa = c_2 c_1^{-1}. \quad (5.4)$$

5.1.2 Habit (225)

Getting over to an interpretation of the real habit-planes, we recall (see Pt. 1.2) that in Fe-C-, Fe-Ni-systems, the observed habit-planes are: Near $\{557\} \div \{111\}$ (up to 0,6 weight % C, up to 29% Ni), $\{225\}$ (0,6 - 1,4 weight % C), $\{259\} \div \{3 \ 10 \ 15\}$ (1,4 - 1,8 % C, 29 - 34% Ni). In accordance with Pt. 7, Sub-Pt. 1.5 of the definition of our task, as well as with our conclusions from Chapters 2 and

3, we shall define, in our description of the waves, pairs of longitudinal (quasi-longitudinal) waves, propagating close to the perpendicular orientations $\langle 001 \rangle$ and $\langle 110 \rangle$ of a fcc-lattice. This way, we can hypothesize that the martensitic transformation is initiated by waves propagating through the austenitic parent areas, delivering or exceeding the required threshold-deformation $\varepsilon \sim \varepsilon_t$ of austenite. In addition, the displacement of lattice atoms, being immediately linked up with the waves, feature just the kind of phase relations being required to perform a Bain-deformation (the geometric pattern of the Bain-deformation has been treated in Pt. 1.4, see also Fig. 1.1).

Let us start with a consideration of martensite with habit planes $\{225\}$: Our particular interest in this habit group is based, on the one hand, on that the crystallographic theory encounters the greatest explanatory difficulties [13] with this group, and on the other hand, on the intermediate position of martensite with these habits, in relation to its carbon-concentration, which may facilitate a comparison of habit planes of martensite belonging to the first and to the third group.

From the outset of our consideration, we note that, if we choose the velocity of one of the waves propagating in direction $\mathbf{c}_1 \parallel [00\bar{1}]$ (Orientation Δ : 4th - order axis of symmetry), then, according (5.2) and (5.3), it will be possible to define the type (h h l) habit, where h, l > 0, by choosing the second wave with a velocity $\mathbf{c}_2 \parallel [11\eta]$, using the condition

$$\varkappa = \frac{c_2}{c_1} = \frac{l - \eta h}{h \sqrt{2 + \eta^2}}. \quad (5.5)$$

Moreover, if we choose waves with reasonable long wave-lengths (see the treatise in Chap. 2), it may be justified to surmise that their role mainly consists in selecting those macro-regions (or meso-regions) comprising the most favorable transformation conditions. Under such a point of view, it suggests itself to perform our interpretation of the particular features of the inner structure of a martensite lamella (with a thin structure), using the notion of coordinated action of long- and short-waves. It may be reminded that a lamella with habit (225) consists of thin twinning lamella (110), among which the main axes [100] and [010] of Bain-deformation alternate in turn. Thus obviously, if we confined ourselves to a description of pure Bain-deformation, it would be justified to choose the velocity of one of the longitudinal waves $\mathbf{c}_1 = \mathbf{c}_\Delta$ in direction $[00\bar{1}]$. The coordinated action of such wave with the short-length displacement waves will then result in a tension of the lattice in the orientation [001], being also required for Bain-deformation with compressive-axes [100] and [010]. As to the wave along $[11\eta]$, both type of twins have equal relevance to it, like in the previously discussed case. Furthermore, if the wave is of the longitudinal type, it will support the Bain-pressure alternating among the directions [010] and [100], the more, the closer η is to zero, i.e. the closer \mathbf{c}_2 is oriented towards Σ .

For a given alloy, the value $\varkappa_0 = \varkappa(\eta_0)$ - corresponding to habit (225) - is

defined by the intersection between the curves determined experimentally $\varkappa_e(\eta)$ and theoretically $\varkappa_{T1}(\eta)$: $\varkappa(\eta_0) = \varkappa_e(\eta_0) = \varkappa_{T1}(\eta_0)$. According to (5.5), the curve $\varkappa_{T1}(\eta)$ descends monotonously - within the interval $0 < \eta < 1$ - from $\varkappa(0) \approx 1,77$ down to $\varkappa(1) \approx 0,87$. Obviously, an unequivocal solution \varkappa_0 exists within the interval $0 < \eta < 1$, if the path of curve $\varkappa_e(\eta)$ ascends monotonously, with an initial value $\varkappa_e(0)$ out of the interval: $0,87 < \varkappa_e(0) < 1,77$. As longitudinal waves normally satisfy the inequality $c_\Delta < c_\Sigma < c_\Lambda$, the requirement of monotonous ascent of curve $\varkappa_e(\eta)$ also is satisfied, in addition: $\varkappa_e(0) = c_\Sigma c_\Delta^{-1} > 1$, thus the only remaining restriction is $\varkappa_e(0) < 1,76$. Under consideration of the aforementioned restriction, which most certainly will be satisfied for the systems of our interest, there must exist an unequivocal solution. The results of our analysis are presented in the first part of Fig. 5.1, where the nearly horizontal curve \varkappa_e represents the weakly pronounced dependence on orientation of a longitudinal wave during a transition from the Σ - to the Λ - orientation, resembling a 3rd order of symmetry axis. As already mentioned, those \mathbf{c}_2 -orientations being close to the Σ - orientation will find our greatest interest. Obviously from Fig. 5.1, this approximation occurs with increasing $\varkappa_e(0)$.

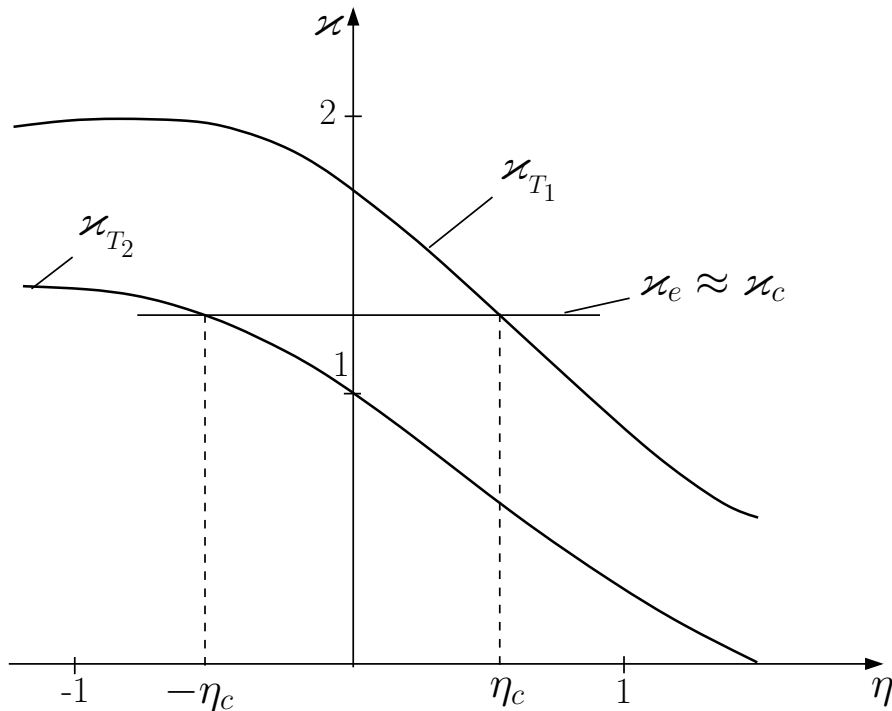


Figure 5.1. Graphic pattern for determination of the η_0 , which determines the orientation $[11\eta_0]$ of propagation of a quasi-longitudinal displacement-wave. Shown is the "critical" case: The value $\eta_0 = \eta_c$ corresponds to the habit plane (225) and the value $\eta_0 = -\eta_c$ to habit plane (557). Then functions $\varkappa_T(\eta)$ and $\varkappa_e(\eta)$ are defined in the text.

5.1.3 Habit (557). Criterion for transition from habitus (557) to (225)

The affiliation of habitus (557) to the type (h h l), also being common with (225), and the possibility of their coexistence in the limit region of carbon-concentration near 0,6 % C, suggest to describe these lamellae by a pair of waves $\mathbf{c}_1 \parallel [00\bar{1}]$, $\mathbf{c}_2 \parallel [11\eta]$, in a similar way as habitus (225). Even though such a description is possible, the solution of the equation $\varkappa(\eta_0) = \varkappa_{T_2}(\eta_0) = \varkappa_e(\eta_0)$ is defined in the negative region $-1 < \eta_0 < 0$. In the left side of Fig. 5.1, the curve $\varkappa_{T_2}(\eta)$ has been drawn in accordance with (5.5), for the habit (557), which ascends monotonously from $\varkappa_{T_2}(0) \approx 1$ up to $\varkappa_{T_2}(-1) \approx 1,386$. The larger $\varkappa_e(0) > 1$ becomes, the more the direction of velocity \mathbf{c}_2 will deviate from that of Σ . In other words, it behaves just the opposite way as in the case of habit (225). Obviously, there must exist a value η_c (let us call it the critical value), for which $\varkappa_{T_1}(\eta_c) = \varkappa_c = \varkappa_{T_2}(-\eta_c) \approx \varkappa_e(0)$. This equation corresponds to $\eta_c \approx 0,55$, with $\varkappa_c \approx 1,285$. The quantitative criterion for separation of these cases, for which apparently the dynamical conditions for development of only one of the habits must be more favorable, has a simple structure:

$$\begin{aligned} (225) - -\varkappa_e(0) &> \varkappa_c, \\ (557) - -\varkappa_e(0) &< \varkappa_c. \end{aligned} \quad (5.6)$$

Obviously, both habits can coexist in the region $\varkappa_e(0) \approx \varkappa_c$. Further assuming that an increase of carbon-concentration leads to a slow increase of $\varkappa_e(0)$, and that the value \varkappa_c is attained near 0,6 % C, then any further increase of $\varkappa_e(0) > \varkappa_c$ must be associated with a transition from habit (557) to (225).

This specific effect of carbon can be explained in a qualitative manner: Those carbon atoms accumulating in voids [13] hybridize their 2p - functions with the 3d-functions of the iron atoms with e_g - symmetry (as shown under Pt. 4.6), and thus reduce the effective positive charges Z of the ions, in the field of which the free 4s-electrons are moving. This must cause a local reduction of longitudinal velocity of sound, as - in accordance with the "jelly"-model [192] - the velocity of sound is $c \sim Z^{1/2}$. Presumably due to the anisotropy of the 2p-functions in Fe-C-systems, the increase of the parameter $\varkappa_e(0) = c_{\Sigma}c_{\Delta}^{-1}$ is mainly associated with the decrease of c_{Δ} with increasing carbon-concentration (note that any comparison of the c_{Δ} - values of different alloys must be performed at the same temperature). In the more general case, a situation is also conceivable in which an increase of $\varkappa_e(0)$ is related to the more rapid increase of the velocity c_{Σ} in relation to c_{Δ} .

Remarkably, the lack of a noticeable region of Ni-concentration for habit (225) in Fe-Ni-systems is in accordance with our criterion (5.6). Experimental evidence reported in [38] shows that $\varkappa_e(0)$ can only attain the value \varkappa_c for 33 % Ni in ferromagnetic austenite. In this case, $\varkappa_e(0)$ attains the values $1,12 \div 1,15$ until reaching magnetic ordering, clearly being less than \varkappa_c .

Having applied this approach for the case of perpendicular waves

$\mathbf{c}_1 \parallel [\eta/2 \ \eta/2 \ \bar{1}]$, $\mathbf{c}_2 \parallel [1 \ 1 \ \eta]$ - where \mathbf{c}_1 already is non-parallel to $[00\bar{1}]$ - and with consideration of the variation of habit from (557) to (111), we get the results listed in Table 5.1.

Table 5.1. Values \varkappa_c , η_c , θ_c , for three pairs of habits

habit-pairs	\varkappa_c	η_c	θ_c , Degree
(225), (557)	1,3083	0,1962	7,8966
(225), (667)	1,1923	0,2619	10,4913
(225), (111)	1,1061	0,3166	12,6197

Here, θ_c - angle between $[11\eta_c]$ and $[110]$; η_c being determined on the basis of equivalence of the velocity-modules ratios $\varkappa = c_2 c_1^{-1}$, for different habits of the types $(h_1 \ h_1 \ l_1)$ and $(h_2 \ h_2 \ l_2)$, as given by

$$\eta_c = \sqrt{2 + b^2} - b, \quad b = \frac{2 h_1 h_2 + l_1 l_2}{h_1 l_2 - h_2 l_1}, \quad (5.7)$$

while \varkappa_c can be determined by substituting $\eta = \eta_c$ in the expression

$$\varkappa = \frac{c_2}{c_1} = \frac{(l - h\eta)\sqrt{2}}{2h + l\eta}. \quad (5.8)$$

In (5.7) and (5.8) the indices $l = l_2 = 5$, $h = h_2 = 2$ correspond to positive η . As can be seen from the data in Table 5.1 for perpendicular wave-pairs \mathbf{c}_1 and \mathbf{c}_2 , an increase of \varkappa supports the transition from the habit (557) to (225), in conjunction with a reduction of the angle of deviation θ among the axes of symmetry of second and fourth order. We also note that the deviation of the first wave from the axis $[00\bar{1}]$ opens up the possibility to significantly reduce the deviation of the second wave from the axis $[110]$, in comparison with the case $\mathbf{c}_2 \parallel [00\bar{1}]$. Of course, for $\varkappa \approx \varkappa_c$, a coexistence of crystals with habits (557) and (225) is possible. This way, e.g. in [165] a similar kind of coexistence has been observed during rapid quenching of steels with $< 0,6 \%$ C

5.1.4 Habits $\{15 \ 3 \ 10\} \div \{9 \ 2 \ 5\}$

The characteristic feature of martensite with these habit-planes is associated with internal twinning. For the habits (15 3 10) and (9 2 5), the Bain-pressure axes in the twins correspond to $[010]$ and $[001]$. Thus, in analogy with habit (225), we have to choose as the first wave contributing to lattice expansion of both twins during Bain-deformation, the longitudinal wave with velocity $\mathbf{c}_1 \parallel [\bar{1}00]$. Then we determine from (5.2) the velocity of the second wave: $\mathbf{c}_2 \parallel [\eta \ 0 \ 3 \ 1]$ and $\mathbf{c}'_2 \parallel [\eta \ 0 \ 4 \ 1]$ (in the following, we mark with $'$ the results relating to the description of habit (9 2 5)). If we construct, on the basis of (5.4), the curves $\varkappa_T(\eta)$ within

a region $0 \leq \eta \leq 0,3$, and $\varkappa'_T(\eta)$ within a region $0 \leq \eta \leq 0,4$, then we can easily convince ourselves that they descend monotonously, attaining the following values at the limits of those regions: $\varkappa_T(0) \approx 1,44$, $\varkappa_T(0,3) \approx 1,1$; $\varkappa'_T(0) \approx 1,67$, $\varkappa'_T(0,4) \approx 1,22$. Obviously, there exist unequivocal solutions of the equations $\varkappa_e(\eta) = \varkappa_T(\eta)$, $\varkappa'_e(\eta) = \varkappa'_T(\eta)$, corresponding to the experimentally determined curves $\varkappa_e(\eta)$, $\varkappa'_e(\eta)$, which ascend monotonously with increasing η , in the regions: $1,1 < \varkappa_e(0) < 1,44$; $1,22 < \varkappa'_e(0) < 1,67$. Let us now take the data of [38] for Fe - 33% Ni and use them to calculate the longitudinal velocities of sound, related to the axes of symmetry of cubic crystals [193], in order to determine $\varkappa_e(0) \approx 1,1$, $\varkappa_e(0,3) \approx 1,22$ for the second wave: $\mathbf{c}_2 \parallel [0,22 \ 0,3 \ 1]$, $\mathbf{c}'_2 \parallel [0,34 \ 0,4 \ 1]$. It should be noted here that the twins no longer can be treated equally in relation to the second wave, if compared with the case of habit (225). Obviously, the second wave delivers more pressure towards direction [001]. The experimental result published in [13] gives evidence for our conclusion that the thickness of the respective twins effectively is more in comparison to the width of the twins with Bain-pressure directed in axis [010].

A very convenient form of notation of axes and planes, being particularly useful for the description of morphologic characteristics of twinned martensitic crystals, can easily be obtained for any given habit, out of a totality $\{h \ k \ l\}$ under the assumption $|h| < |k| < |l|$.

Then the direction $\langle 0 \ 0 \ l/|l| \rangle$ for $\{h \ k \ l\}$ -habits $\{3 \ 10 \ 15\} \div \{2 \ 5 \ 9\}$ (the position of the 1 corresponds with the position of the largest modulus of the index l) will be collinear with the direction of wave-propagation with velocity \mathbf{c}_1 , which initiates the $\gamma - \alpha$ - transformation in the phase of tension. The axis $\langle 0 \ k/|k| \ 0 \rangle$ (position of the 1 corresponds to the position of the intermediate module of index k) determines the direction of the main Bain-pressure axis and the axis $\langle h/|h| \ 0 \ 0 \rangle$ (the position of the 1 corresponds to the position of the smallest module of index h) the direction of the Bain-pressure axis for the volumetrically smaller twin components. The twinning-plane can be noted in the form $\{h/|h| \ k/|k| \ 0\}$.

The same symbols can also be used for definition of the direction of the normals $\langle h \ k \ l \rangle$ to habits $\{h \ k \ l\}$, in a stereographic projection, being commonly used in crystallographic analysis. Namely: the pole $\langle h \ k \ l \rangle$ is located within a stereographic triangle, its corners

$$\langle 0 \ 0 \ \frac{l}{|l|} \rangle, \quad \langle 0 \ \frac{h}{|k|} \ \frac{l}{|l|} \rangle, \quad \langle \frac{h}{|h|} \ \frac{k}{|k|} \ \frac{l}{|l|} \rangle \quad (5.9)$$

correspond with the projections of the axes of symmetry of the fourth, second and third order, respectively. Following (5.9), e.g. the normal $[15 \ \bar{3} \ 10]$ corresponds with the stereographic triangle $[100] - [101] - [1\bar{1}1]$. We can easily convince ourselves that there exists a totality of twenty-four orientational variants, all of them corresponding with the normals $\langle h \ k \ l \rangle$. By consideration of the notes in the previous section we see that the corner $\langle 0 \ 0 \ l/|l| \rangle$ of the triangle, being confronted with the $\{h \ k \ l\}$ - habit, indicates the direction of the austenitic ex-

pansion during formation of a martensite crystal. We also note that the corner $\langle h/|h| \quad k/|k| \quad l/|l| \rangle$ of the stereographic triangle points into the direction of the normal of the plane of densely packed austenite, out of a totality of four planes $\{111\}$, belonging to the orientational relationship of the lattices of the γ - and α - phases (see Pt. 1.2), with respect to a materialized habit of the $\{h \ k \ l\}$ family, which also feature the smallest angle with the habit-plane in relation to the remaining $\{111\}$ planes. The latter circumstance most likely is linked up with the minimization of free energy of the phase-boundary, during its gradually staged microscopic coupling, as commonly known for grain-boundaries [194].

5.2 Grouping laws for packet-martensite crystals

Research on lath- or packet-martensite is a highly demanding scientific task. The papers [24, 195–205] provide us with a relatively comprehensive and contemporary image on the development of concepts and the structure of packet-martensite. The habits of packet-martensite near to $\{557\}$ were firstly mentioned in [195], for Fe - 0,2% C-, Fe - 0,6% C-systems (and confirmed in [197, 205]), where the conformance of a pair of Miller-indices only is approximated. Thus in reality, the normal of the habit-plane is located within the stereographic triangle (see end of Pt. 5.1) corresponding to its habit, and not at the border of two triangles. In our wave-pattern used in Pt. 5.1 for a description of habits $\{h \ h \ l\} - \{557\} \div \{225\}$, an unequivocal orientation of the habits near $\{557\}$, $\{225\}$ will arise if the directions defined by $\mathbf{c}_2 \parallel \langle 11\eta \rangle$ are "split" into pairs $\langle 1 \pm \eta_1, 1 \mp \eta_2, \eta \rangle$, $|\eta_{1,2}| < \eta$. Then we get instead of $\{h \ h \ l\}$ the corresponding expression $\{h \pm \delta_1, h \mp \delta_2, l\}$, where $|\delta_{1,2}| < 1$. Using (5.3) and the relation $\mathbf{c}_1 \parallel [00\bar{1}]$, $\mathbf{c}_2 \parallel [1 + \eta_1, 1 - \eta_2, \eta]$ we can determine the vector \mathbf{N} , being collinear to the normal of the habit-plane

$$N \parallel [1 + \eta_1, 1 - \eta_2, \varkappa \sqrt{(1 + \eta_1)^2 + (1 - \eta_2)^2 + \eta^2 + \eta}], \quad (5.10)$$

where $\varkappa = c_2 c_1^{-1}$. Then we can determine from (5.10), e.g. for $\eta_1 = \eta_2 = 0,03$, $\eta = -0,21$, $\varkappa = 1,2$, the habit (4,79 4,51 7), whose normal is located within the stereographic triangle $[001] - [101] - [111]$.

Let us further assume that, for initiation of a $\gamma - \alpha$ - transformation resulting in packet-martensite, there are required certain phase-relationships among the relative displacements of the lattice atoms associated with the waves, in a similar way as for lamellar martensite (see Pt. 5.1.4). Then we compare in the crystals with habits of the type $\{5 + \delta_1, 7, 5 - \delta_2\}$, for $\delta_{1,2} > 0$, the direction of expansion - $\langle 010 \rangle$ and the direction of compression $\langle 100 \rangle$, where positions 1 correspond with those habit-plane indices where the modules attain the largest or the mean value, respectively.

Further assuming that the strain-amplitudes of the waves are sufficiently large to initiate plastic deformation, (see Chap.3), then it will be possible to determine the direction of macro-shear \mathbf{S} (lacking the correct sign), as the pair of waves

propagating into directions $\langle 001 \rangle$, $\langle 1+\eta_1, 1-\eta_2, \eta \rangle$, will prefer one of the twelve slip-systems $\{111\} \langle \bar{1}\bar{1}0 \rangle$ of the fcc-lattice. The real selection will then be performed in accordance with the Schmid-relationships for shear-stress δ_c (see e.g. [206]):

$$\delta_c \sim \cos \varphi_1 \cos \varphi_2, \quad (5.11)$$

resulting from the requirement of maximum angular factor modulus (5.11) for the mechanical stress associated with the waves. φ_1, φ_2 in (5.11) are the angles between the direction of applied normal stress (being close to the direction of propagation of the longitudinal wave) and the directions of the normal $\langle 111 \rangle$ to the slip plane - $\{111\}$ or shear $\langle \bar{1}\bar{1}0 \rangle$, respectively. As a result of this analysis, the habits $\{5 \pm \delta, 5 \mp \delta, 7\}$ will naturally form groups of sextets $\{h k l\}$ close to the common slip planes $\{111\}$. An example of such grouping is presented in Table 5.2, for $\eta < 0$. This grouping corresponds to a package of crystals [196–198]

Table 5.2. Directions of wave propagation and some characteristics of packet-martensite (slip-plane (111))

Nr.	Habit	Direction of \mathbf{c}_2	Direction \mathbf{c}_1	Compressive-axis	Direction \mathbf{S}
1	$(5 + \delta_1, 5 - \delta_2, 7)$	$[1 + \eta_1, 1 - \eta_2, \eta]$	$[00\bar{1}]$	$[100]$	$[\bar{1}01]$
2	$(5 - \delta_1, 5 + \delta_2, 7)$	$[1 - \eta_1, 1 + \eta_2, \eta]$	$[00\bar{1}]$	$[010]$	$[0\bar{1}1]$
3	$(7, 5 + \delta_1, 5 - \delta_2)$	$[\eta, 1 + \eta_1, 1 - \eta_2]$	$[\bar{1}00]$	$[010]$	$[1\bar{1}0]$
4	$(7, 5 - \delta_1, 5 + \delta_2)$	$[\eta, 1 - \eta_1, 1 + \eta_2]$	$[\bar{1}00]$	$[001]$	$[10\bar{1}]$
5	$(5 - \delta_1, 7, 5 + \delta_2)$	$[1 - \eta_1, \eta, 1 + \eta_2]$	$[0\bar{1}0]$	$[001]$	$[01\bar{1}]$
6	$(5 + \delta_1, 7, 5 - \delta_2)$	$[1 + \eta_1, \eta, 1 - \eta_2]$	$[0\bar{1}0]$	$[100]$	$[\bar{1}10]$

with six orientations close to the common plane (111), forming part of the orientational relationship. Obviously there exist three similar groups of crystals with six orientations in each group, comprising other common planes out of the totality of $\{111\}$. It is also obvious from Table 5.2 that, if the crystals with six orientations are equally partitioned in such a package, then, during a martensitic transformation, the region occupied by such a package must be subjected to a quasi-isotropic volumetric change, as the directions of maximum compressive and tensile stress correspond to all three variants of Bain-deformation, while the alternating orientations of lattice-displacement \mathbf{S} make possible a macroscopic neutralization of totalized local displacements within a packet. In [196–198], just these rules were pointed out.

Due to a missing more stringent definition of the term "Packet-martensite crystal" it came about that, apart from methodological problems, different results were obtained in the determination of the number of orientations associated with martensite packet crystals. Thus in [199], one or two, in [205] only one, and in [196–198], six orientations within a common plane $\{111\}$ were considered. If one describes the term "packet" as a totality of martensite-crystals (with habits near $\{557\}$) and with six orientations close to a common plane out of $\{111\}$, as practically done in [196–198], then the determined reduced number of orientations must be associated with a certain local zone of the packet, which would comprise a reduced number of orientations. In [202], the existence of four zonal types was determined in one packet. Type 1 represents triplets of orientations, i.e. habit-triplets of numbers 1, 3, 5, or 2, 4, 6 as shown in Table 5.2. Type 2 represents pairs of orientations, i.e. habit-pairs 1, 4; 2, 5; 3, 6 as shown in Table 5.2. Type 3 represents pairs of twin-orientations, corresponding to pairs of habits 1, 2; 3, 4; 5, 6 as shown in Table 5.2. Type 4, with only one orientation, corresponds to any of the habits shown in Table 5.2. For equal volumetric fractions of crystals with different orientations in zone of type 1, a quasi-isotropic change of volume in conjunction with neutralization of shear-deformation may be possible. In the zone of type 2 (as well as in the zones of type 3 and 4), the volumetric changes become anisotropic, but a neutralization of displacement-deformation still is possible. This however is no longer possible for zones of type 3 and 4, that is becoming evident by comparison of the \mathbf{S} -directions in Table 5.2. Obviously, the used definition of the packet implicitly takes for granted that the transforming austenite comprises a sufficiently large volume. In other words, this definition is critical with respect to the austenitic volume size. The results obtained with pseudo-monocrystals in [203,204] fit well with the findings in [196–198]. In [200], being related to the case of coexistence of lamellae with habits $\{225\}$ and laths, a package is defined as a totality of "blocks" composed of lamellae and laths (each lamellae being connected with laths embodying two twinning-orientations), in such a way that within this definition, the requirement of six orientations lives on for packet-martensite. A comparison with the a.m. data [202] shows that, due to the presence of lamellae with habits $\{225\}$, to which a dominant role during formation of packets is assigned in [200], only the zone of type 3 is segregated out of four types of local packing zones in lath-shaped crystals. We also note that the association of plane (111) in Table 5.2 with the plane of least slip resistance correlates well with the concepts in [13] on stress-relaxation, during the isothermal martensitic transformation by shear-processes within the austenite-matrix surrounding the martensite crystal. The orientation \mathbf{S} , being precisely determined by the Schmid-rule (with exception of the sign), correlates with the macroscopic direction of displacement of a martensite crystal of this orientation [200,201].

5.3 Effect of the magnetic state of austenite and of an externally applied magnetic field on the martensitic $\gamma - \alpha$ - transformation

5.3.1 Possible causes for the transition of habit-planes

After our matching of the habits with pairs of waves, it will be easy to estimate which parts of the electronic spectrum are actively involved in a martensitic transformation. Following such general characteristics, it is possible to associate crystals with habit-planes near $\{557\}$, $\{225\}$, as the pairs of waves, propagating near the axes of symmetry of the second and fourth order, can be put in relation with the electronic states being localized in the vicinity of the S-surfaces: $S_{\langle 001 \rangle}$, $S_{\langle 110 \rangle}$ (see Chap. 2). In the case of the habit $(15\ 3\ 10)$, already mentioned under Pt. 5.1.4, the direction of \mathbf{c}_2 defines an angle $\theta_1 = 20, 3^\circ$, $\theta_2 = 69, 8^\circ$, $\theta_3 = 34, 7^\circ$ in relation to the axes $[001]$, $[110]$, $[111]$. It is therefore justified to assume that the habits $\{15\ 3\ 10\}$ need only to be matched with the waves propagating near the fourth-order symmetry-axes, being linked up with the $S_{\langle 001 \rangle}$ surfaces. Thus the causes for the first and second change of habits, i.e. $\{557\} \rightarrow \{225\}$ in Fe-C-systems, and for the second change, i.e. $\{225\} \rightarrow \{259\}$ in Fe-C-systems and $\{557\} \rightarrow \{3\ 10\ 15\}$ in Fe-Ni-alloys, apparently must be different.

In the first case, no change of the class of waves governing the growth of a martensitic lamellae occurs; while the velocity-vector \mathbf{c}_2 of the second wave remains within the directional cone near $\langle 110 \rangle$, and only the sign of the projection \mathbf{c}_2 on the direction $\langle 00\bar{1} \rangle$ (close to direction of propagation of the first wave (see Pt. 5.1.3)) changes. The causes for this behavior may be:

1. Increase of the velocity-ratio $\varkappa = c_2 c_1^{-1}$ with increasing carbon-concentration, leading to improved conditions for Bain-deformation for $\varkappa > \varkappa_c$ (see Table 5.1) (i.e. to smaller threshold-deformation ε_t), in case of changing sign of the projection of \mathbf{c}_2 on $\langle 00\bar{1} \rangle$.
2. The appearance of a short-wave displacement component, being responsible for the thin (twinned) structure of macro-lamellae in the case of crystals with habits $\{225\}$. From a dynamical point of view, the appearance of short-wave displacement (of about half the wave-length with an order of magnitude of about the thickness of twins) at lower temperatures (related to the M_S - temperature of lath-martensite) should be possible in principle, as a reduction of T will inevitably lead to a reduction of phonon-extinction and, consequently, also of the threshold-value σ_t of an inverted occupational difference (see (3.10) in Pt. 3.1). The latter argument fits well with the commonly used interpretation in [13], stating that during a martensitic transformation, the relaxation of internal stress at low temperatures is mainly linked up with

twinning-processes.

The second change of habits apparently is caused by a reduction of the activity of electronic states localized near the $S_{\langle 110 \rangle}$ surfaces, in relation to the states located near $S_{\langle 001 \rangle}$. The relative passiveness near $S_{\langle 110 \rangle}$ may be related to the magnitudes of the parameters Γ and $\varepsilon_d - \mu$, at the surfaces $S_{\langle 110 \rangle}$ and $S_{\langle 001 \rangle}$. We recall that ε_d represents certain mean-value $\bar{\varepsilon}$ of the energies of the d-electrons on the S-surface and Γ is an extinction of s-electrons of energy $\varepsilon_s \approx \varepsilon_d$. As a common cause of the different values of the Γ parameter at different S-surfaces, it is possible to define the anisotropy of s-d-scattering, the degree of which varying with concentration of the alloying elements. The variation of $\varepsilon_d - \mu$ for non spin-polarized states with $\varepsilon_d - \mu > 0$ (see Pt. 4.5) is mainly caused by a the variation of the lattice-parameter a , whereas the rate of variation of $\varepsilon_d - \mu$ may differ for different S-surfaces, due to the non-correspondence of the rates of change of energies ε_d . If, for example, the tight binding approximation in [104] was used with consideration of the first and second neighbors, as well as the expressions of the matrix-elements $V_{ij} \sim a^{-5}$ for the electronic transitions among the knots given in [183], then it would easily be recognized that the characteristic energies (see Pt. 2.5) ε_{X_5} , ε_{X_2} , ε_{L_3} decrease with increasing a , while the rate of decrease is largest for ε_{X_5} and least for ε_{L_3} . For spin-polarized states, the value of $\varepsilon_{d\uparrow} - \mu < 0$ will also depend on the magnitude of exchange-splitting, which probably increases at temperatures below the magnetic ordering temperature, and in the case of anisotropic splitting, may be an additional cause of passivation of electronic states near $S_{\langle 110 \rangle}$ for the Fe-Ni-system (with $C_{Ni} > 29\%$), in which magnetic ordering of the γ - phase precedes the martensitic transformation.

The influence of the magnetic state of austenite on reaction kinetics has been highlighted in [207] and [208], in connection with a qualitative consideration of the causes of a selective influence of a magnetic field on the kinetics of the $\gamma - \alpha$ - transformation. The most important law published in [15] is related to the effect of magnetic field bursts with field-strengths H up to $2,8 \cdot 10^7$ A/m (≈ 350 ke) on Fe-Ni-alloys. This law states that a magnetic field stimulates the athermal transformation into lamellar-martensite of Fe-Ni-alloys with Ni-concentration of more than 25 %. In addition, such magnetic field burts cause a non-monotonous increase of the point M_S by ΔM_S , as depicted in Fig. 5.2.

According to [15], the positive shifting $\Delta M_S > 0$ is deducible from the larger inherent magnetization of the α - phase, and, consequently, from the larger incremental free-energy reduction of the α - phase in a magnetic field, in relation to the γ - phase. Non-monotonous character of the shifting ΔM_S is attributable to the exceptionally large volumetric magnetostriction of the para-process defined in [209, 210], with consideration that the lower concentration limit of the non-monotonous magnetic field relationship corresponds with the lower limit of the ΔM_S - relationship (see Fig. 5.3, borrowed from [211]). A similar correlation also exists for steel with a super-paramagnetic γ - phase [209, 212] as well as for Fe-Ni-Mn-alloys with $Fe_{70+x}Ni_{30-2x}Mn_x$ ($0 < x < 4$), which have been in-

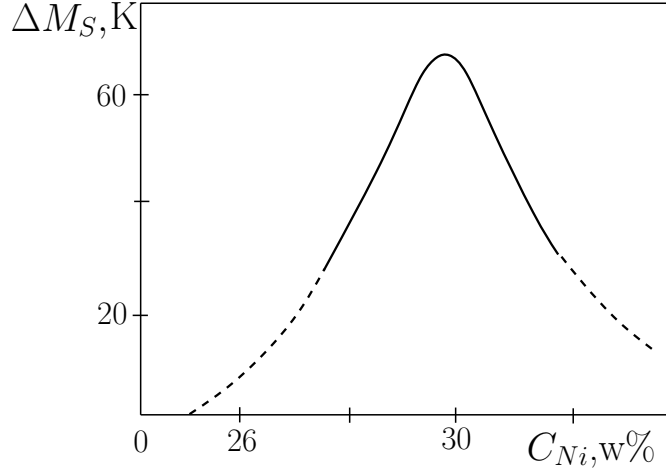


Figure 5.2. Relationship between the shifting of M_S in a magnetic field of $2,6 \cdot 10^7$ A/m and Ni-concentration (weight %) [15]

vestigated in [213, 214]. A linear extrapolation of the relationship between the volumetric increment $\Delta V/V$ and the quantity H , as shown in Fig. 5.4 (borrowed from [209]), results in a value of $\Delta V/V \sim 10^{-3}$ for $H = 2,8 \cdot 10^7$ A/m. The growth of specific volume in a magnetic field also correlates well with an increase of magnetization [213]. This suggests that "quasi-ferromagnetic" ordering exists in a strong magnetic field, being also associated with the transition towards athermal transformation kinetics [208]. The emergence of this state presumably is caused by magnetic-field induced exchange-splitting, which in turn results from the dependence of the exchange integral on the atomic distances (lattice parameter) or specific volume, respectively. As a reasonable basis for analysis and description of this effect, the exchange-contraction model may be suggested (see e.g. [215]).

5.3.2 Single peak density of states (DOS) model, exchange-splitting and electronic redistribution

If the Fermi-level μ of the non-magnetic state of the γ - phase of a Fe-Ni-alloy is located at the boundary of a step-like change of the DOS-function (right in front of the last peak of the density of states function of the d-band in Fig. 2.9), then the process of exchange splitting must be associated with an overflow of a part of the s-electrons into d-states [216,217]. By comparison of a modeled DOS with two characteristic values g_1 and g_2 , as shown in Figs. 5.5a and 5.5b, it becomes evident that the exchange-splitting $\Delta\varepsilon_{exch}$ must lower the Fermi-level by forcing the spin-up states into states with greater occupational density g_2 . The new Fermi-level μ' of the sub-system of d-electrons (dashed line in Fig. 5.5b) can be determined using the condition of equality of the hatched areas for the sub-bands $d \uparrow$, $d \downarrow$ as shown in Fig. 5.5b. With consideration that the difference of the areas of the $d \uparrow$, $d \downarrow$ sub-bands - below the level μ' - determines the atomic magnetic momentum $\bar{\mu} \mu_B^{-1}$

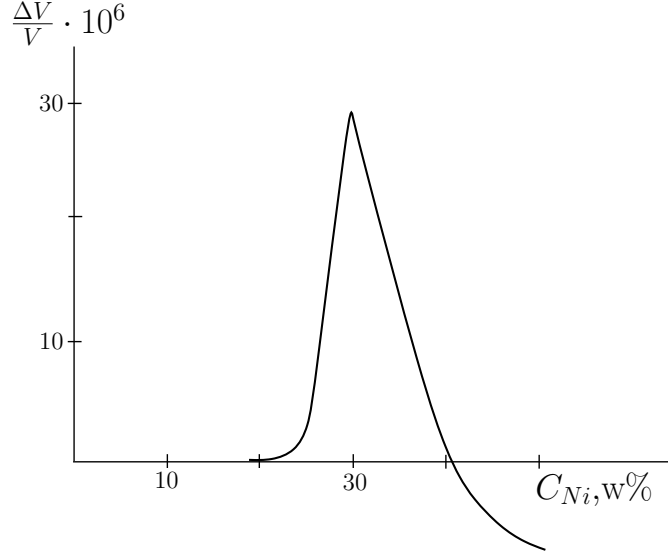


Figure 5.3. Relative change of volume due to magnetostriction in a magnetic field of $8,4 \cdot 10^4$ A/m [211] (Ni-weight %)

(expressed in units of Bohr's magneton μ_B), then we get for the ferromagnetic phase

$$\Delta \varepsilon_{exch} = \frac{g_1 + g_2}{g_1 g_2} \frac{\bar{\mu}}{2 \mu_B}, \quad \mu - \mu' = \frac{g_2 - g_1}{g_1 g_2} \frac{\bar{\mu}}{4 \mu_B}. \quad (5.12)$$

In the parabolic s-band, being characterized by a monotonously changing density of states g_s (see Pt. 4.3), the variation of the Fermi-level $\mu = \mu_s$ of the subsystem, being related to exchange-splitting of the s-electrons, can be ignored, i.e., a separate consideration of the s- and d-band will deliver $\mu' = \mu_d < \mu_s = \mu$. If an equality of the Fermi-levels of d- and s-electrons was required, then it would be possible to estimate the number of electrons flowing over from the s- into the d-band (related to a single atom):

$$\Delta n_s \approx 2 g_s(\mu) (\mu - \mu'), \quad (5.13)$$

where the factor 2 accounts for both projections of the electron-spin (note that in Pt. 4.3 we have $g_s(\mu)$ with only one spin-projection). For a width of the s-band $W_s = 10$ eV, and $Z_M \approx 1$, we get from (4.27) $g_s \approx 0,12 eV^{-1} \text{ atom}^{-1}$. Further assuming that the width of the d-band $W_d = 4,5$ eV, and the width of the rectangular peak 0,5 eV, $g_1 \approx 1 eV^{-1} \text{ atom}^{-1}$, $g_2 \approx 2 eV^{-1} \text{ atom}^{-1}$, $\bar{\mu} \mu_B^{-1} = 1,7$, which, in accordance with [218], almost represents the alloy $Fe_{0,65}Ni_{0,35}$, then

$$\Delta \varepsilon_{exch} \approx 1,28 eV, \quad \mu - \mu' \approx 0,21 eV, \quad \Delta n_s \approx 0,05. \quad (5.14)$$

Of course this pattern features an illustrative character, in that it only gives us an estimated order of magnitude $\mu - \mu' \sim 0,1$ eV, $\Delta n_s \sim 10^{-2}$. Presumably, the value

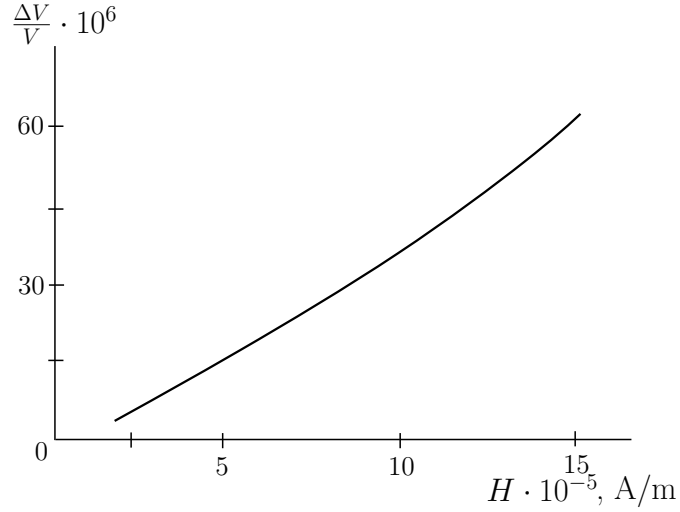


Figure 5.4. Relative change of austenite volume in the steel 40X2H20 in a magnetic field up to $1,5 \cdot 10^6$ A/m , at temperature of 77 K [209]

$\Delta n_s \approx 0,05$ is too large, as firstly, in the non-magnetic case shown in Fig. 5.5a, the shape of the DOS-peak, as well as the location of the Fermi-level, correspond to the maximum value of Δn_s , and, secondly, the relative shift of the d- and s-bands has not been properly taken into consideration. According to [111], the transition from configuration $3d^6 4s^2$ to $3d^7 4s^1$ of the γ - phase of iron is associated with an upward shift of the d-band by 5,5 eV - at an energetic scale - due to an increase of the repulsive energy-potential of the d-electrons. Then, due to an s-electron overflow of $\Delta n_s = 10^{-2}$ into the d-band, we get the following estimate for the upward shift of the d-band: $\Delta\mu' = 5,5 \cdot 10^{-2}$ eV. If we further consider that for $g_s \approx 0,12$ eV $^{-1}$ atom $^{-1}$, an s-electron overflow of $\Delta n_s = 10^{-2}$ would reduce the value of $\mu = \mu_s$ by $4,2 \cdot 10^{-2}$ eV (using the same g_1 and g_2), we got a value of only $\Delta n_s \approx 0,022$, being less than half of our initial estimate (5.14). Thus, the reduction of the Fermi-level $\mu - \mu'$ proves not to be greater than 0,11 eV.

Of larger interest however is the shift of the Fermi-level being related to the bottom of the d-band: In the ferromagnetic state, the bottom of the d-band is equal to the bottom of the $d \uparrow$ - sub-band. Let us designate by $\Delta\mu_{d\uparrow}$ the shift (towards the upper edge of the band). Then the quantity $\Delta\mu_{d\uparrow}$ can be determined, using the condition of equality of the hatched areas in Fig. 5.5b:

$$\Delta\mu_{d\uparrow} = \frac{g_1 \Delta \varepsilon_{exch}}{g_1 + g_2} \approx \frac{1}{3} \Delta \varepsilon_{exch} \approx 0,43 eV, \quad (5.15)$$

where the value $\Delta \varepsilon_{exch}$ has been taken from (5.14). A substantial difference among the values $\Delta\mu_{d\uparrow}$ and $\mu - \mu'$, namely the weak dependence on the relative shift of the s- and d-bands, (note that the shift $\Delta\mu_{d\uparrow}$ is mainly caused by re-distribution of electrons within the $d \downarrow \rightarrow d \uparrow$ sub-bands) as well as disappearing difficulties related to the selection of the origin of energy-reference, are arguments in support

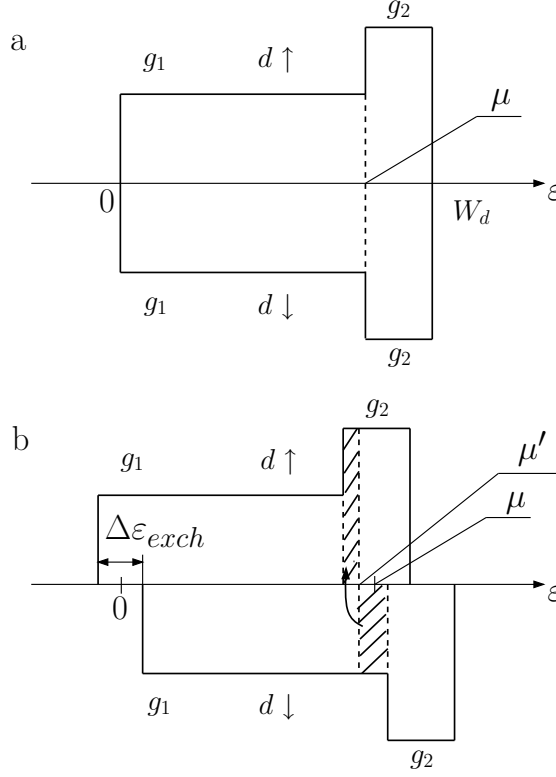


Figure 5.5. Modeled (single-peak) DOS-function of d-electrons, in the paramagnetic (a) and ferromagnetic (b) phase

of $\Delta\mu_{d\uparrow}$, when compared with the measurement conditions of the parameters $\Delta\mu_{d\uparrow}$ and $\mu - \mu'$. Obviously in our model, the heating process, being associated with the destruction of ferromagnetic ordering, will result in a relocation of the Fermi-level relative to the d-band, by about the same magnitude as (5.15), linked with a shift corresponding to the inverted electron overflow $d \uparrow \rightarrow d \downarrow$ ($d \rightarrow s$). These findings are in accordance with data presented in [220, 221], in which a relationship between the Fermi-level and the temperature of invar-alloys has been observed, during photo-electronic X-ray spectroscopy. During heat-up of two Fe-Ni-alloys with about 34,87 atom-% Ni and 35,8 atom-% Ni, from 100 K to 600 K, the shift $\Delta\mu_{d\uparrow}$ towards the bottom of the d-band was about 0,51 eV and 0,36 eV, respectively. Considering of the simplified character of our model, this correspondence of the measured values with our estimate by (5.15) appears fairly well.

We should however note here that, during magnetic ordering, the associated $s \rightarrow d$ redistribution of electrons must result in a reduction ΔC_l of the elastic modulus C_l , which, according to the Bohm-Staver-formula [192], is proportional to the ion-charge-number Z , while a variation of Z must correspond with the quantity $-\Delta n_s$. Thus obviously

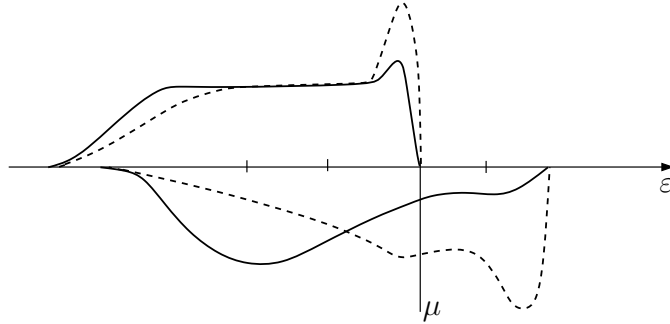


Figure 5.6. Contribution of iron - (dashed line) and nickel-atoms (solid line) to the single-peak DOS- function of the $Fe_{0,6}Ni_{0,4}$ - alloy [219]

$$\Delta C_l \approx \frac{\Delta Z}{Z} C_l,$$

and with $\Delta Z \approx -0,02$, $Z \approx 1$, we get $\Delta C_l \approx -0,02C_l$, being about 10% of the of the elastic modulus reduction¹ associated with the magnetic ordering process, as reported in [38].

Despite their low amount, the number Δn_s of electrons participating on the $s \rightarrow d$ - transition can be regarded as an informative parameter, due to the high sensitivity of the isomer-shift δ of the γ - nuclear resonance absorption-line, in conjunction with to the $s \rightarrow d$ - transition. In particular, the γ - resonance increases during $s \rightarrow d$ - transitions and decreases during $d \rightarrow s$ - transitions (see e.g. [222]). If we now use the relationship between the isomer-shift of Fe^{57} and the charge-density of the 3d- and 4s-electrons (see Fig.16 in [222]), in the configuration $3d^{8-z}4s^z$, for $Z \approx 1$, $\Delta Z \approx -\Delta n_s \approx -0,022$, then we can determine that the isomer-shift increases by $\Delta\delta \approx 6,4 \cdot 10^{-5}$ m/s. This estimate matches fairly well within the interval of $\Delta\delta = (0,6 \div 1) \cdot 10^{-4}$ m/s, as reported in [223] for the isomer-shift in $Fe - (28 \div 75)\%$ Ni-alloys during magnetic transitions (however a somewhat less $\Delta\delta = (4 \div 5) \cdot 10^{-5}$ m/s has been reported in [224], for Fe-33% Ni-alloys).

Single-peak DOS-models have successfully been developed for the fcc-lattice structure of Fe-Ni-alloys (see e.g. [219, 225, 226]). Using a realistic (nearly triangular) shape of the peak, the following characteristics of such DOS-functions were obtained, on the basis of a coherent-potential approximation:

- An appreciable difference among the DOS-functions for sub-bands $d \uparrow$ and $d \downarrow$, being evident in Fig. 2.9;
- Changes of the shape of the sub-band DOS-functions (in most cases, the shape of the $d \downarrow$ - band) will vary with the composition of the alloy;

¹The basic contribution to a softening of elastic modulus gives the redistribution of d-electrons. So e.g. at $\bar{\mu} = 1,7\mu_B$ from states with small density g_1 into states with major density $g_2 = 0,85$ electron/atom overflows. Then $\Delta Z/Z \approx \Delta C/C \approx -0,85/7$.

- Splitting of the DOS into partial contributions of Fe - and Ni - atoms. An example for this splitting, pertaining to the $Fe_{0,6}Ni_{0,4}$ - alloy, borrowed from [219], is shown in Fig. 5.6.

The relative success of the hard-zone model used for these estimates can mainly be deduced to the conservation of the shape of the $d \uparrow$ band for partial components of the iron- and nickel-atoms, as well as to the weakly pronounced variation of the DOS of the $d \downarrow$ band at the Fermi-level, with varying alloying composition. It has to be noted however that the considered mechanism of variation of the isomer-shift through $s \rightarrow d$ - overflow is limited to such Ni-concentrations starting from which the process of $d \downarrow \rightarrow d \uparrow$ - electron redistribution doesn't cause an appreciable downshift of the Fermi-level of the d-electrons subsystem. According to the data in [219], this particular concentration is about 40% Ni, thus the process of $s \rightarrow d$ - overflow can contribute the most part to $\Delta\delta$, within the region of concentration of our interest of 29 ÷ 34% Ni.

Our qualitative notion of these processes however deserves at least another remark, namely: Due to significant inhomogeneities of concentration and magnetic order (see e.g. [227,228]), the transition into a magnetic state of order is remarkably blurred. Thus, with decreasing temperature, the structure of an inhomogeneity can vary from a quasi-paramagnetic up to a chaotically-frozen spin distribution, akin to a spin-glass ([229]). According to [230,231], the cause of the emergence of a non-collinear magnetic structure is the blended character of exchange-interaction, being a common feature of many binary transition-metal alloys. For example, the exchange-integrals of pairs of Fe-Fe atoms in Fe-Ni - alloys are of negative sign, i.e. $J_{Fe-Fe} < 0$, and of Fe - Ni -, Ni - Ni- pairs, of positive sign, i.e. $J_{Fe-Ni} > 0$, $J_{Ni-Ni} > 0$. The notion of an anti-ferromagnetic character of the exchange interaction of Fe-Fe in iron and its alloys with fcc-lattice has for the first time been postulated in [232]. The values of exchange-interactions $J_{Fe-Fe} = -9$ meV, $J_{Fe-Ni} = 39$ meV, $J_{Ni-Ni} = 52$ meV, as determined in [233], are evidence in support of these concepts, i.e., below the Curie temperature T_c , strictly (collinear) magnetic structure not exists in the pre-martensitic austenite, thus the assumption of a ferromagnetic state of the fcc-austenite should only be regarded as a reasonable approximation.

During various neutron-spectroscopic investigations on austenitic Fe-Ni - invar alloys (see e.g. [234-236] and further references therein), there have been discovered super-structures of the γ' , γ'' , γ''' type. The first of them already appearing in the paramagnetic region $T > T_c > M_S$, the second one at $T \leq T_c$ ($T > M_S$), being linked up with the onset of ferromagnetic ordering, while the third one appears at $T \leq T_N$ (T_N - Neel-temperature, $T_N < M_S$) and reflects the onset of antiferromagnetic long-range ordering. We note that the γ'' -phase has been considered as an intermediate phase in [237, 238], thus ensuring the necessary symmetry-link between the γ - and the α - phases, which will finally lead to the Nishiyama orientational relationship of the γ - and α - phases.

Evidence of a rather complex nature of the magnetic transition is also given by

the results of [239] (more detailed see [240]), in which two different stages of the magnetic transition of austenite have been determined, in a temperatures range of $0,8 \leq T \cdot T_c^{-1} \leq 1$, on the basis of a very detailed analysis of the isomer-shift of Fe-Ni-alloys with (28, 5 ÷ 31, 3) wt.-% Ni. The first stage occurs in a temperature range of about 25 ÷ 30 K below T_c and is characterized by an increase of the isomer-shift of Fe^{57} nuclei in the ferromagnetic areas of the fcc-phase, by about $(\Delta\delta)_{fm} \approx 5 \cdot 10^{-5}$ m/s, while the δ -values of the paramagnetic areas remain unchanged, i.e. $(\Delta\delta)_{pm} = 0$. In the second stage, the isomer-shift decreases, exhibiting slightly larger incremental decreases of $(\Delta\delta)_{pm} \approx -6 \cdot 10^{-5}$ m/s in the paramagnetic areas than in the ferromagnetic areas, with $(\Delta\delta)_{fm} \approx -4,5 \cdot 10^{-5}$ m/s. The positive shift $(\Delta\delta)_{fm}$ in the first stage matches fairly well with the estimates of the shift $\Delta\delta$ being associated with $s \rightarrow d$ - electron overflow. However, experimental results reported in [239, 240], which aimed at an explanation of the particularities of the second stage of the magnetic transition, by relating them to the increases of hydrostatic pressure during formation of an "infinite" ferromagnetic cluster within the system, provided $\Delta\delta$ -values which would only correspond to an isomer-shift of about 15 to 20 % of the observed values. Thus it cannot be excluded that the missing (main) part of the observed effect is related to the processes of $d \rightarrow d$ - electron redistribution between iron- and nickel-atoms, being mainly caused by the significant relative differences among their affected spectral density regions, i.e. where the partial contributions of the iron- and nickel-atoms are largest. Thus for example it is obvious from Fig. 5.6 that the increase of exchange-splitting must lead to a reduction of the number of $d \downarrow$ - electrons of the iron-atoms, and to a corresponding increase for the nickel-atoms. This kind of $d \downarrow \rightarrow d \downarrow$ - electron redistribution among alloying components must result in a decrease of isomer-shift, as the decrease of the number of d-electrons of iron-atoms must elevate the charge-density of s-electrons at the nucleus [222]. Such minor effects however, as well as those of a possible polarization of quasi-paramagnetic areas, in conjunction with the formation of internal or external antiferromagnetic order (being put in relation with the ferromagnetic areas), will not deserve further consideration in our further analysis.

5.3.3 Oriented lattice-growth of athermal martensite in an externally applied magnetic field

The orientational effect of an externally applied magnetic field on the growth of martensite crystals mainly consists in a preferred orientation of the long axes of martensite crystals parallel to the magnetic field, as highlighted in [15, 241]. The conclusions in [242] on the orientational effect of a magnetic field had been drawn from investigations of the magnetic anisotropy of a specimen exposed to a magnetic field during and after a $\gamma - \alpha$ - MT. A thermodynamical analysis in [15] explains the predominance of small-angle orientations among martensite-lamellae in cubic crystals, mainly by attributing them to the minimization effect on the

magnetic field energy contribution to the thermodynamic potential, being closely related to the proper magnetic field produced by the magnetic spin-moments of electrons in the ferromagnetic α - phase. As commonly known for the specific case of an ellipsoidal magnetic specimen, this energy resembles a quadratic function of all magnetization-components, the coefficients of which being proportional to the components of the demagnetization-tensor. For small-angle orientations, the proper magnetic energy is proportional to the square of magnetization and to the least of the three eigenvalues of the demagnetization-tensor, being many times less than 1 for small slices (lamellae). And vice-versa, for lamellae with large-angle orientation, the demagnetization factor is of an order of magnitude of 1, thus its contribution by proper magnetic energy becomes largest. It has however to be considered that the orientational influence of the demagnetization-fields, as well as that of magnetic anisotropy, on the growth of martensite crystals not exceeding $8 \cdot 10^5$ A/m $\sim 10^4$ Oe, dwindles with increasing externally applied magnetic field strength, finally disappearing for magnetic fields of $H \geq 10^7$ A/m $\sim 10^5$ Oe [209]. Within this context, in case of strong magnetic fields, those factors which increase with increasing external magnetic field can come to the fore. Among them, there is the non-equilibrium addend to the electronic distribution function.

Let us assume that the athermal martensitic transformation would only be related with those electronic states being localized in the proximity of the $S_{\langle 001 \rangle}$ surfaces (see Pt. 5.3.1). Thus we shall consider the effect of a magnetic field \mathbf{H} on the non-equilibrium addend $f - f^0$ of the electronic distribution function f^0 . In accordance with [243], we can use the following approximation, being linear in \mathbf{H} :

$$f - f^0 = -\Phi' \frac{\partial f^0}{\partial \varepsilon}, \quad (5.16)$$

$$\Phi' = (\tau \mathbf{P}, \mathbf{v}) + \frac{e\tau}{c_0 \hbar} (\mathbf{H}, [\mathbf{v}, \vec{\nabla}]) (\tau \mathbf{P}, \mathbf{v}),$$

where e - electron charge; τ - average free path time of existence of an electron; c_0 - speed of light; $\vec{\nabla}$ - gradient-operator in \mathbf{k} - space, while the explicit form of the vector \mathbf{P} , including the temperature-, chemical and electrical potential-gradients, not being worth to be considered in our further analysis.

We shall further confine our analysis to the calculus of the contribution of non-equilibrium addends to the electronic distribution functions, related to states in the proximity of the reduced 1st face of the $S_{[001]}$ surface, which in this case corresponds with the square-shaped border of the 1st BZ. In our calculus of the group-velocity \mathbf{v} and its derivatives, it will be justified to use a dispersion law in the tight binding approximation, which considers fairly satisfactory the particularities of the electronic energy spectrum within a weakly dispersed band, being enumerated by X_5 on sheet Nr.1. For example, we can obtain from (2.16) $\varepsilon = 4\varepsilon_1 = \text{const}$ along the line X_5W (weak dispersion will only appear after consideration of the resonance-transition integrals with the second neighbor). Let $\mathbf{H} \parallel [001]$ and assume

that the predominant contribution to the rate of change with \mathbf{k} under the numeral of $\vec{\nabla}_{\mathbf{k}}$ brings in \mathbf{v} , then we get from (2.16) and (5.16):

$$\Phi' - (\tau \mathbf{P}, \mathbf{v}) = \frac{2 e \tau^2 \varepsilon_1^2 a^3}{c_0 \hbar^3} H (J_x + J_y + J_z), \quad (5.17)$$

$$\begin{aligned} J_x &= \sin x (\cos x + \cos z) (1 + \cos z \cos y) P_y, \\ J_y &= -\sin y (\cos y + \cos z) (1 + \cos z \cos x) P_x, \end{aligned} \quad (5.18)$$

$$\begin{aligned} J_z &= \sin z \sin x \sin y (\cos x - \cos y) P_z, \\ v_x &= 2 \varepsilon_1 a \hbar^{-1} \sin x (\cos y + \cos z), \\ v_y &= 2 \varepsilon_1 a \hbar^{-1} \sin y (\cos x + \cos z), \\ v_z &= 2 \varepsilon_1 a \hbar^{-1} \sin z (\cos x + \cos y). \end{aligned} \quad (5.19)$$

In (5.18), (5.19) we used instead of the designations η_1, η_2, η_3 in (2.16) the designations x, y, z , without index. During U-processes among states in the proximity of the sheets Nr. 1, the velocity component oriented normal to sheets Nr. 1 inverts its sign (the $V_{x,y,z}$ in (5.19) include odd sine-functions), and the differences of the non-equilibrium terms $\sim (\tau \mathbf{P}, \mathbf{v})$ will sum up, which, in effect, leads to maximum inverted occupational difference (IOD) for ES-pairs. As a result of (5.18), the field-terms containing the J_x, J_y and also deliver an additional contribution to the IOD, being related to ES - pairs located in the proximity of the sheets Nr. 1 with normals [100] and [010], have the same characteristics. The term $\sim J_z$ however is odd with respect to the inversion $x \leftrightarrow y$, Therefore, ES - pairs near sheet Nr. 1 with normal [001] do not contribute to IOD as J_z is integrated in the region which is symmetric with relation to the $x \leftrightarrow y$ inversion. Within usual definitions, this behavior of the field-supplements reflects transversal thermo-magnetic and galvano-magnetic effects. As a result, a field $\mathbf{H} \parallel [001]$ will support the generation of waves with \mathbf{q} near [100] and [010]. Thus, in accordance with the two-wave pattern, there can be expected habits $\{\underline{l} \ k \ \underline{h}\}$, whose smallest angle with \mathbf{H} will be ($|\underline{l}| > |k| > |\underline{h}|$), where the underlined indices mark their position being fixed, i.e.; $\{\underline{l} \ k \ \underline{h}\} - (l \ k \ h), (k \ l \ h), (k \ l \ \bar{h}) \dots$ Accordingly, $\{\underline{l} \ h \ \underline{k}\}$ and $\{h \ k \ \underline{l}\}$ represent the totalities of the medium- and large angle habits. For $\mathbf{H} \parallel \langle 111 \rangle$, this orientational effect must vanish. This latter conclusion is important in order to clarify the causes of the observed orientations, as there also exist thermodynamical reasoning [15] in favor of the small-angled orientation of the first martensite lamellae, being independent of the orientation of \mathbf{H} . The lack of an appreciable orientation at $\mathbf{H} \parallel \langle 111 \rangle$, in relation to $\mathbf{H} \parallel [001]$, would imply that the dynamic mechanism plays a decisive role. Of course, the effect of \mathbf{H} on the generation of lattice-displacement waves becomes appreciable as soon as the magnitude of field-supplement becomes comparable with the initial supplement $(\tau \mathbf{P}, \mathbf{v})$. It is however more convenient to average the supplemental terms when performing such comparison, by integrating the expressions (5.17) and (5.18) over those areas being parallel to faces Nr. 1. Then their ratio will be

$$\psi \approx \frac{e \tau a^2 \varepsilon_1}{5 c_0 \hbar^2} \frac{P_y}{P_x} H. \quad (5.20)$$

For $P_y \approx P_x$, $\tau \sim 10^{-12}$ s, $a = 3,5 \cdot 10^{-10}$ m, $\varepsilon_1 = 5 \cdot 10^{-20}$ J (corresponding to the width of the band $\Delta\varepsilon = 16\varepsilon_1 = 5$ eV), $H = 8 \cdot 10^6$ A/m $\sim 10^5$ Oe (being typical experimental results published in [15]), we get from (5.20) $\psi \approx 0,2$. Thus the field-supplement is a non-negligible quantity.

It has however to be emphasized here that the conclusion related to the transversal character of the thermo- and galvano-magnetic effects at $\mathbf{H} \parallel [001]$, having been drawn during our previous consideration of the electronic states in the proximity of the $S_{\langle 001 \rangle}$ surfaces, will remain valid during an analysis of the non-equilibrium terms for states in the proximity of the curved sheets Nr. 2 of surfaces $S_{\langle 001 \rangle}$. To convince oneself, it will suffice to recall the definition (2.11) of a S-surface, taking into consideration that the vector $[\mathbf{v}, \vec{\nabla}]$ appearing in the field-supplement (5.16) is perpendicular to \mathbf{v} . Consequently, the scalar product $(\mathbf{H}, [\mathbf{v}, \vec{\nabla}])$ vanishes for $\mathbf{v} \parallel \mathbf{H}$ attaining a maximum for $\mathbf{v} \perp \mathbf{H}$. This means that our conclusion of the preference of small-angled orientations of martensite lamellae for $\mathbf{H} \parallel [001]$ also applies for the field supplements to the electronic distribution function f in the proximity of sheets Nr. 2 of the $S_{\langle 001 \rangle}$ surfaces, thus being a general conclusion.

In the case of magnetically ordered austenite, the local field-induction vector has to be used instead of vector \mathbf{H} and also the effect of magnetostriction has to be taken into account as the emerging lattice deformations can modify the orientational effect. At $\mathbf{H} \parallel [001]$ and for a magnetostrictive constant of $\lambda_{100} < 0$ there will be produced compressive stress in the orientation $[001]$ and, in the orientations $[100]$, $[010]$ equal magnitudes of tensile strains (see §2, Chap. 23 in [159]). Considering the rule of matching between the compressive and tensile axes and the habit planes indices, as discussed in Pt. 5.1.4, then there can also be expected medium-angled $\{l \ h \ \underline{k}\}$ habits, in addition to the small-angled $\{l \ k \ \underline{h}\}$ habits. It is worth to note that if \mathbf{H} is oriented near $[001]$, so that a larger dilatation along one of the transversal axes is ensured, e.g. along $[010]$, then the emergence of $\{k \ \underline{l} \ \underline{h}\}$ and $\{h \ \underline{l} \ \underline{k}\}$, with two fixed indices positions will be most likely for the small- and medium-angled habits. For $\lambda_{100} > 0$ (i.e. dilatation along $[001]$), also large-angled habits $\{h \ k \ \underline{l}\}$ must arise, apart from the small-angled habits.

We emphasize that the above orientational effect of an externally applied magnetic field can be discriminated with satisfactory reliability from orientational effects related to uni-axial elastic stress (like that produced by magnetostriction or by externally applied stress), which would result in the appearance of medium-angled (for compressive stress) and large angled (for tensile stress) orientations of the lamellae in athermal martensite.

In sufficiently strong magnetic fields, the contribution of a non-equilibrium electronic field-supplement to the orientational effect, which would have to become more pronounced with increasing \mathbf{H} , can be discriminated from the background

of statical orientational effects are caused by the existence of demagnetization- and anisotropy magnetic fields, the general impact of which will decrease with increasing \mathbf{H} .

In [244], the predominance of small-angled orientations of martensitic lamellae has been reported, based on reproducible experiments with samples of 50X2H22, 77X2H22 steel, being characterized by low autocatalysis of the $\gamma - \alpha$ - transformation, both in magnetic field bursts and in constant field conditions. In these cases, the orientational relationship is most pronounced if \mathbf{H} is oriented parallel to the $\langle 001 \rangle$ -axes. This matches fairly well with our above prediction drawn from our analysis of the effect of the non-equilibrium field supplement. Characteristic of this effect is that an increase of \mathbf{H} over a critical magnitude of $\mathbf{H}_c = 1,1 \cdot 10^7$ A/m (related to the steel 50X2H22, where \mathbf{H}_c is the magnetic field for which, at a given temperature $T_{exp} = 203$ K, the first martensite crystals emerge, i.e. $T_{exp} - M_S \approx 100$ K) results in an increase of the orientational effect, if $\mathbf{H} \parallel [001]$. Similar results were obtained for the steel 77X2H22 (at $T_{exp} = 77$ K, with a critical field $H_c \approx 8,76 \cdot 10^6$ A/m). Unfortunately, the results reported in [244], pertaining to $\mathbf{H} \parallel \langle 111 \rangle$, only relate to the specific case $\mathbf{H} = \mathbf{H}_c$, thus the dependence of the orientational relationship on the magnetic field strength \mathbf{H} has not been investigated. In accordance with the above considerations, it can also be concluded that in the special case of $\mathbf{H} \parallel \langle 111 \rangle$ an increase of \mathbf{H} must lead to a reduction of the orientational effect. In general, the results presented in [244] give evidence in support of our findings based on the notion of the control of the growth process of athermal martensite by longitudinal waves propagating near the $\langle 001 \rangle$ directions and, accordingly, also on the dominating role of the electronic states being localized near the $S_{\langle 001 \rangle}$ surfaces.

5.4 Summary of chapter 5

Following our interpretation of the morphological characteristics of martensite within the notion of a two-wave pattern, the main conclusions that we can draw here are:

1. The habits of the Fe-Ni- and Fe-C-systems can be associated with a two-wave pattern, where one of the waves, belonging to the longitudinal type, propagates in the $\langle 001 \rangle$ direction, while the second wave is of a quasi-longitudinal type, which can be determined on the basis of experimental data of elastic-moduli at a given temperature M_S .
2. The habits near $\{557\}$ and $\{225\}$ are characterized by the pairs of waves propagating near the perpendicular axes of symmetry of the fourth and second order $\langle 110 \rangle$, $\langle 001 \rangle$. By means of the criterion discriminating the most favorable conditions for materialization of habits $\{557\}$: $\varkappa = c_{\Sigma} c_{\Delta}^{-1} < \varkappa_c$

and $\{225\}$: $\varkappa = c_{\Sigma}c_{\Delta}^{-1} > \varkappa_c$ enables us, in principle, to explain the default of habit $\{225\}$ in Fe-Ni-systems.

3. The habits near $\{259\}$, $\{3\ 10\ 15\}$ are only associated with those waves propagating near the fourth-order axes of symmetry. Possible causes for the passivation of electronic states (located near the surfaces $S_{\langle 110 \rangle}$), being associated with wave-generation in the $\langle 110 \rangle$ - direction, can be the anisotropy of s-d-scattering processes and differences of the parameter $\varepsilon_d - \mu$, depending on the size of lattice-parameters as well as on the magnetic state of austenite.
4. The large-scale growth process of martensite is being controlled by long displacement waves, acting in coordination with short displacement waves which form the fine structure. It is possible e.g. to describe the formation of a twinning-plane $\{110\}$ analogous to that of a habit plane, in such a way that a twinning-plane resembles the imprinted path of the moving line of intersection of a pair of perpendicular short-wave fronts, including the pairs of waves propagating perpendicular to $\langle 001 \rangle$. This of course does not impede the description of the transformation of small areas within the concept of stationary waves, as short-wave displacements can perform a multitude of oscillations within half a period of the long-wave oscillations, whenever favorable transformation conditions materialize, thereby enabling the lattice to perform the transformation under optimized conditions. The oscillation period can easily be estimated if one considers that the widths of the macro- and micro-lamellae of the twins is within the order of magnitude of half of a wave-length each of the long and the short displacements.

Of course, the general possibility of twinning being driven by the need for periodic discharge of accumulated elastic strain energy, through lattice rearrangement, is no contradiction to our two-wave lattice control pattern, which only emphasizes the main component.

On the other hand, the long-wave displacements, featuring a slower rate of decay than short-wave displacements, are effective carriers of information controlling the transformation of various regions of the specimen. Long-wave displacements thus can attain a leading role in the formation of crystal ensembles.

5. The knowledge of phase-relationships characterizing atomic displacements being most favorable for the initiation of the martensitic transformation by waves enables us to define rules related to the comparison of habits with the directions of compressive and tensile stresses of the Bain-deformation (based on a stereographic projection) (see end of Pt. 5.1.4). Using these rules it is easily possible, among other things, to determine the predominant orientation of martensite crystals, based on an orientational relationship with the unidirectional elastic stress field arising at temperatures above the M_S - temperature.

6. The rules derived from observations on packet-martensite are in accordance with the conceptual view of martensite growth in which growth is controlled by pairs of elasto-plastic waves. Within this notion, the deviations of the habit planes of lath-crystals from the relevant pairs of Miller-indices, resulting in unequivocal orientation of martensite lamellae, can be put in relation with the orientational deviations from the $\{1\bar{1}0\}$ planes of the waves propagating near the $\langle 110 \rangle$ axes.
7. The new mechanism of controlled lattice growth of athermal martensite within an externally applied magnetic field, having been predicted after an analysis of the non-equilibrium field-supplement to the electronic distribution function, is confirmed by experimental analysis on the morphology of ensembles of martensitic mono-crystals, emerging within the austenitic single-crystals when being subjected to the orientational action of an external magnetic field.

Some additional remarks

1. The simple formalism establishing a link between the habit-plane and a given pair of waves can be used for a phenomenological analysis of the involved longitudinal and transversal waves, independently of causes and conditions of their emergence, like generation under non-equilibrium conditions, local lattice deformation associated with the nucleation of phases, or even excitation by external sources. To take an example reported in [90], experiments have been performed which aimed at an interpretation of habits of the type $\{h\ h\ l\}$, being observable during the $\beta \rightarrow \gamma', \beta''$ - martensitic transformation of copper and gold based alloys [245], using a combined transversal and longitudinal two-wave pattern.
2. An experimental verification of the relationship between a two-wave pattern and the habits must, in the first step, comprise the determination of the \varkappa - parameters for a given pairs of waves at M_S , as well as the selection of the preferable parameters. Of course it suggests itself to confine our measurements to those velocities of sound (for cubic crystals, at the orientations Δ, Σ, Λ) being sufficient for determination of the elastic moduli. This will then enable us to calculate \varkappa for any given pair of waves. In the second step, it will be possible, by means of a pair of external hypersound generators ($\nu \sim 10^9 \div 10^{10} \text{ s}^{-1}$), to excite the selected pair of waves in the single crystal. This would raise, during a crystallographic analysis, the probability for discovery of a habit-plane (already being known at the outset). It should be noted here that the knowledge on the orientations of propagation and the types of the waves which materialize a thermodynamically relatively stable habit, should make it possible to perform such experiments even with low-power generators. Moreover, using high-power generators, it should be

possible to achieve habits not occurring under natural conditions, in a given type of crystal. For example, a habit (225) in the Fe-Ni-system. Most promising would be an experiment for the case of a parameter \varkappa being close to the critical value \varkappa_c . This way, using a predetermined orientation of \mathbf{c}_1 , e.g. $\mathbf{c}_1 \parallel [00\bar{1}]$, it should be possible to materialize the cases shown in Table 5.3, simply by varying the orientation of \mathbf{c}_2 .

Table 5.3. Miller-Indices of some habit-planes formed by a pair of waves, for a variety of orientations of the second wave velocity \mathbf{c}_2 ($\mathbf{c}_1 \parallel [00\bar{1}]$)

Orientation of \mathbf{c}_2	η	Habit
$[1 + \eta_1, 1 - \eta_2, \eta]$	$- \eta_c \leq \eta < 0$	$(5 + \delta_1, 5 - \delta_2, 7)$
$[1 - \eta_1, 1 + \eta_2, \eta]$		$(5 - \delta_1, 5 + \delta_2, 7)$
$[1 + \eta_1, 1 - \eta_2, \eta]$	$0 < \eta \leq \eta_c $	$(2 + \delta_1, 2 - \delta_2, 5)$
$[1 - \eta_1, 1 + \eta_2, \eta]$		$(2 - \delta_1, 2 + \delta_2, 5)$

A large variety of possibilities for exertion of direct influence on directed generation and growth of martensitic structures in austenitic single crystals is opened up by the combined application of magnetic, hypersound and conventional treatment. We also want to point at future potential for development of methods with two or three sources of ultrasound aiming at direct control of the direction of crystallization immediately out of the melting (upon cooling) and in the amorphous condition (upon heating), while these methods can be of interest both for stationary as well as for moving waves. In the latter case, it should be possible e.g. to produce of a chessboard-pattern structure with alternating amorphous and crystalline regions, by usage of two external sources of perpendicular waves.

3. The attractiveness of the two-wave pattern is mainly due to its potential to materially demonstrate the possibility of flexible behavior of a dynamic system, still being able to preserve the conditions for realization of thermodynamically favorable phase-coupling, in spite of variations of key parameters (in our case $\varkappa_e(0)$). The materialization e.g. of habit (557) could thus be attained due to the increasing deviation of the orientation of the velocity vector \mathbf{c}_2 from the direction $\langle 110 \rangle$, occurring coincidentally with an increase of the parameter $\varkappa_e(0)$. As the energy being released during the transformation serves as the source of a non-equilibrium, those waves producing the most favorable conditions of generation (as needed for preservation of temperature- and chemical potential gradient) will develop and predominate. Due to the continuous feedback effect, the system will enter into a condition enabling it to flexibly follow and adapt itself to the most favorable thermodynamical path, on the one hand, by its ability to tune the spectrum of generated waves

(i.e. mode selection), and on the other hand, to select various velocities \mathbf{c}_2 out from an orientational cone around the $\langle 110 \rangle$ axis. Obviously, this point of view is free of contradictions with general thermodynamical reasoning and broadens them by an image of transformation dynamics.

4. Within the approach combining martensite growth with wave generation by non-equilibrium electrons, it is obvious that the conceptual view of nuclear growth can be complemented by means of a soliton-like description of the motion of the phase-boundary, as the conditions required for their generation (i.e. temperature- and chemical potential gradients) exist in the proximity of the boundary.

The most important results relating to an interpretation of morphological characteristics of martensite, within the frame of a wave-pattern, have been published in [99], [56], [246–248]. The re-distribution of electrons during the development of ferromagnetic ordering within a single-peak DOS environment is discussed in [216, 217], the results of which were used in [124].

Chapter 6

Wave-model of motion for a martensitic lattice boundary

The wave model under development for reconstructive martensitic transformations is essentially based on the conceptual view of the stage of growth of the new phase as a lattice deformation propagating in a wave-mode. As already discussed in Chap. 1, there exists sufficient experimental evidence for a metastable condition in the lattice of the pre-martensitic γ - phase at M_S temperature. This means the transition into the new lattice structure is inevitably associated with the need to overcome the interfacial energy barrier, for any degree of supercooling, only becoming possible if the magnitude of lattice deformation ε exceeds a given threshold value $\varepsilon_{th}(M_S)$. In our wave-model, we got $\varepsilon = 4u\lambda^{-1}$, where u - wave-amplitude and λ - wavelength, further assuming $\varepsilon_{th}(M_S) \sim 10^{-3}$.

Under a condition of strongly pronounced supercooling, the transformation of the austenitic lattice is associated with release of transformation heat and with a sudden (jump-like) increase of volume. From the outset, the emerging martensite crystal exerts a thermal, electrical and mechanical influence on the interfacial region $B_{\gamma-\alpha}$ between the phases, thereby causing a deviation of the local thermodynamic state from equilibrium conditions. Under such non-equilibrium conditions, amplification of atomic oscillations is generally possible, through the generation and selective amplification of displacement-waves by means of non-equilibrium electrons (i.e. instability of lattice oscillations by phonon-maser action). The displacement waves in turn ensure a lattice-deformation close to threshold-deformation. With regard to the aforementioned, it is obvious to consider the non-equilibrium region $B_{\gamma-\alpha}$ as an active and highly excited medium, being capable to generate, preserve and amplify cooperative waves, which in turn induce a transition at $\varepsilon \sim \varepsilon_{th}(M_S)$. This way the phonon-maser effect can be defined as an effect based on positive feedback, by conversion of a fraction of the released transformation energy into the energy of displacement waves. Further surmising that these waves in turn ensure the overcoming of the energetic barrier, then it is conclusive to interpret martensitic lattice growth as a self-sustaining

wave-like process, during which the transforming $B_{\gamma-\alpha}$ region propagates in conjunction with lattice displacement waves.

6.1 Coordinated propagation of a displacement-wave with a switching-wave of chemical potential or temperature

We designate in general by a vector \mathbf{u} the displacement of atoms participating on an arbitrary wave motion in a non-transformed lattice area. Let us further theorize that the wave is longitudinal with wave-length $\lambda = 2\pi/q \gg a$, where a - lattice-parameter; q - modulus of the wave-vector \mathbf{q} . Then, in a continuous lattice model, we can express the equations of motion for displacements \mathbf{u} in the following way, using a frame of reference where the x-axis is collinear to \mathbf{u} :

$$\ddot{u} - c^2 u''_{xx} = \chi c u'_x, \quad (6.1)$$

$$\chi = -\varkappa_{\mathbf{q}} \left\{ 1 - \frac{\sigma_0}{\sigma_{th}} \left[1 + \frac{G_e^2 t_\sigma}{\hbar^2 \Gamma_e} (u'^2_x + q^2 u^2) \right]^{-1} \right\}. \quad (6.2)$$

Here, c - velocity of sound; $\varkappa_{\mathbf{q}}$ - wave-extinction without phonon-generation; t_σ - period for emergence of an occupational inversion σ_0 ; σ_{th} - threshold-inversion; Γ_e - extinction of electrons active during generation; G_e - resonance overlap integral, which determines the width of an electronic band in tight binding approximation. Eq. (6.1) can most easily be derived by confining our consideration of phonon generation to single-mode (related to the case of perfect resonance) and to adiabatic approximation, leading to Eq. (3.49) for slowly varying phonon-field amplitudes $\tilde{b}_{\mathbf{q}}^+$, $\tilde{b}_{\mathbf{q}}$. The expression of effective extinction (6.2) is the same as in (3.49). The transition to expression (6.2) can easily be performed by insertion of the explicit form (2.4) of matrix-element W_1 in (3.49), using the relations

$$\begin{aligned} \tilde{b}_{\mathbf{q}}^+ &\approx \left[\frac{M N \omega_{\mathbf{q}}}{2 \hbar} \right]^{\frac{1}{2}} \exp[-i(\omega_{\mathbf{q}} t - q x)] \left(\frac{\dot{u}}{i \omega_{\mathbf{q}}} + u \right), \\ \tilde{b}_{\mathbf{q}} &\approx \left[\frac{M N \omega_{\mathbf{q}}}{2 \hbar} \right]^{\frac{1}{2}} \exp[i(\omega_{\mathbf{q}} t - q x)] \left(u - \frac{\dot{u}}{i \omega_{\mathbf{q}}} \right), \\ \frac{\partial u}{\partial t} &\equiv \dot{u} \approx -c u'_x \end{aligned}$$

for the transformation of $\tilde{b}_{\mathbf{q}}^+$, $\tilde{b}_{\mathbf{q}}$ in (3.49).

Eq. (6.1) can be resolved, provided the class of relationship among the parameters appearing therein and the parameters x and t can be substantiated. Most important is the relationship $\sigma_0 = \sigma_0(x, t)$, whereas the relationships of the remaining parameters ($c, \varkappa_{\mathbf{q}}, \sigma_{th}, t_\sigma, \Gamma_e, G_e$) with x and t is more or less irrelevant and can thus be ignored, without introducing any significant error. According to (3.23), (3.24), the quantity $\sigma_0(x, t)$ implicitly also depends on local temperature T ,

chemical potential μ and on their local gradients. Assuming steady motion of the phase-boundary with a velocity $\mathbf{V} \sim \mathbf{c}$, then it suggests itself to describe temperature and chemical potential by means of "solitary fronts" which propagate with the velocity of sound: i.e. switching-waves (see e.g. [80, 249]). Thus the frontal width l of such a switching wave practically determines the thickness of the transforming region $B_{\gamma-\alpha}$, being characterized by highly pronounced gradients ∇T , $\nabla \mu$, which in turn satisfy the threshold-conditions $D_0 \equiv \sigma_0 \sigma_{thM}^{-1} - 1 > 0$ for phonon generation. Taking this into proper consideration, we can assume $\sigma_0 = \sigma_0(x-Vt)$. As the amplification of a displacement-wave only is possible within the region of $B_{\gamma-\alpha}$, propagating at velocity V , a coordinated propagation of stationary switching waves and displacement waves can only be realized if $V = c$. Taking this for granted, then we can search the solution of Eq. (6.1) in form of expression

$$u = u(x - ct) \equiv u(\xi). \quad (6.3)$$

After insertion of (6.3) in (6.1) we get a set of equations

$$\frac{\partial u}{\partial \xi} = 0, \quad \left(\frac{\partial u}{\partial \xi} \right)^2 + q^2 u^2 - \frac{D_0(\xi)}{\beta_0} = 0, \quad (6.4)$$

where $\beta_0 = \hbar^{-2} G_e^2 t_\sigma \Gamma_e^{-1}$. The first equation in (6.4) delivers a trivial solution, not matching with our expected spatially inhomogeneous distribution of local displacement at the starting moment. Solutions of the second equation of (6.4) only exist for $D_0 \geq 0$, i.e. in the $B_{\gamma-\alpha}$ region. If we characterize the region of $B_{\gamma-\alpha}$ by means of inequalities $-l \leq \xi \leq 0$, further assuming that T and μ linearly depend on ξ - within the $B_{\gamma-\alpha}$ region - then we can use the following expression for D_0

$$D_0(\xi) = \begin{cases} const_1 \geq 0, & \xi \in [-l, 0]; \\ const_2 < 0, & \xi \notin [-l, 0]. \end{cases} \quad (6.5)$$

Thus the solution of the second equation in (6.4), being confined to the region $B_{\gamma-\alpha}$, will look as follows:

$$u(\xi) = \frac{1}{q} \left[\frac{D_0(\xi)}{\beta_0} \right]^{\frac{1}{2}} \sin(q \xi + \varphi). \quad (6.6)$$

The value of the phase-term φ in (6.6) can be determined from the additional conditions imposed on u at the starting moment $t = 0$, at the boundaries of the segment $[-l, 0]$.

Solution (6.6) is based on the requirement of equality of the velocities of the displacement-wave and of the switching-waves for T and μ . Within this context it is reasonable to discuss here the limitations imposed on our model-parameters by the above requirement. According to [80], a switching-wave can be defined by a non-linear equation of the diffusion-type:

$$\dot{\psi} = F(\psi) + d \psi''_{xx}, \quad (6.7)$$

where d - diffusion coefficient, ψ - dimensionless variable of the type $\psi = \psi_T = (T - T_\gamma)/(T_\alpha - T_\gamma)$, or $\psi = \psi_\mu = (\mu - \mu_\gamma)/(\mu_\alpha - \mu_\gamma)$ and $F(\psi)$ - non-linear function. Assuming that $F(\psi) \geq 0$ and Eq. $F(\psi) = 0$ only has two solutions, namely $\psi = 0$ and $\psi = 1$, corresponding to the values of ψ in the γ - and α - phases, then we get for velocity V [80]:

$$2(d F'_\psi(0))^{1/2} = 2 \left(d \frac{dF}{d\psi} \Big|_{\psi=0} \right)^{1/2} \equiv V_{\min} \leq V. \quad (6.8)$$

In accordance with (6.8) the equality $V = c$ is possible for $V_{\min} \leq c$. We estimate V_{\min} by assuming that $V_{\min} \neq 0$. For it, $F(\psi)$ must be materialized. A function $F(\psi)$, being compatible with the conditions $F(0) = F(1) = 0$, $F'_\psi(0) \neq 0$, can always be expressed in the form

$$F = \tau^{-1} \psi (1 - v(\psi)), \quad (6.9)$$

where $v(\psi) = 1$ only for $\psi = 1$ and $v(0) = 0$, τ - constant with temporal dimension. It follows from (6.9), that $F'_\psi(0) = \tau^{-1}$ and $V_{\min} = 2(d/\tau)^{1/2}$:

$$V_{\min} = 2 \left(\frac{d_{T,\mu}}{\tau} \right)^{1/2}. \quad (6.10)$$

In the case of a temperature-wave (T-wave) the coefficient $d \equiv d_T$ is the temperature- conductivity ($d_T \sim 10^{-5} \text{ m}^2\text{s}^{-1}$ for iron-alloys). In the case of chemical potential (μ - wave), the coefficient $d \equiv d_\mu$ can be determined in accordance with (3.46) by means of the specific conductivity σ_γ in the form of

$$d_\mu = \frac{2 \sigma_\gamma \mu_\gamma}{3 e^2 n_\gamma} \quad \text{and} \quad d_\mu \sim 4 \cdot 10^{-4} \text{ m}^2/\text{s}.$$

Let us come back to the condition $V = V_{\min} = c$ and estimate τ from (6.10) for $c = 5 \cdot 10^3 \text{ m/s}$. This delivers $\tau \equiv \tau_T \sim 2 \cdot 10^{-12} \text{ s}$, $\tau \equiv \tau_\mu \sim 6 \cdot 10^{-11} \text{ s}$. Using a linear approximation for the profile of the frontal region of the switching wave, we get for l the following relationship with τ , using the condition $V_{\min} = c$: $l = A \tau c$, where A - a figure not larger than a few units, depending on the form of expression $v(\psi)$ in (6.9). For $v(\psi) = \psi$, e.g., we have $A = 4$, according to [249], thus $l = l_T \sim 4 \cdot 10^{-8} \text{ m}$ or $l = l_\mu \sim 10^{-6} \text{ m}$, respectively. Taking into account that the optimum size of the region being deformed by the displacement-wave corresponds to $\lambda/2$ in the wave model, then we can assess the minimum value q in (6.6) using the relation $l \sim \lambda/2 = \pi/q$: $q = q_T \sim 10^{-2} \pi/a$ for $l = l_T$ and $q = q_\mu \sim (10^{-4} \div 10^{-3}) \pi/a$ at $l = l_\mu$.

Strictly speaking, expression (6.5), when used for resolving (6.4), would require the following form of the function ψ :

$$\psi = \theta(-\eta - 1) - \eta [\theta(\eta + 1) - \theta(\eta)], \quad (6.11)$$

$$\eta = \frac{(x - ct)}{l} \equiv \frac{\xi}{l},$$

which will only be satisfied after replacement of expression (6.9) for $F(\psi)$ by a rectangularly shaped pulse-function:

$$F(\psi) = \frac{1}{\tau} \theta(\psi) \theta(1 - \psi). \quad (6.12)$$

In (6.11), (6.12) the function θ - Heaviside unit-function:

$$\theta(\psi) = \begin{cases} 1, & \psi > 0, \\ 0, & \psi < 0. \end{cases}$$

Such an approximation of the wave profile and of $F(\psi)$ should be fully satisfactory for a qualitative consideration, after having determined the speed of propagation of the switching-wave.

6.2 Coordinated propagation of a pair of displacement-waves with the switching-wave of $T(\mu)$

Let us extend the results of Pt. 6.1 to the case of a pair of longitudinal waves propagating with the velocities \mathbf{c}_1 and \mathbf{c}_2 in non-collinear directions of axes x_1 and x_2 , in that we surmise, as done in Chapter 5, that the formation of a martensite lamellae of thickness $\sim \lambda_1, \sim \lambda_2$ ($\lambda_{1,2}$ - wave lengths) is performed by the association of the areas subjected to synchronized tensile and compressive stress, the main axes of which being oriented parallel to x_1 and x_2 , respectively. If we start our conceptual view with a pair of waves of type (6.6), featuring infinite flat fronts, it will be obvious that the specific region in which the combination of tensile and compressive stress being required for a martensitic transformation (also combined with the release of transformation energy) is granted, is identical with the region of wave-imposition, propagating in the same direction and with the same velocity $\mathbf{c} = \mathbf{c}_1 + \mathbf{c}_2$ (if $\mathbf{c}_1 \perp \mathbf{c}_2$), that is the line of intersection of the (perpendicular) wave fronts. Consequently, the stationary wave pattern must correspond with the region $B_{\gamma-\alpha}$ bound in both x_1 and x_2 directions and moving with velocity \mathbf{c} . In other words, a stationary propagation of the pair of displacement-waves in cooperation with the switching wave is feasible, if the latter one propagates with a velocity \mathbf{V}

$= \mathbf{c} = \mathbf{c}_1 + \mathbf{c}_2$. This also means that, in the case of a displacement-wave, the requirement $\mathbf{V} = \mathbf{c}$ is to be replaced by the requirement $V_{x_1} = c_1, V_{x_2} = c_2$. Within our following considerations, the actual orientation of the axes x_1 and x_2 will be of no fundamental importance. Thus we shall further on consider $x_1 \perp x_2$. With consideration of (6.6) it is possible to note the expression for the displacements u_i , with $i = x_1, x_2$ in the form

$$u_i = \frac{1}{q_i} \left[\frac{D_{0i}}{\beta_{0i}} \right]^{\frac{1}{2}} \sin (q_i \xi_i + \varphi_i). \quad (6.13)$$

However, the term D_{0i} already depends on two variables $\xi_1 = x_1 - c_1 t$ and $\xi_2 = x_2 - c_2 t$, as the region of $B_{\gamma-\alpha}$, in which $D_{0i} > 0$, is in simultaneous motion both in the x_1 - and x_2 - directions, while featuring limited dimensions $\sim l_1, l_2$ in both directions. This means that each of the expressions (6.13) describes a stationary wave bundle moving together with the switching wave. The most simple switching-wave model (see Fig. 6.1), corresponding to the wave beams (6.13), can be prescribed by the expression

$$\begin{aligned} \psi = & \left[1 + \frac{c_2}{c_1} \eta_2 \right] \left[\theta \left(\eta_2 + \frac{c_1}{c_2} \right) - \theta(\eta_2) \right] \theta \left(-\eta_1 - \frac{c_2}{c_1} \eta_2 - 1 \right) + \\ & + \left[1 - \frac{c_2}{c_1} \eta_2 \right] \left[\theta(\eta_2) - \theta \left(\eta_2 - \frac{c_2}{c_1} \right) \right] \theta \left(-\eta_1 + \frac{c_1}{c_2} \eta_2 - 1 \right) - \\ & - \eta_1 [\theta(\eta_1 + 1) - \theta(\eta_1)] \left[\theta \left(\eta_1 + \frac{c_2}{c_1} \eta_2 + 1 \right) - \theta \left(-\eta_1 + \frac{c_1}{c_2} \eta_2 - 1 \right) \right], \end{aligned} \quad (6.14)$$

$$\eta_1 = (c_1 \xi_1 + c_2 \xi_2) \tilde{d}^{-1}, \quad \eta_2 = (c_2 \xi_1 - c_1 \xi_2) \tilde{d}^{-1},$$

where $\tilde{d} = c_1 l_1 + c_2 l_2$; the coordinates η_1, η_2 are mutually perpendicular and located in the plane ξ_1 and ξ_2 , where the axis η_1 is oriented parallel to \mathbf{V} . If the definition of the Heaviside θ - function is taken into consideration, it will be easy to understand that the first row of Eq. (6.14) describes the distribution of the reduced temperatures (chem. potentials) ψ in the region $OA_3A_1A'_1$, the second row in the region $OA_3A_2A'_2$, and the third row in the region $A_1O_1A_2A_3$ as illustrated in Fig. 6.1. Put in another way, (6.14) is sub-divided into terms corresponding to the flat sectors of the triclinic surface ψ .

The peripheral points of the plane (x_1, x_2) , supposed to be reached by the switching-wave at an instant t , are the points of segment A_1A_2 of the straight line $\eta_1 = 0$ (see Fig. 6.1) on which $\psi = const = 0$. Consequently, this segment belongs to the switching-wave front (note that in an orientation perpendicular to x_1 and x_2 , the switching-wave front is unlimited). The velocity of motion of the points belonging to the segment A_1A_2 , related to the frame of reference x_1, x_2 , is easy to find, after having noted that the conditions $\dot{\eta}_1 = 0, \dot{\eta}_2 = 0$ are

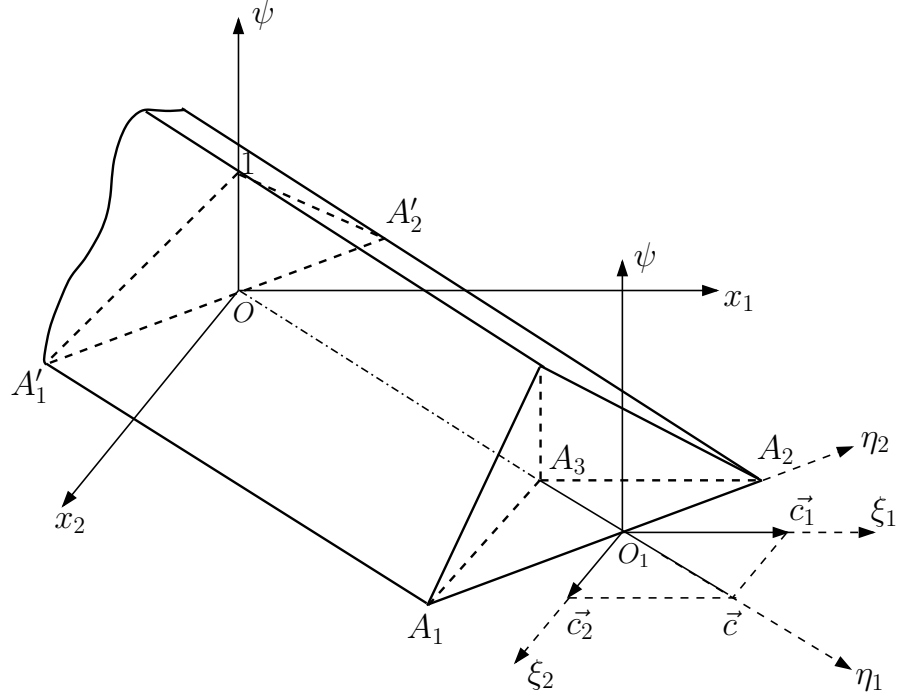


Figure 6.1. Model of a switching-wave propagating in conjunction with two wave-beams. The coordinates of the points are: A_1 : $(\eta_1 = 0, \eta_2 = -c_1/c_2)$, A_2 : $(\eta_1 = 0, \eta_2 = c_2/c_1)$, A_3 : $(\eta_1 = -1, \eta_2 = 0)$; further explanations are given in the text.

satisfied for any point of segment A_1A_2 , from which it can be concluded that - in the frame of reference x_1, x_2 - the velocity $\dot{\mathbf{r}}$ of the wave-front is equal to $\mathbf{V} = \mathbf{c}_1 + \mathbf{c}_2$. Obviously, for $\dot{\eta}_2 \rightarrow \pm 0$ the expression (6.14) transforms into (6.10). Then it will be possible to determine the expressions for the time τ and the coefficient of diffusion d , assuming that the quantity $V = (c_1^2 + c_2^2)^{1/2}$ corresponds to the minimum velocity of the switching-wave $2(d\tau^{-1})^{1/2}$, and by consideration of the relationship $\dot{\psi} = \psi'_{\eta_1} \dot{\eta}_1 = -\dot{\eta}_1 = \tau^{-1}$, resulting from (6.7), (6.10) and (6.11), where $\dot{\eta}_1 = -c^2/\tilde{d}$:

$$\tau = \frac{\tilde{d}}{V^2}, \quad d = \frac{1}{4} V^2 \tau = \frac{1}{4} \tilde{d}. \quad (6.15)$$

For a given d , relationship (6.15) delivers the connection between l_1 and l_2 , and thus also among the lengths of the displacement-waves, propagating along the x_1 and x_2 -directions, because $l_1 \sim \lambda_1 \sim q_1^{-1}$ and $l_2 \sim \lambda_2 \sim q_2^{-1}$.

Finally we have to note that, within the notion of a solitary wave front separating regions with different stationary values of T and μ , the description of T and μ only is an approximation, as the diffusion-processes proceeding perpendicular to \mathbf{V} will modify the profile of a two-dimensional wave with increasing time. Thus the real profile of the T - and μ - waves would only feature a shape near their

stationary value if they were located close to the $B_{\gamma-\alpha}$ region.

6.3 Stationary wave of relative spatial deformation $\tilde{\varepsilon}$ during the $\gamma - \alpha$ - transformation

6.3.1 $\tilde{\varepsilon}$ - trigger-switching - wave in absence of displacement-waves

The displacement-waves generated in the $B_{\gamma-\alpha}$ region ensure the lattice deformation required for a cooperative overcoming of the energy-threshold separating the structural α and γ states. These structural α - and γ - states are characterized by different values of static (permanent) displacements. However, the states of the α - and γ - phases feature different T -, μ - values, a fact not having been explicitly considered in our previous treatise. We shall now focus our analysis on the static deformations and only consider the relative change of volume during the transformation or, put in other words, characterize the γ - and α - phases by their relative volume deformation $\tilde{\varepsilon}$, where $\tilde{\varepsilon}_\gamma = 0$ and $\tilde{\varepsilon}_\alpha = 2,4 \cdot 10^{-2}$, being a value typical of the volume effect of the Bain-deformation (see also Pt. 1.4). The tilde-sign (\sim) is introduced to distinguish the relative volume deformation $\tilde{\varepsilon}$ from the associated linear deformation ε being produced by a displacement-wave. In a system comprising two stable states ($\tilde{\varepsilon} = \tilde{\varepsilon}_\alpha$, $\tilde{\varepsilon} = \tilde{\varepsilon}_\gamma$), being separated by certain barrier, the propagation of a trigger-switching wave (TSW) is possible in principle [80, 250]. However, for its generation, an initial level of excitation ($\tilde{\varepsilon} = \tilde{\varepsilon}_0$) is required, which must at least exceed the threshold-value ($\tilde{\varepsilon} = \tilde{\varepsilon}_{th}$). It is also known that an $\tilde{\varepsilon}$ - wave of the triggering type, propagating along the x-orientation, satisfies the relationship

$$\dot{\tilde{\varepsilon}} = d_{\tilde{\varepsilon}} \tilde{\varepsilon}''_{xx} + F(\tilde{\varepsilon}), \quad (6.16)$$

for which, in contrast to (6.7), the non-linear function $F(\tilde{\varepsilon})$ for $\tilde{\varepsilon} = \tilde{\varepsilon}_\gamma = 0$, $\tilde{\varepsilon} = \tilde{\varepsilon}_{th} > 0$, $\tilde{\varepsilon} = \tilde{\varepsilon}_\alpha > \tilde{\varepsilon}_{th}$ must vanish. The most simple expression for $F(\tilde{\varepsilon})$ thus may look as follows:

$$F(\tilde{\varepsilon}) = -\frac{1}{\tau_{\tilde{\varepsilon}}} \tilde{\varepsilon} (\tilde{\varepsilon} - \tilde{\varepsilon}_{th}) (\tilde{\varepsilon} - \tilde{\varepsilon}_\alpha), \quad (6.17)$$

where $\tau_{\tilde{\varepsilon}}$ - constant with the dimension of time. The stationary solution $\tilde{\varepsilon} = \tilde{\varepsilon}(x - V_{\tilde{\varepsilon}} t) \equiv \tilde{\varepsilon}(\xi)$ of wave-equation (6.16), comprising a non-linearity (6.17), will look as follows:

$$\tilde{\varepsilon} = \frac{1}{2} \tilde{\varepsilon}_\alpha [1 - \tanh(2 \xi l_{\tilde{\varepsilon}}^{-1})], \quad (6.18)$$

$$l_{\tilde{\varepsilon}} = \frac{4}{\tilde{\varepsilon}_\alpha} (2 d_{\tilde{\varepsilon}} \tau_{\tilde{\varepsilon}})^{\frac{1}{2}}. \quad (6.19)$$

In contrast to the T - and μ - waves - resembling so called phase - switching waves (PSW) [250]), which dispose of a velocity-continuum $V \geq V_{min}$ - a TSW only features a single (discrete) velocity:

$$V_{\tilde{\varepsilon}} = \left[\frac{d_{\tilde{\varepsilon}}}{2 \tau_{\tilde{\varepsilon}}} \right]^{\frac{1}{2}} (\tilde{\varepsilon}_{\alpha} - 2 \tilde{\varepsilon}_{th}). \quad (6.20)$$

In order to interpret these results, we recall that Eq. (6.16) can be expressed in the notation of the Landau-Halatsnikov-Equation (see e.g. [251]):

$$\dot{\tilde{\varepsilon}} = -\Gamma \frac{\delta \Phi}{\delta \tilde{\varepsilon}},$$

where Γ - kinetic coefficient (not to be confounded with electron-extinction); Φ - fraction of free energy depending on $\tilde{\varepsilon}$; $\delta \Phi / \delta \tilde{\varepsilon}$ - functional derivative of Φ by $\tilde{\varepsilon}$,

$$\Phi = \int dV \left\{ \frac{A}{2} \tilde{\varepsilon}^2 + \frac{1}{3} B \tilde{\varepsilon}^3 + \frac{1}{4} G \tilde{\varepsilon}^4 + \frac{1}{2} P \left(\frac{\partial \tilde{\varepsilon}}{\partial x} \right)^2 \right\}, \quad (6.21)$$

where $A/G = \varepsilon_{th} \tilde{\varepsilon}_{\alpha}$, $B/G = -(\tilde{\varepsilon}_{\alpha} + \tilde{\varepsilon}_{th})$, $\Gamma G = \tau_{\tilde{\varepsilon}}^{-1}$, $\Gamma P = d_{\tilde{\varepsilon}}$. Our model (6.21) for Φ represents a 1st order phase - transformation, because $A > 0$, $B < 0$, $G > 0$. If, in addition, $dB/dT < dA/dT < 0$, then the elastic moduli will feature a normal temperature dependence during cooling, $\tilde{\varepsilon}_{th}$ and the level of the energy-threshold $\Phi_0(\tilde{\varepsilon}_{th})$, which separates the states $\tilde{\varepsilon} = \tilde{\varepsilon}_{\gamma}$, $\tilde{\varepsilon} = \tilde{\varepsilon}_{\alpha}$, will subside and remain a finite quantity. If we use the notation Φ_0 for Φ at $\partial \tilde{\varepsilon} / \partial x = 0$, and consider that

$$\Phi_0(\tilde{\varepsilon}_{\gamma}) = 0, \quad \Phi_0(\tilde{\varepsilon}_{\alpha}) = \frac{V A \tilde{\varepsilon}_{\alpha}^2 (2 \tilde{\varepsilon}_{th} - \tilde{\varepsilon}_{\alpha})}{12 \tilde{\varepsilon}_{th}}, \quad (6.22)$$

$$\Phi_0(\tilde{\varepsilon}_{th}) = \frac{V A \tilde{\varepsilon}_{th}^2 (2 \tilde{\varepsilon}_{\alpha} - \tilde{\varepsilon}_{th})}{12 \tilde{\varepsilon}_{\alpha}},$$

where V - volume of the system, it becomes obvious from (6.20) and (6.22), that $V_{\tilde{\varepsilon}} \sim (\Phi_0(\tilde{\varepsilon}_{\gamma}) - \Phi_0(\tilde{\varepsilon}_{\alpha}))$, being proportional to the driving-force of the transformation, and $V_{\tilde{\varepsilon}} = 0$ at $T = T_0$, being corresponded by the value of $\tilde{\varepsilon}_{th} = 1/2 \tilde{\varepsilon}_{\alpha}$. We should however remark that, in order to excite a TSW, being in motion with non-vanishing velocity $V_{\tilde{\varepsilon}}$ at a temperature T near T_0 , there would be required large initial values of $\tilde{\varepsilon}_0$ of about $\sim 1/2 \tilde{\varepsilon}_{\alpha}$.

The frontal width $l_{\tilde{\varepsilon}}$ of a TSW, as defined by (6.19) (with linear approximation of its profile), is determined by parameters A and P in the function (6.21), in the form

$$l_{\tilde{\varepsilon}} = 4 \left[\frac{2 \tilde{\varepsilon}_{th} P}{A \tilde{\varepsilon}_{\alpha}} \right]^{\frac{1}{2}}. \quad (6.23)$$

To perform an evaluation of $l_{\tilde{\varepsilon}}$, let us first express P by means of the specific surface-energy E_s and A by the additional assumption

$$E_s = \int_{-\infty}^{\infty} dx P \left(\frac{\partial \tilde{\varepsilon}}{\partial x} \right)^2. \quad (6.24)$$

After substitution by (6.18) in (6.24), and with consideration of (6.23) we get:

$$E_s = \frac{1}{6} \left[\frac{\tilde{\varepsilon}_{\alpha} P A}{2 \tilde{\varepsilon}_{th}} \right]^{\frac{1}{2}} \tilde{\varepsilon}_{\alpha}^2, \quad (6.25)$$

i.e.

$$P = 72 E_s^2 \frac{\tilde{\varepsilon}_{th}}{A \tilde{\varepsilon}_{\alpha}^5}.$$

Using (6.22), we can express $\tilde{\varepsilon}_{th}$ by the following notation:

$$\tilde{\varepsilon}_{th} = A \tilde{\varepsilon}_{\alpha}^3 \left[2 A \tilde{\varepsilon}_{\alpha}^2 - 12 \left(\frac{\Delta \Phi_0}{V} \right) \right]^{-1}. \quad (6.26)$$

According to the calculus in [58], it is justified to assume for the $\gamma - \alpha$ - transformation of iron-based alloys: $\Delta \Phi_0(M_S)/V \approx (4/3) Q$, where Q - specific reactive heat (it will be surmised that one fourth part of $\Delta \Phi_0/V$ is needed for the formation of the phase-boundary, thus providing an explanation for the factor $(4 / 3)$ associated with Q). E.g. for the alloy H30: $Q \approx 3 \cdot 10^8 \text{ J m}^{-3}$ [22]. Thus we get for $A \approx 2 \cdot 10^{11} \text{ J m}^{-3}$ - being a typical value of the compressive modulus - from (6.26): $\tilde{\varepsilon}_{th} \approx 5,4 \cdot 10^{-4}$. Taking a value of $0,2 \text{ J m}^{-2}$ for E_s [252], we can determine from (6.25) and (6.23): $P \approx 10^{-6} \text{ J m}^{-1}$, $l_{\tilde{\varepsilon}} \approx 1,9 \cdot 10^{-9} \text{ m} \approx 5 a$, i.e., the width of the front $l_{\tilde{\varepsilon}}$ is about 5 times as large as the lattice-parameter of the γ - phase.

Some additional remarks:

1. The data presented in [252] mainly relate to the surface energy of a static phase-boundary, whereas, in our above compilation of E_s , we used the solution (6.18) pertaining to a moving phase-boundary, which, strictly speaking, would only be justified for the case of a temperature close to T_0 , and with $V_{\tilde{\varepsilon}} \approx 0$. In case of an arbitrary temperature, the value E_s of a static phase-boundary can however be calculated using the general approach related to

the determination of the boundary energy of a ferromagnetic domain in [71]:

$$\begin{aligned}
E_s = & \left(\frac{PA}{2} \right)^{\frac{1}{2}} \frac{\tilde{\varepsilon}_\alpha^2}{27 n^2} \left\{ 6 \sqrt{2(n-1)} (n^2 - n + 1) - \right. \\
& - \sqrt{3(n-2)} (n-2) (n-1) + \frac{2}{\sqrt{n}} (2n-1) (n-2) (n+1) \times \\
& \left. \times \ln \left| \frac{2(2n-1) + 3\sqrt{2n(n-1)}}{n-2 + \sqrt{3n(n-2)}} \right| \right\} \quad (6.27)
\end{aligned}$$

where $n = \tilde{\varepsilon}_\alpha \tilde{\varepsilon}_{th}$. A comparison between (6.27) and (6.25) shows that for $T = T_0$, ($\tilde{\varepsilon}_\alpha = 2 \tilde{\varepsilon}_{th}$), ($n = 2$) the expressions for E_s match, as required. For $T = M_S$, if $n \gg 1$, we get from (6.27):

$$\begin{aligned}
E_s \approx & \frac{(PAn)^{\frac{1}{2}}}{27 \sqrt{2}} \tilde{\varepsilon}_\alpha^2 \left\{ 6 \sqrt{2} - \sqrt{3} + \right. \\
& \left. + 4 \ln \left| \frac{4 + 3\sqrt{2}}{\sqrt{3} + 1} \right| \right\} \approx 0,3 (PAn)^{\frac{1}{2}} \tilde{\varepsilon}_\alpha^2, \quad (6.28)
\end{aligned}$$

being about 2,5 - fold larger than the result obtained from (6.25). Thus we obtain with $E_s \approx 0,2 \text{ J m}^{-2}$ the values $P \approx 4 \cdot 10^{-7} \text{ J m}^{-1}$ and $l_\varepsilon \approx 2a$.

2. In the papers [17, 19], dealing with E_s , a ratio of

$$E_s \approx \frac{\Phi_0(\tilde{\varepsilon}_{th})}{V} l_\varepsilon,$$

was used, which can also be expressed by

$$E_s \approx \frac{1}{3} \left(\frac{PA \tilde{\varepsilon}_{th}}{\tilde{\varepsilon}_\alpha} \right)^{\frac{1}{2}} \left(2 - \frac{\tilde{\varepsilon}_{th}}{\tilde{\varepsilon}_\alpha} \right) \tilde{\varepsilon}_{th}^2, \quad (6.29)$$

after consideration of (6.22), (6.23). At $T = T_0$, $\tilde{\varepsilon}_\alpha = 2 \tilde{\varepsilon}_{th}$, Eq. (6.29) realistically delivers the order of magnitude of the quantity E_s , however at $T = M_S$ and $\tilde{\varepsilon}_\alpha \geq 10 \tilde{\varepsilon}_{th}$, the ratio between E_s , as determined from (6.25) or (6.27), and the value of E_s derived from (6.29), is of an order of magnitude of $(\tilde{\varepsilon}_\alpha/2 \tilde{\varepsilon}_{th})^3 \geq 10^4$, thus we can conclude that the assessment from (6.29) is not realistic in principle.

3. If the motion of the phase-boundary resembles a thermally activated process, being controlled e.g. by a diffusion-process, then the quantities V_ε and thus also Γ , d_ε and τ_ε should exhibit a strongly pronounced (exponential) dependence on temperature.

4. In order to determine Γ , $d_{\tilde{\varepsilon}}$ and $\tau_{\tilde{\varepsilon}}$ by means of our model (6.21) of the potential Φ , it should suffice to know the experimentally determined value $V_{\tilde{\varepsilon}}$, provided the quantities A , $\tilde{\varepsilon}_{\alpha}$, $\tilde{\varepsilon}_{th}$, P are previously given. We shall use the expressions suffixing Eq. (6.21), and write $V_{\tilde{\varepsilon}}$ in the form

$$V_{\tilde{\varepsilon}} = \Gamma \left[\frac{PA}{2\tilde{\varepsilon}_{th}\tilde{\varepsilon}_{\alpha}} \right]^{\frac{1}{2}} (\tilde{\varepsilon}_{\alpha} - 2\tilde{\varepsilon}_{th}) \quad (6.30)$$

thus highlighting the proportionality between $V_{\tilde{\varepsilon}}$ and Γ .

5. Besides the potential (6.21) there is frequently used a potential which only depends on even powers of ε , i.e. $\tilde{\varepsilon}^2$, $\tilde{\varepsilon}^4$, $\tilde{\varepsilon}^6$. In this particular case, being qualitatively analogous to that relating to (6.21), it is easily possible to perform a consideration of the triggering-switching wave (TSW), using the results of [253].

6.3.2 Effect of the displacement-waves on the velocity of the $\tilde{\varepsilon}$ - switching-wave

The relationship between the velocity $V_{\tilde{\varepsilon}}$ and the temperature, in conjunction with the parameters included in (6.20), is not typical of the $\gamma - \alpha$ - MT. That is no surprise, as the mechanism being responsible for the cooperative character of the transformation is not expressed explicitly neither in Eq. (6.16) nor in Eq. (6.21). In the two-wave model however, the cooperative nature of the lattice-transformation is linked up with displacement-waves, which, during their propagation, ensure the attainment of the threshold-deformation-level in the $B_{\gamma-\alpha}$ region. As soon as this threshold-deformation is surpassed, irreversible deformations up to the value of $\tilde{\varepsilon} = \tilde{\varepsilon}_{\alpha}$ will be produced, resulting in the development of an $\tilde{\varepsilon}$ - wave. Obviously, this conceptual view of martensite crystal growth must take for granted the motion of the $\tilde{\varepsilon}$ -wave into x-direction with a velocity \mathbf{c} , being equal to the geometric sum of the velocities of each individual displacement wave. That becomes a possibility when, as a result of the interaction of the $\tilde{\varepsilon}$ - TSW and the displacement waves, the $\tilde{\varepsilon}$ - TSW is converted into a wave featuring more than one discrete velocity $V_{\tilde{\varepsilon}}$, i.e. a velocity continuum, like a PSW. In mathematical terms, the effect of the displacement waves at the points of the $B_{\gamma-\alpha}$ region is expressed in such a way that there occur in sequence the events of approaching, confluence and finally, of disappearance (so-called "Folding-Catastrophe" [254]) of two singular points $\tilde{\varepsilon}_{\gamma}$ and $\tilde{\varepsilon}_{th}$. As a result, only a singular stable point $\tilde{\varepsilon}_{\alpha}$ will remain, to which the system tends (see Fig. 6.2).

In the latter case, the $\tilde{\varepsilon}$ - wave can generally propagate with any arbitrary velocity, since the region deformed by the displacement waves becomes unstable against any positive fluctuation. As the aforementioned vanishing process of particular points, propagating with velocity \mathbf{c} in space, is caused by the action of

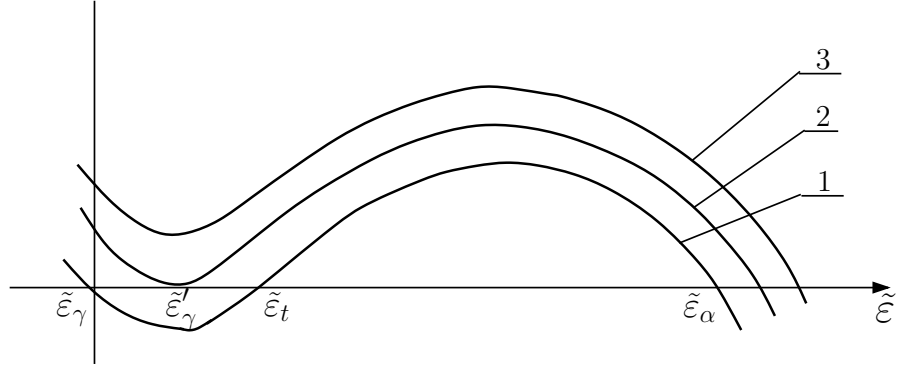


Figure 6.2. Development of a "Catastrophe" of the folding-type: Curve 1 - path of the function (6.17) in absence of displacement waves; Curves 2 and 3 are associated with the confluence and disappearance of discrete points $\tilde{\varepsilon}_\gamma$, $\tilde{\varepsilon}_{th}$, respectively.

displacement waves, just this velocity proves to be the only one highlighted in the velocity continuum of the modified $\tilde{\varepsilon}$ - wave. The vanishing of the discrete points $\tilde{\varepsilon}_\gamma$ and $\tilde{\varepsilon}_{th}$ of the function $F(\tilde{\varepsilon})$ can be taken into consideration by adoption of an addend of the "field-type" in (6.21): $-\tilde{\sigma}(\tilde{\varepsilon}_u) \tilde{\varepsilon}$, where $\tilde{\sigma}(\tilde{\varepsilon}_u)$ - pressure and $\tilde{\varepsilon}_u$ - volume deformation associated with the displacement-waves. If we further infer that $\tilde{\sigma}(\tilde{\varepsilon}_u) = K\tilde{\varepsilon}_u$, with $K > 0$, and equalize the conditions for confluence $\tilde{\varepsilon}_\gamma$, $\tilde{\varepsilon}_{th} \rightarrow \tilde{\varepsilon}'_\gamma = \tilde{\varepsilon}'_{th} \approx \tilde{\varepsilon}_{th}/2$ of the discrete points $\tilde{\varepsilon}_\gamma$ and $\tilde{\varepsilon}_{th}$ with the condition $\tilde{\varepsilon}_u = \tilde{\varepsilon}'_\gamma$, then we can determine $K = A/2$. Thus, within the framework of our considered model, $\tilde{\varepsilon}_{th}(M_S) = \tilde{\varepsilon}'_\gamma \approx \tilde{\varepsilon}_{th}/2$.

This way our consideration of displacement waves, which ensure the cooperative lattice transformation in the growth-stage, leads to a conceptual view of the motion of the martensite lattice-boundary with a velocity \mathbf{c} , only weakly depending on T , its magnitude corresponding to that of the velocity of sound. More than that, if \mathbf{c} is the geometric sum of \mathbf{c}_1 , \mathbf{c}_2 , than \mathbf{c} can even exceed the velocity of sound in the direction given by \mathbf{c} . We recall that supersonic speed of growth has been observed during the passage of a detonation wave through steel [30,31].

6.3.3 The $\tilde{\varepsilon}$ - Modified-Switching-Wave

Let us now consider in more detail the $\tilde{\varepsilon}$ - Modified-Switching-Wave ($\tilde{\varepsilon}$ - MSW), related to the case of the confluence of the discrete points $\tilde{\varepsilon}_\gamma$, $\tilde{\varepsilon}_{th}$ (Curve 2 in Fig. 6.2): $\tilde{\varepsilon}'_\gamma = \tilde{\varepsilon}'_t \approx \tilde{\varepsilon}_{th}/2$. Such a wave can generally be described by an equation of the form

$$\dot{\tilde{\varepsilon}} = d_{\tilde{\varepsilon}} \tilde{\varepsilon}''_{xx} + \frac{1}{\tau_{\tilde{\varepsilon}}} (\tilde{\varepsilon} - \tilde{\varepsilon}'_{th})^2 (\tilde{\varepsilon}_\alpha - \tilde{\varepsilon}), \quad (6.31)$$

in which, by way of contrast to (6.16), the non-linear function $F(\tilde{\varepsilon})$ only features two values $\tilde{\varepsilon}'_{th}$, $\tilde{\varepsilon}_\alpha$, corresponding to the requirement $F(\tilde{\varepsilon}) = 0^1$. Let us now introduce the designations

$$Z = \frac{\tilde{\varepsilon} - \tilde{\varepsilon}'_{th}}{\tilde{\varepsilon}_\alpha - \tilde{\varepsilon}'_{th}}, \quad \tilde{\tau} = \frac{\tau_{\tilde{\varepsilon}}}{(\tilde{\varepsilon}_\alpha - \tilde{\varepsilon}'_{th})^2}, \quad (6.32)$$

and a dimensionless time \tilde{t} and spatial coordinate \tilde{x} :

$$\tilde{t} = \frac{t}{\tilde{\tau}}, \quad \tilde{x} = x \left(\frac{1}{d_{\tilde{\varepsilon}} \tilde{\tau}} \right)^{\frac{1}{2}}. \quad (6.33)$$

Then we can write Eq. (6.31) in the form

$$\dot{Z}_{\tilde{t}} = Z''_{\tilde{x}\tilde{x}} + Z^2 (1 - Z). \quad (6.34)$$

The solution Z is of the travelling-wave type $Z = Z(\xi)$

$$Z(\xi) \equiv Z(\tilde{x} + \tilde{c}\tilde{t}), \quad (6.35)$$

where \tilde{c} - dimensionless wave-velocity

$$\tilde{c} = c \left(\frac{\tilde{\tau}}{d_{\tilde{\varepsilon}}} \right)^{\frac{1}{2}}, \quad (6.36)$$

corresponds to the equation

$$Z''_{\xi\xi} - \tilde{c} Z'_{\xi} + Z^2 (1 - Z) = 0. \quad (6.37)$$

In case of large values $\tilde{c}^2 \gg 1$ it is possible to use a simplified procedure for resolving Eq. (6.37), by introduction of a row of additive terms with increasing powers of the small parameter \tilde{c}^{-2} . This procedure is described in detail in [249]. Taking the velocity $c = |\mathbf{c}_1 + \mathbf{c}_2|$ as given (see Pt.6.3.2) and the condition $\tilde{c}^2 \gg 1$ as satisfied, then we will be able to assess the frontal width of the $\tilde{\varepsilon}$ - SW. Following [249], we designate

$$\varphi = -\tilde{c} Z'_{\xi} \quad (6.38)$$

and transform (6.37) into the coordinate frame of a phase plane:

$$\frac{1}{\tilde{c}^2} \frac{d\varphi}{dZ} = \frac{\varphi - Z^2 (1 - Z)}{\varphi}. \quad (6.39)$$

Let us now search for a solution of (6.39) in the form of

$$\varphi(Z, \tilde{c}^{-2}) = g_0(Z) + \tilde{c}^{-2} g_1(Z) + (\tilde{c}^{-2})^2 g_2(Z) + \dots. \quad (6.40)$$

¹Notice that equation (6.31) has the solution (6.18) for the solitary wave front propagating with velocity (6.20)

After insertion of (6.40) in (6.39) and equalizing the terms with identical powers (\tilde{c}^{-2}) we get:

$$g_0(Z) = Z^2(1 - Z), \quad (6.41)$$

$$g_1(Z) = g_0 \frac{d g_0}{d Z} = Z^3 (1 - Z) (2 - 3 Z), \quad (6.42)$$

$$g_2(Z) = \frac{d}{d Z} (g_0 g_1) = 2 Z^4 (1 - Z) (1 - 2 Z) (5 - 6 Z). \quad (6.43)$$

We determine the dimensionless frontal width \tilde{l} of the $\tilde{\varepsilon}$ - PSW from [249] by the ratio

$$\tilde{l} \sim \frac{1}{Z'_\xi(Z_0)}, \quad (6.44)$$

in which Z_0 is a solution of the equation

$$\frac{d \varphi}{d Z} = 0 \quad (6.45)$$

corresponding to the flex point of the function $Z(\xi)$, i.e. $Z''_{\xi\xi} = 0$ for $Z = Z_0$. From (6.45) and (6.40) - (6.43) we can immediately find

$$Z_0 = \frac{2}{3} + \frac{14}{27} \tilde{c}^{-2} + O(\tilde{c}^{-4}). \quad (6.46)$$

After insertion of (6.46) in (6.40), and with consideration of (6.38), we get

$$Z'_\xi(Z_0) = \frac{1}{\tilde{c}} \frac{4}{27} + O(\tilde{c}^{-5}). \quad (6.47)$$

Making use of (6.44), (6.47), we get

$$\tilde{l} \sim \frac{27}{4} \tilde{c}. \quad (6.48)$$

If we turn over to dimensional quantities with consideration of (6.36) and (6.33), we get from (6.48)

$$l \sim 7 c \tilde{\tau} = \frac{7 c \tau_{\tilde{\varepsilon}}}{(\tilde{\varepsilon}_\alpha - \tilde{\varepsilon}'_{th})^2} \approx \frac{7 c \tau_{\tilde{\varepsilon}}}{\tilde{\varepsilon}_\alpha^2}, \quad (6.49)$$

in which the condition $\tilde{\varepsilon}'_{th} \ll \tilde{\varepsilon}_\alpha$ is appropriately considered.

Up to now, the constant $\tau_{\tilde{\varepsilon}}$ with the dimension of time played the role of a free phenomenological parameter, the determination of which would have to consider certain additional condition. This condition results from the general requirement of coordinated propagation of atomic displacement waves (the waves ensure the attainment of a threshold-deformation $\tilde{\varepsilon}'_{th}$) with coexistent temperature

(T) chemical potential (μ) and $\tilde{\varepsilon}$ - switching waves, as this requirement takes for granted that the a.m. conditions of equalized wave-propagation velocity as well as that of equalized spatial scale of the frontal widths of the T -, μ - and $\tilde{\varepsilon}$ - SW's. In fact, an unambiguous relationship between electrochemical potential μ and electron-concentration (and thus also with specific volume) inhibits the materialization of a PSW of the μ - type with frontal width l_μ , which would substantially differ from the frontal width of the $\tilde{\varepsilon}$ -wave. It is nonetheless justified to assume that also the process of heat-emission, being represented by the non-linear function $F(\psi)$ introduced in Eq. (6.7), will occur in a region with $\tilde{\varepsilon} > \tilde{\varepsilon}'_{th}$, i.e. in the frontal area of the $\tilde{\varepsilon}$ - MSW. Thus it is justified to introduce the following additional condition:

$$l \sim l_\mu \sim l_T \sim \lambda/2, \quad (6.50)$$

where λ - length of a displacement-wave with magnitude of about $(10^{-7} \div 10^{-6})$ m. For the aforementioned region of λ we can determine from (6.50) and (6.49) with $c \sim 5 \cdot 10^3$ m/s $\tau_{\tilde{\varepsilon}} \sim 2(10^{-15} \div 10^{-14})$ s. The time $\tilde{\tau} = \tau_{\tilde{\varepsilon}}/(\tilde{\varepsilon}_\alpha - \tilde{\varepsilon}'_{th})^2$, which, according to (6.49), determines the frontal width l , is of an order of magnitude of 10^{-11} s for $\tilde{\varepsilon}_\alpha \sim 2, 4 \cdot 10^{-2}$.

Now it is easy to convince ourselves that, for $\tau_{\tilde{\varepsilon}} \sim (10^{-15} \div 10^{-14})$ s, our initial assumption $\tilde{c}^2 \gg 1$, used for our above analysis, is satisfied. Thus we can also use the relationships linking up the quantities $d_{\tilde{\varepsilon}}$, $\tau_{\tilde{\varepsilon}}$ with Γ , P , A , $\tilde{\varepsilon}_\alpha$, $\tilde{\varepsilon}_{th}$, appearing in Eq. (6.21), to determine

$$\frac{d_{\tilde{\varepsilon}}}{\tilde{\tau}} = \frac{P \tilde{\varepsilon}_{th} \tilde{\varepsilon}_\alpha}{\tau_{\tilde{\varepsilon}} \tilde{\tau} A} \approx \frac{P \tilde{\varepsilon}_{th} \tilde{\varepsilon}_\alpha^3}{A \tau_{\tilde{\varepsilon}}^2}. \quad (6.51)$$

From (6.51), we can determine for $P \sim 4 \cdot 10^{-7}$ J/m, $A = 2 \cdot 10^{11}$ J/m³, $\tilde{\varepsilon}_{th} \sim 10^{-3}$, $\tilde{\varepsilon}_\alpha \sim 2, 4 \cdot 10^{-2}$, $\tau_{\tilde{\varepsilon}} \sim (10^{-15} \div 10^{-14})$ s the value of $d_{\tilde{\varepsilon}}/\tilde{\tau} \sim (10^2 \div 10^4)$ m²/s². Then we obtain from (6.36) the quantity \tilde{c}^2 for $c \sim 5 \cdot 10^3$ m/s, delivering $\tilde{c}^2 \sim (10^5 \div 10^3) \gg 1$.

Remarkably, for the same values of P , A , $\tilde{\varepsilon}_{th}$, $\tilde{\varepsilon}_\alpha$, and $\tau_{\tilde{\varepsilon}} \sim 10^{-14}$ s, we obtain a kinetic coefficient $\Gamma \sim 10^{-2}$ m³/(J s), and then, in accordance with (6.30), the velocity of the TSW $V_{\tilde{\varepsilon}} \sim 10$ m/s is almost three orders of magnitude smaller than the speed of growth of a martensite crystal.

Large values of \tilde{c}^2 justify the omission of two addends of an order of magnitude of \tilde{c}^{-2} and, all the more, those of an order of magnitude of \tilde{c}^{-4} , \tilde{c}^{-5} appearing in Eqs. (6.47), (6.46) without introducing any significant error. This also means that, when breaking down Eq. (6.40), it is justified to confine our further analysis to the first addend. This approximation corresponds to an omission of the second derivative $Z''_{\xi\xi}$ in Eq. (6.37). After elementary integration of Eq. (6.37) we are able to find the expression defining the shape of the $\tilde{\varepsilon}$ - modified-wave:

$$\frac{Z}{(1-Z) \exp(Z^{-1})} = \exp\left(\frac{\xi}{\tilde{c}}\right). \quad (6.52)$$

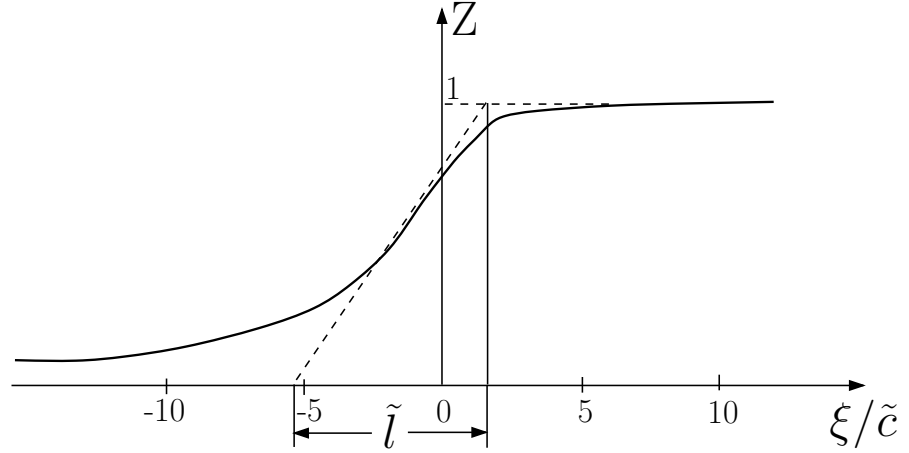


Figure 6.3. Phase-Switching-Wave (PSW) profile of relative volume deformation.

As a result of (6.52), we obtain $Z \rightarrow 0$ for $\xi \rightarrow -\infty$, and $Z \rightarrow 1$ for $\xi \rightarrow +\infty$. Fig. 6.3 shows the profile of the $\tilde{\varepsilon}$ - wave, as obtained from Eq. (6.52), as well as the width \tilde{l} as obtained from Eqs. (6.44) and (6.48). It is obvious from Fig. 6.3 that the wave-profile is asymmetric in relation to the point with coordinates $Z = 1/2$, $\xi/\tilde{c} = -2$, which does not correspond to the flex point ($Z = 2/3$, $\xi/\tilde{c} \approx -0,807$) of the function (6.52), and is characterized by a more moderate variation at $Z \rightarrow 0$ in relation to a variation at $Z \rightarrow 1$. This in turn justifies to some degree the usage of the band-structure of the fcc-phase of iron for an analysis of the conditions for displacement-wave generation.

6.4 Summary of Chapter 6

Let us summarize as follows:

1. Within the framework of the wave-model, our qualitative approach as proposed in Chap. 6 is mainly based on the presumption that several of the mutually - connected processes, which are propagated in a wave regime, determine the growth mechanism of martensite crystals.
2. In the particular case of missing atomic displacement-waves, the width of the moving boundary between the adjacent phases is mainly determined by the frontal width $l_{\tilde{\varepsilon}}$ of the $\tilde{\varepsilon}$ - TSW, corresponding to some lattice-constants.

In the case of non-vanishing atomic displacement-waves, which ensure the required threshold-deformation, the $\tilde{\varepsilon}$ - wave transforms into a modified-switching wave of frontal width l , being characterized by a displacement-wavelength λ . For $\lambda/2 \sim (10^{-7} \div 10^{-6})$ m, the quantity l is about two to three orders of magnitude larger than $l_{\tilde{\varepsilon}}$. The region $B_{\gamma-\alpha}$, comprising

highly pronounced inhomogeneities of temperature and chemical potential, basically corresponds with the frontal structure of the modified $\tilde{\varepsilon}$ - wave.

The complicated structure of the wave-process justifies the introduction of the special term "transformation-wave", closely related to the growth stage of martensite, also having been used in [77], but without specification of the wave-structure.

3. The cooperative character of the structural transformation, being the most typical phenomenological feature of martensitic transformations, is ensured by a phonon-maser effect occurring in the $B_{\gamma-\alpha}$ - region, which transforms a fraction of total reaction energy into energy of the atomic displacement waves.
4. The specification of the pattern of growth control of a martensite crystal by a pair of waves, as developed in Chap. 5, is reduced with the replacement of the lattice displacement waves with infinite frontal dimensions by wave-beams. The notion of wave-beams, i.e. of displacement-waves with finite frontal dimensions, suggests itself for the description of the growth process of a cylindrical macronucleus (see Pt. 1.3), whose lateral dimension will just determine the minimum dimension of the wave front.
5. In order to provide further evidence for our interpretation by the notion of wave- beams, it may be of crucial interest to investigate how efficiently crystal-growth can be stimulated by means of two external sources of hyper-sound, and its relationship with the dimensions of the wave-front sources, with the aim of an improved specification of the transformation pattern treated in the final part of Chap. 5. In particular, getting over to closely located and properly oriented linear emitters with lateral dimensions of about $\leq 10^{-6}$ m might make possible the simulation of a generation mechanism with long-wave components of the displacement waves, during the development of a single nucleus. It cannot be excluded that a single linear emitter (with the special orientation) may be a successful tool for simulation of the development of a single cylindrical macronucleus.

It is obvious from the description of the habits near $\{557\}$, $\{225\}$ in the two-wave pattern that, in order to excite waves propagating near the axes $\langle 00\bar{1} \rangle$, $\langle 110 \rangle$, the emitter must be oriented in the direction of $\langle 1\bar{1}0 \rangle$, lying in the habit-plane. The success of such an experiment might be evidenced by the emergence of crystals with a limited choice of habits (i.e. from 1 to 4) of the type $(h \pm \delta, h \mp \delta, \pm l)$ with $\delta < 1$. Such result would testify the benefit of nucleation of the martensitic crystals in elastic fields of dislocations with typical Burgers-vectors of fcc-lattice structures. It would also be promising to try to simulate the process of energy irradiation during the nucleation process, by means of narrow (with lateral dimensions of about $\sim 10^{-6}$ m)

directed electron-, ion- or photon- beams, with a profile ensuring a linear trace of interaction on a single crystal-surface, with a period of interaction of $t_i \sim 10^{-10} \div 10^{-11}$ s.

6. The mutual interaction of wave beams among themselves and with PSW of the T - or μ - type is expressed by the requirement of their coordinated propagation, i.e. $\mathbf{V} = \mathbf{c} = \mathbf{c}_1 + \mathbf{c}_2$.
7. In the case of the $\gamma - \alpha$ - MT, the volumetric effect as well as the macroscopic shear with a typical magnitude of 0,2, serve as macroscopic characteristics. It can however easily be shown that the aforementioned model of thermodynamic potential (6.21), being related to the macroshear, will deliver a threshold-level of macroscopic shear exceeding the threshold of volume deformation by one power, even for an A-value equivalent to the minimum shear-modulus $C' = (C_{11} - C_{12})/2$. Thus it can be expected that macroscopic shear-distortion will only play a subordinate role, in that it would only appear in regions which already lost their stability by volume deformation, due to the action of longitudinal displacement waves. In other words, the relative volumetric change (actually playing the role of an ordering-parameter) might be the better choice as a macro-parameter. This point of view is close to the position of the author of [77], highlighting the leading role of longitudinal waves during the development of the central zone (the "midrib") of lenticularly shaped martensite crystals.
8. In the case of lenticularly shaped martensite crystals, the quantity c determines the greatest (frontal) midrib-growth velocity and thus features an important characteristic of the process. This circumstance implies the requirement for a precise measurement - by more than only of its order of magnitude - of the velocity c by an independent measuring principle. For example, the method described in [27] could be improved by triggering the martensitic transformation of certain specimen exhibiting a pronounced two-stage transformation, by means of a strong magnetic field [34, 36]. On the one hand, this would allow a distinguished identification of the first, rapidly processing transformation stage and, on the other hand, a reduction of possible orientations of martensite, by proper consideration of the orientation of the pre-martensitic austenitic single crystals (see Pt. 5.3.3), in addition to allowing an improved determination of the dimensions of the crystals.

Some additional remarks:

1. In [255], the temperature-field at the boundary of the growing martensitic crystal with the shape of an ellipsoid cylinder with small ratio of the cross-section axes has been treated. The task treated in [255] is like the freezing-problem of humid ground [256]: The equation of heat-conduction is devoid

of sources, and the speed of boundary motion is assumed to be proportional to the temperature-gradient within the boundary. However, this approach differs remarkably from the one we used. Nonetheless, it is interesting to note that the estimate of the radius of curvature of the martensite-boundary $\rho \sim 10^{-6}$ m (as determined in [255]), at which adiabatic crystal growth mode becomes effective, confirms the possibility of adiabatic growth of the cylindrical macro-nucleus with a radius of an order of magnitude of about 10^{-6} m.

2. The description of martensitic growth as a lattice-deformation process suggests itself as most natural. In our above consideration, we distinguished between the deformation controlling the growth process of martensite, by means of displacement-waves, and the observable macroscopic deformation. Obviously, from a phenomenological point of view, this interpretation represents one of some possible variants of description, within the framework of a pattern of cooperating micro- and macroscopic ordering parameters [1]. We also drew the attention to [257], focusing on the selection of an ordering-parameter not being deducible to the observed macro-deformation, and on the applicability of a striction-model for an interpretation of thermodynamic laws, being typical of thermoelastic martensite.
3. For large propagation velocities of the phase boundary, it is generally required to take into consideration the systematic motion of the electrons with the velocity of local lattice motion analogously to the systematic motion of the electrons with the local velocity of ions in an elastic wave (see e.g. Chap. 3 in [258]). The results published in [29, 259] give evidence for the dragging-effect of electrons by a moving boundary. However it is easy to prove that the contribution of such dragging effect on the occupational inversion would only be of an order of magnitude of $\Delta\sigma_0 \sim 10^{-4}$ and thus have no appreciable effect on the rate of phonon-generation, as becoming obvious after comparison with the σ_0 - values in Table 3.1.
4. In addition to the description of the phase boundary by means of a functional of type (6.21) we also would like to draw attention on the work of Lihachev [260], which, within the framework of continuum-mechanics, suggests to consider boundary layers in the solid state (without specifying their structure) as independent planar-defects.

The results related to the qualitative analysis of coordinated propagation of switching- and displacement-waves, which simulate the motion of the phase-boundary during the $\gamma - \alpha$ - MT, are published in papers [261–264]. The substantiation of Chap. 6 mainly follows the work published in [262].

Synopsis and outlook

Based on analysis of experimental data and theoretical notions, a new conceptual approach for the description of rapid (frontal) crystal growth during fcc - bcc ($\gamma - \alpha$) martensitic transformations in ferrous alloys has been developed. The particularities in the course of this transformation (e.g. supersonic velocity of growth, anomalous magnitude of supercooling below the point of phase-equilibrium, missing phonon mode softening in the temperature region before the onset of a martensitic transformation) are considered as strong evidence for setting off the spontaneous martensitic transformation as a peculiar kind of "limiting case" among diffusionless transformations, contrasting most pronouncedly with the opposed "limiting case" of structural transformations, described most conveniently under the notion of soft-phonons.

Basically, the martensite growth stage is considered as a process of propagation of lattice deformation, being controlled by wavelike atomic displacements of relatively large wavelengths $\lambda \sim (10^{-7} \div 10^{-6})$ m. However, the cooperative character of atomic displacement can only become effective if significant deviations from equilibrium conditions in the sub-system of 3d-electrons are present, thus implying the requirement of the existence of 3-d-electron sub-systems embodying a macroscopic number of pairs of equidistant, inversely occupied states. This way, electronic transitions among inversely occupied electronic states lead to the generation of cooperative macroscopic lattice-displacement waves by stimulated emission of phonons (phonon-maser effect). Because, from a quantum-mechanical point of view, the propagating atomic displacement wave represents a macroscopic amount of phonons of non-vanishing frequency, the previously defined notion of martensitic transformations, being essentially based on the propagation of displacement waves, is equivalent to a description within the conceptual framework of "hard" phonon modes, conforming to the new scientific tendency of theoretical research on $\gamma - \alpha$ - martensitic transformations.

The survey of results presented in the final sections of Chaps. 2 to 6 of this monograph is showing that the tasks determined in Pt. 1.5 have been resolved, at least at a qualitative level. Nonetheless, let us now review once more the most important findings considered essential for the new description of the $\gamma - \alpha$ - martensitic transformation in ferrous alloys, as well as some remarkable quantitative key-evaluations obtained for the stage of nucleation of martensite, as well as some predictions derived from the theory and their future developments, respec-

tively.

Most important findings

1. In the stage of rapid martensite crystal growth there exists a boundary area between the phases being characterized by intensive electron currents within coexisting strongly pronounced temperature and even more important - chemical potential gradients.
2. An electronic drift current leads to an inverted occupation of those pairs of electronic states being localized in the proximity of the S - surfaces in quasi-momentum space. S - surfaces are defined by the condition that the projection of electronic group velocity towards the orientations of $\vec{\nabla}T$ or $\vec{\nabla}\mu$ must vanish at all points of the S-surfaces.
3. The number of pairs of inversely occupied electronic states of the 3d - bands of iron is a macroscopic quantity.
4. The process of generation of atomic displacement waves is energized by stimulated emission of phonons during transitions of the non-equilibrium 3d-electrons between the inversely occupied states. This process is similar to the radiation of photons in a maser.
5. The displacement waves controlling the process of martensitic crystal growth are of the longitudinal type (or quasi-longitudinal) with frequencies of $\nu \sim 10^{10} \text{ s}^{-1}$ (region of hypersound) and amplitudes ensuring the required level of lattice deformation of $\varepsilon \sim 10^{-3}$ needed for initiation of the $\gamma - \alpha$ - martensitic transformation. The mode of initial excitation of waves during the nucleation stage of the α - phase is a hard mode.
6. Certain combinations of displacement waves are important but not separate waves. Thus for instance, the stage of rapid growth of a martensitic lamellae is correlated with the propagation of a pair of perpendicularly oriented waves, stimulating the process of flat lattice deformation of a combined tensile-compressive type.
7. The displacement waves exist in the shape of the wave bundles propagating in coordination with the spatially limited front of a wave of relative volume deformation and making the function of "pilot-waves", paving the way for the martensitic reaction in their wake.

Key quantitative evaluations

1. Obviously, the electronic (chemical) potential gradient $\vec{\nabla}\mu$ is the main non-equilibrium source within an electron-subsystem. The assessment of the quantity $\vec{\nabla}\mu$ requires that the difference of chemical phase potentials $\Delta\mu =$

$\mu_\gamma - \mu_\alpha$ as well as the width l of the region among the phases are known. The value $\Delta\mu \approx 0,16$ eV has been determined for the s - and d - electron sub - systems under Pts. 1.5 and 4.5.3. The quantity l can be assessed by means of Eq. (6.49). Taking into account that the constant τ_ε included in (6.49) plays the role of the minimum time-constant characterizing the Bain-deformation process, it suggests itself to take the physically consistent value $\tau_\varepsilon \sim 10^{-14}$ s, corresponding to the period in which a lattice - atom will be displaced - at near-sound velocity - by a distance of about $0,1 a$ (a - lattice-parameter). Then we get from (6.49) the value $l \sim 10^{-6}$ m and $\nabla\mu \sim \Delta\mu/l \sim 10^5$ eV/m.

2. Within the frame of the proposed wave-model of martensite-growth the requirement for satisfaction of the condition $\sigma_0 > g_{th}$ for displacement-wave generation, as outlined under Pt. 3.1, attains a key role. An assessment of the inverted population difference of a pair of electronic states, associated with an electron drift in a field $\vec{\nabla}\mu$, delivers $\sigma_0(\nabla\mu) \geq 10^{-3}$. The threshold-value $\sigma_{th} \sim 10^{-4} \div 10^{-3}$ had been determined under Pt. 3.1 from Eq. (3.10). After further evaluation of σ_{th} , it becomes obvious that the number of pairs of inversely occupied states $R_{\mathbf{q}}$, being proportional to the area $\Sigma_{\mathbf{q}}$ of the reduced sheet of the S-surface, is of paramount importance. For $\Sigma_{\mathbf{q}} \approx 20(\pi/a)^2$, the condition $\sigma_0 > \sigma_{th}$ is satisfied for ordinary values of the matrix-elements of electron-phonon-interaction $W_{\mathbf{q}}$ ($W_{\mathbf{q}}$ is taken in the tight binding approximation). We emphasize that the instability of a metal lattice, being linked up with the amplification of an acoustic wave by the mechanism of stimulated emission of phonons (see e.g. [265]) has generally been supposed as not realizable in metals.
3. The magnitude of maximum lattice deformation ε_m maintainable in a displacement wave also is of fundamental importance. An evaluation of ε_m has been performed under Pt. 3.3 by means of Eq. (3.42), being correct for stationary conditions. Using this methodology, a value of $\varepsilon_m \sim 10^{-3}$ was obtained for $\sigma_0 \approx 2,5 \sigma_{th}$.

The inequality $t_u \gg t_\nabla$, being included in Pt. 3.3, refers to the settling time - t_u - of the stationary amplitude (or of the deformation ε_m) within the displacement wave. The lifetime of the chemical potential gradient t_∇ shows that a usage of the stationary ε_m - estimate is only justified for a hard mode of wave excitation. With this approach, it is possible to link up the growth of martensite with displacement waves, while we believe that near M_S the austenitic lattice remains essentially stable against deformations being less than 10^{-3} , thus suggesting the following conclusion:

the nucleation process of martensite crystals is associated with the hard mode excitation of displacement waves of an estimated strain amplitude

$$\varepsilon_m \sim 10^{-3}.$$

4. An evaluation of the threshold value $\tilde{\varepsilon}_{th}(M_S)$ of relative volume deformation $\tilde{\varepsilon}$ at temperature M_S also is of crucial importance. The point here is that coordinated propagation of displacement waves with an interphase boundary would only be possible if the relative volume deformation $\tilde{\varepsilon}_u$ within the displacement waves exceeded the value $\tilde{\varepsilon}_{th}(M_S)$. Otherwise, ($\tilde{\varepsilon}_u < \tilde{\varepsilon}_{th}(M_S)$), the motion of the phase boundary would be described by a triggering-switching wave with the sole velocity being distinctly smaller than the magnitude of the sound velocity. In Pts. 6.3.2, 6.3.1, there has been shown that $\tilde{\varepsilon}_{th}(M_S) \approx 2,5 \cdot 10^{-4}$, so that the condition $\tilde{\varepsilon}_u > \tilde{\varepsilon}_{th}(M_S)$ is easily satisfied for $\varepsilon_m \sim 10^{-3}$.

Proposed experiments for further verification of the growth model

1. Measurement of the contact-potential difference $\Delta\varphi$ among the γ - and α - phases (see Pt. 2.5). The value and sign of $\Delta\varphi$ are needed to determine the inverted occupational difference $\sigma_0 \sim \Delta\varphi$, as well as the direction of propagation of the displacement waves in relation to $\vec{\nabla}\mu$ (see legend of table 2.1).
2. Measurement of the ratio of the velocity moduli of the longitudinal waves $\varkappa_e = c_{(110)}/c_{(001)}^{-1}$ in austenite at the temperature M_S , as a function of the concentration of the alloying element C_{ae} , in order to check the criterion for the first change of the habit-planes ($\{557\} \rightarrow \{225\}$). A positive result of the experiments would be an increase of \varkappa_e with increasing C_{ae} while approaching to the concentration at which the habit $\{225\}$ obviously becomes stabilized (see Pt. 5.1.3).
3. Precise measurement of the rapid frontal growth velocities of martensite crystals and comparison with the values $|\mathbf{c}| \approx |\mathbf{c}_1 + \mathbf{c}_2|$ predicted by theory, while the velocities \mathbf{c}_1 and \mathbf{c}_2 could be calculated on the basis of measured elastic moduli of austenite at M_S .
4. Observation of oriented growth of the martensite crystals during simultaneous influence of hypersound and strong magnetic fields, as well as of the effects of laser radiation pulses impinging on the surface of a specimen, directed along a trace near to a linear form.

We note here that the discovery of a predicted orientational effect in a magnetic field of $H \sim 10^7$ A/m [244], exceeding in order of a magnitude both demagnetization- and magnetic anisotropy fields, delivers strong evidence in favor of the maser-effect during phonon-generation, and, moreover, confirms our conclusion on the connection of the second change of habit $\{557\} \rightarrow \{3\ 10\ 15\}$ in the Fe-Ni-system, and $\{225\} \rightarrow \{259\}$ in the Fe-C-system, with exclusion of the quasi-longitudinal waves with velocity directions near the second-order axes of symmetry of the fcc-lattice from the total spectrum of generated waves.

If we mention further research, we want to note, above all, that a comprehensive understanding of the processes occurring in the stage of growth of martensite crystals should also contribute to the definition of physical models of the preceding stage of nucleation, as well as of the subsequent stage of accommodation of the coexisting phases. This way, for instance, the requirement for coordination of the nucleation stage with the growth stage, caused by the non-equilibrium conditions at the interphase boundary and being controlled by displacement waves, will lead to new findings on the rapid emergence of the macro-nucleus, as treated under Pt. 1.3.

Synthesis of concepts of the heterogeneous nucleation and of the wave growth of martensitic crystals

The presently achieved success in improved understanding of the nucleation stage can mainly be attributed to the consolidation of the notions of heterogeneous (dislocation-) nucleation as well as of the wave-controlled growth of martensite [266–272]. A calculus of the elastic fields of linear dislocations, being typical of the parent- γ - phase, have shown that even single mixed dislocations can play the role of nucleation centers (NC) of martensite crystals. NC-characteristics and macroscopic morphological features of martensite are (genetically) mutually linked up. In result there exist 24 different variants of matching patterns in the "NC-crystal".

The elastic field of dislocations disarranges the original lattice symmetry by selecting regions being most favorable for martensitic nucleation. Such a region features the shape of a perpendicular parallelepiped, its edges being oriented along the eigenvectors $\vec{\xi}_i$ of the strain tensor $\hat{\varepsilon}$, its eigenvalues ε_i satisfying the following conditions:

$$\varepsilon_1 > 0, \quad \varepsilon_2 < 0, \quad |\varepsilon_3| \ll |\varepsilon_{1,2}|,$$

thus ensuring the existence of slightly distorted surfaces (SDS) which are close to planes with normals

$$(\mathbf{N}_{SDS})_{1,2} \parallel \vec{\xi}_2 \mp \vec{\xi}_1 \sqrt{\varepsilon_1/|\varepsilon_2|}, \quad |\vec{\xi}_{1,2}| = 1.$$

Obviously, from a point of view of minimization of elastic distortion energy, phase-coupling is supported by weakly distorted (with $\varepsilon_3 = 0$ invariants) planes. Thus it would be reasonable to expect that the normal of the habit-plane of the martensite crystal should match with one \mathbf{N}_{SDS} .

In fact, among the \mathbf{N}_{SDS} , there exist $\langle h k l \rangle$ situated near $\langle 557 \rangle$, $\langle 225 \rangle$ (for 60° - dislocations with lines $\langle 1\bar{1}0 \rangle$) and situated near $\langle 259 \rangle$, $\langle 3\ 10\ 15 \rangle$ (for 30° - dislocations with lines $\langle 1\bar{2}1 \rangle$), being evidence of certain differences among the NC of packet- vs explosive-martensite.

Moreover, in the orientational relationship of the phase-lattice, there are included the slip-plane and the dislocation line, the latter one acting as a nucleation center, which suggests us to give preference to the Kurdjumov-Sachs- or Nishiyama-relationships, for various NC.

The question related to the orientation of macroscopic shear \mathbf{S} will be resolved in conjunction with the choice of one of the two orientations of the normal \mathbf{N}_{SDS} . For this aim, let us consider the notation of the distortional tensor of the elastic field, being represented as the sum of two diad products, and discriminate the part containing two addends

$$\mathbf{S}_1 \cdot \mathbf{N}_1 + \mathbf{S}_2 \cdot \mathbf{N}_2, \quad |\mathbf{N}_{1,2}| = 1.$$

We recall that the diad product $\mathbf{S} \cdot \mathbf{N}$ defines a deformation with an invariant plane, where \mathbf{N} - normal of a plane and \mathbf{S} - vector characterizing the shape deformation. Further considering that austenite is metastable at the beginning of the martensitic transformation at M_S - temperature, it is justified in the case of $|\mathbf{S}_1| > |\mathbf{S}_2|$, to surmise that the plane with the normal \mathbf{N}_1 is distinguished, and that the anticipated orientation of macroscopic shear is close to \mathbf{S}_1 . And vice-versa, for $|\mathbf{S}_2| > |\mathbf{S}_1|$, the components \mathbf{N}_2 and \mathbf{S}_2 will be discriminated, respectively. In the case of the straight $\gamma - \alpha$ - transformation, the results of this approach are in good accordance with experimental results.

With this approach, all macroscopic morphological characteristics of martensite attain a reasonable interpretation within the conceptual notion of nucleation at dislocations, where dislocations act as centers of forces disturbing the original lattice symmetry, their effect not being confined to the nuclear volume.

These findings match in detail with the ideas of the wave theory of growth, presupposing that the transformation starts with the emergence of an excited state with the shape of a parallelepiped, built up of vectors $\vec{\xi}_i$, its pairs of edges oscillating in opposed phase, thereby exciting controlling displacement waves orientated in the wave-normal $\mathbf{n}_{1,2}$ close to $\vec{\xi}_{1,2}$. In the most simple approximation of the equations

$$\mathbf{n}_1 = \vec{\xi}_1, \quad \mathbf{n}_2 = \vec{\xi}_2,$$

the requirement of correspondence of \mathbf{N}_{WDS} with the wave-habit (5.3) delivers the following condition:

$$\varkappa = \frac{c_2}{c_1} \approx \left[\frac{\varepsilon_1}{|\varepsilon_2|} \right]^{\frac{1}{2}}$$

which, if satisfied, ensures the possibility of a kinematic agreement of the wave description with the deformation description of the habit. Obviously, given the case that the ratio of tensile and compressive deformation in the wave-mode corresponds with \varkappa^2 , then dynamic agreement will also be achieved. We further note that for the $\gamma - \alpha$ - transformation, which proceeds with increase of specific volume: $\varepsilon_1 > |\varepsilon_2|$. Consequently, $c_2 > c_1$, so that the tensile strain can be prescribed by the wave propagating with the smaller velocity c_1 , whereas compressive strain can be prescribed by the wave propagating with the larger velocity c_2 (In the case of the $\alpha - \gamma$ - transformation, the situation will just be inverted). Specifically, the latter finding provides a physical criterion for the realistic choice of phase tuning of the waves controlling the transformation, as outlined in Chap. 5, as well as for the selection for the principal axes of tensile and compressive strain. Undoubtedly, the rules of deviation of the normal $\mathbf{n}_{1,2}$ of the controlling waves from the axes of symmetry of an ideal cubic lattice are dictated by the symmetry of the elastic field of the NC in the nucleation stage, in conjunction with a hard mode of wave generation. It is further worth to note that the orientation of the axis $\vec{\xi}_3$ of the cylindrical nucleus of the α - phase can significantly deviate from the line of dislocations (most pronouncedly for the 30° - dislocation line).

Our specification of the nucleation stage, which also enabled us to define the orientation $\vec{\xi}_3$, besides lifetime, energy and spatial contour of the state of excitation, suggested possibilities for their physical simulation [273, 274]. The effect of laser impingement close to a linear trace, with a period of $\sim 2 \cdot 10^{-11}$ s and sufficient power density for atomic vaporization, could induce the onset of a $\gamma - \alpha$ - in Fe-31,5 Ni-single crystals, at a temperature some degrees above M_S , however only in cases where the orientation of the trace of impingement of laser radiation was close to the calculated orientation $\vec{\xi}_3$ on the flat surface of the specimen. Obviously, besides the envisaged precise measurement of the speed of growth of α - martensite, the already obtained results are fundamental for proving true the developed dynamical theory of the transformation.

In order to get over to the dynamical description of the final stage, it would be useful, from our point of view, to represent the displacement waves by extremely small bundles of waves (with one of its transversal frontal dimensions of an order of magnitude of about one half wave-length), existing in the form of half-wave pulses (the dimensions of such pulses of order $\lambda/2$ in their direction of propagation). In fact, given a level of deformation $\varepsilon \sim 10^{-3}$, with $\lambda/2 \sim 10^{-6}$ m, the utmost displacement associated with the wave-pulse would be $u_{max} \approx 1/4 \varepsilon \lambda$, i.e., of similar order of magnitude as the lattice-parameter. Consequently, such wave-pulses must destroy the continuity of the medium, by causing the following effects: Generation of structural de-

fects; rotational distortions of the transforming lattice (being equivalent to the onset of "rotational modes" [275]), which re-establish the macroscopic continuity of the medium, as known from [11, 13, 275], also leading to the emergence of a characteristic relief at the surface of the specimen subjected to a $\gamma - \alpha$ - transformation. Of course, all these processes, including the nucleation stage, are closely associated with the stage of growth and thus can only partly be put in relation with the stage of accommodation of co-existing phases. Nonetheless it is reasonable to classify as fundamental the identification of processes controlling the martensitic transformation, as well as a more detailed investigation of the microscopic mechanism of their development, within the frame of a comprehensive description of the growth mechanism of martensite.

The identification of dislocation centers linked with martensite-nucleation opens up new possibilities for an interpretation of the laws and rules governing the formation of lattice-ensembles, by definition of the spectrum of new centers of nucleation, being immanent in the newly emerged α - phase crystal.

Further progress of the general theory of martensitic $\gamma - \alpha$ - transformations will undoubtedly be associated with the following topics:

- Theoretical research on the dynamics of lattice-fluctuations including investigations on the effects of elastic dislocation fields on the nucleation stage of martensite. It can already be anticipated that the fluctuations leading to the above defined state of lattice-excitation in the form of an elongated parallelepiped, are most probable;
- Specification of the area in which the state of excitation is localized, within the field of dislocation (i.e. the shortest distance to the line of dislocation), as well as of its probable transversal dimension;
- Specification of the structure of the electronic spectrum in the proximity of the dislocation-nucleation center (DNC) and of the $B_{\gamma-\alpha}$ - region. Doing so, the following aspects have to be considered:
 - 1) The potential coexistence of a mixture of electronic configurations of the iron-atoms (the basic pattern of calculus of a band-spectrum has already been proposed in [276]);
 - 2) The effect of lattice-distortions on the shape of the S-surfaces as well as of energy-dispersion at the S-surfaces, in the proximity of the Fermi-surface.

Finally, we remark that S-surfaces resemble individual objects in quasi-momentum space, thus classifying electronic states with respect to their contribution to transport-processes. Furthermore, for investigations and interpretations of phenomena in transition-metal alloys, which can most con-

veniently be described on the basis of a first-order coherent-potential approximation [277], it will be necessary to evaluate the possible existence of S-surfaces with large areas. Obviously, our proposed wave-model of growth control for an α - crystal will be universally applicable for most rapidly proceeding (1st - order) martensitic transformations, being related to a dislocation-nucleation mechanism. The threshold-deformation for such martensitic transformation comprises combined tensile and compressive strain, their main axes being oriented perpendicularly. For atoms in an intermediate phase region, the energy barrier can be overcome in a cooperative manner by a wave-mode. This way, the controlling displacement-waves imprint macroscopic characteristics in the martensite-crystals, however without determining the final positions of the atoms. The latter will mainly depend on the pattern of local interactions among the atoms. The atomic displacements towards their new equilibrium-positions can be initiated by waves of shorter wavelength (in relation to the control-waves), both in the pretransitional stage and in the growth-stage. Such an additional system of waves, in parallel with the accommodation-processes, must define the internal fine structure of the martensite plates.

Final conclusions

As a final conclusion, it can be stated that the obtained results provide sufficient evidence of the onset of a new qualitative stage of research on the large field of $\gamma - \alpha$ - martensitic transformations, within the frame of the wave-approach, thus making possible, on principle, to establish and to describe the following fundamental chain of relationships of cause and effect:

- dislocation-nucleation-center
- initial state of excitation
- non-equilibrium conditions
- particularities of the electronic structure
- spectrum of the generated displacement-waves
- observed morphological characteristics.

It is apparent that just the growth-controlling displacement-waves carry the information about the elastic field created by the nucleation-center in the region of nucleation location, thereby ensuring a genetic correspondence of the characteristics of macroscopic martensite-crystals with those of the nucleation-center. It is also obvious that, within the developed dynamical theory of $\gamma - \alpha$ - martensitic transformation, the growth-controlling displacement-waves play the role of the previously missing link among micro- and macroscopic description.

Our general conclusion is that the new comprehensive model of growth of the martensite crystals in a wave regime is basically consistent with observations and phenomenological theories, now being complemented by contemporary dynamics of lattice, and also by thermodynamical and quantum theoretical aspects, missed or only partially considered in previous theories.

The author hopes that near-future research will confirm most of the predictions, enabling an extension of the insights of the wave-model of α - martensite-growth in ferrous alloys onto a variety of other solid-state martensitic transformations.

Bibliography

- [1] Iziunov Iu.A. and V.N. Syromiatnikov. *Fazovye perekhody i simmetriia kristallov*. M.: Nauka, 1984.
- [2] Vaks V.G. *Vvedenie v mikroskopicheskuiu teoriiu segnetoelektrikov*. M.: Nauka, 1973.
- [3] Gufan Iu. M. *Strukturnye fazovye perekhody*. M.: Nauka, 1982.
- [4] Brus A. and Kauli P. *Strukturnye fazovye perekhody*. M.: Mir, 1984.
- [5] Vaks V.G., Zinenko V.I., and Shneíder V.E. *Mikroskopicheskie teorii strukturnykh fazovykh perekhodov tipa poriadok-besporiadok v kristallakh*. UFN, 141(4):629–673, 1983.
- [6] Strukov B.A. and Levaniuk A.P. *Fizicheskie osnovy segnetoélektricheskikh iavlenií v kristallakh*. M.: Nauka, 1983.
- [7] Kaufman L. and Koén M. *Termodinamika i kinetika martensitnykh prevrashchenií*. Uspekhi fiziki metallov, IV:192–289, 1961.
- [8] Warlimont H., Hausch G., Prasetyo A., and Renaud F. *Relations between elastic properties and diffusionless structural transition*. Proceedings of the first JIM Int. Symposium on „New aspects of martensitic transformation“, pages 153–158, 1976.
- [9] Warlimont H. *On the classification of structural phase transformation*. J. Microsc. Spectrosc. Electron., 2:333–344, 1977.
- [10] Kristian D. *Teoria prevrashchenií v metallakh i splavakh*, volume 1. M.: Mir, 1978.
- [11] Umanskií Ia.S. and Iu.A. Skakov. *Fizika metallov*. M.: Atomizdat, 1978.
- [12] Kurdjumov G.V. *Iavleniia zakalki i otpuska stali*. M.: Metallurgizdat, 1960.
- [13] Kurdjumov G.V., Utevskií L.M., and Éntin R.I. *Prevrashchenia v zheleze i stali*. M.: Nauka, 1977.

- [14] Lysak A.I. and Nikolin B.I. *Fizicheskie osnovy termicheskoi obrabotki stali*. Kiev: Tekhnika, 1975.
- [15] Krivoglaz M.A., Sadovskii V.D., L.V. Smirnov, and i dr. *Zakalka stali v magnetnom pole*. M.: Nauka, 1977.
- [16] Bernshtein M.L., Zaïmovskii V.A., L.M. Kaputkina, and i dr. *Termomekhanicheskaiia obrabotka stali*. M.: Metallurgiiia, 1983.
- [17] Roitburd A.L. *Sovremennoe sostoianie teorii martensitnykh prevrashchenii. Nesovershenstva kristallicheskogo stroeniia i martensitnye prevrashcheniia*, pages 7–32, 1973.
- [18] Roitburd A.L. and Éstrin É.P. *Martensitnye prevrashcheniia*. In *Itogi nauki i tekhniki. Metallovedenie i termicheskaiia obrabotka*, pages 5–102. M.: VINITI, 1970.
- [19] Roitburd A.L. *Martensitic transformation as a typical phase transformation in solids. Solid state physics: Advance in research and application*, 33:327–390, 1978.
- [20] N. Seljakow, G. Kurdjumov, and Goodtzow N. *Eine röntgenographische untersuchung der struktur des kohlenstoffstahls. Zeitschrift für Physik*, 45:384–408, 1927.
- [21] Fridkin V.M. *Dinamika reshetki i fazovye perekhody. Sovremennaia kristallografia*, 2:262–296, 1979.
- [22] Vinnikov L. Ia., Georgieva I.Ia., and i dr. *Vydelenie énergii pri obrazovanii martensita v zhelezo-nikelevykh splavakh i osobennosti ego struktury. Metallofizika*, (55):24–27, 1974.
- [23] Robin M. and Gobin P.F. *Etude par amplification electronique rapide de la propagation de la martensite dans un alliage ferrum-nickel. Scripta Metall.*, 11:669–674, 1977.
- [24] Izotov V.I. and Khandarov P.A. *Klassifikaciia martensitnykh struktur v splavakh zheleza. FMM*, 34:332–338, 1972.
- [25] Georgieva I.Ia. and Nikitina I.I. *DAN SSSR*, 186(1):85–87, 1969.
- [26] Zambrzhitzkii V.N., Maksimova O.P., and Shcherbedinskií G.V. *O novom kineticheskom variante martensitnogo prevrashcheniia. DAN SSSR*, 272(1):90–94, 1983.
- [27] Bunshah R.F. and Mehl R.F. *Rate of propagation of martensite. Trans. AIME*, 197:1251–1258, 1953.

- [28] Mukherjee K. On the dynamics of martensitic transformations. *Trans. AIME*, 242:1494–1501, 1968.
- [29] Robin M., Lormand G., and Gobin P.F. Electrical emission associated with the martensitic burst of Fe-Ni alloy. *J. Phys. (Fr.)*, 43(12):485–490, 1982.
- [30] Lokshin F.L. Skorost' martensitnogo prevrashcheniia. *Nauchnye doklady vysheí shkoly*, (2):205–208, 1968.
- [31] Lokshin F.L. Dinamicheskaiia teoriia martensitnogo prevrashcheniia, volume 771/85. Tr. Novocherkas. Politekhn. instituta, 1967.
- [32] Takashima K., Higo Y., and Nunomura S. The propagation velocity of the martensitic transformation in 304 stainless steel. *Phil. Mag. A.*, 49(2):231–241, 1984.
- [33] Arskii V.N. Vremya obrazovaniia martensitnogo kristalla. *Metallovedenie i obrabotka metallov*, (11):26–29, 1966.
- [34] Sadovskii V.D. and Romashev L.N. Rost kristallov martensita, obrazovavshikhsia pod deístviem impul'snogo magnitnogo polia. *DAN SSSR*, 238(2):342–344, 1978.
- [35] Schastlivtsev V.M., Romashev L.N., Iakovleva I.L., and Sadovskii V.D. Élektronnomikroskopicheskoe issledovanie struktury kristallov martensita, zarodivshikhsia pod deístviem impul'snogo magnitnogo polia. *FMM*, 52(4):773–782, 1981.
- [36] Schastlivtsev V.M., Iakovleva I.L., and Romashev L.N. Élektronnomikroskopicheskoe issledovanie struktury kristallov martensita, zarodivshikhsia pod deístviem impul'snogo magnitnogo polia. *FMM*, 52(2):271–279, 1983.
- [37] Serebriakov V.G. and Éstrin É.I. Pereokhlazhdenie „vzryvnogo“ martensitnogo prevrashcheniia v monokristallakh splavov Fe-Ni. *DAN SSSR*, 237:322–324, 1977.
- [38] Haush G. and Warlimont H. Single crystalline elastic constants of ferromagnetic face centered cubic Fe-Ni invar alloys. *Acta Met.*, 21(4):401–414, 1973.
- [39] Delaey L., Gobin P.F., Guenin G., and Warlimont H. Premartensitic phenomena. *Proceedings of the International Conference on Martensitic Transformations ICOMAT-79*, pages 400–414, 24–29 June, 1979.
- [40] Hallman E.D. and Brockhause B.N. Crystal dynamics of nickel-iron and copper-zinc alloys. *Canadian Journ. Phys.*, 47(10):11–17, 1969.

- [41] Endoh Y. Lattice dynamics in ferromagnetic invar alloys. *J. Magn. and Magn. Mat.*, (10):177–182, 1969.
- [42] Zverev V.M. and Silin V.P. Zavisimost' skorosti zvuka ot namagnichenosti v ferromagnitnykh metallakh. Preprint T-19272. M.: FI AN SSSR.
- [43] Zverev V.M. and Silin V.P. K invarnoi probleme. *Kratkie soobshcheniia po fizike*, (6):46–49, 1984.
- [44] Cech R.E. and Turnbull D. Heterogeneous nucleation of the martensitic transformation. *Trans. AIME*, 206:124–132, 1956.
- [45] Vintaikin E.Z. Martensitnye prevrashcheniia. *Itogi nauki i tekhniki. Metallovedenie i termicheskaiia obrabotka.*, 17:3–63, 1983.
- [46] Iurchikov E.E. and Men'shikov A.Z. Issledovanie sostoianii austenita pered martensitnym prevrashcheniem metodom éffekta messbauéra. *FMM*, 32(1):168–170, 1971.
- [47] Tiapkin Iu. D., Pushin V.G., Romanova P.P., and Buinov N.N. Issledovanie struktury γ - i α -faz v splavakh zhelezo-nikel' vblizi tochki martensitnogo prevrashcheniia. 1. diffuznoe rasseianie élektronov i rentgenovskikh lucheí. *FMM*, 41(5):1040–1047, 1976.
- [48] Kondrat'ev V.V. and Pushin V.G. Predperekhodnye sostoianii v splavakh vblizi martensitnykh prevrashchenií. *Fazovye prevrashcheniia i struktura metallov i splavov*. Sverdlovsk: UNTs AN SSSR, pages 18–25, 1982.
- [49] Sarrak V.I. and Suvorova S.O. Ob osobennostiakh sostoianii austenita v predmartensitnom intervale temperatur. *Izv. AN SSSR, Metally*, (6):90–97, 1982.
- [50] Kondrat'ev V.V. O termodinamicheskoi ustoičivosti strukturykh sostoianii pri martensitnykh prevrashcheniiax. *FMM*, 47(1):102–109, 1979.
- [51] Falk F. Ginzburg-Landau theory and solitary waves in shape-memory alloys. *Z. Phys. B.*, 54:159–167, 1984.
- [52] Krivoglaz M.A. Fluktuonnye sostoianii élektronov. *UFN*, III(4):618–654, 1973.
- [53] Roítburd A.L. Zarozhdenie na dislokatsiakh pri martensitnykh prevrashcheniiax. *DAN SSSR*, 256(1):80–84, 1981.
- [54] Gurevich A.B. and Mints R.G. Lokalizovannye volny v neodnorodnykh sredakh. *UFN*, 142(1):61–84, 1984.

- [55] Petrov Iu. N. Defekty i bezdiffuzionnoe prevrashchenie v stali. Kiev: Naukova dumka, 1978.
- [56] Kashchenko M.P. and Vereshagin V.P. Dynamic lattice stability during reconstructive martensitic transformations in the phonon maser model. Phys.Met. Metall., 58(3):28–34, 1984.
- [57] Roítburd A.L. Neutron scattering study of the magnetic structure of cupric oxide. FTT, 10(12):3619–3627, 1968.
- [58] Krizement O., Gudremon É., and Vefer F. K termodinamike austenitno-martensitnogo prevrashcheniia. In Fazovye prevrashcheniia v stali, pages 263–271. M.:Metallurgizdat, 1961.
- [59] Mogutnov B.M., Tomilin I.A., and Shvartsman L.A. Termodinamika zhelezo-uglerodistykh splavov. M.: Metallurgiiia, 1972.
- [60] Landau L.D. and Lifshits E.M. Statisticheskaiia fizika. M.: Nauka, 1976.
- [61] Ziner K. Rol' éntropii v stabilizatsii faz. In Ustoíchivost' faz v metallakh i splavakh, pages 96–109. M.:Mir, 1970.
- [62] Dovgopol S.P. and Zaborovskaia I.A. Élektronnaia struktura, magnetizm i stabil'nost' faz 3d-metallou i splavov v tverdom i zhidkom sostoianiiakh. Obsory po teplofizicheskim svoístvam veshchestv. M.: IVTAN, 1982.
- [63] Miodownik A.P. The effect of magnetic transformation on phase diagrams. Bull. Alloys Phase Diagr., 2:406–412, 1982.
- [64] Hasegawa H. and Pettifor D.G. Microscopic theory of the temperature – pressure phase diagram of iron. Phys. Rev. Let., 50:130–133, 1983.
- [65] Barret Ch.S. and Massal'skií T.B. Struktura metallov. PartII. M.: Metallurgiiia, 1984.
- [66] Roítburd A. L. Teoriiia formirovaniia geterofaznoí struktury pri fazovykh prevrashcheniiax v tverdom sostoianii. UFN, 113(1):105–128, 1974.
- [67] Patel J.R. and Cohen M. Criterion for the action of applied stress in the martensitic transformation. Acta Metall., 1(5):531–538, 1953.
- [68] Kosenko N.S., Roítburd A.L., and Khandros L.G. Vliianie vneshnego napriazheniia na termodinamiku i strukturu produktov martensitnogo prevrashcheniia. In Martensitnye prevrashcheniia: Dokl. mezhdunar. konf."ICOMAT-77", pages 74–78. Kiev: Naukova dumka, 1978.

- [69] Pankova M.N. and Roítburd A.L. Orientiruiushchee vliianie vneshnego napriazheniia na martensitnoe prevrashchenie v splavakh na osnove zheleza. FMM, 58(4):716–726, 1984.
- [70] Roítburd A.L. O nekotorykh ocobennostiakh rosta kristallov v kondensirovannykh sistemakh. Kristallografiia, 7(8):292–299, 1962.
- [71] Landau L.D. and Lifshits E.M. 'Elektrodinamika sploshnykh sred. M.: Nauka, 1982.
- [72] Roítburd A.L. Osobennosti razvitiia fazovykh prevrashchenií v kristallakh. In Problemy sovremennoí kristallografi, pages 345–369. M.: Nauka, 1975.
- [73] Khirt Dzh. and Lote I. Teoriia dislokatsií. M.: Atomizdat, 1972.
- [74] Kottrel A. Teoriia dislokatsií. M.: Mir, 1969.
- [75] Udarnye volny i iavleniia vysokoskorostnoí deformatsii metallov. M.: Metallurgiiia, 1984.
- [76] Machlin E.S. and Cohen M. Habit phenomenon in the martensitic transformation. Trans. AIME, 191:1019–1029, 1951.
- [77] Meyers M.A. On the growth of lenticular martensite. Acta Metall., 28:757–770, 1980.
- [78] Lokshin F.L. Primenenie teorii udarnykh voln k opisaniiu protsessa rosta kristallov martensita. In Nauchnye doklady vysheí shkoly, number 1, pages 146–150. M.: Metallurgiiia, 1969.
- [79] Crussard C. Application de theorie de ondes explosives a la croissance de la martensite. Compt. Rend., 240(24):2313–2315.
- [80] Rabinovich M.I. and Trubetskov D.I. Vvedenie v teoriu kolebanií i voln. M.: Nauka, 1984.
- [81] Wasilewski R.J. On the nature of the martensitic transformation. Metall.Trans., 6A:1405–1418, 1975.
- [82] Kayser U. The activation of the martensitic phase transformation in ferrous alloys by stimulated emission of phonons. J. Phys. F., 2:60–64, 1972.
- [83] Zvelto O. Fizika lazerov. M.: Mir, 1979.
- [84] Panin V.E., Egorushkin V.E., Khon Iu.A., and Elsukova T.F. Atomvakansionnye sostoianiia v kristallakh. Izv. vuzov SSSR. Ser. Fizika, (12):5–28, 1982.

- [85] Zhang J. The non-equilibrium phase transition theory of martensitic transformation. *J. Phys. F.*, 14(3):769–783, 1984.
- [86] Naí Dzh. *Fizicheskie svoítva kristallov*. M.: Mir, 1967.
- [87] Zaíman Dzh. *Prinzipy teorii tverdogo tela*. M.: Mir, 1974.
- [88] Kashchenko M.P. Lazernaia model' martensitnogo prevrashcheniia v splavakh perekhodnykh metallov. In *Martensitnye prevrashcheniia v metallakh i splavakh: Dokl. mezhdunar. konf. „ICOMAT-77“*, pages 137–141. Kiev: Naukova Dumka, 1979.
- [89] Kashchenko M.P. and Mints R.I. Mechanism of martensitic transformation due to the disequilibrium of the electron-phonon system. *JETP Lett.*, 26(6):309–310, 1977.
- [90] Kashchenko M.P. Sravnenie dvukh istochnikov neravnovesnosti élektronnoí podsystemy pri uchete zatukhaniia élektronov. *Izv. vuzov SSSR. Ser. Fizika*, (3):113–114, 1982.
- [91] Afanas'ev A.M. and Kagan Iu. M. Ob osobennostiakh v zakone dispersii fononov, sviazannykh s élektron-fononnym vzaimodeístviem. *ZhÉTF*, 43(10):1457–1463, 1962.
- [92] Bulaevskii L.N. Strukturnyi (paíerlsovskii) perekhod v kvaziodnomernykh sistemakh. *UFN*, 115:263–300, 1975.
- [93] Egorushkin V.E., Kulkov S.N., and Kulkova S.E. Electronic structure and the theory of phase transformation in NiMn. *Physics*, 123:61–68, 1983.
- [94] Kulikov N.I. and Tugushev V.V. Volny spinovoí plotnosti i zonnyí antiferromagnetizm v metallakh. *UFN*, 144(4):643–680, 1984.
- [95] Gor'kov L.P. Ob osobennostiakh élektronnogo spektra soedinenii so strukturoí β -W. *Pis'ma v ZhÉTF*, 20(8):571–574, 1974.
- [96] Gor'kov L.P. and Dorokhov O.N. Sverkhprovodiashchie svoítva i strukturnyí perekhod v soenineniiax s reshetkoí A-15. *ZhÉTF*, 71(5(11)):1934–1950, 1976.
- [97] Vonsovskii S.V., Iziumov Iu.A., and Kurmaev Z.Z. *Sverkhprovodimost' perekhodnykh metallov, ikh splavov i soedinenii*. M.: Nauka, 1977.
- [98] Léks M. *Fluktuatsii i kogerentnye iavlénia*. M.: Mir, 1975.
- [99] Kashchenko M.P. and Mints P.I. Kolebatel'nye analogi deformatsii beína i morfoogiia martensita v tverdykh pastvorakh sistem γ (Fe-Ni). *FTT*, 19(2):329–334, 1977.

- [100] Erenreíkh G. and Shvarts L. *Élektronnaia struktura splavov*. M.: Mir, 1976.
- [101] Vediaev A.V. Metod kogerentnogo potentsiala v teorii neuporiadochennykh splavov. *TMF*, 31(3):392–404, 1977.
- [102] Egorushkin V.E. and Kul'ment'ev A.I. *Élektronnaia struktura splavov perekhodnykh metallov s proizvol'nym dal'nim poriadkom*. *Izv. vuzov SSSR. Ser. fizika*, (12):29–49, 1982.
- [103] Kallueí D. *Teoriia énergeticheskoi zonnoi struktury*. M.: Mir, 1969.
- [104] Slater J.C. and Koster G.F. Simplified L C A O method for potential problem. *Phys. Rev.*, 94:1498–1512, 1954.
- [105] Dzhons G. *Teoriia zon Brilliuéna i élektronnye sostoiانيا v kristallakh*. M.: Mir, 1968.
- [106] Wood I.H. Energy bands in iron via the augmented plane wave method. *Phys. Rev.*, 126:517–527, 1962.
- [107] Bagayoko D. and Callaway J. Lattice - parameter dependence of ferromagnetism in bcc and fcc iron. *Phys. Rev.B.*, 28:5419–5422, 1983.
- [108] Zornberg E.I. Band structure and fermi surface of ferromagnetic nickel. *Phys. Rev.B.*, 1:244–251, 1970.
- [109] Connolly J.W.D. Energy bands in ferromagnetic nickel. *Phys. Rev.*, 159:415–418, 1967.
- [110] Jarlborg T. and Freeman A.J. Self-consistent semi-relativistic energy band structure of fcc and tetragonal Ni metals. *J. Magn. Magn. Mater*, 22(1):6–13, 1980.
- [111] Snow E.C. and Waber J.T. The APW energy bands of the body centered and face centered cubic modifications of the 3d-transition metals. *Acta Metall.*, 17:623–635, 1969.
- [112] Roy D.M. and Pettifor D.G. Stoner theory support for the two-state hypothesis for iron. *J.Phys.F.*, 7:183–187, 1977.
- [113] Samsonov G.B., Priadko I.F., and Priadko L.F. *Élektronnaia lokalizatsiia v tverdom tele*. M.: Nauka, 1976.
- [114] Liakutkin A.V., Grigorovich V.K., and Ivakhnenko I.S. Issledovanie fazovykh perekhodov chistogo zheleza metodom magnitnoi vospriimchivosti. *DAN SSSR*, 257(2):398–400, 1981.

- [115] Liakutkin A.V. Vozmozhnost' izomorfnoġo okhlazhdeniia chistogo zheleza posle kristallizatsii iz rasplava. FMM, 54(1):129–136, 1982.
- [116] Wilkinson M.K. and Shull C.G. Neutron diffraction studies on iron at high temperatures. Phys. Rev., 103:516–524, 1956.
- [117] Brown P.J. and et al. Ferromagnetic correlations in both the α - and γ -phases of paramagnetic iron. J. Magn. Magn. Mater, 30:335–339, 1983.
- [118] Grebennikov V.I., Prokop'ev Iu.I., Sokolov O.B., and Turov E.A. Metod lokal'nykh fluktuatsii v teorii magnetizma perekhodnykh metallov. FMM, 52(4):679–694, 1981.
- [119] Tauer K.J. and Weiss R.J. Unusual magnetic structure of face-centered cubic Fe. Bull. Amer. Phys. Soc., 6:125, 1961.
- [120] Kaufman L., Clougherty E.V., and Weiss R.J. The lattice stability of metals - III iron. Acta Metal., 11:323–335, 1963.
- [121] Poulsen U.K., Kollart J., and Andersen O.K. Magnetic and cohesive properties from canonical bands. J. Phys., 6(9):241–247, 1976.
- [122] Kübler J. Magnetic moments of ferromagnetic and anti-ferromagnetic bcc and fcc iron. Phys. Lett., 81A(1):81–83, 1981.
- [123] Kulikov N.I. Élektronnaia struktura perekhodnykh metallov pod davleniem. Izv. vuzov SSSR. Ser. Fizika, (12):50–62, 1982.
- [124] Éiřhinskiġ E.R. Dva élektronnykh sostoianiia atomov zheleza v ego gtsk i otsk modifikatsiakh. Dep. v VINITI, (number 1082), 1984.
- [125] Keller J., Fritz J., and Garritz A. Cluster method multiple scattering calculation of density of states of liquid transition metals, rare earth metals and their alloys. J. de Phys., 35(5):379–385, 1974.
- [126] Kondorskiġ E.I. Zonnaia teoriia magnetizma. Part I. M.: Izd-vo Mosk.un-ta, 1976.
- [127] Krenkell A. and Wong K. Poverkhnost' Fermi. M.: Atomizdat, 1978.
- [128] Kashchenko M.P. Interpretation of some characteristic morphological indicators of martensite of systems Fe-Ni, Fe-C using the phonon maser model. Phys.Met. Metall., 58(5):24–31, 1984.
- [129] Vereshchagin V.P. and Kashchenko M.P. Optimal'naia struktura zonnogo spektra élektronov v modeli fononnoġo mazera. Dostizheniia v oblasti metallovedeniia i termicheskoi obrabotki metallov. Tez. zonal'noi konf. (IX Ural'skoi shkoly metallovedov - termistov). Sverdlovsk: In-t fiziki metallov UNTs AN SSSR, pages 93–95, 1985.

- [130] Vereshchagin V.P. and Kashchenko M.P. Principles of selection of pairs of electronic states which are potentially active in phonon generation. *Phys.Met. Metall.*, 61(2):23–30, 1986.
- [131] Khanin Ia.I. *Kvantovaiia radiofizika*. M.: Sov. radio, 1975.
- [132] Khaken G. and Vaídlikh V. *Kvantovaiia teoriia lazera*. In *Kvantovye fluktuatsii izlucheniia lazera*, pages 143–205. M.: Mir, 1974.
- [133] Khaken G. *Sinergetika*. M.: Mir, 1980.
- [134] Makomber Dzh. *Dinamika spektroskopicheskikh perekhodov*. M.: Mir, 1979.
- [135] Khaken G. *Statistika lazernogo izlucheniia s toчки zreniia teorii fazovykh perekhodov*. In *Spektroskopiia opticheskogo smeshcheniia i korreliatsiia fotonov*, pages 493–517. M.: Mir, 1978.
- [136] Taker Dzh. and Rémp-ton V. *Giperzvuk v fizike tverdogo tela*. M.: Mir, 1975.
- [137] *Teploprovodnost' tverdykh tel. Spravochnik*. M.: Ènergoatomizdat, 1984.
- [138] Gantmakher V.F. and Levinson I.B. *Rasseianie nositelei toka v metallakh i poluprovodnikakh*. M.: Nauka, 1984.
- [139] Agranat M.B., Ashitkov S.I., Granovskií A.B., and Rukman G.I. *Vzaimodeístvie pikosekundnykh lazernykh impul'sov s élektronnoi spinovoi i fononnoi podsystemami nikelia*. *ZhÉTF*, 86(4):1376–1379, 1984.
- [140] Kashchenko M.P. and Mints R.I. *Mikroskopicheskií mekhanizm martensitnogo prevrashcheniia v sisteme Fe-Ni*. *ZhÉTF*, 75(6(12)):2280–2289, 1978.
- [141] Kashchenko M.P. *Usloviia generatsii voln, sopostavliaemykh deformatsii Beína*. *FMM*, 49(5):937–946, 1980.
- [142] Vereshchagin V.P. and Kashchenko M.P. *Vydelenie markovskogo priblizheniia v metode neravnovesnogo statisticheskogo operatora*. *Fizicheskie metody issledovaniia tverdogo tela*. Sverdlovsk, (3):57–67, 1979.
- [143] Vereshchagin V.P. and Kashchenko M.P. *Markovskaia forma neravnovesnogo statisticheskogo operatora dlia sistem so slabym vzaimodeístviem*. *TMF*, 42(1):133–138, 1980.
- [144] Vereshchagin V.P. and Kashchenko M.P. *Postroenie kineticheskikh uravnenii dlia neravnovesnykh kvantovykh sistem*. Sverdlovsk. *Rukopic' predstavlena Ural. lecotekh. in-tom. Dep. v VINITI 2 avg. 1979, No. 2893-79*, 1979.

- [145] Vereshchagin V.P. and Kashchenko M.P. Kineticheskie uravneniia dlia sistemy vzaimodeistvuiushchikh élektronov i fononov. Sverdlovsk. Rukopic' predstavlena Ural. lecotekh. in-tom. Dep. v VINITI 7 dek. 1979, No. 4177-79, 1979.
- [146] Vereshchagin V.P. and Kashchenko M.P. Prostranstvenno-lokal'nye kineticheskie uravneniia dlia élektronov i fononov. Usloviia generatsii uprugikh voln. Sverdlovsk. Rukopic' predstavlena Ural.lecotekh. in-tom. Dep. v VINITI 5 avg. 1980, No. 3455-80, 1980.
- [147] Vereshchagin V.P. Osobennosti neravnovesnoí dinamiki sistemy vzaimodeistvuiushchikh élektronov i fononov v tverdykh telakh:. Diss. ... kand. fiz.-mat. nauk. Sverdlovsk: Ural. politekhn. in-t, 1980.
- [148] Zubarev D.N. Neravnovesnaia statisticheskaiia termodinamika. M.: Nauka, 1971.
- [149] Kalashnikov V.P. Metod neravnovesnogo statisticheskogo operatora i ego prilozhenie k kinetike paramagnitnykh iavlenii v provodiashchikh kristallakh. Diss.... dokt. fiz.-mat. nauk. Sverdlovsk: In-t fiziki metallov UNTs AN SSSR, 1971.
- [150] Zubarev D.N. and Kalashnikov V.P. Teoriia vozmushchenii i integral'nye uravneniia dlia neravnovesnykh statisticheskikh operatorov. TMF, 5(3):406–416, 1970.
- [151] Pustovoit V.I. Vzaimodeistvie élektronnykh potokov s uprugimi volnami reshetki. UFN, 97(2):257–306, 1969.
- [152] Bonch-Bruevich V.L. and Kalashnikov S.G. Fizika poluprovodnikov. M.: Nauka, 1977.
- [153] Zheru I.I. Nizkochastotnye rezonansy éksitonov i primesnykh tsentrov. Kishinev: Shtiintsa, 1976.
- [154] Kopvillem U.Kh. and Saburova R.V. Paraélektricheskií rezonans. M.: Nauka, 1982.
- [155] Andreev A.V., Emel'ianov V.I., and Il'inskií Iu.A. Kollektivnoe spontannoe izluchenie (sverkhizluchenie Dike). UFN, 131(4):653–694, 1980.
- [156] Bogachev I.N. and Egolaev V.F. Struktura i svoistva zhelezomargantsevykh splavov. M.: Metallurgiiia, 1973.
- [157] Zyrianov P.S. and Klinger M.I. Kvantovaiia teoriia iavlenii élektronnogo perenosa v kristallicheskiikh poluprovodnikakh. M.: Nauka, 1976.

- [158] Weiss R.J. and Marotta A.S. Spin-dependence of the resistivity of magnetic metals. *J. Phys. Chem. Sol.*, 9:302–309, 1959.
- [159] Vonsovskii S.V. *Magnetizm*. M.: Nauka, 1971.
- [160] Auslender M.I. and Kalashnikov V.P. Proizvodiashchii funktsional dlia neravnovesnoi sistemy élektronov i fononov. *TMF*, 25(3):370–381, 1975.
- [161] Kheine V., Cohen M., and Uéir D. *Teoriia pseudopotentsiala*. M.: Mir, 1973.
- [162] Mirzaev D.A., Morozov O.P., and Shteinberg M.M. O sviazi prevrashchenii v zheleze i ego splavakh. *FMM*, 36(3):560–568, 1973.
- [163] Shteinberg M.M., Mirzaev D.A., and Ponomareva T.N. Gamma al'fa prevrashchenie pri okhlazhdenii splavov zhelezo-marganets. *FMM*, 43(1):166–172, 1977.
- [164] Mirzaev D.A., Shteinberg M.M., Ponomareva T.N., and i dr. Fasovye $\gamma \rightarrow \alpha$ prevrashcheniia v binarnykh splavakh zheleza s med'iu, kobal'tom, ruteniem i platinoi. *FMM*, 51(2):364–375, 1981.
- [165] Mirzaev D.A., Shteinberg M.M., Ponomareva T.N., and Schastlivtsev V.M. Vliianie skorosti okhlazhdeniia na polozhenie martensitnykh toчек. Uglerodistye stali. *FMM*, 47(1):125–135, 1981.
- [166] Mirzaev D.A., Shteinberg M.M., Ponomareva T.N., and Schastlivtsev V.M. Vliianie skorosti okhlazhdeniia na polozhenie martensitnoi tochki II. Legirovannye stali. *FMM*, 47(5):986–992, 1979.
- [167] Gudenaf D. *Magnetizm i khimicheskaiia sviaz*. M.: Metallurgiiia, 1968.
- [168] Akhiezer A.I. *Obshchaia fizika. Élektricheskie i magnitnye iavleniia: spravochnoe posobie*. Kiev: Nauk. dumka, 1981.
- [169] Beilin V.M., Zeinalov T.I., and Rogel'berg I.L. Ob opredelenii vremeni élektron-fononnoi relaksatsii v nikle i ego splavakh. *Mekhanizmy relaksatsionnykh iavlenii v tverdykh telakh*. Kaunas: Kaunas.politekh. in-t, pages 44–46, 1974.
- [170] Vnukovskii N.I. *Izluchatel'nye kharakteristiki khromistykh splavov: Avtoref. Diss. ... kand. fiz.-mat. nauk*. Sverdlovsk: Ural. politekh. in-t, 1982.
- [171] Noskov M.M. *Opticheskie i magnetoopticheskie svoistva metallov*. Sverdlovsk: UNTs AN SSSR, 1983.
- [172] Shirokovskii V.P., Kirillova M.M., and Shilkova N.A. Anomaliia opticheskogo pogloshcheniia v zheleze. *ZhÉTF*, 82(3):784–792, 1982.

- [173] Bolotin G.A., Noskov M.M., and Sasovskaia I.I. Mezkhzonnoe opticheskoe pogloshchenie v ferromagnitnom kobal'te. Sviaz' s plotnost'iu sostoianii. FMM, 35(4):699–705, 1973.
- [174] Kaufman L. and Cohen M. The martensitic transformation in the iron-nickel system. Trans. AIME, 206:1393–1401, 1956.
- [175] Sasovskaia I.I., Noskov M.M., and Men'shikov A.Z. Opticheskie i rentgenovskie spektry splava zheleza s 30% nikelia v gtsk i otsk strukturnykh sostoianiiakh. FMM, 27(2):272–279, 1969.
- [176] Bendic W. and Pepperhoff W. Temperature dependence of the electrical resistivity of fcc iron alloys. J. Phys. F. Metal. Phys., 8(12):2535–2544, 1978.
- [177] Kidin I.N., Shtremel' M.A., and Andreev Iu.G. Elektrosoprotivlenie uglerodistogo martensita. FMM, 28(5):874–878, 1969.
- [178] Andreev Iu.G. Issledovanie svoistvu uglerodistogo martensita: Diss. ... kand. tekh. nauk. M.: MISiS, 1969.
- [179] Kekalo I.B. Fizicheskie svoistva metallov i splavov. M.: MISiS, 1979.
- [180] Krivoglaz M.A. Difraktsiia rentgenovskikh lucheí i neítronov v nei-deal'nykh kristallakh. Kiev: Nauk. dumka, 1983.
- [181] Nakamura Y. The invar problem. I E E E Trans. Magn., MAG.-12:278–291, 1976.
- [182] Tanji Y. and Nakamura Y. Steinemann anomalous elastic properties of Fe-Ni (fcc) alloys and their invar. Physica, B 119:109–114, 1983.
- [183] Kharrison U. Élektronnaia struktura i svoistva tverdykh tel, volume 2. M.: Mir, 1983.
- [184] Kamenetskaia D.S., Piletskaia I.B., and Shiriaev V.I. Zhelezo vysokoí stepeni chistoty. M.: Metallurgiiia, 1978.
- [185] Zaíman Dzh. Modeli besporiadka. M.: Mir, 1982.
- [186] Gel'd P.V., Dovgopol S.P., Dovgopol M.G., and Radovskij I.Z. Magnitnaia vospriimchivost' i struktura blizhnego poriadka zhelezo-uglerodistykh rasplavov. DAN SSSR, 236(4):853–856, 1977.
- [187] Kalinovich D.F., Kovenskií I.I., and Smolin M.D. Sostoiianie ugleroda, rastvorenogo v γ -zheleze. Izv. AN SSSR. Metally, (4):105–107, 1974.

- [188] Mirzaev D.A., Ponomareva T.N., and Shteinberg M.M. O stupeniakh prevrashcheniia v splavakh zheleza, vyivliaiushchikhsia pri uvelichenii skorosti okhlazhdeniia do $4 \cdot 10^5$ grad/sek. In *Mezhdunar. konf., Martensitnye prevrashcheniia*. Tez.dokl. Kiev, pages 142–143, 1977.
- [189] Kashchenko M.P. Soglasovanie kontsentratsionnoi zavisimosti temperatur martensitnykh prevrashchenii v sistemakh Fe-Ni, Fe-Mn s usloviiami generatsii v modeli fononnogo mazera. *FMM*, 50(3):671–672, 1980.
- [190] Kashchenko M.P. and Èishinskiĭ E.R. Determination of the optimum temperature for fonon generation by non-equilibrium électrons in binary alloys of iron. *Phys.Met. Metall.*, 56(4):47–54, 1983.
- [191] Èishinskiĭ E.R. Magnitnye i magnitoob“emnye svoístva Fe i Fe-Ni splavov v modeli vydelennykh sostoianii atomov zheleza: Diss. ... kand. fiz.-mat. nauk. Sverdlovsk: Ural. politekhn. in-t, 1984.
- [192] Shriifer Dzh. *Teoriia sverkhprovodimosti*. M.: Nauka, 1970.
- [193] Fedorov F.I. *Teoriia uprugikh voln v kristallakh*. M.: Nauka, 1965.
- [194] Novikov I.I. *Defekty kristallicheskogo stroeniia metallov*. M.: Metallurgii, 1975.
- [195] Marder A.R. and Krauss G. The formation of low-carbon martensite in Fe-C alloys. *Trans. Quart.*, 62(4):957–964, 1969.
- [196] Schastlivtsev V.M. Strukturnye osobennosti martensita v konstruktsionnykh staliakh. *FMM*, 33(2):326–334, 1972.
- [197] Schastlivtsev V.M. Élektronnomikroskopicheskoe issledovanie struktury martensita konstruktsionnykh stalei. *FMM*, 38(4):326–334, 1974.
- [198] Schastlivtsev V.M., Koptseva N.V., and Artemova T.V. Élektronnomikroskopicheskoe issledovanie struktury martensita v malouglerodistykh splavakh zheleza. *FMM*, 41(6):1251–1260, 1976.
- [199] Izotov V.I. Morfologiia i kristallogometriia rechnogo (massivnogo) martensita. *FMM*, 34(1):123–132, 1972.
- [200] Izotov V.I. Struktura zakalenoĭ konstruktsionnoĭ stali. Sostoianie peregreva. *FMM*, 39(4):801–814, 1975.
- [201] Éterashvili T.V., Spacckiĭ M.N., Utevskii L.M., and Tulikov G.N. Razvitie plasticheskoi deformatsii paketnogo martensita. *FMM*, 46(4):772–780, 1978.

- [202] Éterashvili T.V., Utevskii L.M., and Spacckii M.N. Struktura paketnogo martensita i lokalizatsiia ostatochnogo austenita v konstruktsionnykh stalakh. FMM, 48(4):807–815, 1979.
- [203] Andreev Iu.G., Devchenko L.N., Shelekhov E.V., and Shtremel' M.A. Upakovka kristallov martensita v psevdomonokristalle. DAN SSSR, 237(3):574–576, 1977.
- [204] Andreev Iu.G., Devchenko L.N., Zarkova E.I., and Shtremel' M.A. Kristallogometriia martensitnogo sdviga v krupnom pakete. FMM, 56(4):783–790, 1983.
- [205] Sandvic B.P.I. and Wayman C.M. Electron microscopy studies of martensitic. J. Phys. (Fr.), 43(12):557–562, 1982.
- [206] Urusovskaia A.A. Mekhanicheskie svoítva kristallov. In *Sovremennaiia kristallografiia*, volume 4, pages 47–152. 1981.
- [207] Georgieva I.Ia. and Nikitina I.I. Izotermicheskoe i atermicheskoe martensitnye prevrashcheniia. MiTOM, (5):68–72, 1972.
- [208] Men'shikov A.Z. O vliianii magnitnogo sostoianiia austenita na kharakter martensitnogo prevrashcheniia. FMM, 40(4):853–856, 1975.
- [209] Zolotarevskii I.V., Snezhnoi V.L., and Sheiko L.M. O magnitostrikt-sii paraprotsessa austenitnykh splavov vblizi martensitnoi točki. FMM, 47(6):1312–1313, 1979.
- [210] Zolotarevskii I.V., Kosenko N.S., and Krivoglaz M.A. Vliianie magnitostrikt-sii na sdvig točki martensitnogo prevrashcheniia v sil'nom magnitnom pole. Metallofizika, 1(2):17–22, 1979.
- [211] Belov K.P. Uprugie, teplovyie i élektricheskie iavleniia v ferromagnitnykh metallakh. M.-L.: GITTL, 1951.
- [212] Romashev L.N. Vliianie magnitnogo sostoianiia γ -fazy stalei na ($\gamma \rightarrow \alpha$) – martensitnoe prevrashchenie pod deístviem magnitnogo polia. In *Fazovye prevrashcheniia i struktura metallov i splavov*, pages 32–39. Sverdlovsk : UNTs AN SSSR, 1982.
- [213] Zolotarevskii I.V., Snezhnoi V.L., Georgieva I.Ia., and Matiushenko L.A. Magnitostrikt-siia austenita zhelezo-nikel'-margantsevykh splavov, obladaiushchikh dvoínoi kinetikoí martensitnykh prevrashchenii. FMM, 51(3):669–672, 1981.
- [214] Zolotarevskii I.V., Snezhnoi V.L., and Sheiko L.M. Magnitostrikt-siia austenita zhelezo-nikel'-margantsevykh splavov i martensitnoe prevrashchenie pod deístviem sil'nogo magnitnogo polia. FMM, 55(3):548–553, 1983.

- [215] Zavadskii É.A. and Val'kov V.I. *Magnitnye fazovye perekhody*. Kiev: Naukova dumka, 1980.
- [216] Èíshinskií E.R. and Kashchenko M.P. *Izmenenie skorosti zvuka za schet pereraspredeleniia élektronov pri magnitnom fazovom prevrashchenii*. ZhTF, 51(11):2396–2398, 1981.
- [217] Èíshinskií E.R. and Kashchenko M.P. *Izmenenie skorosti zvuka za schet pereraspredeleniia élektronov v slabykh kollektivizirovannykh ferromagnetikakh, imeiushchikh pik v plotnosti sostoianií d-élektronov*. Tez. dokl. XV Vsesoiuz. konf. po fizike magnitnykh iavlenií. Perm': UNTs AN SSSR. Part I, pages 34–35, 1981.
- [218] Crangle J. and Hallam G.C. *The magnetization of face centered cubic and body centered cubic iron + nickel alloys*. Proc. Roy. Soc., A. 272:119–132, 1963.
- [219] Tikadzumi S. *Fizika ferromagnetisma. Magnitnye svoístva veshchestva*. M.: Mir, 1983.
- [220] Zakharov A.I. *Vliianie temperatury na rentgenovskii fotoélektronnyí spektr valentnykh élektronov splava Fe-Ni invarnogo sostava*. Pis'ma v ZhÉTF, 24:276–278, 1976.
- [221] Zakharov A.I. and Narmonev A.G. *Temperaturnye izmeneniia v rentgenovskikh fotoélektronnykh spektrakh valentnykh i ostovnykh élektronov splava Fe-Ni invarnogo sostava*. Metallofizika, 4:113–115, 1982.
- [222] Vertkheím G. *Éffekt Messbauéra*. M.: Mir, 1966.
- [223] Iurchikov E.E. *Issledovanie metodom IaGR magnitnogo i strukturnogo sostoiania Fe-Ni splavov: Avtoref. diss. ... kand. fiz.-mat. nauk*. Sverdlovsk: In-t fiziki metallov UNTs AN SSSR, 1971.
- [224] Hesse J., Müller J.B., Wiechmann B., and Ullrich H. *Local magnetization of Fe atoms in Fe-Ni alloys*. J. Magn.Magn.Mater., 15-18. Part 3:1195–1196, 1980.
- [225] Nakamura Y. *The invar problem*. IEEE Trans.Magn., MAG-12:278–291, 1976.
- [226] Hasegawa H. and Kanamori J. *An application of the coherent potential approximation to ferromagnetic alloys*. J. Phys. Soc. Jap., 31:382–393, 1971.
- [227] Men'shikov A.Z. and Shestakov V.A. *Magnitnye neodnorodnosti v invarnykh zhelesonikelevykh splavakh*. FMM, 43(4):722–733, 1977.

- [228] Goman'kov V.I., Mokhov B.N., and Nogin N.I. Kotsentratsionnye ferro-antiferromagnitnye perekhody v sistemakh na osnove Fe. *ZhETF*, 77(2(8)):630–639, 1979.
- [229] Kuz'min N.N. and Men'shikov A.Z. Nizkotemperaturnoe kriticheskoe rasseyanie neitronov v splavakh zhelezo-nikel' i nikel'-marganets. *FMM*, 49(2):433–437, 1980.
- [230] Sidorov S.K. and Doroshenko A.V. O magnitnoi strukture splavov NiFe, imeiushchikh granetsentrirovannuiu kubicheskuiu reshetku. *FMM*, 19(5):786–788, 1965.
- [231] Iziumov Iu.A. and Medvedev M.V. *Teoriia magnitouporiadochennykh kristallov s primesiami*. M.: Nauka, 1970.
- [232] Kondorskiĭ E.I. O prichinakh osobennostei fizicheskikh svoistv invarnykh splavov. *ZhETF*, 37:1819–1820, 1959.
- [233] Hatherly M., Hirakawa K., Lowde R.D., and et al. Spin wave energies and exchange parameters in iron-nickel alloys. *Proc. Phys. Soc.*, 84:55–62, 1964.
- [234] Dubinin S.F., Teploukhov S.G., and Sidorov S.K. Neitron-difraktsionnye efekty iskazhenii struktury splava Ni – 67,7 at.% Fe v magnitouporiadochenom sostoianii. *FMM*, 55(6):1160–1164, 1983.
- [235] Dubinin S.F., Teploukhov S.G., and Sidorov S.K. Utochnenie parametrov sverkhstruktury Fe-Ni invarov. *FMM*, 59(6):1158–1164, 1985.
- [236] Dubinin S.F., Teploukhov S.G., Evtukh A.A., Koliadin V.P., Skorobogatov V.P., and Sidorov S.K. Atomnaia i magnitnaia sverkhstruktura ostatochnogo austenita v splave Ni – 66,8 at.% Fe s nezavershennym γ – α prevrashcheniem. *FMM*, 59(6):1165–1176, 1985.
- [237] Dubinin S.F., Izyumov Yu.A., Sidorov S.K., Syromyatnikov V.N., and Teploukhov S.G. The role of the incommensurable atomic structure in the mechanism of the martensite transformation in the invar alloys. *Phys.stat. sol. (a)*, 67(1):75–82, 1981.
- [238] Dubinin S.F., Teploukhov S.G., Izyumov Yu.A., Syromyatnikov V.N., and Sidorov S.K. O simmetriinoi sviazi faz pri martensitnom prevrashchenii invarnykh Fe-Ni splavov. *FMM*, 50(6):1276–1284, 1980.
- [239] Bukhalenkov V.V. Izmenenie elektronnoi struktury splavov Fe-Ni s GTsK reshetkoi pri magnitnom fazovom perekhode. *FMM*, 55(4):826–829, 1983.
- [240] Bukhalenkov V.V. Issledovanie magnitnogo i strukturnogo fazovykh perekhodov v Fe-Ni splavakh metodom IaGR: Diss. ... kand. fiz.-mat. nauk. Sverdlovsk: Ural. politekhn. ins-t, 1983.

- [241] Bernshtein M.L. Termomagnitnaia obrabotka stali. M.: Metallurgiiia, 1968.
- [242] Ermolenko A.S., Men'shikov A.Z., and Malinen P.A. Vozniknovenie odnoocnoi magnitnoi anizotropii pri martensitnom prevrashchenii v magnitnom pole. FMM, 26(1):76–80, 1968.
- [243] Blatt F. Fizika élektronnoi provodimosti v tverdykh telakh. M.:Mir, 1971.
- [244] Leont'ev A.A., Schastlivtsev V.M., and Romashev L.N. Gabitus i orientatsiia kristallov martensita, obrazuiushchikhsia pod deistviem magnitnogo polia. FMM, 58(5):950–957, 1984.
- [245] Varlimont Kh. and Dilei L. Martensitnye prevrashcheniia v splavakh na osnove medi, srebra i zolota. M.:Nauka, 1980.
- [246] Kashchenko M.P. Opisanie gabitusnykh ploskosteí (hh1) v volnovykh modeliakh rosta splavov na osnove medi, zolota i zheleza. Izv. vuzov SSSR. Ser. Fizika, (3):41–43, 1982.
- [247] Kashchenko M.P. Opisanie gabitusnykh ploskosteí v volnovykh modeliakh rosta martensita. gabitusy (225), (557), (925). Izv. vuzov SSSR. Ser. Fizika, (2):7–9, 1982.
- [248] Kashchenko M.P. The habit planes (hh1) description in wave models of the martensite growth for Cu-, Au- and Fe-based alloys. Abstract bulletin ICOMAT-82, Belgium, page 23, 1982.
- [249] Marri Dzh. Nelineinye differentsial'nye uravneniia v biologii. Lektsii o modeliakh. M.:Mir, 1983.
- [250] Iakhno V.G. Avtovolnovye protsessy v odnomernykh relaksatsionnykh sistemakh. Avtovolnovye protsessy v sistemakh s diffuziei. Gor'kií: In-t prikladnoi fiziki AN SSSR, pages 46–76, 1981.
- [251] Patashinskií A.Z. and Pokrovskií V.L. Fluktuatsionnaia teoriia fazovykh perekhodov. M.:Nauka, 1982.
- [252] Missol V. Poverkhnostnaia énergiiia razdela faz v metallakh. M.:Metallurgiiia, 1978.
- [253] Iakhno V.G. O raschete skorosti voln v vzbudimoi srede. Biofizika, 21(3):547–550, 1984.
- [254] Gilmor R. Prikladnaia teoriia katastrof. Kn. 1. M.: Mir, 1984.

- [255] Liubov B.Ia. and Roítburd A.L. Temperaturnye usloviia na poverkhnosti rastushchego martensitnogo kristalla. DAN SSSR, 131(4):809–812, 1960.
- [256] Lykov A.V. Teoriia teploprovodnosti. M.: Vysshiaia shkola, 1967.
- [257] Likhachev A.A. and Koval' Iu.N. O vozmozhnosti primeneniia fenomenologicheskoi teorii Landau dlia opisaniia martensitnykh prevrashchenii. Kiev: Institut metallofiziki AN USSR, 1983.
- [258] Fizicheskaiia akustika. T. 7/ Pod red. Mazona, U.M. M.: Mir, 1974.
- [259] Bobrov V.S. and Lebedkin M.A. Nabliudenie élektricheskikh éffektov pri nizkotemperaturnom dvoínikovanii niobii. Pis'ma v ZhÉTF, 38(7):334–336, 1983.
- [260] Likhachev V.A. Kooperativnaia plastichnost', obuslovlennaia dvizheniem granits razorientatsii i granits razdela faz. Izv. vuzov SSSR. Ser.Fizika, (6):83–102, 1982.
- [261] Kashchenko M.P. and Vereshchagin V.P. Dvizhenie granitsy martensitnogo kristalla kak avtovolnovoi protsess. Dostizheniia v oblasti metallovedeniia i termicheskoi obrabotki metallov. Tez. zonal'noi konf. (IX Ural'skoi shkoly metallovedov-termistov). Perm': Permskii politekhn. in-t, pages 4–5, 1985.
- [262] Kashchenko M.P. and Vereshchagin V.P. Migration of the boundary of a martensite crystal in the phonon maser mode. Phys.Met. Metall, 60(5):18–26, 1985.
- [263] Kashchenko M.P. and Vereshchagin V.P. Skorost' dvizheniia granitsy martensitnogo kristalla v volnovykh modeliakh rosta. Vsesoiuz. nauch. konf., Sverkhuprugost', éffekt pamiati formy i ikh primeneniie v novoi tekhnike": Tez. dokl. Tomsk: Isd-vo Tom. un-ta, pages 11–12, 1985.
- [264] Kashchenko M.P. and Vereshchagin V.P. Usloviia statsionarnogo dvizheniia granitsy martensitnogo kristalla v modeli fononnogo mazera. Vsesoiuz. nauch. konf., Sverkhuprugost', éffekt pamiati formy i ikh primeneniie v novoi tekhnike": Tez. dokl. Tomsk: Isd-vo Tom. un-ta, pages 54–55, 1985.
- [265] Paíns D. Élementarnye vozbuzhdeniia v tverdykh telakh. M.: Mir, 1965.
- [266] Kashchenko M.P. and Vereshchagin V.P. Tsentry zarozhdeniia i volnovye skhemy rosta martensita v splavakh zheleza. Izv. vuzov SSSR. Ser. Fizika, (8):16–20, 1989.

- [267] Kashchenko M.P. and Vereshchagin V.P. Uchet uprugogo polia priamo-lineinoi dislokatsii v ramkakh volnovogo opisaniia rosta martensita. *Izv. vuzov SSSR. Ser. Fizika*, (8):20–23, 1989.
- [268] Vereshchagin V.P., Kashchenko S.M., and Kashchenko M.P. Uchet osoben-nostei uprugogo polia dislokatsionnogo tsentra zarozhdeniia v volnovoi modeli rosta kristalla α -martensita v splavakh zheleza. *Novye metody v fizike i mekhanike deformiruемого tverdogo tela. Ch. 1. Tomsk: Izd-vo Tom-skogo un-ta*, pages 136–143, 1990.
- [269] Vereshchagin V.P. and Kashchenko M.P. Dislokatsionnye tsentry zarozh-deniiia α -martensita i orientatsionnye sootnosheniia pri $\gamma - \alpha$ prevrashcheniia v splavakh zheleza. *FTT*, 33(5):1605–1607, 1991.
- [270] Vereshchagin V.P., Kashchenko S.M., and Kashchenko M.P. Dislokatsionnye tsentry zarozhdeniia α -martensita v splavakh zheleza. *Izv. vuzov SSSR. Ser. Fizika*, (9):79–83, 1991.
- [271] Vereshchagin V.P., Kashchenko S.M., and Kashchenko M.P. Volnovaia priroda zarozhdenia i rosta α -martensita v splavakh zheleza. *Sil'no vzbuzhdennye sostoianiia v kristallakh. Sbornik trudov Tomskogo IFPM. Tomsk: Izd-vo Tomskogo nauch. tsentra SO AN SSSR*, pages 75–89, 1991.
- [272] Vereshchagin V.P. and Kashchenko M.P. Obobshchenie volnovoi modeli rosta kristalla α -martensita v splavakh zheleza. *Prognozirovanie mekhanich-eskogo povedeniia materialov. Novgorod*, pages 1–5, 1991.
- [273] Kashchenko M.P., Letuchev V.V., Konovalov S.V., and Neskromnyí S.V. Novyí podkhod k napravlennomu formirovaniu struktury α -martensita v splavakh na osnove zheleza. *Mekhanika prochnosti materialov s novymi funktsional'nymi svo'stvami. Rubezhnoe*, pages 232–233, 1990.
- [274] Kashchenko M.P., Letuchev V.V., Konovalov S.V., and Neskromnyí S.V. Physical imitation of α -martensite nucleation. *Phys.Met. Metall.*, 73(1):48–49, 1992.
- [275] Panin V.E., Griniaev Iu.V., Elsukova T.F., and Ivanchin A.G. Strukturnye urovni deformatsii tverdykh tel. *Izv. vuzov SSSR. Ser. Fizika*, (6):5–27, 1982.
- [276] Egorushkin V.E., Kul'ment'ev A.I., and Panin V.E. K probleme peremennoi valentnosti. *DAN SSSR*, 276(5):1104–1106, 1984.
- [277] Vediaev A.V., Granovskií A.B., Kondorskií E.I., and Kotel'nikova O.A. K teorii kineticheskikh iavlenii neuporiadochennykh splavov v priblizhenii kogerentnogo potentsiala. *FTT*, 20(1):166–170, 1978.

Epilogue

The author is sure that readers, who have reached up to the end of the monography, have understood that the mechanism controlling the spontaneous growth of martensite crystals (at cooling or heating) is connected with process of elastic waves generation by nonequilibrium 3d electrons (see also [1,2]). It is self-evident that the content of the monography is not exhausted by exposition of this process as the severe fathoming of the martensitic transformation mechanism in iron alloys needs the knowledge of solid-state physics in full.

Really, the nucleation process exposition of martensite is guessing the knowledge of the elastic fields created by flaws (in particular by dislocations).

It is necessary to understand, on the one hand, features of an energy-band structure in transition metals, and on the other hand, the essence of the kinetic phenomenons in them to explain the generation mechanism of waves.

It is necessary to take into account that not only pure metals must be discussed, but also alloys (in a wide range of concentrations and temperatures); not only paramagnetic state, but also the ferromagnetic state; not only linear, but also nonlinear waves with interior dynamic structure of a wave-front, etc.

The explanations covering the physical essence of solved problems and distinctive role of the martensitic transformation $\gamma - \alpha$ in iron alloys among structural transformations in solids (as an example of phase transition with extremely high speed of growth) ensure worth of the given book for broad enough audience of specialists.

The author has closely overlooked the monography once again and has convinced yourself that there is no need to make any essential changes in the text holding its topical nature (set of fine misprints have been eliminated at editing of translation).

It is worth noting that research directions marked in the monography have received the progress during last decade.

1. Dislocation nucleation centres were established for the martensitic crystals with all types of habit planes [3]. It has allowed to interpret the processes of forming of typical ensembles of the martensitic crystals (see for example [4-6]).
2. The formation of fine twin structure has been described as the consequence

of the coordinated propagation of relatively short-wave and long-wave atomic displacements (see [7–9]).

3. Calculations for the dislocation loops have been shown that their elastic fields (possessing the greater inhomogeneity in comparison with fields of the infinite rectilinear dislocations) create the such compact regions that the nucleation within them leads to observed distributions of habit planes.

Hence the distribution of habit planes gives the additional information for reconstruction of the nucleation process via morphological indications [10–12].

4. The concept of the crystons was found convenient and constructive for description of the lattice losing a stability during propagation of the process controlling the martensite growth [6]. This concept was originally used for interpretation of shear band formation (see for example [13–17]).
5. The cryston model has been extended to exposition of strain martensite.

In this case the crystons (the shear carriers of superdislocation type) are direct carriers of threshold strain (see [18, 19]).

Thus there is clear enough fathoming of physical mechanisms for all alternatives of the $\gamma - \alpha$ martensitic transformation in iron based alloys.

It is significant that concepts of the heterogeneous nucleation and the strain controlling the crystal growth (the last is localized in the frontal region of the growing crystal) are the universal for the exposition of martensite crystal formation.

However the dynamic nature of controlling processes, as well as mechanisms of their energy support, essentially discriminate.

For case of the cooling martensite this is the controlling wave process that is supported in the maser regime by nonequilibrium electrons due to the generation of energy in transforming phase.

For case of the strain martensite this is the processes of the crystons propagation that are supported in basic by energy of exterior stresses.

The author is sincerely grateful to mister U. Kayser-Herold and madam J. Gerlts. The translation that has been carried out by them, adequately transmits the content of the monography in Russian.

Bibliography for epilogue

- [1] Kashchenko M.P. and Letuchev V.V. and Konovalov S.V. and Neskromnyi S.V. Wave mechanism of growth and novel technique for initiation of the martensite nucleation. *Phys.Met. Metall.*, 76(3):300–308, 1993.
- [2] Letuchev V.V. and Konovalov S.V. and Kashchenko M.P. Dynamical Lattice State at the Initial Stage of Martensitic Transformation and Possibilities of its Physical Realization. *Journal de Physique IV, Colloque C2*, 5:53–58, 1995.
- [3] Letuchev V.V. and Vereshchagin V.P. and Alexina I.V. and Kashchenko M.P. Conception of New Phase Dislocation-Based Nucleation at Reconstructive Martensitic Transformations. *Journal de Physique IV, Colloque C8*, 5:151–156, 1995.
- [4] Kashchenko M.P. and Konovalov S.V. and Yablonskaya T.N. Dislocation Centers in α -Martensite Formation and Dual Couplings of Thinly-Laminated Martensite Crystals. *Russian Physics Journal*, 37(6):567–570, 1994.
- [5] Kashchenko M.P. and Konovalov S.V. and Yablonskaya T.N. Dislocation Centers for Nucleation of α -Martensite and Pairwise Joining of Martensite Crystals with Habits $\{hhl\}$. *Russian Physics Journal*, 37(4):363–366, 1994.
- [6] Kashchenko M.P. and Letuchev V.V. and Konovalov S.V. and Yablonskaya T.N. Model of packet martensite formation. *Phys.Met. Metall.*, 83(3):237–242, 1997.
- [7] Kashchenko M.P. and Chashchina V.G. Dinamicheskii mekhanizm dvoinkovaniia martensitnogo kristalla. *Mekhanizmy deformatsii i razrusheniia perspektivnykh materialov. Sb. trudov XXXV seminara "Aktual'nye problemy prochnosti"*. Part I. Pskov: PPI SPbGTU, pages 14–19, 1999.
- [8] Kashchenko M.P. and Chashchina V.G. Vliianie neodnorodnosti fronta upravliaushchego volnovogo protsessa na raspredelenie dvoinkov prevrashchenia v kristallakh martesita s gabitusami tipa (259) - (3 10 15). *Fizika*

- protsessov deformatsii i razrushenia i prognozirovanie mekhanicheskogo povedenia materialov: trudy XXXVI mezhdunarodnogo seminara "Aktual'nye problemy prochnosti v 2 chastiakh". Ch.I, Vitebsk, VGTU, pages 81-86, 2000.
- [9] Kashchenko M.P. and Chashchina V.G. Vliianie neodnorodnosti fronta upravliaushchego volnovogo protsessa na raspredelenie dvoinikov prevrashchenia v kristallakh martesita s gabitusami tipa (225). Nauchnye trudy IV mezhdunarodnogo seminara "Aktual'nye problemy prochnosti v 2 t." T.I, Velikii Novgorod, NGU, pages 156-158, 2000.
- [10] Kashchenko M.P. and Nefedov A.V. and Vereshchagin V.P. and Letuchev V.V. Nucleation of α martensite crystals with (hhl) habits in elastic fields of dislocation loops. Phys.Met. Metall., 85(4):392–402, 1998.
- [11] Dzhemilev K.N. and Kashchenko M.P. and Nefedov A.V. Vlianie tochechnykh defektov na uprugie polia dislokatsionnykh tsentrov zarozhdenia martensita. Fizika protsessov deformatsii i razrushenia i prognozirovanie mekhanicheskogo povedenia materialov: trudy XXXVI mezhdunarodnogo seminara "Aktual'nye problemy prochnosti v 2 chastiakh". Ch.II, Vitebsk, VGTU, pages 506-511, 2000.
- [12] Dzhemilev K.N. and Kashchenko M.P. and Nefedov A.V. Vlianie tochechnykh defektov na uprugie polia prizmaticheskikh dislokatsionnykh petel'. Nauchnye trudy IV mezhdunarodnogo seminara "Aktual'nye problemy prochnosti v 2 t.". T.I, Velikii Novgorod, NGU, pages 195-199, 2000.
- [13] Kashchenko M.P. and Letuchev V.V. and Teplyakova L.A. and Yablonskaya T.N. A model of formation of macroshear bands and strain-induced martensite with (hhl) boundaries. Phys.Met. Metall., 82(4):329–336, 1996.
- [14] Kashchenko M.P. and Teplyakova L.A. and Sokolova O.A. and Konovalov S.V. Formations of planar shear bands with $\{123\}$ boundaries in fcc single crystals. Phys.Met. Metall., 86(1):27–30, 1998.
- [15] Kashchenko M.P. and Teplyakova L.A. and Dzhemilev K.N. and Chashchina V.G. Conditions for the generation of crystons and the interpretation of the $\sigma - \varepsilon$ curve for Ni_3Fe single crystals. Phys.Met. Metall., 88(3):223–227, 1999.
- [16] Kashchenko M.P. and Chashchina V.G. and Semenovih A.G. The mechanism of formation of the shear bands with orientations of boundaries $\{hhl\}$ in cubic crystals. In *Advances in mechanical behaviour, plasticity and damage*. Proceedings of EUROMAT 2000, V.I., pages 305–310, Amsterdam: Elsevier science Ltd., 2000.

- [17] Kashchenko M.P. and Chashchina V.G. and Semenovih A.G. Kristonnyi mekhanizm formirovania α' martensita deformatsii v prisutstvii martensita napriazhenia. *Voprosy materialovedenia*, 1(29):253–259, 2002.
- [18] Kashchenko M.P. and Chashchina V.G. and Semenovih A.G. Kristonnaia model' formirovania α' martensita deformatsii v splavakh na osnove zheleza. *Fizicheskaiia mezomekhanika*, 6(3):95–122, 2003.
- [19] Kashchenko M.P. and Chashchina V.G. and Semenovih A.G. Cryston model of strain induced martensite. *J. Phys. IV France*, 112:147–150, 2003.

Kashchenko M.P. "The wave model of martensite growth
for the $\gamma - \alpha$ transformation of iron-based alloys".
2005

Summary

Kashchenko Mikhail Petrovich, professor (Holder of Physics Chair, Urals State Forest Engineering University), doctor of physical-mathematical sciences. The sphere of his scientific interests: physics of solids, high-excited states of solids, martensitic transformations, synergetics.

This book is the first monograph in the scientific literature, dedicated to the $\gamma - \alpha$ transformation in iron-based alloys, in which the dynamical approach is used for the explanation of the martensite growth stage.

The rapid growth of a martensite crystal is considered as a self-organized process controlled by the quasi-longitudinal lattice displacement waves (DW). The regime of the DW initial excitation is rigid. DW have the frequencies $\sim 10^{10} \text{sec}^{-1}$ from the hypersound band and the amplitudes providing the level of deformation $\sim 10^{-3}$. The conditions that are necessary for the generation of DW by non-equilibrium d-electrons are analyzed.

A wide range of questions (from peculiarities of the electronic spectrum to macroscopic morphological indicators), connected with the physical interpretation of the $\gamma - \alpha$ martensitic transformation in iron-based alloys, is discussed.

The short review of results having fundamental meaning for the creation of a physical model describing the martensite nucleation process is given in the monograph's conclusion. It is shown, that processes of the heterogeneous nucleation and wave growth have the genetic connection to the $\gamma - \alpha$ martensitic transformation.